

# **Renewable Biomass Resources: from waste biomass to novel applications *via* green chemical technologies**

**Zhanrong Zhang**

**Doctor of Philosophy**

**University of York**

**Chemistry**

**April 2015**



# Abstract

Waste biomass as a resource represents an interesting opportunity that imbues the principles of green chemistry within the context of sustainability. Herein, potential routes for valorisation of currently low-value and/or underutilised biorenewable waste streams, namely: spruce wood chips; waste office paper; paper deinking residue (DIR), and; waste starch, using green chemical technologies are reported.

Microwave-assisted low-temperature (<200 °C) pyrolysis was conducted on spruce wood chips, waste office paper and paper deinking residue (DIR) to afford three product lines: bio-oil (organic and aqueous phase); bio-char (microwave residue), and; gas. The application of the crude organic phase bio-oils as adhesives for aluminium to aluminium bonding was explored. Maximum tensile strengths, from approximately 2520 N (spruce wood chips) to 2300 N (waste paper) to 400 N (DIR), were observed. A synergistic and/or co-operative effect between various components of waste paper derived bio-oil on adhesive properties is postulated based on evaluation the results from liquid-liquid fractionation. This is the first reported application of bio-oils derived via low-temperature microwave processing for use as adhesives for metal-metal bonding.

The first complete holistic characterization of low-temperature microwave-processed DIR is reported. The residue (78 wt.%) was characterized by solid-state  $^{13}\text{C}$  CP/MAS NMR and XRD, showing it was free from organic matter and primarily comprises calcite and kaolinite. The DIR-derived bio-oil gave the lowest adhesion properties (400 N) compared to paper and wood-derived bio-oil.

The incorporation of expanded high amylose corn starch (HACS) and its propionates, with differing degree of substitution (DS), into potentially biodegradable hot melt adhesives (HMAs) comprising polyvinyl alcohol (PVOH) and glycerol was studied. The expansion process to form HMAs, surface area of HACS was increased from around  $5\text{ m}^2\text{ g}^{-1}$  to  $176\text{ m}^2\text{ g}^{-1}$ , is beneficial towards Al adhesion (ca. 2.0 MPa) as compared to non-expanded HACS (ca. 1.1 MPa).



# List of Contents

<b>Abstract.....</b>	<b>3</b>
<b>List of Contents .....</b>	<b>5</b>
<b>List of Figures.....</b>	<b>11</b>
<b>List of Tables .....</b>	<b>21</b>
<b>Acknowledgement .....</b>	<b>23</b>
<b>Author's declaration .....</b>	<b>25</b>
<b>Chapter 1 Introduction: Aims and Contextualisation.....</b>	<b>27</b>
<b>1.1 Aims and contextualisation.....</b>	<b>29</b>
<b>1.2 Preamble: Sustainable Development .....</b>	<b>30</b>
<b>1.3 (Bio)Waste: a growing problem, but also a growing opportunity.....</b>	<b>31</b>
<b>1.4 Lignocellulosic biomass.....</b>	<b>34</b>
<b>1.4.1 Cellulose.....</b>	<b>36</b>
<b>1.4.2 Hemicellulose.....</b>	<b>37</b>
<b>1.4.3 Lignin .....</b>	<b>38</b>
<b>1.4.4 Starch-based biomass .....</b>	<b>39</b>
<b>1.5 Green Chemistry and Green Chemical Engineering and the Biorefinery Concept .</b>	<b>41</b>
<b>1.5.1 Green Chemistry and Green Chemical Engineering .....</b>	<b>41</b>
<b>1.5.2 The Biorefinery concept.....</b>	<b>45</b>
<b>1.6 Thermochemical conversion techniques.....</b>	<b>47</b>
<b>1.6.1 Incineration.....</b>	<b>49</b>
<b>1.6.2 Gasification .....</b>	<b>49</b>
<b>1.6.3 Pyrolysis.....</b>	<b>50</b>
<b>1.7 Microwave chemistry .....</b>	<b>52</b>
<b>1.7.1 Principles of microwave heating .....</b>	<b>53</b>
<b>1.7.2 Microwave vs. conventional heating – the “microwave-effects” .....</b>	<b>56</b>

<b>Chapter 2 Microwave-assisted pyrolysis of biorenewable waste streams: From wood to paper to deinked residue.....</b>	<b>59</b>
<b>2.1 Summary.....</b>	<b>61</b>
<b>2.2 Wood chips, waste paper and de-inked residue (DIR).....</b>	<b>63</b>
2.2.1 Wood processing waste and wood chips .....	63
2.2.2 Waste paper.....	64
2.2.3 Paper deinking residue.....	65
<b>2.3 Microwave-assisted low-temperature pyrolysis of biorenewable waste streams .....</b>	<b>66</b>
2.3.1 Experimental set-up .....	66
2.3.2 Yield analysis.....	68
<b>2.4 Proximate and ultimate analysis of biorenewable feedstocks and their microwave-assisted low-temperature (&lt;200 °C) pyrolysis products.....</b>	<b>73</b>
2.4.1 Proximate and ultimate analysis .....	73
2.4.2 Mineral content analysis .....	77
<b>2.5 ATR-IR Characterization of feedstocks and their microwave-assisted pyrolysis products.....</b>	<b>81</b>
2.5.1 ATR-IR characterization of spruce wood chips and their pyrolysis products .....	81
2.5.2 ATR-IR characterization of waste office paper and its pyrolysis products .....	85
2.5.3 ATR-IR characterization of DIR and its pyrolysis products.....	87
2.5.4 Summary of the ATR-IR characterization.....	90
<b>2.6 NMR Characterization of bio-oils .....</b>	<b>91</b>
2.6.1 NMR characterization of spruce wood chips derived organic and aqueous phase bio-oils .....	95
2.6.2 NMR characterization of waste office paper derived organic and aqueous phase bio-oils .....	98
2.6.3 NMR characterization of DIR derived organic and aqueous phase bio-oils.....	101
2.6.4 Summary of liquid-state $^1\text{H}$ and $^{13}\text{C}$ NMR characterization of bio-oils .....	103
<b>2.7 GC-MS characterization of bio-oils.....</b>	<b>104</b>
2.7.1 GC-MS characterization of spruce wood chips derived bio-oils .....	105
2.7.2 GC-MS characterization of waste office paper derived bio-oils.....	110

2.7.3 GC-MS characterization of DIR derived bio-oils .....	113
2.7.4 Summary of GC-MS characterization of bio-oils .....	117
<b>2.8 Adhesion properties of organic phase bio-oils .....</b>	<b>118</b>
2.8.1 Adhesion tests of organic phase bio-oils .....	118
2.8.2 Adhesion strengths of organic phase bio-oils.....	121
2.8.3 ATR-IR characterization of scrapings of cured bio-oil polymers .....	130
2.8.4 Solid-state CP/MAS $^{13}\text{C}$ NMR characterization of scrapings of cured bio-oil polymers.....	137
<b>2.9 Liquid-liquid fractionation of waste office paper derived organic phase bio-oil and the adhesive properties of different bio-oil fractions.....</b>	<b>142</b>
2.9.1 Liquid-liquid fractionation of the crude organic phase bio-oil derived from waste office paper.....	143
2.9.2 $^{13}\text{C}$ NMR analysis of different bio-oil fractions .....	146
2.9.3 GC-MS characterization of different bio-oil fractions .....	148
2.9.4 Adhesive strengths of different bio-oil fractions.....	149
2.9.5 ATR-IR characterization of scrapings from cured different bio-oil fractions.....	152
<b>2.10 Model compound study of adhesive properties of organic phase bio-oils .....</b>	<b>154</b>
2.10.1 Adhesion properties of single model compounds .....	156
2.10.2 Adhesion properties of mixtures of two model compounds.....	159
2.10.3 Adhesion properties of mixtures of three model compounds.....	167
<b>2.11 Characterization of DIR derived microwave residue.....</b>	<b>171</b>
2.11.1 Solid-state CP/MAS $^{13}\text{C}$ NMR characterization of DIR and its microwave-residue .....	172
2.11.2 SEM morphology of DIR, microwave residue and TG ashes .....	173
2.11.3 ATR-IR characterization of DIR, microwave residue and TG ashes .....	175
2.11.4 ICP-MS analysis of DIR, its microwave residue and TG ashes.....	176
2.11.5 Powder XRD characterization of DIR, microwave residue and TG ashes.....	178
2.11.6 Solid-state Bloch-decay $^{13}\text{C}$ NMR characterization of DIR microwave residue ..	180
<b>2.12 Conclusions and future work.....</b>	<b>182</b>

<b>Chapter 3 Valorisation of waste starch and the application of expanded starch and its esters in hot melt adhesives .....</b>	<b>187</b>
<b>3.1 Summary.....</b>	<b>189</b>
<b>3.2 Introduction.....</b>	<b>189</b>
3.2.1 Hot melt adhesives.....	189
3.2.2 The development of biodegradable “green” hot melt adhesives.....	193
3.2.3 Expansion of starch.....	196
3.2.4 Esterification of starch .....	199
<b>3.3 Expansion and esterification of high amylose corn starch .....</b>	<b>202</b>
3.3.1 Preparation of expanded high amylose corn starch and its propionate derivatives .	202
3.3.2 ATR-IR characterization of expanded HACS and its esters.....	204
3.3.3 Thermogravimetric characterization of expanded HACS and its esters .....	207
3.3.4 NMR characterization of expanded HACS and its esters .....	209
<b>3.4 Preparation and characterization of hot melt adhesive formulations.....</b>	<b>213</b>
3.4.1 Preparation of hot melt adhesive formulations .....	213
3.4.2 DSC Characterization of hot melt adhesive formulations .....	213
3.4.3 ATR-IR Characterization of hot melt adhesive formulations .....	216
<b>3.5 Adhesion testing of hot melt adhesives.....</b>	<b>217</b>
3.5.1 Adhesion tests of hot melt adhesives .....	217
3.5.2 Tensile stress tests of hot melt adhesives.....	218
<b>3.6 Conclusions and future work .....</b>	<b>220</b>
<b>Chapter 4 Experimental .....</b>	<b>223</b>
<b>4.1 Materials and reagents .....</b>	<b>225</b>
4.1.1 Biomass.....	225
4.1.2 Chemical reagents.....	225
4.1.3 Other used materials .....	225
<b>4.2 Experimental details and instrumentation for chapter 2 .....</b>	<b>226</b>
4.2.1 Microwave-assisted low-temperature (<200 °C) pyrolysis of biorenewable waste streams .....	226

4.2.2 Yield analysis of microwave-assisted low-temperature (<200 °C) pyrolysis of biorenewable waste streams .....	227
4.2.3 Thermogravimetric analysis of paper deinking residue (DIR) .....	228
4.2.4 Proximate and ultimate analysis of raw materials and their microwave-assisted pyrolysis products .....	228
4.2.5 Calorific value measurement.....	230
4.2.6 Karl Fischer Titration.....	230
4.2.7 ICP-MS characterization .....	230
4.2.8 ATR-IR characterization .....	231
4.2.9 Liquid-state NMR characterization of bio-oils.....	231
4.2.10 GC-MS characterization of bio-oils .....	231
4.2.11 Qualitative and quantitative characterization of DIR derived organic phase bio-oil .....	232
4.2.12 Adhesion tests and tensile strength measurement .....	232
4.2.13 Solid-state CP/MAS <sup>13</sup> C NMR characterization of scrapings of cured bio-oil polymers .....	233
4.2.14 Liquid-liquid fractionation of waste office paper derived organic phase bio-oil..	234
4.2.15 Solid-state CP/MAS <sup>13</sup> C NMR characterization of DIR and its microwave residue .....	236
4.2.16 Scanning electron microscopy.....	236
4.2.17 Powder X-ray diffraction.....	236
4.2.18 Solid-state Bloch-decay <sup>13</sup> C NMR spectroscopy.....	236
<b>4.3 Experimental details and instrumentation for chapter 3.....</b>	<b>237</b>
4.3.1 Expansion of high amylose corn starch.....	237
4.3.2 BET surface area measurement.....	237
4.3.3 Esterification of expanded starch .....	238
4.3.4 Determination of degree of substitution.....	239
4.3.5 ATR-IR characterization .....	240
4.3.6 Thermogravimetric analysis.....	240
4.3.7 Solid-state CP/MAS <sup>13</sup> C NMR characterization .....	240

4.3.8 Liquid-state $^1\text{H}$ NMR characterization .....	240
4.3.9 Preparation of hot melt adhesive formulations .....	240
4.3.10 DSC characterization of hot melt adhesives .....	241
4.3.11 Adhesion tests of hot melt adhesives .....	241
<b>Chapter 5 Concluding remarks and Future Work .....</b>	<b>245</b>
<b>Appendix A .....</b>	<b>251</b>
<b>Appendix A: Qualitative and quantitative GC-MS characterization of the organic phase bio-oil generated from microwave-assisted low-temperature (&lt;200 °C) pyrolysis of DIR .....</b>	<b>253</b>
<b>Abbreviations .....</b>	<b>265</b>
<b>References .....</b>	<b>269</b>

# List of Figures

<b>Figure 1:</b> Three spheres of sustainable development, adapted from Reference 3. (Originally in colour).....	30
<b>Figure 2:</b> Illustration of the current version of waste hierarchy, reproduced from reference 34. (Originally in colour).....	33
<b>Figure 3:</b> General constituents in plant/wood biomass, adapted from reference 45 and 46. (Originally in colour).....	35
<b>Figure 4:</b> Chemical structure of cellulose.....	36
<b>Figure 5:</b> Major constituent monosaccharides of hemicellulose. (Originally in colour).....	38
<b>Figure 6:</b> Chemical structures of the three lignin building blocks and representative fragment of the structure of lignin, adapted from reference 70. (Originally in colour).....	39
<b>Figure 7:</b> Chemical structures of amylose and amylopectin. (Originally in colour).....	40
<b>Figure 8:</b> Comparison of petro-refinery and biorefinery, adapted from reference 83. (Originally in colour).....	45
<b>Figure 9:</b> The three types of Biorefineries. <sup>86-88</sup> (Originally in colour).....	46
<b>Figure 10:</b> An overview of thermochemical technologies for conversion of biomass and waste materials, adapted from reference 95. (Originally in colour).....	48
<b>Figure 11:</b> Illustration of several potential applications of pyrolysis products, adapted from reference 95. (Originally in colour).....	52
<b>Figure 12:</b> The electromagnetic spectrum. (Originally in colour).....	53
<b>Figure 13:</b> Illustration of temperature profiles of microwave irradiation and conventional heating, adapted from references 123 and 127. (Originally in colour).....	57
<b>Figure 14:</b> Illustration of potential sources for the three kinds of biorenewable waste streams: wood chips, waste paper and DIR. (Originally in colour).....	61
<b>Figure 15:</b> Experimental set-up for the microwave-assisted low-temperature (<200 °C) pyrolysis of spruce wood chips, waste office paper and DIR. (Originally in colour).....	67
<b>Figure 16:</b> Distribution of product yields for the microwave-assisted low-temperature pyrolysis of Spruce wood chips, waste office paper and DIR (the gas yield was calculated by mass difference). (Originally in colour).....	68

<b>Figure 17:</b> Appearance of raw materials and products from microwave-assisted low-temperature processing of spruce wood chips, waste office paper and DIR. (Originally in colour).....	69
<b>Figure 18:</b> TG traces of DIR in N <sub>2</sub> (black) and in air atmosphere (red), samples heated from 30 °C to 625 °C at a heating rate of 10 °C min <sup>-1</sup> . (Originally in colour).....	71
<b>Figure 19:</b> Appearance of (A) DIR raw material, (B) DIR microwave residue obtained from microwave-assisted pyrolysis of DIR, (C) TG ash of DIR in N <sub>2</sub> atmosphere and (D) TG ash of DIR in air atmosphere. (Originally in colour).....	71
<b>Figure 20:</b> TG trace of microwave residue in N <sub>2</sub> atmosphere (100 mL min <sup>-1</sup> ), sample heated from 30 °C to 625 °C at a heating rate of 10 °C min <sup>-1</sup> . (Originally in colour).....	72
<b>Figure 21:</b> ATR-IR spectra of spruce wood chips and the products generated from microwave-assisted pyrolysis process (except gas fraction): organic fraction bio-oil, aqueous fraction bio-oil and microwave residue. (Originally in colour).....	83
<b>Figure 22:</b> ATR-IR spectra of waste office paper and the products generated from microwave-assisted pyrolysis process (except gas fraction): organic fraction bio-oil, aqueous fraction bio-oil and bio-char. (Originally in colour).....	87
<b>Figure 23:</b> ATR-IR spectra of DIR raw material and the products generated from microwave-assisted pyrolysis of DIR (except gas fraction): organic phase bio-oil, aqueous phase bio-oil and microwave residue, together with those of calcium carbonate (calcite) and kaolinite.....	89
<b>Figure 24:</b> <sup>13</sup> C NMR spectra of organic and aqueous phase bio-oil generated from microwave-assisted processing of spruce wood chips. All spectra used the central resonance of DMSO-d <sub>6</sub> ( $\delta$ C, 39.52 ppm) as internal reference. (Originally in colour).....	96
<b>Figure 25:</b> <sup>1</sup> H NMR spectra of organic and aqueous phase bio-oil generated from microwave-assisted processing of spruce wood chips. (Originally in colour).....	98
<b>Figure 26:</b> <sup>13</sup> C NMR spectra of organic and aqueous phase bio-oil generated from microwave-assisted processing of waste office paper. All spectra used the central resonance of DMSO-d <sub>6</sub> ( $\delta$ C, 39.52 ppm) as internal reference. (Originally in colour).....	99
<b>Figure 27:</b> <sup>1</sup> H NMR spectra of organic and aqueous phase bio-oil generated from microwave-assisted processing of waste office paper.....	101

<b>Figure 28:</b> $^{13}\text{C}$ NMR spectra of organic and aqueous phase bio-oil generated from microwave-assisted processing of DIR. All spectra used the central resonance of DMSO-d <sub>6</sub> ( $\delta\text{C}$ , 39.52 ppm) as internal reference. (Originally in colour).....	102
<b>Figure 29:</b> $^1\text{H}$ NMR spectra of organic and aqueous phase bio-oil generated from microwave-assisted processing of DIR.....	103
<b>Figure 30:</b> GC-MS spectra of (A) organic and (B) aqueous phase bio-oils derived from microwave-assisted pyrolysis of spruce wood chips.....	105
<b>Figure 31:</b> Chemical structures of several representative aromatic compounds derived from thermal degradation of lignin.....	108
<b>Figure 32:</b> Chemical structures of levoglucosan and levoglucosenone.....	109
<b>Figure 33:</b> GC-MS spectra of (A) organic and (B) aqueous phase bio-oils derived from microwave-assisted pyrolysis of milled waste office paper. *Possible artefacts.....	110
<b>Figure 34:</b> GC-MS spectra of (A) organic and (B) aqueous phase bio-oils derived from microwave-assisted pyrolysis of DIR. *Possible artefacts.....	114
<b>Figure 35:</b> Curing procedures for the application of bio-oil as an adhesive for Al – Al bonding. (Originally in colour).....	120
<b>Figure 36:</b> Illustration of tensile strength tests of bio-oil cured Al plates using an Instron 3367 universal testing machine, at a crosshead speed of 5 mm min <sup>-1</sup> . (Originally in colour).....	120
<b>Figure 37:</b> A general extension – load curve generated by the accompanying software of Instron 3367 universal testing machine for bio-oil cured Al plates. (Originally in colour).....	121
<b>Figure 38:</b> Appearances of the Al – bio-oil –Al interfaces of Al plates oven cured by the spruce wood chips derived organic phase bio-oil at various temperatures for 8 h. (Originally in colour).....	122
<b>Figure 39:</b> Appearances of the Al – bio-oil –Al interfaces of Al plates oven cured by the waste office paper derived organic phase bio-oil at various temperatures for 8 h. (Originally in colour).....	122
<b>Figure 40:</b> Appearances of the Al – bio-oil –Al interfaces of Al plates oven cured by the DIR derived organic phase bio-oil at various temperatures for 8 h. (Originally in colour).....	123

<b>Figure 41:</b> Illustration of principles of adhesion and cohesion, together with differences between adhesive and cohesive joint failure patterns, adapted from reference 196. (Originally in colour).....	124
<b>Figure 42:</b> Tensile strengths of spruce wood chips derived organic phase bio-oil (70 mg) cured Al plates.....	125
<b>Figure 43:</b> Tensile strengths of waste office paper derived organic phase bio-oil (70 mg) cured Al plates. (Originally in colour).....	125
<b>Figure 44:</b> Tensile strengths of DIR derived organic phase bio-oil (70 mg) cured Al plates... 126	
<b>Figure 45:</b> Mass loss (wt.%) of spruce wood chips, waste office paper and DIR derived organic phase bio-oil during curing Al in oven at various temperatures for 4 h curing. (Originally in colour).....	128
<b>Figure 46:</b> Mass loss (wt.%) of spruce wood chips, waste office paper and DIR derived organic phase bio-oil during curing Al in oven at various temperatures for 8 h curing. (Originally in colour).....	129
<b>Figure 47:</b> Adhesion strength test of the waste office paper derived organic phase bio-oil. The tested specimen is Al plates adhered by the crude, waste office paper derived organic phase bio-oil at 160 °C for 8 h curing. (Originally in colour).....	130
<b>Figure 48:</b> ATR-IR spectra of spruce wood chips derived organic phase bio-oil, scrapings of the Al-bio-oil-Al interface polymer formed at 140 °C for 4 and 8 h curing (between 4000 cm <sup>-1</sup> and 500 cm <sup>-1</sup> ). (Originally in colour).....	132
<b>Figure 49:</b> ATR-IR spectra of spruce wood chips derived organic phase bio-oil, scrapings of the Al-bio-oil-Al interface polymer formed at 140 °C for 4 and 8 h curing (between 2000 cm <sup>-1</sup> and 500 cm <sup>-1</sup> ). (Originally in colour).....	132
<b>Figure 50:</b> ATR-IR spectra of waste office paper derived organic phase bio-oil, scrapings of the Al-bio-oil-Al interface polymer formed at 160 °C for 4 and 8 h curing. (Originally in colour).....	134
<b>Figure 51:</b> ATR-IR spectra of waste office paper derived organic phase bio-oil, scrapings of the Al-bio-oil-Al interface polymer formed at 160 °C for 4 and 8 h curing (between 2000 cm <sup>-1</sup> and 500 cm <sup>-1</sup> ). (Originally in colour).....	134

<b>Figure 52:</b> ATR-IR spectra of DIR derived organic phase bio-oil, scrapings of the Al-bio-oil-Al interface polymer formed at 160 °C for 4 and 8 h curing (between 4000 cm <sup>-1</sup> and 500 cm <sup>-1</sup> ). (Originally in colour).....	136
<b>Figure 53:</b> ATR-IR spectra of DIR derived organic phase bio-oil, scrapings of the Al-bio-oil-Al interface polymer formed at 160 °C for 4 and 8 h curing (between 2000 cm <sup>-1</sup> and 500 cm <sup>-1</sup> ). (Originally in colour).....	136
<b>Figure 54:</b> Solid-state <sup>13</sup> C CP/MAS NMR spectrum of spruce wood chips derived bio-oil / Al scraping (black) and <sup>13</sup> C CP/MAS NMR spectrum of spruce wood chips derived bio-oil / Al scraping with dipolar dephasing (red), overlapped with the liquid-state <sup>13</sup> C NMR spectrum of organic phase bio-oil from spruce wood chips. (Originally in colour).....	138
<b>Figure 55:</b> Solid-state <sup>13</sup> C CP/MAS NMR spectrum of waste office paper derived bio-oil / Al scraping (black) and <sup>13</sup> C CP/MAS NMR spectrum of waste office paper derived bio-oil / Al scraping with dipolar dephasing (red), overlapped with the liquid-state <sup>13</sup> C NMR spectrum of organic phase bio-oil (*possible artefacts). (Originally in colour).....	139
<b>Figure 56:</b> Solid-state <sup>13</sup> C CP/MAS NMR spectrum of DIR derived bio-oil / Al scraping (black) and <sup>13</sup> C CP/MAS NMR spectrum of DIR derived bio-oil / Al scraping with dipolar dephasing (red), overlapped with the liquid-state <sup>13</sup> C NMR spectrum of organic phase bio-oil from DIR. (Originally in colour).....	140
<b>Figure 57:</b> Liquid-liquid fractionation of the waste office paper derived organic phase bio-oil. (Originally in colour).....	144
<b>Figure 58:</b> Appearances of the “neutral” ethyl acetate fraction, “acidic” ethyl acetate fraction and aqueous fraction bio-oil. (Originally in colour).....	146
<b>Figure 59:</b> Yield of liquid-liquid fractionation of waste office paper derived organic phase bio-oil. (Originally in colour).....	146
<b>Figure 60:</b> <sup>13</sup> C NMR spectra of “neutral” ethyl acetate fraction, “acidic” ethyl acetate fraction and aqueous fraction bio-oil yielded from liquid-liquid fractionation of waste office paper derived organic phase bio-oil (all spectra used the central resonance of DMSO-d <sub>6</sub> ( $\delta$ C, 39.52 ppm) as internal reference). *possible artefacts.....	147

<b>Figure 61:</b> GC-MS spectra of “neutral” ethyl acetate fraction, “acidic” ethyl acetate fraction and aqueous fraction bio-oil generated from liquid-liquid separation of waste office paper derived organic phase bio-oil. *possible artefacts. (Originally in colour).....	149
<b>Figure 62:</b> Tensile strengths of waste office paper derived organic phase bio-oil, “neutral” and “acidic” ethyl acetate and aqueous fraction bio-oil, and a mixture of the “neutral” and “acidic” ethyl acetate fraction bio-oil cured Al plates (Specimens cured at 160 °C for 4 h. (Originally in colour).....	150
<b>Figure 63:</b> Appearances of the Al – bio-oil –Al interfaces of Al plates oven cured by the “neutral” ethyl acetate fraction, “acidic” ethyl acetate fraction and aqueous fraction bio-oil at 160 °C for 4 h. (Originally in colour).....	151
<b>Figure 64:</b> Mass loss (wt.%) of waste office paper derived organic phase bio-oil, “neutral” ethyl acetate fraction, “acidic” ethyl acetate fraction and aqueous phase fraction bio-oil during curing Al plates in oven at 160 °C for 4 h curing. (Originally in colour).....	152
<b>Figure 65:</b> ATR-IR spectra of (A) “neutral” ethyl acetate fraction bio-oil and scrapings of cured polymer of this fraction (B) “acidic” ethyl acetate fraction bio-oil and scrapings of cured polymer of this fraction (specimens cured at 160 °C for 4 h). (Originally in colour).....	154
<b>Figure 66:</b> Chemical structures of the three selected model chemical compounds (catechol, HMF and levoglucosan).....	156
<b>Figure 67:</b> Appearances of the Al – single compound –Al interfaces of Al plates oven cured by single model compound (70 mg) at 140 °C for 4 h. (Originally in colour).....	157
<b>Figure 68:</b> ATR-IR spectra of HMF and the residue at the Al-HMF-Al interface after curing at 140 °C for 4 h. (Originally in colour).....	158
<b>Figure 69:</b> ATR-IR spectra of catechol and the residue at the Al-catechol-Al interface after curing at 140 °C for 4 h. (Originally in colour).....	158
<b>Figure 70:</b> ATR-IR spectra of levoglucosan and the residue at the Al-levoglucosan-Al interface after curing at 140 °C for 4 h. (Originally in colour).....	159
<b>Figure 71:</b> Appearances of the Al–mixture–Al interfaces of Al plates oven cured by mixtures of two model compounds (70 mg) at 140 °C for 4 h. (Originally in colour).....	161
<b>Figure 72:</b> Illustration of a potential reaction pathway for phenolic compounds and furans in the presence of acid catalysts ( <i>e.g.</i> , carboxylic acids, phenolic compounds).....	163

<b>Figure 73:</b> ATR-IR spectra of mixtures of HMF and levoglucosan with molar ratio 5 : 5 and the residue at the Al–mixture–Al interface after curing at 140 °C for 4 h. (Originally in colour).....	164
<b>Figure 74:</b> ATR-IR spectra of mixtures of catechol and HMF with molar ratio 1 : 9 and the residue at the Al–mixture–Al interface after curing at 140 °C for 4 h. (Originally in colour).....	165
<b>Figure 75:</b> ATR-IR spectra of mixtures of catechol and levoglucosan with molar ratio 1 : 9 and the residue at the Al–mixture–Al interface after curing at 140 °C for 4 h. (Originally in colour).....	165
<b>Figure 76:</b> Tensile strengths of Al plates cured by catechol and HMF mixtures with various molar ratios (1 : 1, 3 : 7 and 5 : 5), specimens cured at 140 °C for 4 h. (Originally in colour).....	166
<b>Figure 77:</b> Appearances of the Al – mixture –Al interfaces of Al plates oven cured by mixtures of three model compounds (70 mg) with various molar ratios at 140 °C for 4 h. C: catechol; H: HMF; L: levoglucosan. (Originally in colour).....	169
<b>Figure 78:</b> Tensile strengths of catechol, HMF and levoglucosan mixtures with variable molar ratios cured Al plates, samples cured at 160 °C for 4 h. (Originally in colour).....	170
<b>Figure 79:</b> ATR-IR spectra of mixture of catechol, HMF and levoglucosan with molar ratio 28 : 36 : 36 and the residue at the Al-mixture-Al interface after curing at 160 °C for 4 h. (Originally in colour).....	171
<b>Figure 80:</b> Solid-state CP/MAS <sup>13</sup> C NMR spectra of DIR raw material (upper) and its microwave residue (lower).....	173
<b>Figure 81:</b> Representative SEM micrographs of (A) DIR raw material, (B) microwave residue, (C) TG ash of DIR (in N <sub>2</sub> ), (D) TG ash of DIR (in air) on 100 µm scale. (Originally in colour).....	174
<b>Figure 82:</b> Representative SEM micrographs of (A) DIR raw material, (B) microwave residue, (C) TG ash of DIR (in N <sub>2</sub> ), (D) TG ash of DIR (in air) on 10 µm scale. (Originally in colour).....	174
<b>Figure 83:</b> ATR-IR spectra of DIR raw material, microwave residue, TG ashes of DIR obtained in N <sub>2</sub> and air atmosphere. (Originally in colour).....	176
<b>Figure 84:</b> Powder XRD patterns of DIR raw material, microwave residue, TG ashes of DIR obtained in N <sub>2</sub> and air atmosphere together with commercial CaCO <sub>3</sub> (calcite) and kaolinite (k: kaolinite; cel: cellulose; c: calcite).....	179

<b>Figure 85:</b> $^{13}\text{C}$ Bloch-decay solid-state NMR spectra of DIR raw material, microwave residue resulting from microwave-assisted pyrolysis of DIR, TG ash of DIR ( $\text{N}_2$ ), TG ash of DIR (air) and commercial $\text{CaCO}_3$ (calcite), with full width at half height (FWHH) of each signal indicated (background corrected).....	181
<b>Figure 86:</b> Summary of microwave-assisted low-temperature ( $<200\text{ }^\circ\text{C}$ ) pyrolysis of three biorenewable waste streams. (Originally in colour).....	182
<b>Figure 87:</b> Illustration of a potential route for valorisation of DIR in the concept of biorefinery. (Originally in colour).....	186
<b>Figure 88:</b> Illustration of a typical temperature – time curve for hot melt adhesive, adapted from reference 225 and 226. (Originally in colour).....	191
<b>Figure 89:</b> Primary constituents of a typical hot melt adhesive and the general properties and functions of each constituent, according to references 225 - 228. (Originally in colour).....	192
<b>Figure 90:</b> The shift from petrochemical derived materials to biorenewable materials derived products in hot melt adhesive formulations, adapted from references 240 and 258. (Originally in colour).....	195
<b>Figure 91:</b> Illustration of gelatinisation and retrogradation of starch granules, adapted from reference 274. (Originally in colour).....	197
<b>Figure 92:</b> Illustration of collapsing of starch porous structures if water is directly removed from the aqua gel matrix without solvent exchange, adapted from reference 276. (Originally in colour).....	198
<b>Figure 93:</b> Illustration of the concept of the work within this chapter. (Originally in colour).....	201
<b>Figure 94:</b> Mechanism for esterification of starch using propionic anhydride (esterifying reagent) and DMAP (catalyst). (Originally in colour).....	201
<b>Figure 95:</b> Effects of (A) amounts of esterifying reagent <i>i.e.</i> propionic anhydride for 6 h reaction and (B) reaction time on DS of starch propionates.....	204
<b>Figure 96:</b> ATR-IR spectra of expanded HACS and its propionates. (Originally in colour)....	206
<b>Figure 97:</b> TGA traces for expanded HACS and its propionates, samples heated from $30\text{ }^\circ\text{C}$ to $625\text{ }^\circ\text{C}$ at a heating rate of $10\text{ }^\circ\text{C min}^{-1}$ . (Originally in colour).....	208
<b>Figure 98:</b> dTG traces for expanded HACS and its propionates, samples heated from $30\text{ }^\circ\text{C}$ to $625\text{ }^\circ\text{C}$ at a heating rate of $10\text{ }^\circ\text{C min}^{-1}$ . (Originally in colour).....	208

<b>Figure 99:</b> Solid-state $^{13}\text{C}$ CP/MAS NMR spectra of (A) expanded HACS and (B) starch propionate (DS, 1.00). The repeating unit shown in Figure 99 B is with the ester group connected to the most probable C position (C – 6). <sup>287</sup> .....	210
<b>Figure 100:</b> $^1\text{H}$ NMR spectra of expanded HACS and its propionates (DS: 0.38, 1.46, 1.99 and 2.54) in DMSO-d <sub>6</sub> . * Possible artefact.....	212
<b>Figure 101:</b> Illustration of the potentially biodegradable hot melt adhesive formulations. (Originally in colour).....	213
<b>Figure 102:</b> DSC traces of the 2 <sup>nd</sup> heating run of expanded HACS and starch propionates (DS: 0.38; 1.00; 1.82; 2.54) based HMAs. (Originally in colour).....	215
<b>Figure 103:</b> DSC traces of the 2 <sup>nd</sup> cooling run of expanded HACS and starch propionates (DS: 0.38; 1.00; 1.82; 2.54) based HMAs. (Originally in colour).....	215
<b>Figure 104:</b> DSC traces of the 2 <sup>nd</sup> to 5 <sup>th</sup> heat – cool cycle of starch propionate (DS, 1.00) based HMA formulation. (Originally in colour).....	216
<b>Figure 105:</b> ATR-IR spectra of (A) expanded HACS, expanded HACS based HMA before and after DSC measurement, (B) starch propionate (DS, 1.82), starch propionate (DS, 1.82) based HMA before and after DSC measurement. (Originally in colour).....	217
<b>Figure 106:</b> A typical failure pattern of formulated HMA bonded Al plates, sample shown is the Al – HMA – Al interface of expanded HACS based HMA cured Al plates. (Originally in colour).....	218
<b>Figure 107:</b> Normalized tensile stress of non-expanded HACS, expanded HACS and its starch propionates based HMA formulations (50 mg) bonded Al plates. (Originally in colour).....	219
<b>Figure 108:</b> Illustration of the experimental set-up used for the microwave-assisted low-temperature (<200 °C) pyrolysis, sample shown in the microwave vessel is DIR. (Originally in colour).....	226
<b>Figure 109:</b> Proximate analysis (moisture content, volatile matter, fixed carbon and ash content) of spruce wood chips. (Originally in colour).....	229
<b>Figure 110:</b> Illustration of the procedure for liquid-liquid separation of waste office paper derived organic phase bio-oil and the appearances of samples at crucial separation stages. (Originally in colour).....	235

<b>Figure 111:</b> Illustration of effective bonding area (the area covered by HMA polymer). (Originally in colour).....	242
<b>Figure 112:</b> Overall gas chromatogram of the DIR derived organic phase bio-oil.....	260
<b>Figure 113:</b> Specified gas chromatogram identification of the DIR derived organic phase bio-oil (0-25 min).....	261
<b>Figure 114:</b> Specified gas chromatogram identification of the DIR derived organic phase bio-oil (25-50 min).....	262
<b>Figure 115:</b> Specified gas chromatogram identification of the DIR derived organic phase bio-oil (50-75 min).....	263
<b>Figure 116:</b> Specified gas chromatogram identification of the DIR derived organic phase bio-oil (75-100 min).....	264

# List of Tables

<b>Table 1:</b> Typical cellulose, hemicellulose and lignin contents of several selected plant resources and biorenewable waste materials <sup>48-51</sup> .....	35
<b>Table 2:</b> The twelve principles of green chemistry. <sup>78</sup> .....	42
<b>Table 3:</b> The twelve principles of green chemical engineering. <sup>80</sup> .....	43
<b>Table 4:</b> Loss factors ( $\tan\delta$ ) of several common solvents <sup>a</sup> .....	56
<b>Table 5:</b> Proximate and ultimate characterization of spruce wood chips and their microwave-assisted pyrolysis products.....	75
<b>Table 6:</b> Proximate and ultimate characterization of waste office paper and its microwave-assisted pyrolysis products.....	76
<b>Table 7:</b> Ultimate characterization of DIR and its microwave-assisted pyrolysis products.....	77
<b>Table 8:</b> Mineral contents of spruce wood chips and their relative low-temperature microwave-assisted pyrolysis products as determined by ICP-MS.....	78
<b>Table 9:</b> Mineral contents of waste office paper and its relative low-temperature microwave-assisted pyrolysis products as determined by ICP-MS.....	79
<b>Table 10:</b> Mineral contents of DIR and its relative low-temperature microwave-assisted pyrolysis products as determined by ICP-MS.....	80
<b>Table 11:</b> Classification of bio-oil carbon contents in accordance with the chemical shift range <sup>182</sup> .....	93
<b>Table 12:</b> Classification of bio-oil hydrogen contents in accordance with the chemical shift range <sup>182</sup> .....	94
<b>Table 13:</b> Major identified compounds in spruce wood chips derived organic phase bio-oil <sup>a</sup> ..	106
<b>Table 14:</b> Major identified compounds in spruce wood chips derived aqueous phase bio-oil <sup>a</sup> .....	107
<b>Table 15:</b> Major identified compounds in waste office paper derived organic phase bio-oil <sup>a</sup> .....	112
<b>Table 16:</b> Major identified compounds in waste office paper derived aqueous phase bio-oil <sup>a</sup> .....	113
<b>Table 17:</b> Major identified compounds in DIR derived organic phase bio-oil <sup>a</sup> .....	115

<b>Table 18:</b> Major identified compounds in DIR derived aqueous phase bio-oil <sup>a</sup> .....	116
<b>Table 19:</b> Assignments of carbon resonance signals in the solid-state $^{13}\text{C}$ CP/MAS NMR spectra with and without dipolar dephasing in accordance with the chemical shift range.....	142
<b>Table 20:</b> Tensile strengths of Al plates cured by mixtures of each two model compounds (70 mg) with various molar ratios.....	160
<b>Table 21:</b> Mineral contents of DIR raw material, microwave residue, TG ashes of DIR obtained in nitrogen and air atmosphere as determined by ICP-MS.....	177
<b>Table 22:</b> Current benefits of hot melt adhesives and potential benefits of bio-based hot melt adhesives, reproduced from reference 240.....	194
<b>Table 23:</b> Esterification reaction conditions and degree of substitutions (DS) of resultant starch propionates. <sup>a</sup> .....	203
<b>Table 24:</b> Summary of the assignments of major bands in the ATR-IR spectra of expanded HACS and its propionates.....	207
<b>Table 25:</b> Summary of esterification reaction conditions.....	238
<b>Table 26:</b> Summary table of GC-MS characterization of the DIR derived organic phase bio-oil.....	254
<b>Table 27:</b> Detailed GC-MS analysis of the DIR derived organic phase bio-oil.....	255

# Acknowledgements

My first and warmest gratitude must go to Dr. Avtar S. Matharu for his excellent supervision throughout my PhD study in York. With enthusiasm and patience, he has ceaselessly guided, motivated, helped and inspired me in various fields. I feel very lucky to have him as my supervisor during the past three and half years. I'm very grateful for all the opportunities he provided to attend many international conferences, training courses and to participate in lots industrial internships. Importantly, I appreciate Professor James H. Clark for his insightful advice, guidance and all the help during the past several years in my academic life. I appreciate especially Dr. Duncan J. Macquarrie who has been very important for me with his constructive, positive advice and comments on my work.

For financial support, I acknowledge the Department of Chemistry at University of York for a Wild-fund scholarship for PhD study. I also appreciate the Great Britain-China Educational Trust (GBCET) for a scholarship award in 2014, which is really encouraging and rewarding.

I would like to thank Abdulrahman Alwehaibi especially who has been very kind and encouraging for me during the past five years. I appreciate Chris Mortimer for the production of shot-blasted Al plates. Dr. Pedro Aguiar for his help with solid-state  $^{13}\text{C}$  NMR. Huge thanks must go to Dr. Hannah Briers, Paul Elliott and Charlotte Brannigan for their technical assistance. I acknowledge all the previous and current members of the Green Chemistry Centre of Excellence for all their help and friendship.

In particular, I would like to make a very special thank you to Ms. Shanshan Guan, for all her dedication, inspiration, understanding, patience, and lots help.

Finally and most importantly, the greatest gratitude goes to my dearest parents (父亲：张全峰；母亲：杨彩霞) and sister (张家荣), for all their love and support in the past 27 years which allowed me to get to this point.



# Author's declaration

Some of the results presented herein were obtained by, or in collaboration with other co-workers. They are all fully acknowledged in the list below along with their corresponding institution. All other results are the work of the author.

Zhanrong Zhang

April 2015

Piece of work	Collaborator/institution
Elemental (CHN) analysis	Chemistry Department service, University of York
Sulfur content analysis	Yara analytical services, York, UK
Total organic carbon analysis	Yara analytical services, York, UK
GC – MS analysis of DIR derived organic phase bio-oil	Thunen Institute, University of Hamburg, Germany
SEM microscopy	Dr. Meg Stark, Department of Biology, University of York
ICP-MS analysis	Dr. Helen Parker, Green Chemistry Centre
Solid-state <sup>13</sup> C NMR analysis	Dr. Pedro Aguiar, Department of Chemistry, University of York
Al plates production and pretreatment (blasting)	Chris Mortimer, Department of Chemistry, University of York

Aspects of work described in this thesis have been presented in several publications:

- Z. Zhang, D. J. Macquarrie, P. M. Aguiar, J. H. Clark and A. S. Matharu, *Environmental Science & Technology*, 2015, **49**, 2398-2404.
- Z. Zhang, D. J. Macquarrie, M. De bruyn, V. L. Budarin, A. J. Hunt, M. J. Gronnow, J. Fan, P. S. Shuttleworth, J. H. Clark and A. S. Matharu, *Green Chemistry*, 2015, **17**, 260-270.
- Z. Zhang, D. J. Macquarrie, J. H. Clark and A. S. Matharu, *RSC Advances*, 2014, **4**, 41947-41955.



# Chapter 1

## *Introduction: Aims and Contextualisation*



## **1.1 Aims and contextualisation**

This project aims to study potential routes for valorisation of several currently underutilised biorenewable waste streams within the concept of a biorefinery. Waste valorisation practices should be performed in a way that allows for the recovery of high-value and marketable products for both existing and new markets, in order to offer added revenues for industry. In this context, exploring innovative uses of the products generated from biorefinery processes is particularly important. Herein, the conversion of several types of biorenewable waste streams: wood chips; waste paper; paper deinking residue (DIR), and; waste starch, using green chemical technologies and processes into potentially valuable products and applications is studied.

Chapter 2 describes the microwave-assisted low-temperature (<200 °C) pyrolysis of three biorenewable waste streams (*i.e.*, spruce wood chips, waste office paper and DIR) for the generation of bio-oil, bio-char (microwave residue) and gas. The properties of pyrolysis products were comprehensively studied with particular emphasis on the application of the crude organic phase bio-oils as adhesives towards metal bonding. As an attempt to gain some understanding of the adhesive behaviours of bio-oil, a liquid – liquid fractionation of the waste office paper derived organic phase bio-oil was performed and the adhesive properties of the thus derived different fractions of bio-oil were investigated. Moreover, a compound study using 5-(hydroxymethyl)-2-furaldehyde (HMF), catechol and levoglucosan was conducted to get further understanding of the adhesion of bio-oil towards aluminium bonding. At last, holistic characterization of the largest part of the pyrolysis products derived from DIR (*i.e.*, microwave residue) was performed, aiming for its valorisation.

Chapter 3 illustrates a potential route for valorisation of waste starch (high amylose corn starch, HACS) and the applications of expanded HACS, and its propionate derivatives, in potentially biodegradable hot melt adhesive (HMA) formulations. The influences of amounts of esterifying reagent (propionic anhydride) and reaction time on the degree of substitution (DS) of starch propionates were investigated. Expanded HACS and its propionates were formulated into HMA

formulations comprising polyvinyl alcohol (PVOH) and glycerol. The adhesion properties of thus derived HMA formulations towards Al bonding were studied.

Chapter 4 and 5 describe the experimental procedures employed and conclusions for the PhD project (including future work), respectively.

## 1.2 Preamble: Sustainable Development

The term “sustainable development” was first coined in 1987 by the United Nations World Commission on Environment and Development (WCED) in their report entitled “*Our common future*”, also known as the “Brundtland report”.<sup>1</sup> Sustainable development is defined as “development that meets the needs of the present without compromising the ability of future generations to meet their own needs”.<sup>1</sup> As shown in Figure 1, the concept of sustainable development aims to achieve a balance between social, economic, and environmental needs.<sup>2–4</sup>

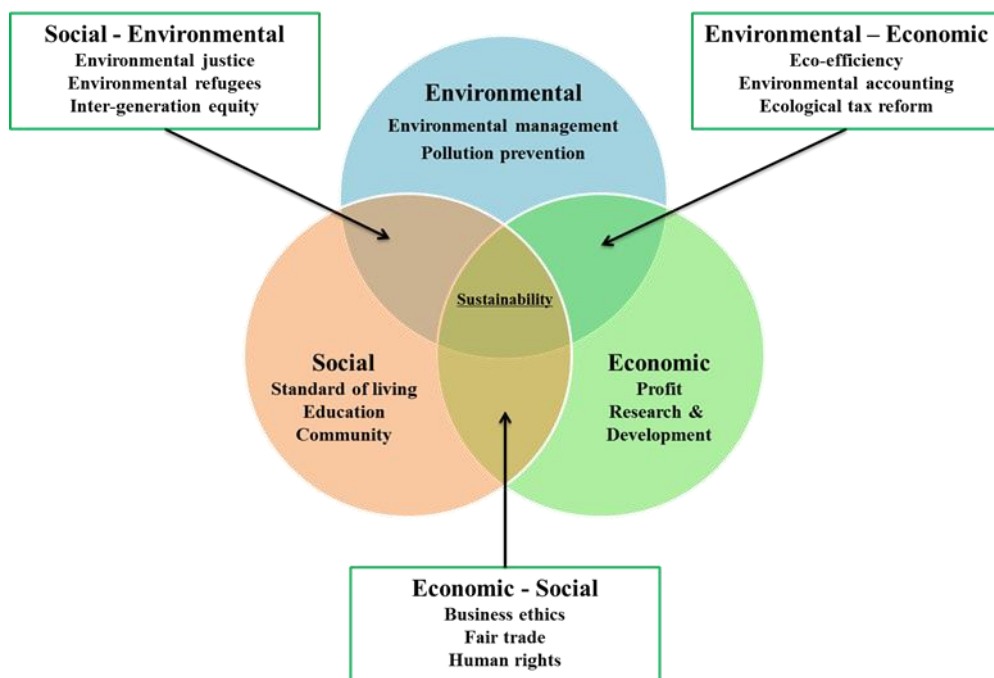


**Figure 1:** Three spheres of sustainable development, adapted from Reference 3. (Originally in colour)

The last one hundred years has seen global population multiply four-fold to 6.4 billion, global economic output increase more than twenty-fold and global material consumption increase eight-fold.<sup>5</sup> To date, about 72 billion metric tonnes (Gt) of materials are been consumed by humanity per annum and this number is projected to reach 100 Gt by 2030.<sup>6</sup> Industrialised economies are energy- and raw material-intensive, and heavily dependent upon non-renewable fossil fuels, such as oil, to meet their societal energy, chemicals and material needs. The International Energy Agency (IEA) announced that the demand for oil will continuously increase from 90 million barrels per day in 2013 to 104 million barrels per day in 2040 due to increased use for transport and petrochemicals, although the pace of overall consumption is gradually constrained by price fluctuations and new policies.<sup>7</sup> However, continued reliance on fossils fuels is unsustainable because it is not an infinite resource, but limited, and its continual burning represents a major environmental concern. In 2015, McGlade and Ekins reported if we are to limit global warming to no more than 2 °C by 2020 then over 80% of coal, 50% of gas and 30% of oil reserve are un-burnable, thus putting more pressure on alternative feedstocks.<sup>8</sup> To this effect, global governments are realizing the importance of transitioning from a petro- to a biorenewable-based economy enabling an environmentally-friendly, sustainable, future 21<sup>st</sup> century.<sup>9 - 16</sup>

### **1.3 (Bio)Waste: a growing problem, but also a growing opportunity**

Our current society is suffering from worldwide escalating waste problems, which is becoming increasingly important and alarming in less developed and developing countries such as the five BRICS nations (*i.e.*, Brazil, Russia, India, China and South Africa), as well as in developed countries.<sup>17 - 20</sup> The World Bank estimates that at least 1.3 billion tonnes (Gt) of municipal solid waste is currently generated by world cities per year and this is expected to increase to 2.2 Gt by 2025, representing an increase of solid waste management cost from today's annual \$205.4 billion to around \$375.5 billion in 2025.<sup>21</sup> Based on their origin, different types of wastes mainly includes industrial, agricultural, sanitary and solid urban residues.<sup>22</sup> According to the World Bank, the solid urban residues mainly include organic waste (46%), paper and cardboard (17%), plastics (10%), glass (5%), metal (4%) and others (18%).<sup>21</sup> There is an urgent need to

recover value from (valorise) these “wastes” rather than commit it to landfill and/or other disposal methods (*e.g.*, burning with energy recovery, composting, anaerobic digestion).<sup>22, 23</sup> The twin problem faced by modern society (*i.e.* increasing dependence on non-renewable fossil resources, escalating waste problems) could be solved by employing these wastes as valuable raw materials for biorefineries for the generation of high-value products.<sup>24 – 26</sup> Processes using renewable feedstocks are often closer to being carbon neutral than those using conventional petrochemical routes.<sup>23, 25, 27</sup> Making use of renewable raw materials may also strengthen the current agricultural and forest industry, by increasing their efficiency, capability and profitability.<sup>25, 28</sup> In addition, it is even better to use (large volume) biorenewable waste streams and/or unavoidable losses as feedstocks for the generation of value-added useful products.<sup>22 - 25</sup>

(Bio)waste as a resource has been recognised to be of national importance by the UK Government following their 2015 report, “Building a high value bioeconomy - Opportunities from Waste”<sup>29</sup> as a result of the House of Lords Science and Technology Committee report, “Waste or resource? Stimulating a Bioeconomy”<sup>30</sup> published a year earlier, both evoking the need for a UK bioeconomy for future sustainable development. The reports highlight a significant market for renewable chemicals, already estimated at \$57 billion worldwide and forecast to rise to \$83 billion by 2018.<sup>29, 30</sup> Similarly, the United States Department of Agriculture (USDA) report on the potential for bio-based products indicates 10% chemical market penetration by 2015 with ultimately 50,000 eco-products, representing a global market value of \$1 trillion and the creation of over 200,000 jobs in the US alone.<sup>31</sup> Small and medium enterprises (SME’s) are an important driver for new growth as the EU bioeconomy (not restricted to waste feedstocks) has a turnover of about €2 trillion, employs around 22 million people, mainly in rural areas and often SME’s, and represents 9% of total employment in the EU. Each euro invested in EU-funded bioeconomy research and innovation is estimated to enable €10 of value added in bioeconomy sectors by 2025.<sup>10</sup>

EU policy makers encourage the diversion of biodegradable waste streams away from the totally wasteful and polluting landfill sites. For example, it is required in the Landfill directive 99/31/EC that the amount of biodegradable waste must be reduced 65% by weight against

1995's level by 2016 with intermediate reduction targets.<sup>32</sup> This is also reflected in the recently revised Waste Framework Directive 2008/98/EC (the rWFD), which introduced the revised "waste hierarchy" (Figure 2).<sup>33</sup> The waste hierarchy places priority on waste prevention and the lowest priority on disposing to landfill (the worst option). Among the intermediate waste management choices, re-use and recycling of biodegradable waste (*e.g.*, for the generation of high-value chemicals, fuels and useful materials) is preferred in comparison with energy recovery (*i.e.* incineration, anaerobic digestion *etc.*).<sup>32 - 34</sup> As a result, the costs for waste disposal in landfills have been significantly increased. For instance, the landfill gates fees continuously increased from £40 – 74 to £80 – 121 plus the landfill tax between 2009 and 2013 in the UK.<sup>35</sup>

Hence, making innovative use of currently low-value, underutilised biorenewable waste streams, especially unavoidable losses resulted from industrial practices (*e.g.*, manufacturing, recycling) for the production of bio-derived chemicals, fuels, and other value-added functional materials is particularly important and attractive. Such waste valorisation practices also represent an imperative grand research challenge and a promising topic globally from both an environmental and economic point of view.<sup>36</sup>

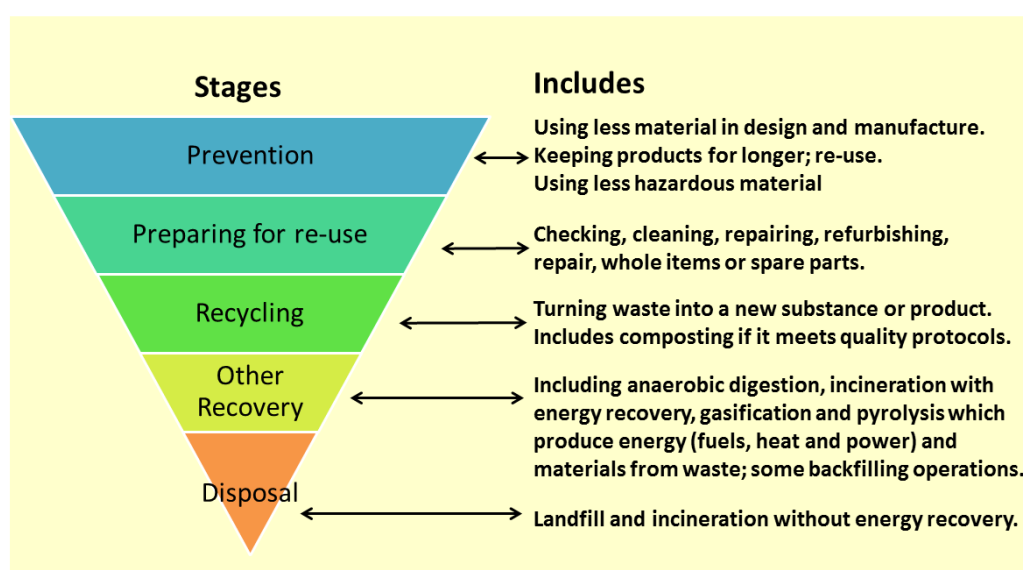


**Figure 2:** Illustration of the current version of waste hierarchy, reproduced from reference 34.  
(Originally in colour)

## 1.4 Lignocellulosic biomass

In the scope of this thesis waste wood, paper and starch are considered as feedstocks and thus this section briefly overviews the chemistry of lignocellulosic biomass comprising lignin, cellulose and hemicellulose and starch-based biomass. For a detailed account the reader is directed to references 37 – 42.

Lignocellulosic biomass (wood and other plant biomass) comprises the bulk of the dry weight of both woody and grassy plant materials, hence it is one of the most abundant naturally occurring biochemicals on the planet and the industrial yield of lignocellulose is expected to be higher than that of starch.<sup>43</sup> Major sources of lignocellulose include so-called “energy crops” (*e.g.*, switchgrass, willow, poplar *etc.*) and agricultural and forestry industrial by-products (*e.g.*, corn stover, wheat and rice straw, wood waste, waste paper *etc.*).<sup>43</sup> Globally, around  $200 \times 10^9$  tonnes of biomass are produced each year, of which over 90% is lignocellulosic matter. Among these, around  $8 - 20 \times 10^9$  tonnes end up as wastes, representing an attractive feedstock for biorefineries, especially in so-called future integrated forestry biorefineries.<sup>42, 44</sup>

Lignocellulose is essentially a composite material constructed primarily from three oxygen-containing high-molar-mass organic polymers, namely cellulose, hemicellulose and lignin, as well as minor amounts of low-molar-mass extraneous materials: mainly organic extractives (*e.g.*, terpenes and oils) and inorganic minerals.<sup>45–47</sup> The weight percentage of each component varies and depends on the wood/plant species, but in general, typical wood biomass contains 35 – 50% cellulose, 25 – 30% hemicellulose, 15 – 30% lignin and 5 – 10% organic extractives and inorganic minerals.<sup>45, 46</sup> Figure 3 illustrates the general constituents of wood biomass and Table 1 summarizes the cellulose, hemicellulose and lignin content of several selected plant resources and biorenewable waste materials.

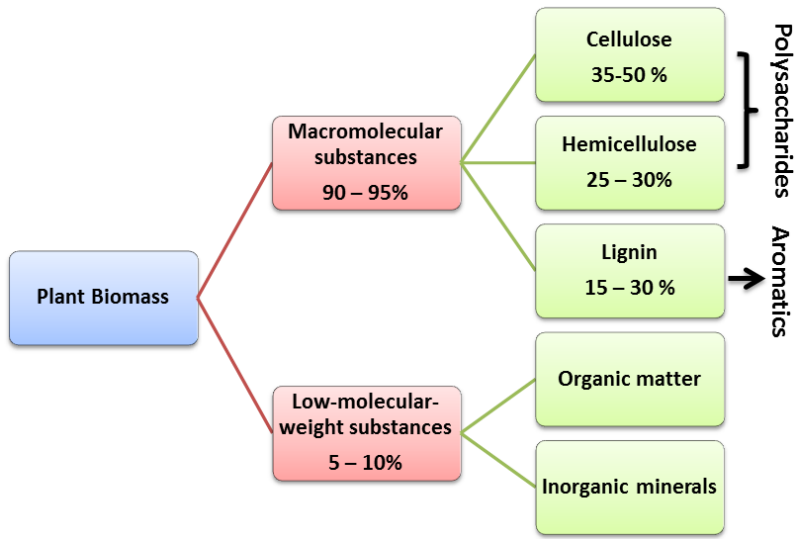


**Figure 3:** General constituents in plant/wood biomass, adapted from reference 45 and 46.  
(Originally in colour)

**Table 1:** Typical cellulose, hemicellulose and lignin contents of several selected plant resources and biorenewable waste materials<sup>48-51</sup>

Material	Cellulose (%)	Hemicellulose (%)	Lignin (%)
Wood	35 – 50	20 – 30	25 - 30
Wheat straw	33 – 40	20 – 25	15 – 20
Switch grass	30 – 50	10 – 40	5 – 20
Sugarcane bagasse	19 – 24	32 – 48	23 – 32
Spruce wood	50.8	21.2	27.5
Corn stove	28	35	16 – 21
Waste paper	60 – 70	10 - 20	5 – 10
Rice straw	32	24	18
Pine	46	23	28

The thermal behaviour of certain biomass is strongly dependent on its chemical composition and structure, and the thermal decomposition (thermolysis) generally occurs within temperature ranges from 200 °C to 400 °C.<sup>52</sup> Indeed, the thermal behaviour of cellulose rich biomass tends to be more similar with that of pure cellulose; while lignin rich biomass behaves more similarly to

lignin itself.<sup>52, 53</sup> Thus, a better understanding of these three major biomass constituents is vital to achieve optimisation of process conditions and product distributions, and improved efficiency for biomass processing.<sup>54</sup>

### 1.4.1 Cellulose

Cellulose is a high-molecular-weight linear polysaccharide polymer consisting of anhydroglucose units connected via  $\beta$ -(1 $\rightarrow$ 4)-glycosidic bonds in a fully equatorial  $^4C_1$  conformation, which stabilises the chair structure and facilitates the formation of well extended linear structures.<sup>45, 55</sup> As the  $\beta$ -(1 $\rightarrow$ 4)-glycosidic bonds cause alternate glucose rings to be rotated by 180°, the basic repeating unit of cellulose polymers contains two glucose anhydride units (*i.e.* a cellobiose unit).<sup>45</sup> The chemical structure of cellulose is illustrated in Figure 4.

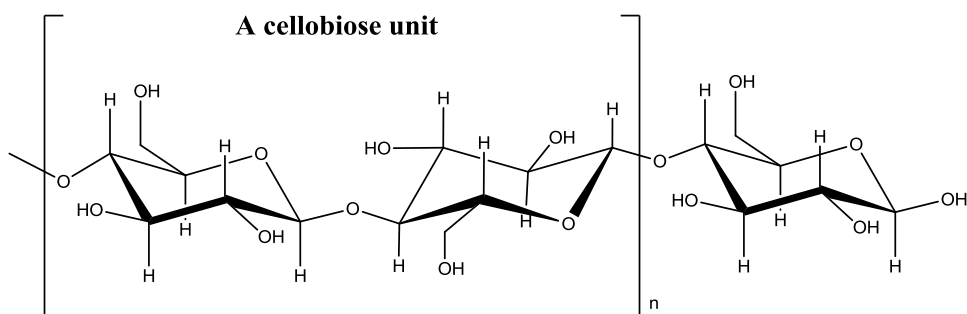


**Figure 4:** Chemical structure of cellulose

Both the two hydroxyl groups (OH-2, 3) on C-2, 3 and the hydroxymethyl group (C6-OH) on C5 adopt the equatorial conformation, which leads to the equatorial hydrophilic and axial lipophilic nature of cellulose.<sup>56</sup> The abundant hydroxyl groups (OH-2, 3, 6) within cellulose form an extensive network of intra- and intermolecular hydrogen bonds, which hold the network flat, give rise to the crystallinity of cellulose, and consequently, render cellulose completely insoluble in aqueous solutions and resistant to swelling in water.<sup>45, 57</sup> However, cellulose is soluble in near supercritical water, aqueous solutions of zinc chloride, and some ionic liquids for example.<sup>45, 58</sup> Thus, owing to its rigid structure, it is not an easy process to degrade and/or convert cellulose. Indeed, efficient degradation/conversion of cellulose depends on several

factors associated with the origin of cellulose, such as crystallinity index (CrI), degree of polymerisation (DP), and the fraction of reducing ends ( $F_{RE}$ ).<sup>58</sup>

Any occasional faults in the order of anhydroglucose units within cellulose chains leads to the formation of amorphous regions, which are more susceptible to chemical conversions, such as hydrolysis and are probably the association points with hemicelluloses in biomass.<sup>58, 59</sup> Taking advantage of this property, several pre-treatment approaches were developed to convert the rigid crystalline cellulose to more “accessible” amorphous cellulose. According to Dhepe and Fukuoka, such pre-treatment methods mainly include physical approaches such as milling, grinding, steaming *etc.* and chemical approaches such as alkali/acid pre-treatment, dissolution, swelling and oxidation.<sup>58</sup> These approaches should and could be incorporated with any microwave-assisted conversion processes in a biorefinery to obtain desired, or optimised, product distribution, if necessary.

#### **1.4.2 Hemicellulose**

Unlike cellulose, which only contains glucose in its structure, hemicellulose has a heteropolysaccharide makeup and is a branched polymer consisting of various polymerised monosaccharides.<sup>60</sup> Major constituent monosaccharides include C5 sugars (pentoses) such as xylose, arabinose, and C6 sugars (hexoses) such as mannose, glucose and galactose, as well as some uronic acids (*e.g.*, glucuronic acid), as shown in Figure 5.<sup>45, 60</sup> The ratio of these constituent monomers varies dramatically depending on the origins of biomass.<sup>45, 60</sup> Hemicellulose has lower molecular weights than cellulose with only around 150 repeating monosaccharide units compared to that of repeating glucose units in cellulose (5000 – 10000).<sup>45</sup> Hemicellulose surrounds/interacts with cellulose through hydrogen bonding and acts as a linkage between cellulose and lignin.<sup>60, 61</sup> Also different from cellulose, hemicellulose is mainly amorphous due to its random polymerised nature and the presence of side chains, which prevents the formation of ordered rigid crystalline structures and renders it much more susceptible/reactive and less stable than cellulose.<sup>43, 59, 62</sup>

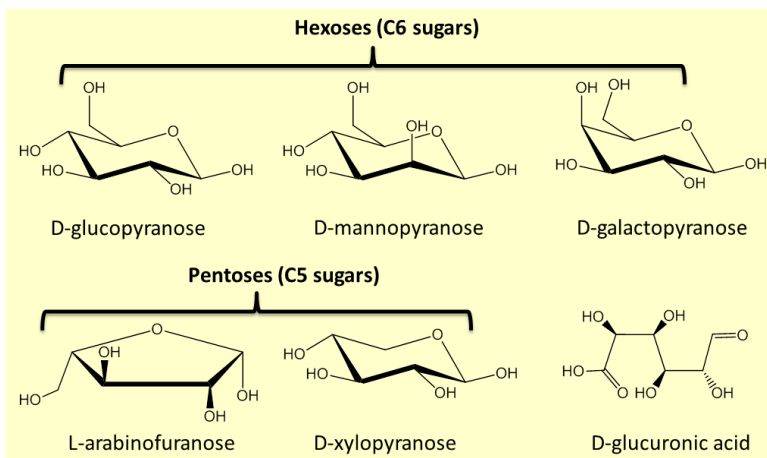


**Figure 5:** Major constituent monosaccharides of hemicellulose. (Originally in colour)

### 1.4.3 Lignin

Lignin is Nature's dominant aromatic polymer and the only large-volume renewable material composed of aromatic molecules, which also currently represents the most underutilised fraction of lignocellulosic biomass.<sup>63, 64</sup> More specifically, lignin is a highly complex cross-linked three-dimensional amorphous resin that surrounds the outer layers of polysaccharide fibers, protecting the inside cellulosic fibers from microbial and/or fungal destruction while providing structural integrity and rigidity.<sup>65–67</sup> Lignin is a complex, highly branched and recalcitrant polyphenolic macromolecule substance consisting of a wide irregular variety of “hydroxyl” and “methoxy-” substituted phenylpropane type units.<sup>68, 69</sup> Despite the pathway for biosynthesis of lignin still remains uncertain, typically, three monolignol (monomer units of lignin) building blocks are present in lignin, namely *p*-coumaryl alcohol, coniferyl alcohol and sinapyl alcohol, as shown in Figure 6.<sup>63, 64</sup> These monolignols further generates corresponding phenyl propanoids: *p*-hydroxyphenyl (H), guaiacyl (G) and syringyl (S) lignin subunits, in which forms they are incorporated into lignin macromolecules.<sup>63, 64</sup>

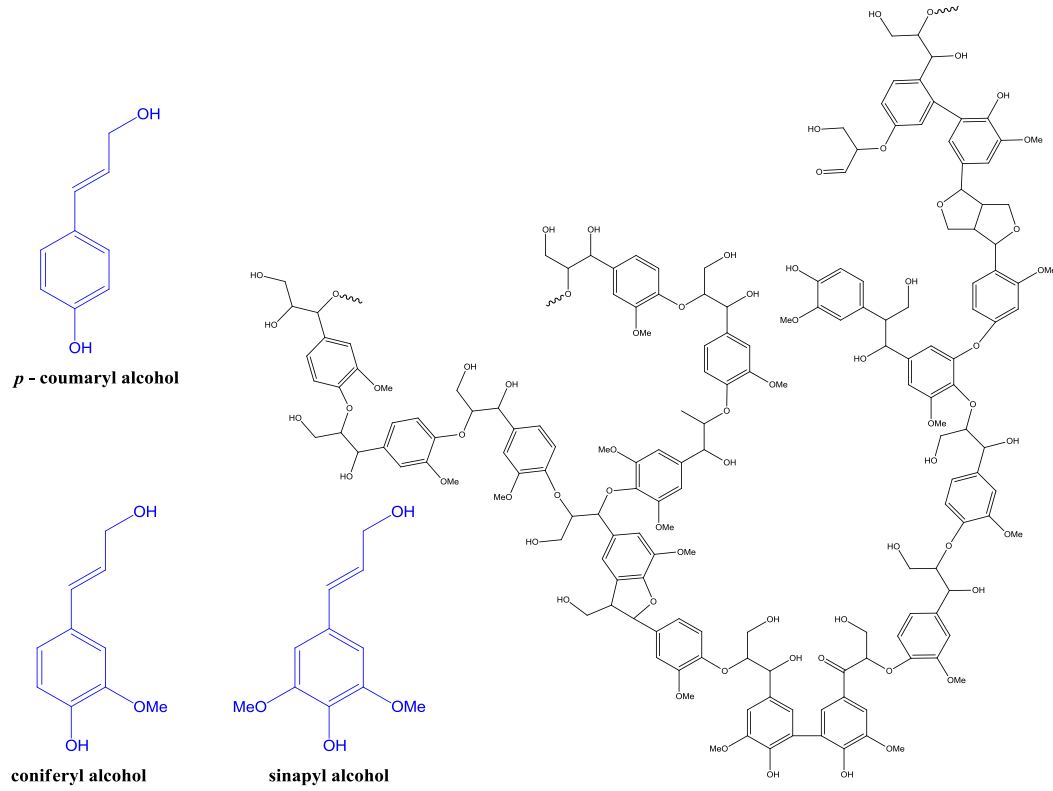


**Figure 6:** Chemical structures of the three lignin building blocks and representative fragment of the structure of lignin, adapted from reference 70. (Originally in colour)

#### 1.4.4 Starch-based biomass

Starch is one of the most abundant natural polysaccharides. It is a carbohydrate source used for energy storage in plants and is generally stored in the form of granules.<sup>71</sup>

Around 2.5 billion tonnes of starch is produced by crop plants globally per year.<sup>72</sup> Taking advantage of genetic engineering of crop plants, the starch (especially rice) grain production in China is expected to increase to around 540 million tonnes by 2020, doubling the current quantity of starch being generated in China.<sup>72, 73</sup> In Europe, around 9.4 million tonnes of starch was produced in 2008. Among these, about 8.7 million tonnes of starch and its derivatives were consumed for both food and non-food (around 39%) applications.<sup>72</sup> Therefore, it can be estimated that significant amounts of starch are currently being underutilised and wasted. Hence, it is necessary to explore alternative valorisation routes for starch.<sup>74</sup>

Chemically, the compositions of starches vary according to their botanical origins, such as the origin and type of plant. The origin of starch not only influences starch composition, structure and properties, but also affects the form, shape and functionality of starch.<sup>75</sup> In general, starch granules are composed of two types of  $\alpha$  - glucans (*i.e.* amylose and amylopectin) which account for approximate 98 – 99% of dry weight with small amounts of lipids, free fatty acids, protein and relatively small quantities (<0.4%) inorganic minerals.<sup>75</sup> The ratio of these two types of polymers in starch significantly affects and determines some of its key properties, such as gelatinization temperature, gelling rate, viscosity and the strength of film formed.<sup>76</sup>

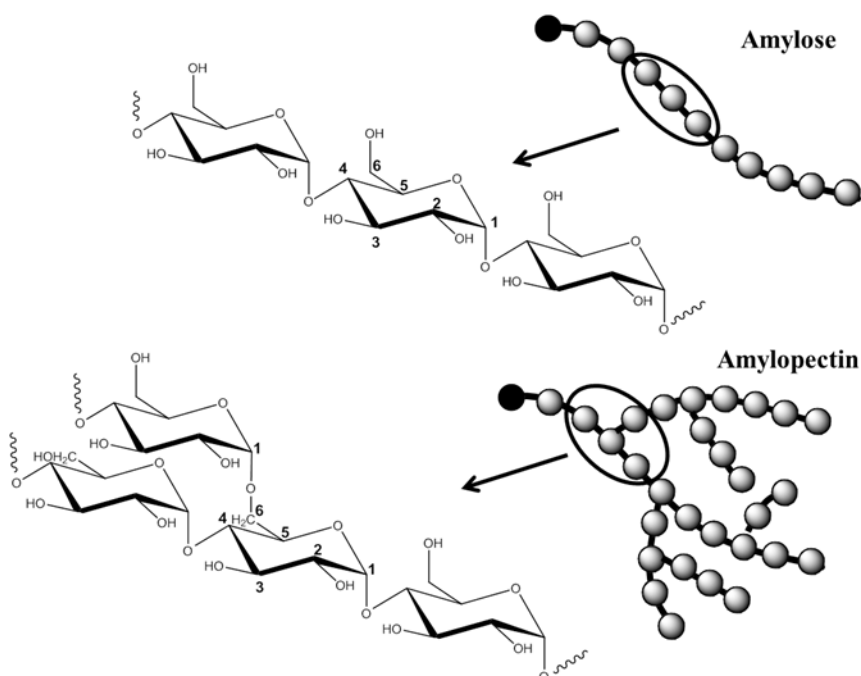


**Figure 7:** Chemical structures of amylose and amylopectin. (Originally in colour)

Amylose is a linear polymer consisting (around 99%) of unbranched ( $1\rightarrow 4$ ) linked  $\alpha$  - glucan. On the contrary, amylopectin has chains of ( $1\rightarrow 4$ ) linked  $\alpha$  – glucoses arranged in a highly branched structure with  $\alpha$  – ( $1\rightarrow 6$ ) branching links.<sup>75, 77</sup> The chemical structures of amylose and amylopectin are illustrated in Figure 7. The molecular weight of amylose is generally in the range of  $10^5$  –  $10^6$  Da (when the degree of polymerization is between 1000 – 10,000 glucose units) while amylopectin is a much larger polymer than amylose, with a molecular weight around  $10^8$  Da.<sup>75, 77</sup> The amylose contents of starches vary according to their botanical origins. Normally, maize starches contain approximately 25% amylose and 75% amylopectin.

## **1.5 Green Chemistry and Green Chemical Engineering and the Biorefinery Concept**

In order to aid sustainable development *via* a bio-based economy that utilises waste as a resource, the principles and practices of green chemistry, green chemical engineering and the biorefinery concept need to be considered.

### **1.5.1 Green Chemistry and Green Chemical Engineering**

Green Chemistry is both a philosophy and a methodology in the pursuit of sustainability. In the 1990s, Anastas and Warner at the US Environmental Protection Agency (EPA) first described green chemistry as “the utilisation of a set of principles that reduces or eliminates the use or generation of hazardous substances in the design, manufacture, and application of chemical products”, with the introduction of twelve principles of green chemistry (Table 2).<sup>78</sup> During the past 20 years, with a globally rising awareness and concerns over the fast depleting fossil fuel reserves and pollution associated with wasteful processes, as well as promoted by tougher legislations and regulations, the development of green chemistry quickly gained momentum, which has led to and nurtured the now well-recognized clean technologies (*i.e.*, green chemical technologies).<sup>79</sup> In the pursuit of sustainability at the molecular, product, process and system levels and to achieve the goals outlined by the 12 principles of green chemistry, innovations in the development of new low-environmental-impact technologies and in the evaluation and improvement of existing chemical processes are required. In 2003, a set of 12 principles of green chemical engineering were subsequently proposed by Anastas and Zimmerman (Table 3),<sup>80</sup> which together with the 12 principles of green chemistry, provide a framework for designing new products (*e.g.*, chemicals, materials, energy *etc.*), processes and systems, maximising efficiency and sustainability while minimising negative environmental impacts.<sup>80, 81</sup> According to the Pike research report on Green Chemistry, adoption of green chemistry principles and practices, in particular making use of renewable raw materials, will save the current chemical industry \$65 billion by 2020, and create a bio-based market worth about \$98.5 billion from its current value (2013) of approximately \$3 billion.<sup>82</sup>

**Table 2:** The twelve principles of green chemistry.<sup>78</sup>

---

## 1. Prevention

*It is better to prevent waste than to treat or clean up waste after it is formed.*

## 2. Atom economy

*Synthetic methods should be designed to maximise the incorporation of all materials used in the process into the final product.*

## 3. Less hazardous chemical syntheses

*Wherever practicable, synthetic methodologies should be designed to use and generate substances that possess little or no toxicity to human health and the environment.*

## 4. Designing safer chemicals

*Chemical products should be designed to preserve efficacy of function while reducing toxicity.*

## 5. Safer solvents and auxiliaries

*The use of auxiliary substances (e.g. solvents, separation agents, etc.) should be made unnecessary wherever possible and, innocuous when used.*

## 6. Design for energy efficiency

*Energy requirements should be recognised for their environmental and economic impacts and should be minimised. Synthetic methods should be conducted at ambient temperature and pressure.*

## 7. Use of renewable feedstocks

*A raw material of feedstock should be renewable rather than depleting wherever technically and economically practicable.*

## 8. Reduce derivatives

*Unnecessary derivatisation (blocking group, protection/deprotection, temporary modification of physical/chemical processes) should be avoided whenever possible.*

## 9. Catalysis

*Catalytic reagents (as selective as possible) are superior to stoichiometric reagents.*

## 10. Design for degradation

*Chemical products should be designed so that at the end of their function they do not persist in the environment and break down into innocuous degradation products.*

## **11. Real-time analysis for pollution prevention**

*Analytical methodologies need to be further developed to allow for real-time, in-process monitoring and control prior to the formation of hazardous substances.*

## **12. Inherently safer chemistry for accident prevention**

*Substances and the form of a substance used in a chemical process should be chosen so as to minimise the potential for chemical accidents, including releases, explosions, and fires.*

---

**Table 3:** The twelve principles of green chemical engineering.<sup>80</sup>

---

### **1. Inherent rather than circumstantial**

*Designers need to strive to ensure that all materials and energy inputs and outputs are as inherently non-hazardous as possible.*

### **2. Prevention instead of treatment**

*It is better to prevent waste than to treat or clean up waste after it is formed.*

### **3. Design for separation**

*Separation and purification operations should be designed to minimise energy consumption and materials use.*

### **4. Maximise efficiency**

*Products, processes, and systems should be designed to maximise mass, energy, space and time efficiency.*

### **5. Output-pulled versus input-pushed**

*Products, processes, and systems should be “output pulled” rather than “input pushed” through the use of energy and materials.*

### **6. Conserve complexity**

*Embedded entropy and complexity must be viewed as an investment when making design choices on recycle, reuse, or beneficial disposition.*

### **7. Durability rather than immortality**

*Targeted durability, not immortality, should be a design goal.*

## **8. Meet need, minimise excess**

*Design for unnecessary capacity or capability (e.g., “one size fits all”) solutions should be considered a design flaw.*

## **9. Minimise material diversity**

*Material diversity in multicomponent products should be minimised to promote disassembly and value retention.*

## **10. Integrate material and energy flows**

*Design of products, processes, and systems must include integration and interconnectivity with available energy and materials flows.*

## **11. Design for commercial “afterlife”**

*Products, processes, and systems should be designed for performance in a commercial “afterlife”.*

## **12. Renewable rather than depleting**

*Material and energy inputs should be renewable rather than depleting.*

---

On examining the twelve fundamental principles of green chemistry as well as those of green chemical engineering, the use of renewable (bio-derived) resources instead of non-renewable diminishing fossil fuel reserves as feedstock raw material adheres to some of the above outlined principles, *i.e.* principle 7 of the 12 principles of green chemistry (*A raw material or feedstock should be renewable rather than depleting wherever technically and economically practicable*), and principle 12 of the 12 principles of green chemical engineering (*Material and energy inputs should be renewable rather than depleting*). The incorporation of renewable raw materials, especially biorenewable waste streams, into innovative chemical processes for the production of a diverse range of new products leads to the creation of a new paradigm: the biorefinery concept.

## 1.5.2 The Biorefinery concept

Essentially analogous to the well-established oil-based refineries, a biorefinery makes use of low-value (waste) biomass materials as major feedstocks, and converts them into a diverse array of industrially useful intermediates and final marketable products (Figure 8).<sup>83</sup> These intermediates and final products have the potential to replace their petroleum-derived analogues.<sup>83</sup> More specifically, the International Energy Agency (IEA) Bioenergy Task 42 defined biorefining as “*the sustainable processing of biomass into a spectrum of bio-based products such as food, feed, chemicals, materials and bioenergy such as biofuels, power and heat*”.<sup>84</sup> According to the National Renewable Energy Laboratory (NREL), the term biorefinery refers to “*a facility that integrates biomass conversion processes and equipment to produce fuels, power, and chemicals from biomass*”.<sup>85</sup>

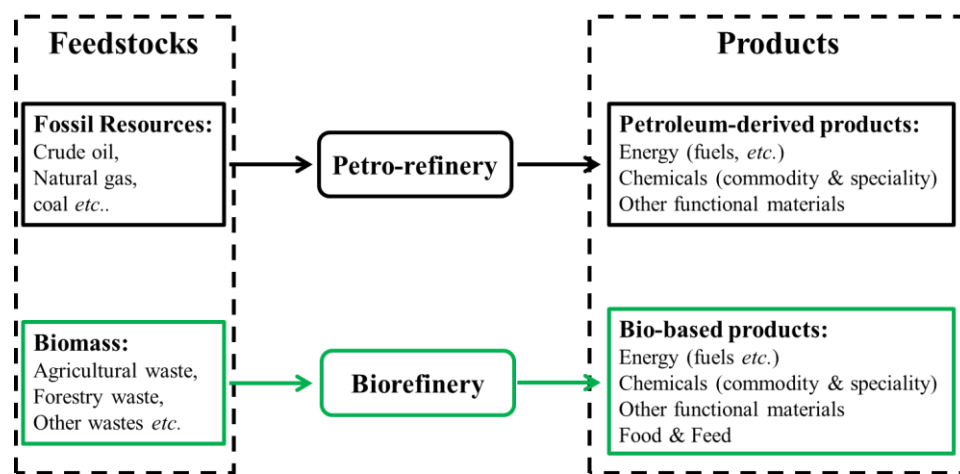


**Figure 8:** Comparison of petro-refinery and biorefinery, adapted from reference 83. (Originally in colour)

Future sophisticated biorefineries should be capable of producing low-value, high-volume products such as fuels mainly including biodiesel and bioethanol, commodity products and generating high-value low-volume speciality chemicals and materials.<sup>83, 86</sup> The core idea should be maximise the value of products, while minimising and/or eliminating waste streams.<sup>83, 86</sup>

As described by Fernando *et al.*,<sup>86</sup> Kamm and Kamm,<sup>87</sup> Van Dyne *et al.*,<sup>88</sup> and Clark and Deswarte,<sup>83</sup> three types of biorefineries are reported in the literature, namely phase I, II and III biorefineries. Figure 9 demonstrates the three types of biorefineries.

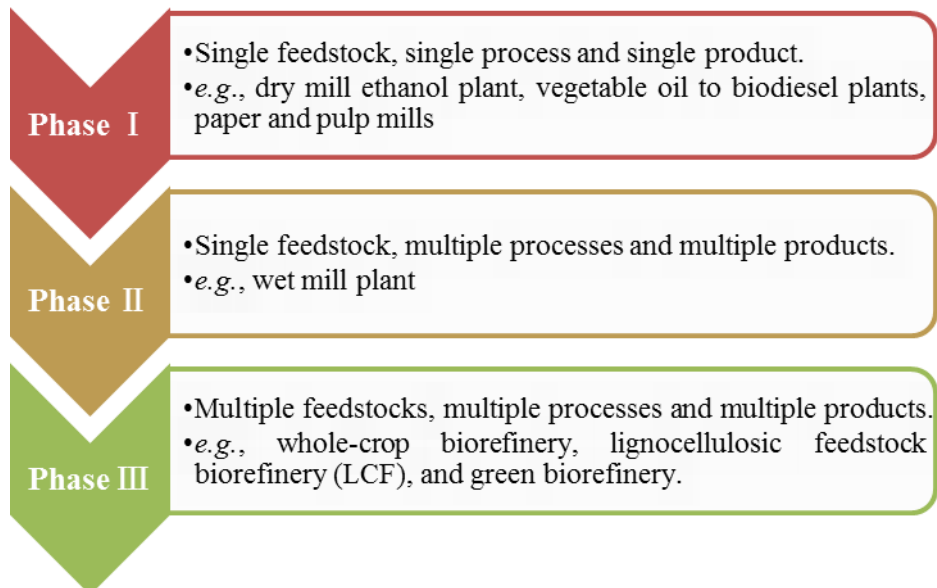


**Figure 9:** The three types of Biorefineries.<sup>86 - 88</sup> (Originally in colour)

A phase III biorefinery is much more advanced and sophisticated, in which various feedstock materials could be converted to a much more diverse range of energy, chemicals and materials employing various (combined) technologies.<sup>86 - 88</sup> The multi-input, multi-technique and multi-output nature of phase III biorefineries provides them much more flexibility in terms of responding to changing market demands and feedstock supply chains, and maximising profitability. Hence, phase III biorefineries represent the most favoured type of biorefinery in research and design.<sup>86 - 88</sup>

Traditionally, industrial investment and research effort has been mainly devoted to biofuels production (e.g., bio-diesel, bioethanol) to substitute a fraction of petroleum derived fuels. With rapid cost reductions and continued financial support (e.g., the global subsidies for developing renewable energy technologies amounted to \$120 billion in 2013), the use of biofuels is expected to triple to 4.6 million barrels per day in 2040, and almost half of the increase in total electricity generation to 2040 will be based on renewables including wind power (34%),

hydropower (30%) and solar technologies (18%).<sup>7</sup> However, global fossil-fuel subsidies were still four-times more than for renewables, reaching \$550 billion in the same year.<sup>7</sup> This renders it even less effective and profitable for biofuel production alone. It has been gradually realized that the production of high-value chemicals, and other functional materials in addition to biofuels production, could generate more value than current biofuel production processes. For example, the production of chemicals and polymer resins from waste biomass could create two to four times more added value and six to eight times more employment, while requiring less percentage of feedstocks compared with biofuel production.<sup>89</sup>

Constantly feedstock supply will be one of the major problems and challenges faced by a biorefinery.<sup>83, 86</sup> Unlike fossil resources, geographically, biomass is widely distributed. Moreover, the cost for transportation of biomass will be high, due to the low bulk density and high water content of biomass. Densification of biomass is thus crucial for developing future biorefinery infrastructures capable of processing biomass raw material with substantial quantities, while reducing operation costs.<sup>83, 86</sup> The perishable character and the susceptibility to degradation of biomass, especially fresh biomass, represent another important issue that needs to be taken into consideration. In addition, again unlike fossil resources, the availability of biomass is seasonal. To overcome these problems, biomass may need to be stabilised prior to long-term storage. In developing future biorefineries, fundamental logistics of a consistent, orderly flow of biomass raw materials is of great importance in order to achieve the economic success.<sup>83, 86, 87, 88</sup>

In the scope of this thesis the opportunities and challenges in terms of developing future biorefineries will not be discussed further and the reader is directed to references 90, 91 and 92 for a fuller account.

## 1.6 Thermochemical conversion techniques

Current research and practices on valorisation of waste lignocellulosic biomass are primarily based on two platforms: the biochemical platform and thermochemical platform.<sup>85, 93</sup> Each of

these two types of conversion approaches has its own advantages and drawbacks. Biochemical conversion of waste biomass is generally through the use of biological microorganisms, such as enzymes, to degrade complex wastes and produce fuel. The biochemical conversion processes are selective and conducted at low temperatures. However, this approach tends to be slow and requires batch-wise manufacturing processes.<sup>93, 94</sup>

Thermochemical conversion technologies provide important economic and environmental options for waste valorisation by converting wastes into industrially useful and value-added materials, fuels and chemicals.<sup>93, 95</sup> Such processes tend to be relatively quick and could be continuously conducted. Compared with biochemical routes, thermochemical methods could essentially convert all the organic components of biomass, hence fully capitalizing on its chemical and fuel potential. However, these processes are generally operated at high temperatures, resulting in a complex mixture of processes and products with uncontrollable properties.<sup>93, 94</sup> This section provides an overview of general thermochemical approaches for waste valorisation with particular emphasis on pyrolysis.

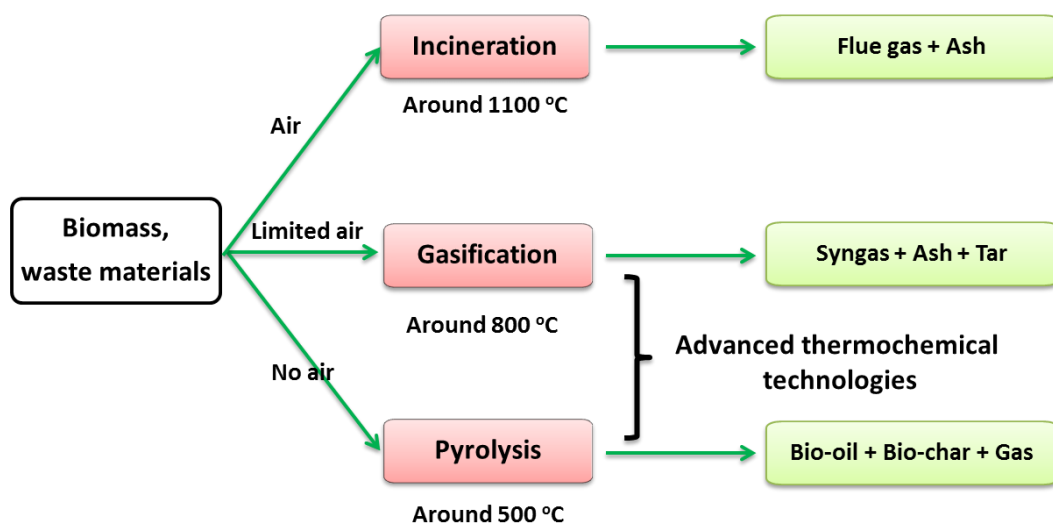


**Figure 10:** An overview of thermochemical technologies for conversion of biomass and waste materials, adapted from reference 95. (Originally in colour)

Advanced thermochemical conversion processes employ a wide range of thermal decomposition techniques such as gasification, pyrolysis, and/or combined pyrolysis and gasification, decomposing waste materials into smaller molecules that can be used as energy sources or feedstocks for the synthesis of new products.<sup>93, 95</sup> Traditionally, thermochemical conversion processes are broadly divided into three categories: incineration, gasification, and pyrolysis, depending on the amount of oxygen supplied to thermal reactors.<sup>95</sup> The major operational differences between incineration, gasification, and pyrolysis are demonstrated in Figure 10.

### **1.6.1 Incineration**

Incineration is commonly employed to recover energy value of waste materials. In an excess supply of oxygen, this approach involves complete oxidation of wastes to produce energy in the form of electricity and/or heat, yielding carbon dioxide, water, ash and some other products (*e.g.*, metals, trace hydrocarbons, acid gases).<sup>95</sup> However, only the energy content of waste materials could be recovered through incineration. Global concerns over greenhouse gas (GHG) emissions and environmental pollution associated with the toxic emissions render this method increasingly impractical.

The focus of research and industrial practices are shifting towards more advanced thermochemical processing of wastes in a more efficient, environmental benign and economic manner. Gasification and pyrolysis are two important approaches to convert wastes into value-added products, and hold great potential to recover both energy and chemical value of waste materials.<sup>95</sup>

### **1.6.2 Gasification**

Gasification is a high-temperature thermochemical process that converts waste materials into a flammable gas mixture (*i.e.* so called syngas) rich in CO, CO<sub>2</sub>, CH<sub>4</sub> and H<sub>2</sub>, ash and a tar product.<sup>95, 96</sup> This process involves partial oxidation of wastes in the presence of limited, sub-stoichiometric amounts of oxygen in air, steam, CO<sub>2</sub> or pure oxygen, at high temperatures generally above 800 °C.<sup>95, 96</sup> The combustible syngas could be used as a fuel directly to generate heat and electricity. It could also be converted into liquid fuel and chemicals through

post-reaction processing, such as the Fischer–Tropsch process.<sup>95, 97</sup> In recent years, the focus of application of gasification has shifted from production of heat and/or electricity to generation of other high-value products, such as chemicals and liquid transportation fuel.<sup>96, 97</sup> Several technical and economic challenges still remain to be addressed. For instance, the process is energy-intensive and usually requires a capital intensive plant capable of operating on a large scale. Thus the overall energy efficiency of the process should be increased to address the required significant energy-input. Also, robust and efficient technologies for cleaning of the syngas and upgrading of gasification products to valuable chemicals and fuels should be further developed and improved.<sup>95 - 97</sup>

### **1.6.3 Pyrolysis**

Pyrolysis is considered to be a promising method for converting biomass into value-added products and aims to obtain bio-char, gas, and a liquid product (bio-oil) through thermal decomposition of waste biomass in the absence of oxygen. The pyrolysis process is potentially capable of recovering both the energy and chemical value of waste biomass. There are several comprehensive reviews existing in the literature on pyrolysis of biomass/waste material for generation of value-added chemicals, fuels, materials and upgrading methods for pyrolysis products.<sup>98 – 102</sup>

Importantly, the pyrolysis process is versatile and can be manipulated to capture all the components and maximise the output of the desired products, by altering operational parameters such as heating rate, maximum processing temperature and residence time.<sup>95, 102</sup> In accordance with operating conditions, pyrolysis processes are typically divided into three types: slow pyrolysis, fast pyrolysis and flash pyrolysis, although these terms are sometimes arbitrary and are not very precise.<sup>95, 102</sup> Slow pyrolysis has historically been employed for many years to enhance charcoal generation at low-temperature (typically between 300 °C and 500 °C) with a long vapour-residence time ranging from hours to days. Nowadays, in most cases the term pyrolysis refers to fast and/or flash pyrolysis in which smaller molecules (such as bio-oil and gas) are preferred products. The bio-oil and gas products generated from fast and/or flash pyrolysis are more versatile and potentially of higher value.<sup>95, 102</sup> Since fast and/or flash

pyrolysis are capable of processing a wide range of feedstocks (*e.g.*, lignocellulosic biomass, waste plastics, waste tyres), they are considered to be promising alternative approaches for waste valorisation.<sup>98, 99, 102</sup> Fast pyrolysis usually heats the biomass at high heating rates of about 100 °C s<sup>-1</sup> to the relatively moderate temperatures of about 500 °C to 700 °C. The short residence times of hot vapour (around 1 second) in the reaction zone and rapid quenching lead to the production of a mainly liquid product over gas and char. It is reported that liquid product yields could be up to 75% based on the starting dry biomass weight could be achieved in some fast and/or flash pyrolysis reactions.<sup>98, 102</sup> The product distributions vary significantly with pyrolysis processing conditions. For instance, by increasing hot vapour residence time to 10 – 20 s, the liquid yield may drop to around 50%, while the yield of gas and char may increase to 30% and 20% on average.<sup>99, 100, 102</sup>

The liquid product formed by condensation of hot vapour is pyrolysis bio-oil, sometimes known as bio-crude or pyrolysis oil. In general, bio-oil is a dark brown liquid.<sup>98, 100</sup> The composition and properties of bio-oil vary significantly, depending on feedstocks and processing conditions such as pyrolysis reactors, heating rates, pyrolysis temperatures, residence times, collection methods. The bio-oil generated from lignocellulosic wastes contains a complex mixture of oxygenated compounds as a result of degrading of cellulose, hemicellulose and lignin. Hence, bio-oils contain a wide range of chemical compounds such as carbonyl compounds, carboxylic compounds, phenolic compounds, oligosaccharides and anhydrosugars.<sup>98 - 102</sup> Bio-oils also contain water, and the quantity of water depends on the feedstock and pyrolysis conditions ranging from 15 – 50 wt.%.<sup>95, 98</sup> One advantage of converting waste matter into an oil product is that the bio-oil could be readily stored and transported away from the pyrolysis plant, hence de-coupling the waste processing and product utilisation.<sup>95</sup>

Bio-oil is potentially one of the most valuable pyrolysis products. It has promising potential to be used as a renewable liquid fuel for road transportation and aviation purposes and/or an energy source for generation of heat and electricity. It could also be used as a feedstock for production of chemicals.<sup>98</sup> However, although bio-oils have been tested successfully in engines, turbines and boilers, and have been upgraded to high-quality hydrocarbon fuels, their high

energetic and financial costs are still presently unacceptable due to its high oxygen content and high viscosity.<sup>98</sup> The high acidity, corrosiveness and low thermal stability of bio-oil also render it incompatible with existing petroleum refining infrastructure.<sup>95, 98</sup> Due to its complex chemical composition, bio-oil tends to become more viscous as a result of a variety of chemical and physical reactions. In addition, bio-oils are immiscible with standard hydrocarbon fuels. Even though the recovery of pure chemical compounds from the complex bio-oil is technically feasible, it is unattractive economically due to its high costs and low concentrations of specific chemicals.<sup>103</sup> Significant efforts are required to address some of the obstacles mentioned above.

The bio-char and gas products are sometimes considered as by-products in the context of fast and/or flash pyrolysis.<sup>95, 98</sup> Bio-char could be used as a soil improver, solid fuel in boilers or a precursor for the production of activated carbon and carbon nanotubes, and the gas product is potentially an alternative source for chemicals and could provide energy for the pyrolysis process.<sup>95</sup> Several potential applications of pyrolysis products are illustrated in Figure 11.

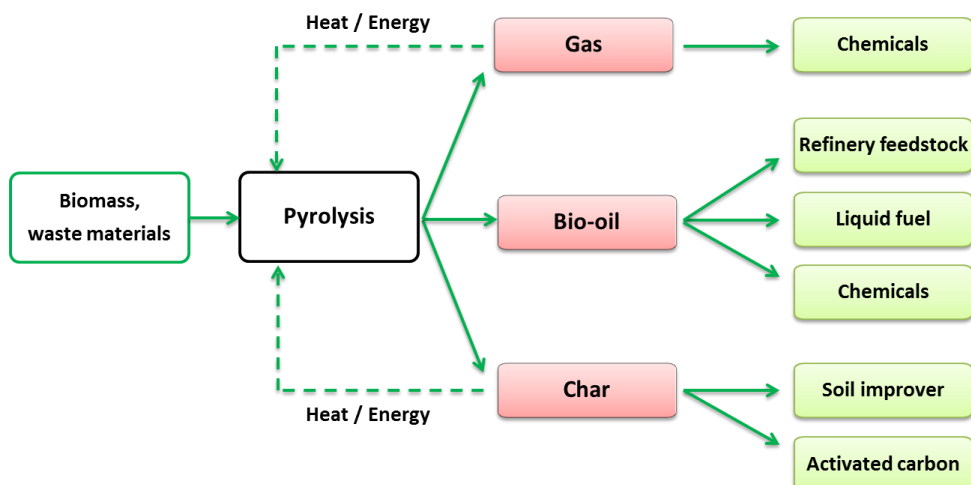


**Figure 11:** Illustration of several potential applications of pyrolysis products, adapted from reference 95. (Originally in colour)

## 1.7 Microwave chemistry

An ideal efficient thermochemical conversion process for valorisation of biomass and other waste materials would combine the advantages of biochemical and thermochemical approaches.

It should be operated continuously and at relatively low temperatures, yielding a narrow spectrum of products on a reasonable timescale.<sup>93</sup> Recently, the integration of microwave with pyrolysis has attracted much attention due to the nature and many advantages of microwave heating, such as uniform and rapid internal heating of large biomass particles, instantaneous response for rapid start-up and shut down, energy efficiency, no need for agitation *etc.*<sup>104</sup> Also, microwave processing has now been widely accepted as an efficient technique for both pilot scale and large continuous processing for waste treatment.<sup>105, 106</sup> Luque *et al.* pointed out that microwave-assisted pyrolysis, especially at low temperatures, is a promising alternative for valorisation and processing of biomass and waste materials, and has great potential to be integrated into future biorefineries.<sup>107</sup> In this context, Lam and Chase reviewed existing processes for converting waste to energy using microwave pyrolysis,<sup>108</sup> and Yin reviewed microwave-assisted pyrolysis of biomass for the production of bio-fuels.<sup>109</sup> In recent years, significant efforts have been devoted to the application of microwave pyrolysis to a vast array of biomass and/or waste materials, such as sewage sludge,<sup>110</sup> algae,<sup>111</sup> straws,<sup>112</sup> plastics,<sup>113</sup> cellulose<sup>114</sup> and other organic wastes,<sup>115 - 120</sup> for valorisation.

### 1.7.1 Principles of microwave heating

In the electromagnetic spectrum (Figure 12), microwave irradiation lies between radio and infrared in the frequency range of 0.3 to 300 GHz, which corresponds to a wavelength range of 1 m to 1 cm.<sup>121, 122</sup>

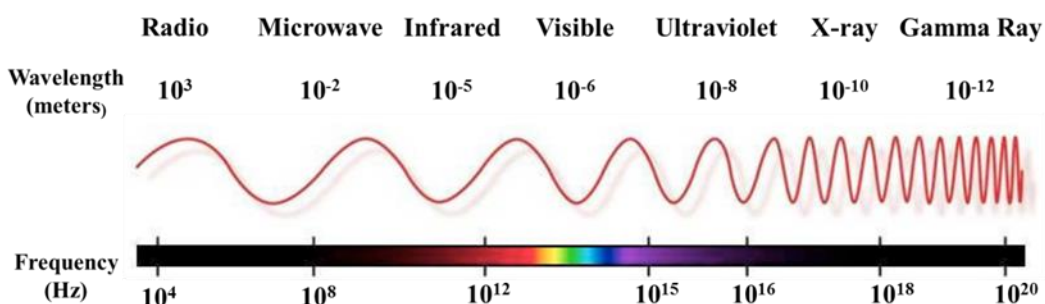


**Figure 12:** The electromagnetic spectrum. (Originally in colour)

As specified by international convention, industrial microwave heating is conducted at frequencies of either close to 900 MHz or 2.45 GHz, to minimise and/or avoid any interference with communication services.<sup>122</sup> Nowadays, both industrial and domestic microwave heating facilities are exclusively operated at 2.45 GHz (which corresponds to a wavelength of 12.24 cm).

Microwave heating is one kind of electrical volumetric heating wherein all the infinitesimal elements containing in the volume of a workload/specimen are heated individually and ideally at the same rate.<sup>122</sup> Microwave-enhanced processes take advantages of the efficient heating of microwaves which result from “microwave dielectric heating effects”.<sup>123</sup> The overall mechanism of how microwave energy is absorbed and dissipated within a material is complicated, but briefly *via* two main mechanisms, namely dipolar polarisation (reorientation) and ionic conduction, as well as interfacial (Maxwell-Wagner) polarisation:<sup>108, 123, 124</sup>

- a) Dipolar polarisation (reorientation): When a workload/specimen which includes polar compounds, in other words possess dipole moments, is subjected to an electromagnetic field, induced dipoles are formed by displacing electrons (electronic polarisation) and /or the atomic nuclei (atomic polarisation) from their equilibrium position. The induced and/or existing permanent dipoles will attempt to reorient themselves to the applied electromagnetic field by rotation. The electromagnetic field oscillates so quickly and the realignments of (induced) dipoles occurs trillions of times each second, and in this process, heat is generated by friction between the rotating molecules within the whole volume of the workload/specimen.<sup>108, 123</sup> In this case water, consisting of permanent dipoles, is a good example and an excellent microwave absorber which is widely used in microwave-enhanced processes. The extent to which a material could be heated is directly related to the frequency of applied electromagnetic field and the ability of the matrix to realign itself with the frequency of electromagnetic field. If the frequency of applied electromagnetic field is too high, the time is too short to allow molecular rotation to occur and hence no heating occurs. On the other hand, at low frequencies, the rotation rate of molecules is slow, resulting in minimal heating effect. At the given frequency of 2.45 GHz, which lies between the above mentioned two extremes at which almost all

commercial facilities operates, the (induced) molecular dipoles have time to align with the applied field rather quickly, but not too fast to follow the oscillating field precisely.<sup>123 - 125</sup> So, not surprisingly, for liquids that do not contain dipole moments, or one in which induced dipoles could not be formed, direct heating by microwave irradiation is not possible. However, this effect could be addressed by adding even very small amounts of a dipolar liquid to a miscible non-dipolar liquid, a uniform heat distribution could be rapidly achieved under microwave irradiation. For gas samples, the molecular distance are too large to generate molecular friction, thus they could not be heated by microwaves.

- b) Ionic conduction: this mechanism is significantly effective if the irradiated workload/specimen contains ions. When subjected to microwave irradiation, the charged ions and/or electrons will move through the material and electric currents are generated.<sup>108</sup> The flowing ions and/or electrons undergo significant collisions under the influence of oscillating applied electromagnetic field and hence the kinetic energy is converted to heat. In some cases, the irradiated workload/specimen has a relatively high electrical resistivity, so the energy generated by flowing ions/electrons is dissipated as heat as well.<sup>108</sup>
- c) Interfacial (Maxwell-Wagner) polarisation: For a heterogeneous workload/specimen, under microwave irradiation, since the conductivities and dielectric constants of the substances at the interfaces are different, charges are built up in contact areas or interfacial areas between different components, resulting in polarisation. This polarisation further leads to field distortions and dielectric loss, and consequent heating effects.<sup>108</sup>

It is the dielectric properties that predominantly determine a material's heating properties and characteristics.<sup>108, 123, 125</sup> More specifically, the loss factor ( $\tan\delta$ ) is an indicative of a material's ability and efficiency in terms of converting absorbed electromagnetic energy into heat, which is dependent on two parameters, namely dielectric constant ( $\epsilon'$ ) and dielectric loss factor ( $\epsilon''$ ), and is expressed as the following equation:

$$\tan\delta = \frac{\epsilon''}{\epsilon'}$$

The dielectric constant ( $\epsilon'$ ) refers to the ability of a material to be polarised by the applied electric field, whereas the dielectric loss factor ( $\epsilon''$ ) indicates the material's efficiency in terms of converting electromagnetic radiation into heat.

The loss factor ( $\tan\delta$ ) mechanism accounts for the observation that materials of similar polarity in some cases heat up at different rates, the numerical value of which is determined experimentally. Also, the higher the “loss factor  $\tan\delta$ ”, the better the material is as a microwave absorber.<sup>108, 123</sup> For instance, carbon materials and inorganic oxides are typically classified as efficient microwave absorbers; while materials with low loss factor ( $\tan\delta$ ), such as plastics, are “resistant” or “transparent” to microwave irradiations. In the latter case, efficient microwave absorbers, such as particulate carbon, are generally added to promote efficient microwave heating. In terms of solvents, generally according to their loss factor ( $\tan\delta$ ), they are broadly classified as high ( $\tan\delta > 0.5$ ), medium ( $0.5 > \tan\delta > 0.1$ ) and low ( $0.1 > \tan\delta$ ) microwave absorbing solvents.<sup>123</sup> The  $\tan\delta$  values of some common solvents are listed in Table 4.

**Table 4:** Loss factors ( $\tan\delta$ ) of several common solvents<sup>a</sup>

Solvent	$\tan\delta$
Ethanol	0.941
Dimethyl sulfoxide (DMSO)	0.825
Methanol	0.659
Acetic acid	0.174
Water	0.123
Chloroform	0.091
Ethyl acetate	0.059
Hexane	0.020

<sup>a</sup> Data obtained from references 123 and 126; 2.45 GHz, 20 °C

### 1.7.2 Microwave vs. conventional heating – the “microwave-effects”

As mentioned above, due to the electrical volumetric heating nature of microwave irradiation, microwave heating offers efficient in-core volumetric heating (also known as internal heating)

by directly coupling microwave electromagnetic energy with molecules contained in the heated matrix. Hence microwave heating is considered to be much more efficient compared with conventional heating, in which case heat is transferred from the surface to the centre of a workload/specimen with the application of an external heat source (*e.g.*, an oil bath or hot plate) mainly through conduction and/or convection.<sup>108, 123</sup> As a result, in conventional heating, the internal temperature distribution of a heated workload/specimen is limited by the thermal diffusivity of the material, which is a physical parameter that is determined by the specific heat, thermal conductivity and density of a material and specifically determines the temperature rise within a material (subjected to a given set of conditions of heating) as a function of depth from the surface and time.<sup>108, 122</sup> To allow direct interactions of molecules within a material and microwave irradiation, microwave vessels are typically produced using (nearly) microwave-transparent materials such as quartz, borosilicate glass or teflon.<sup>123</sup> Under microwave irradiation an inverted temperature gradient effect occurs compared with conventional thermal heating, more specifically, the temperatures of microwave vessels or material surfaces are lower than those of the interior of the material.<sup>123</sup> The inverted temperature gradient effect of microwave heating is illustrated in Figure 13.

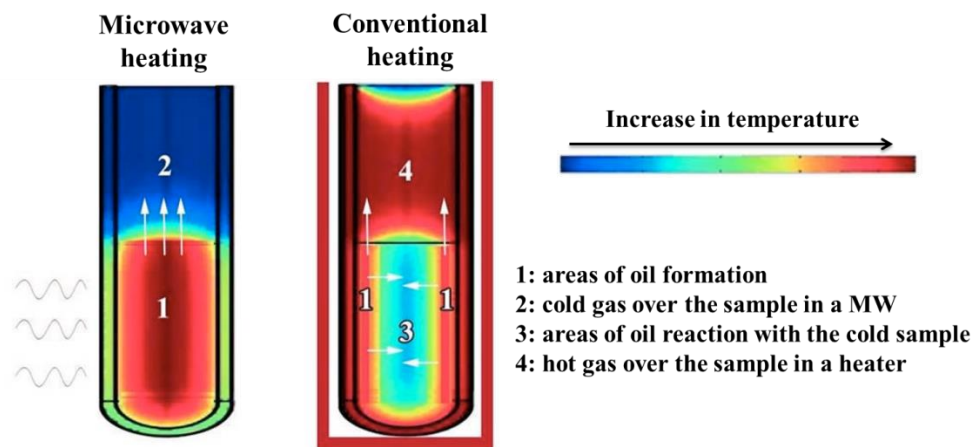


**Figure 13:** Illustration of temperature profiles of microwave irradiation and conventional heating, adapted from references 123 and 127. (Originally in colour)

Attributed to its electrical volumetric heating nature and heating mechanism stated above, microwave heating also shows several “unique” heating effects which generally cannot be

attained or duplicated under conventional heating conditions.<sup>123</sup> For example, a) super heating effect (*e.g.*, polar solvents/liquids could be superheated to temperatures tens degree above their boiling points within rapidly in sealed microwave vessels; the temperature of ionic liquids could dramatically jumps around 200 °C within seconds), b) selective rapid heating of polar or strong microwave absorbing compounds while less or ineffective for less or non-polar substances, c) the hot spot effects (*i.e.*, microscopic hotspots or “molecular radiators” are formed owing to varieties in dielectric properties of compounds within the heated material, leading to significantly higher temperatures of certain positions within the material than the temperature measured in bulk), d) the elimination of the vessel “wall effects” due to the inverted temperature gradient effect under microwave irradiation, e) sometimes altered product distributions compared to experiments conducted with conventional heating approaches. These “specific microwave effects” caused significant debate and controversy previously, but today it is widely accepted that the inherent reason for these “specific microwave effects” is mainly the dramatic accelerated heating rate caused by microwave irradiation and the fundamental/base of these “specific” effects are actually thermal/kinetic effects.<sup>123, 125</sup>

Overall, microwave heating as an alternative heating approach offers several advantages over conventional heating methods. Taking advantage of the above mentioned “unique” features associated with microwave heating, it is possible to improve process efficiency and intensification, modify process product distributions and selectivities, achieve better process controllability and even, in some cases, to perform reactions that generally cannot be conducted with conventional heating approaches.<sup>123</sup>

# **Chapter 2**

## ***Microwave-assisted pyrolysis of biorenewable waste streams: From wood to paper to deinked residue***

Aspects of work described in this chapter have been published in:

Z. Zhang, D. J. Macquarrie, P. M. Aguiar, J. H. Clark and A. S. Matharu,  
*Environmental Science & Technology*, 2015, **49**, 2398-2404

Z. Zhang, D. J. Macquarrie, M. De bruyn, V. L. Budarin, A. J. Hunt, M. J. Gronnow, J. Fan, P.  
S. Shuttleworth, J. H. Clark and A. S. Matharu,  
*Green Chemistry*, 2015, **17**, 260-270

Oral presentation given at 4<sup>th</sup> NORthern Sustainable Chemistry meeting  
(NORSC), Huddersfield, UK, October, 2014

Oral presentation given at 3<sup>rd</sup> International Symposium on Green Chemistry,  
La Rochelle, France, May, 2015

Poster presentation to be given at 11<sup>th</sup> International Conference on Renewable  
Resources & Biorefineries (RRB11), York, UK, June, 2015 (accepted)



## 2.1 Summary

Three kinds of biorenewable waste streams (spruce wood chips, waste office paper and paper deinking residue (DIR)) were converted to value-added products *via* microwave-assisted low-temperature (<200 °C) pyrolysis. The potential applications for the pyrolysis products with particular emphasis on bio-oils and microwave residue (from DIR) were explored. Figure 14 illustrates the possible major sources of these three kinds of biorenewable waste streams. This chapter could also be viewed as three case studies for valorisation of currently under-utilised and low-value biorenewable waste streams in the concept of the biorefinery.

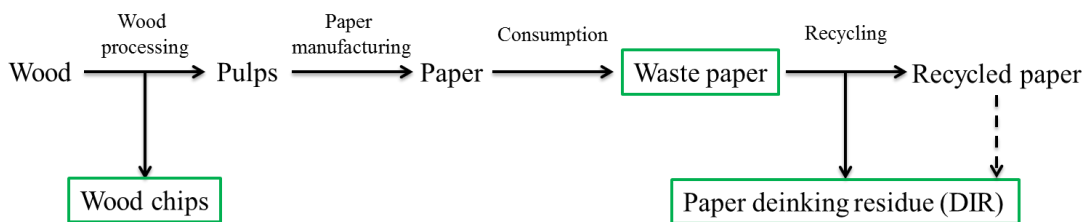


**Figure 14:** Illustration of potential sources for the three kinds of biorenewable waste streams: wood chips, waste paper and DIR. (Originally in colour)

The three biorenewable waste streams (*i.e.* spruce wood chips, waste office paper and paper deinking residue (DIR)) were converted into bio-oil (organic and aqueous phases), bio-char (microwave residue) and gas *via* low-temperature (<200 °C) microwave-assisted pyrolysis within approximately 15 minutes at fixed power (1200 W, 2.45 GHz). Both biorenewable feedstocks and their pyrolysis products (except gas) were characterized by proximate and ultimate analysis, ICP-MS, ATR-IR spectroscopy. Chemical compositions of both the organic and aqueous phase bio-oils generated from microwave-assisted pyrolysis processes were comprehensively studied using  $^1\text{H}$  and  $^{13}\text{C}$  NMR spectroscopy and GC-MS. It was demonstrated that broad categories of compounds indicative of sugars (carbohydrates), (hetero-) aromatics and carbonyl-containing moieties were identified in the organic phase bio-oils. The aqueous phase bio-oils mainly comprise water, carboxylic acids as well as trace amounts of organic matter. In addition, it was found that the microwave-assisted low-temperature (<200 °C)

pyrolysis process is very efficient for simultaneously efficient fast separation and recovery of the organic and inorganic content of DIR.

The utilisation of the organic phase bio-oils derived from spruce wood chips, waste office paper and DIR as adhesives for aluminium – aluminium (Al – Al) bonding was studied. The influences of curing temperatures and time periods on the adhesive strengths (tensile strengths) of the Al plates cured by the organic phase bio-oils were investigated by application of the organic phase bio-oil (70 mg) to Al plates (50 mm × 50 mm) followed by curing at different temperatures (120 °C, 140 °C, 160 °C and 180 °C) and time periods (4 and 8 h). The scrapings of the post-cure material at the Al – bio-oil – Al interfaces post tensile tests were characterized by ATR-IR and solid-state <sup>13</sup>C CP/MAS NMR with and without dipolar dephasing.

To gain an in-depth understanding of the adhesive properties of bio-oil, a liquid - liquid fractionation of the waste office paper derived organic phase bio-oil using alkali and organic solvents were carried out. The results suggest a possible *synergistic* and/or *co-operative* effect within various bio-oil components, while the “acidic” fraction comprising possible (hetero-) aromatic compounds such as furans contribute most towards good adhesion.

Furthermore, a model compound study using 5-(hydroxymethyl)-2-furaldehyde (HMF), catechol and levoglucosan was conducted to investigate bonding behaviour of the bio-oil. Single model compound, mixtures of each two model compounds with various molar ratios and mixtures of the three model compounds with various molar ratios were applied as adhesives for Al bonding. The post cure material and/or residues remaining between the two Al substrates were characterized by ATR-IR.

Finally, since the microwave residue represents the largest fraction of products generated from microwave-assisted low-temperature (<200 °C) pyrolysis of DIR, it was further characterized by solid-state CP/MAS <sup>13</sup>C NMR, SEM, ATR-IR, ICP-MS, powder X-ray diffraction (XRD) and solid-state Bloch-decay <sup>13</sup>C NMR. The results indicate that the microwave-residue is free from organic matter and primarily comprises calcium carbonate (calcite) and kaolinite. Hence, a

potential application for reusing the microwave residue in paper recycling processes to produce recycled paper and/or cardboards is proposed.

## **2.2 Wood chips, waste paper and de-inked residue (DIR)**

### **2.2.1 Wood processing waste and wood chips**

Wood is by far the most widely and intensively used lignocellulosic material worldwide. The application areas of wood are numerous due to its versatile physical and chemical characteristics.<sup>128, 129</sup> Global major industrial wood application areas include heat and/or power generation, saw milling, woodworking, paper and pulp industry as well as wood-based materials industry.<sup>128 - 130</sup>

Industrial round wood is the wood that enters the forest processing industry and used for any purposes except energy and fuel, majorly comprising sawlogs, veneer logs, pulpwood, round and split, as well as other industrial round wood (*e.g.*, used for fence posts and telegraph poles).<sup>131</sup> According to the Food and Agriculture Organization (FAO) of the United Nations, global industrial round wood production increased from 1710 million m<sup>3</sup> in 2012 to 1737 million m<sup>3</sup> in 2013, representing an increase of about 1.6%.<sup>131</sup> Actually, the global round wood production has increased since 2009 and has also exceeded the level of production in 2009 by 13%.<sup>131</sup> The major consumers of industrial round wood are US (16%), China (12%), the Russian Federation (9%), Brazil (9%) and Canada (8%), which are also the top five major producers of industrial round wood worldwide.<sup>132</sup>

Due to the significantly high amounts of wood being produced and consumed each year, the wood processing industry, together with other relative industrial sectors, represents a major industrial domain that generates vast amounts of wood waste.<sup>133, 134</sup> Europe, China, USA, Brazil and Canada are the leading region/countries where most wood residues are generated. Industrial wood residues are primarily generated as co-products of the sawmilling industry, including shavings, sawdust, wood chips and residues of any other forest industry.<sup>133, 134</sup> The volume of industrial wood residues generated globally per year is huge. According to data released by the

FAO, about 8.5% of industrial round wood results in wood residues.<sup>135</sup> For instance, in 2010, among the 1534 million m<sup>3</sup> of consumed industrial round wood, around 131 million m<sup>3</sup> ended up in wood residues.<sup>135, 136</sup> Some wood residues could still find an application depending on the species, quality and properties.<sup>136, 137</sup> For example, wood chips and particles of proper and high quality could be used as feedstock in the paper and pulp industry. Also, some residues (*e.g.*, sawdust, bark, wood shavings) may be suitable for generation of heat and/or power, and a small proportion of this residue is employed for the production of chemicals.<sup>136 - 139</sup> Nevertheless, significant amounts of waste wood residue still remain and can be of diverse quality depending on their origins and the industrial processes. In the context of waste as a resource, these wood residues represent one important source of renewable biomass raw material from which high value-added products could be derived.<sup>133, 134, 140, 141</sup>

## 2.2.2 Waste paper

Globally, paper is one of the most widely recycled materials. For instance, in 2011 the recycling rate of used waste paper was over 70%.<sup>142</sup> In theory, paper can be recycled up to six or seven times, but in reality this is far from true. Paper cannot be recycled indefinitely as cellulose fibers become too short and worn to be useful in creating a new sheet of paper or cardboard box. The current average paper recycling rate in Europe is 3.5; while world-wide the average is only 2.4 times.<sup>142</sup> In an era of confidentiality and data protection, document shredding and/or milling of paper is on the rise, which can render it ineffective for recycling as the resulting fibres become too short. Finely chopped or ground paper also causes maintenance problems and fire hazards when fed into certain types of paper mill machinery, and some mill machines simply cannot recognize small or shredded materials detrimental to paper quality.<sup>143</sup>

Thus, a significant amount of waste paper and board ends up in landfill or incineration, which is a loss of valuable cellulosic raw materials and might have negative impacts on the environment. The recognition of the value of this rejected material is now important, as the economic differential between the price of paper for recycling and the cost of reject management is becoming marginal. Paper destined for recycling should be seen as a source for many valuable components to produce additional high value products alongside paper.<sup>144</sup>

The production of biofuels and other sugar derivatives (such as gluconic acid,<sup>145</sup> lactic acid<sup>146</sup>) from waste paper through biochemical conversion has been reported. Also, it has been estimated that the annual global production of bio-ethanol can be as much as 82.9 billion litres from waste paper, replacing 5.36% of petroleum consumption, with accompanying greenhouse gas (GHG) emission savings between 29.2% and 86.1%.<sup>144</sup> However, one disadvantage of biochemical conversion, which generally involves enzymatic hydrolysis, is the low enzymatic degradation rate of lignocellulosic materials due to the resistant crystalline structure of cellulose and the physical barrier formed by lignin that is associated with the cellulose.<sup>147</sup> Also, the high enzyme cost is another disadvantage for biochemical conversion from an economic point of view.<sup>148</sup>

### **2.2.3 Paper deinking residue**

The Paper and pulp industry is a major industrial sector that generates significant amounts of lignocellulosic wastes.<sup>149, 150</sup> For example, in Europe alone, the paper and pulp industry generates 11 million tonnes of waste annually and around 70% of the waste is attributed to the production of deinked recycled paper.<sup>151</sup> Among these, deinking residue (DIR), also sometimes known as deinking paper sludge (DPS), which is a composite waste material generated from paper deinking processes, accounts for about 2.3 million tonnes of waste generated each year.<sup>152,</sup><sup>153</sup> In general, 15 - 40% by weight of original wastepaper before deinking ends up as DIR on a dry basis, depending on the quality of wastepaper raw material and the type of recycling process.<sup>154</sup> As mentioned above in section 2.2.2, paper is one of the most recycled materials globally,<sup>142</sup> dramatically significant amounts of DIR have been and are still being generated.

The waste paper recycling process generally involves separation of useable pulp fibers from other paper components, yielding “secondary” fibers that are suitable for making new paper products and waste materials.<sup>154</sup> Paper fibers can only be recycled for a limited number of times (around 2.4 worldwide), before they are too short to be useful for making new paper products and must be discarded as part of DIR.<sup>142, 153</sup> Consequently, DIR mainly contains short cellulosic fibers, inorganic mineral fillers (clay, calcium carbonate, and silica *etc.*), ink particles, and coatings depending on the type of recovered paper being processed.<sup>151, 154</sup> Generally, DIR is poorly used and ends up in a landfill and/or land spread. With the increasingly high landfill

costs and tougher legislation, disposal of DIR represents both an economic and environmental burden for recycled paper mills, in particular paper deinking mills, all over the world. Global concerns over the efficiency, competitiveness, and profitability of relative industrial sectors are also key drivers to recover value from major industrial waste streams which are currently underutilized, such as DIR.

Several alternative beneficial ways for valorisation of DIR have been explored and reported. For example, it can be used as soil amendments and a plant nutrient carrier<sup>155</sup> and for the production of particleboard and other composite materials.<sup>156 - 159</sup> It can also be used as a waste biomass feedstock for the production of fuel and chemicals *via* thermochemical methods such as pyrolysis, sub-/supercritical water treatments.<sup>160 - 165</sup> The char generated from pyrolysis of DIR could be used for heavy metal adsorption.<sup>166 - 168</sup>

## **2.3 Microwave-assisted low-temperature pyrolysis of biorenewable waste streams**

### **2.3.1 Experimental set-up**

As described in the experimental section 4.2.1 in chapter 4, the microwave-assisted low-temperature (<200 °C) pyrolysis experiments of various waste raw material feedstocks (*i.e.*, Spruce wood chips, waste office paper and DIR) were performed on a Milestone ROTO-SYNTH Rotative Microwave Reactor (Milestone Srl., Italy) fitted with a vacuum system, which allows for *in-situ* separation, condensation and collection of generated volatile compounds.

The pyrolysis processes were carried out under vacuum and samples were exposed to microwave irradiation at a fixed power (1200 W, 2.45 GHz) within a rotating microwave vessel (2 L), thus even distribution of microwave irradiation energy could be achieved.<sup>169</sup> Process temperatures gradually increased from room temperature (around 25 °C) with reaction time, the microwave-assisted pyrolysis processes generally finished (no volatiles came out from the

microwave vessel) and maximum temperatures (between 190 °C and 200 °C) were reached after about 12 – 13 minutes of irradiation. Using the fitted vacuum system, condensable volatile compounds were collected as two phases of bio-oils (*i.e.*, aqueous phase bio-oil and organic phase bio-oil) and incondensable gaseous products were removed from the reaction system by the vacuum pump, as diagrammatically illustrated in Figure 15.

More specifically, during microwave-irradiation of biomass within the rotating microwave vessel in the microwave chamber, an aqueous phase was firstly generated and collected at the round-bottom flask connected to the water cooled condenser. After 3 to 4 minutes, a dark-brown liquid was produced and collected separately in another round-bottom flask (*i.e.*, organic phase bio-oil). This microwave-assisted pyrolysis experimental set-up was reported to be very efficient at producing organic phase bio-oil which almost free from water.

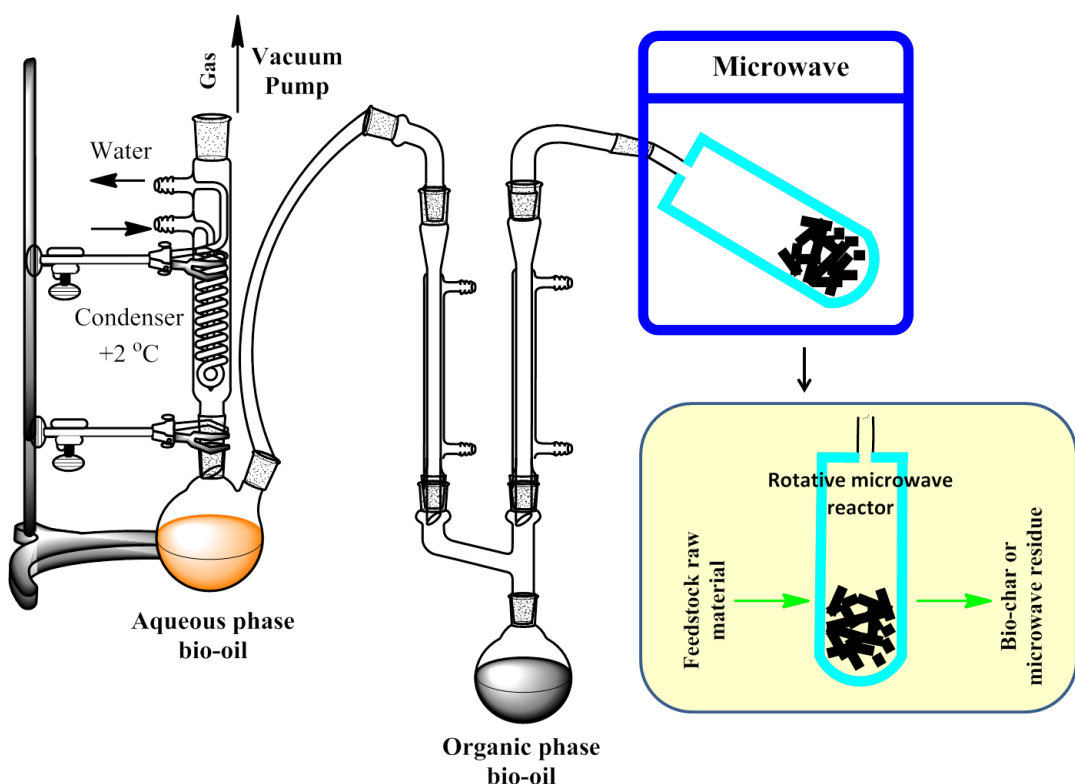


**Figure 15:** Experimental set-up for the microwave-assisted low-temperature (<200 °C) pyrolysis of spruce wood chips, waste office paper and DIR. (Originally in colour)

### 2.3.2 Yield analysis

The distribution of products as a result of microwave-assisted low-temperature (<200 °C) pyrolysis of spruce wood chips, waste office paper and paper deinking residue is shown in Figure 16. The yields of gases were calculated by mass differences as in the current study gaseous products were depleted from the reaction system by the vacuum pump. The appearances of the feedstock raw materials (spruce wood chips, waste office paper and DIR) together with generated pyrolysis products are shown in Figure 17.

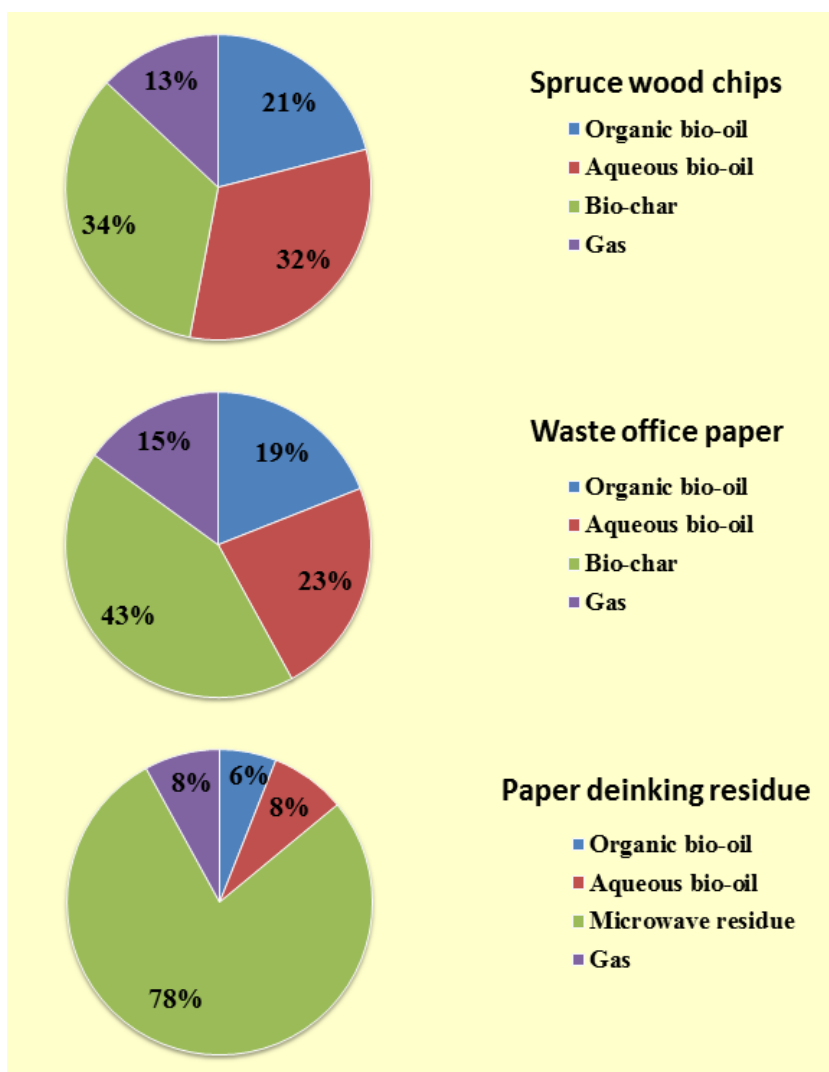


**Figure 16:** Distribution of product yields for the microwave-assisted low-temperature pyrolysis of Spruce wood chips, waste office paper and DIR (the gas yield was calculated by mass difference). (Originally in colour)

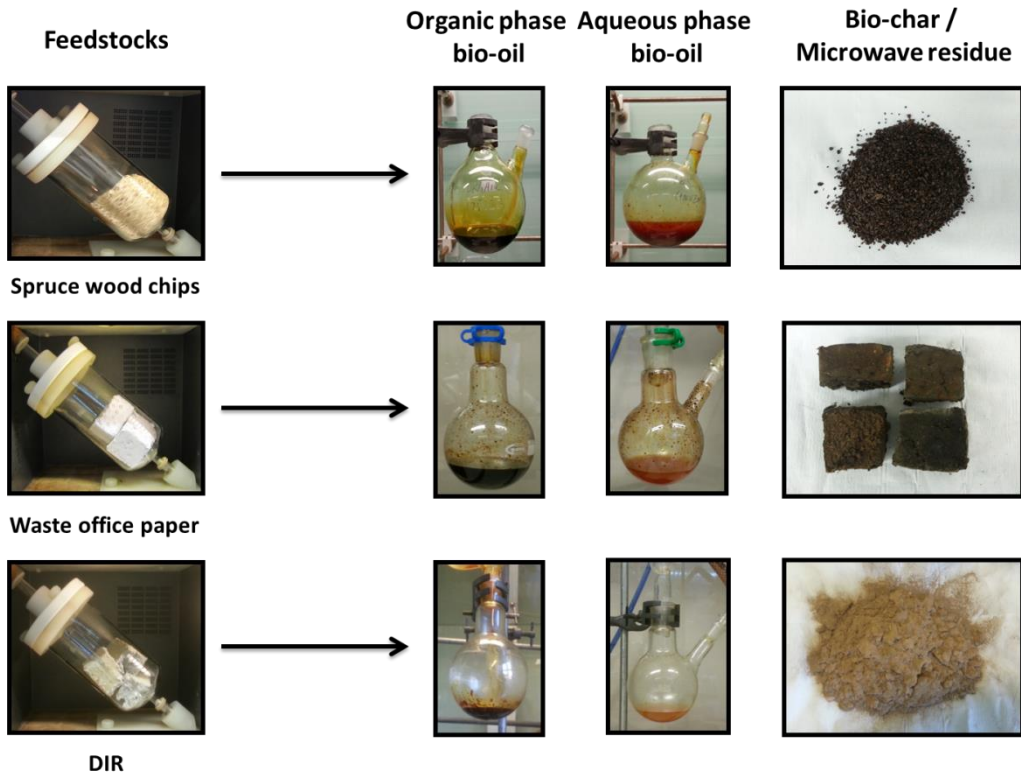


**Figure 17:** Appearance of raw materials and products from microwave-assisted low-temperature processing of spruce wood chips, waste office paper and DIR. (Originally in colour)

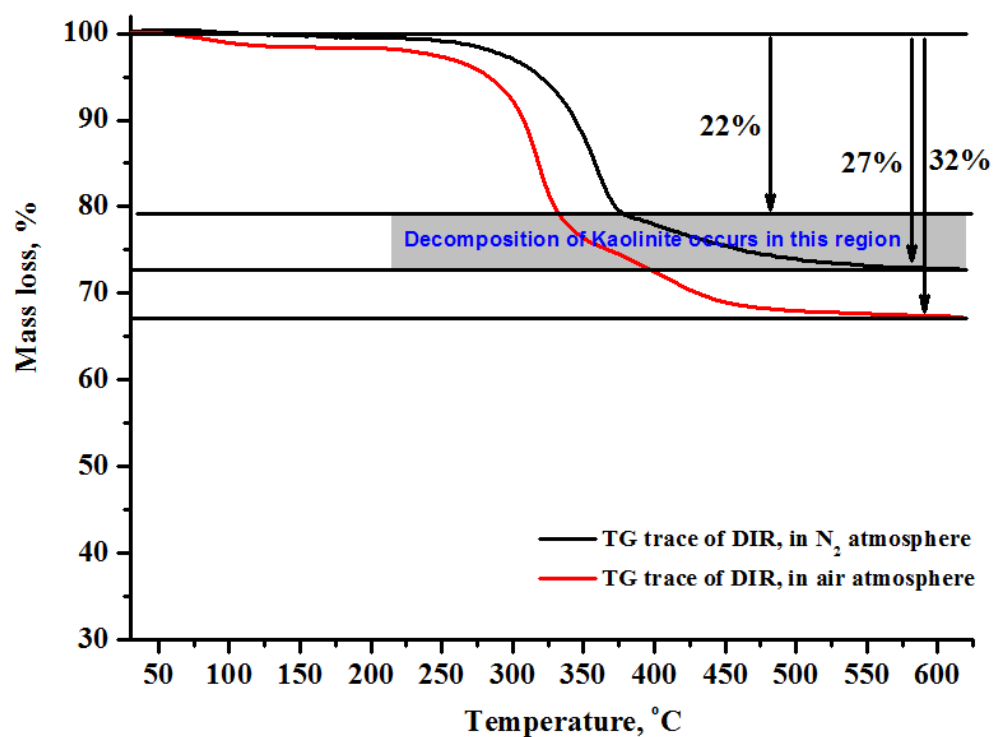
For spruce wood chips and waste office paper, the yield distributions are typical of microwave-assisted low-temperature pyrolysis of waste biomass, such as wheat straw.<sup>169, 170</sup> The yields for the organic and aqueous phase bio-oils derived from spruce wood chips are 21% and 32%, while those for waste office paper generated organic and aqueous phase bio-oils are 19% and 23%, respectively. This microwave-assisted pyrolysis process also yielded a char-like material (bio-char) with yields up to 34% (from spruce wood chips) and 43% (from waste office paper). The yields for gaseous products derived from Spruce wood chips and waste office paper are 13% and 15%, respectively.

Due to the “unique” nature of DIR (mainly inorganic matter and few residual organic lignocellulosic matter), to allow a better evaluation of the microwave-assisted processing of DIR and yields of products derived from DIR, the as-received DIR was initially characterized with thermogravimetric analysis (TGA). TGA of DIR raw material was conducted in both

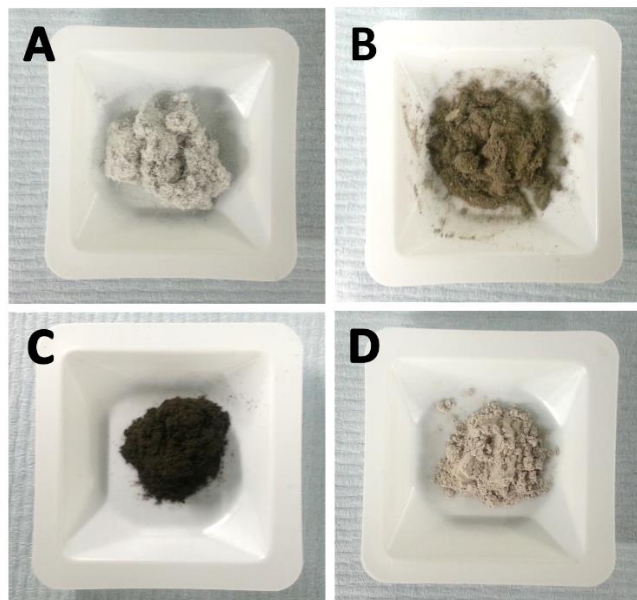
nitrogen and air atmosphere, according to the procedure described in the experimental section 4.2.3 in chapter 4.

Figure 18 highlights the TG traces of DIR in nitrogen (black) and air (red) atmosphere. Samples were heated from 30 °C to 625 °C at a heating rate of 10 °C min<sup>-1</sup>. For the TG trace of DIR in nitrogen atmosphere, weight loss below 200 °C is mainly attributed to water /moisture vaporization. The decomposition of organic matter (mainly short cracked cellulose fibers) is observed between 250 °C and 370 °C. Another weight loss step is observed from 370 °C to 550 °C, which is mainly due to dehydration and dehydroxylation reactions of kaolinite.<sup>166, 171</sup> Decomposition of CaCO<sub>3</sub> was not observed as it generally occurs at temperatures higher than 750 °C.

The TG profile of combustion of DIR (*i.e.*, in air) is similar to that of heating DIR in nitrogen atmosphere. From 30 °C to 200 °C, the weight loss is mainly due to evaporation of water / moisture and probably some dehydration reactions of organic matter. From around 200 °C to 550 °C is attributed to combustion and volatilization of organic matter.<sup>167, 172</sup> Dehydration and dehydroxylation reactions associated with kaolinite also contribute to the weight loss in this temperature range, but mainly for the weight loss between 350 °C to 550 °C. Similar TG profiles were observed before for this kind of waste material.<sup>166, 167, 173</sup> The percentage of weight loss of DIR in N<sub>2</sub> atmosphere (27%) is less than that of DIR in air (32%) at around 600 °C, as all the organic matter in DIR is combusted in air but little residual organic matter still existed after heating in nitrogen atmosphere. The colour of TG ash of DIR in N<sub>2</sub> atmosphere is dark brown, while that of TG ash of DIR in air is grey white, as demonstrated in Figure 19. The TG ashes of DIR obtained from thermogravimetric analysis of DIR in both nitrogen and air atmosphere, together with the microwave residue obtained from microwave-assisted low-temperature (<200 °C) pyrolysis of DIR, will be further characterized and discussed in-depth in section 2.11.



**Figure 18:** TG traces of DIR in  $N_2$  (black) and in air atmosphere (red), samples heated from 30 °C to 625 °C at a heating rate of  $10\text{ }^{\circ}\text{C min}^{-1}$ . (Originally in colour)



**Figure 19:** Appearance of (A) DIR raw material, (B) DIR microwave residue obtained from microwave-assisted pyrolysis of DIR, (C) TG ash of DIR in  $N_2$  atmosphere and (D) TG ash of DIR in air atmosphere. (Originally in colour)

Because of the high inorganic content of the as-received DIR (around 78%) as revealed by the TGA characterization, the largest fraction of pyrolysis products is the microwave residue with yield about 78%. Two phases of bio-oils were generated, namely organic phase (yield: 6%) and aqueous phase bio-oil (yield: 8%). The yield for incondensable gaseous product was 8%. As organic matter accounts for approximately 22% by weight of DIR according to TGA, it is obvious that the microwave-assisted pyrolysis process is very efficient for complete separation of inorganic matter as microwave residue from organic content of DIR. This effect was further proved by a TG characterization of the microwave residue; the weight loss of microwave residue was less than 1% even after heating to 625 °C in nitrogen atmosphere (Figure 20).

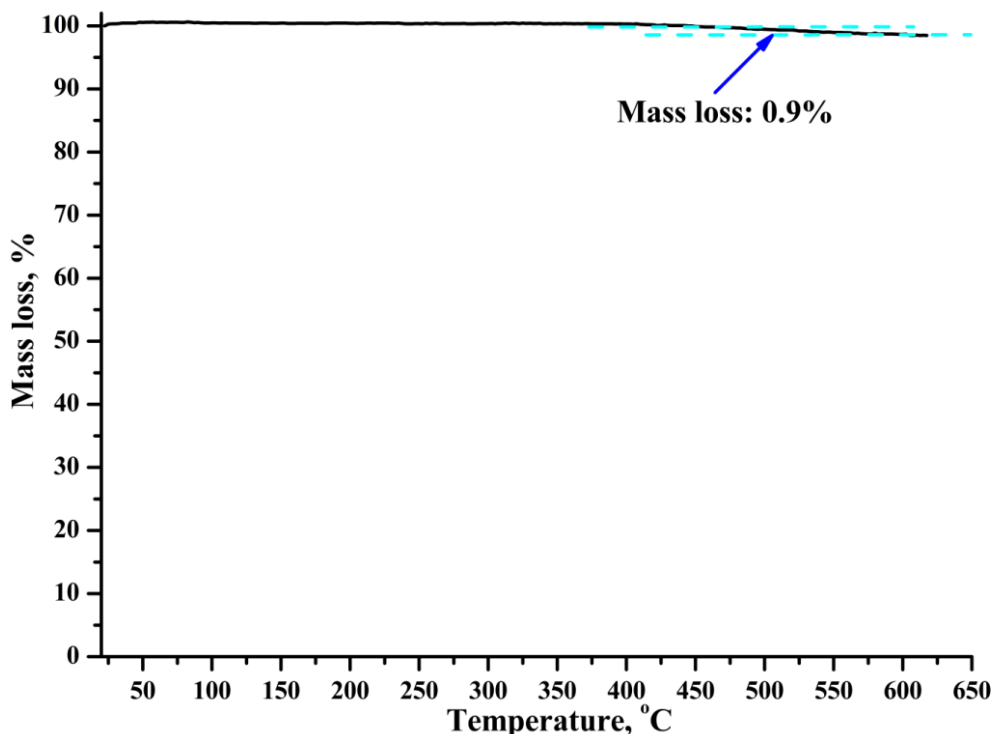


**Figure 20:** TG trace of microwave residue in  $\text{N}_2$  atmosphere ( $100 \text{ mL min}^{-1}$ ), sample heated from 30 °C to 625 °C at a heating rate of  $10 \text{ }^{\circ}\text{C min}^{-1}$ . (Originally in colour)

## **2.4 Proximate and ultimate analysis of biorenewable feedstocks and their microwave-assisted low-temperature (<200 °C) pyrolysis products**

### **2.4.1 Proximate and ultimate analysis**

To achieve a better evaluation of the microwave-assisted low-temperature pyrolysis processes, the proximate and ultimate analysis of spruce wood chips, waste office paper, DIR, as well as their relative pyrolysis products (except incondensable gaseous products) are summarized in Table 5, 6, and 7, respectively. The parameters of proximate analysis include moisture content, volatile matter content, fixed carbon content and ash content, which were determined by a TG characterization of each sample in both N<sub>2</sub> and air atmosphere (where appropriate), as specifically described in the experimental section 4.2.4 in chapter 4. For the ultimate analysis (*i.e.* elemental analysis), the carbon, hydrogen, nitrogen, sulfur and oxygen content of raw materials and their pyrolysis products (except gas) were quantitatively determined. In addition, the calorific values and water content of raw materials and their pyrolysis products (where appropriate) were measured and summarized. Since the DIR raw material was characterized in detail in section 2.3.2, also due to the “unique” composition of DIR, the proximate analysis of DIR was not included in Table 7.

The calorific values of the resulting organic phase bio-oils are all (significantly) higher than those of their relative parent materials, *i.e.*, energy densified. In addition, It is noteworthy that the calorific values of the organic phase bio-oils generated from microwave-assisted low-temperature (<200 °C) pyrolysis of the three biorenewable feedstocks are higher than typical reported calorific values of bio-oils (about 17 MJ kg<sup>-1</sup>).<sup>98, 99, 102</sup> For instance, as shown in Table 5, the calorific value of the spruce wood chips derived organic phase bio-oil (22.75 MJ kg<sup>-1</sup>) is higher than that of the spruce wood chips (18.57 MJ kg<sup>-1</sup>). More significant energy densified effect was observed for waste office paper and DIR. The calorific value of the DIR derived organic phase bio-oil (26.26 MJ kg<sup>-1</sup>) is almost 5 times higher than that of DIR raw material (5.71 MJ kg<sup>-1</sup>).

With an increasing of the amount of inorganic matter (ash content) in the feedstocks from spruce wood chips (0.9%) to waste office paper (12.8%) to DIR (around 68%, Figure 18), the calorific values of these materials decreased accordingly: spruce wood chips ( $18.57 \text{ MJ kg}^{-1}$ ), waste office paper ( $13.6 \text{ MJ kg}^{-1}$ ) and DIR ( $5.71 \text{ MJ kg}^{-1}$ ). The calorific value of the waste office paper derived bio-char ( $11.7 \text{ MJ kg}^{-1}$ ) is lower than that of the original waste paper raw material ( $13.6 \text{ MJ kg}^{-1}$ ), which is due to its elevated content of inorganic matter, namely calcium carbonate ( $\text{CaCO}_3$ ) and clays such as kaolinite, commonly added to paper products during paper manufacturing processes.<sup>174</sup> This trend is even more significant for DIR which has a much higher inorganic content than waste office paper. The calorific value of the DIR derived microwave residue is only around  $1.38 \text{ MJ kg}^{-1}$ , this is attributed to the very low organic content of the resultant microwave residue (<1%) as evidenced by the TG analysis (section 2.3.2, Figure 20). Due to the high amounts of water present in the aqueous phase bio-oils, the calorific values of the aqueous phase bio-oils cannot be measured using the bomb calorimeter as described in section 4.2.5 in chapter 4.

The fact that the organic phase bio-oils generated from microwave-assisted low-temperature (<200 °C) pyrolysis of the three biorenewable feedstocks are energy densified is mainly attributed to the employment of the efficient separation system in the microwave-assisted pyrolysis experiments (Figure 15). Since most water, mainly generated from dehydration reactions within feedstocks during pyrolysis, was trapped into the aqueous phase bio-oils, the water contents of the organic phase bio-oils are relatively low (around 2%).

**Table 5:** Proximate and ultimate characterization of spruce wood chips and their microwave-assisted pyrolysis products

	Spruce wood chips	Organic phase bio-oil	Aqueous phase bio-oil	Bio-char
<b>Proximate analysis (wt.%)</b>				
<b>Moisture</b>	6.2	---	---	2.0
<b>Volatile matter</b>	73.1	---	---	39.9
<b>Fixed carbon</b>	19.8	---	---	55.8
<b>Ash</b>	0.9	<1.0	1.1	2.3
<b>Ultimate analysis</b>				
<b>C (%)</b>	46.10 ± 0.21	52.03 ± 0.31	26.41 ± 0.18	71.33 ± 0.31
<b>H (%)</b>	5.60 ± 0.08	6.40 ± 0.03	7.71 ± 0.02	4.20 ± 0.05
<b>N (%)</b>	N.D. <sup>a</sup>	N.D.	N.D.	N.D.
<b>S (%)</b>	0.020 ± 0.003	0.005 ± 0.001	0.009 ± 0.002	0.041 ± 0.002
<b>O (%)<sup>b</sup></b>	48.3 ± 0.29	41.60 ± 0.34	65.89 ± 0.20	24.5 ± 0.36
<b>Water content (%)</b>	1.1	2.1 ± 0.2	---	<1.0
<b>CV (MJ kg<sup>-1</sup>)<sup>d</sup></b>	18.57 ± 1.32	22.75 ± 1.16	---	27.76 ± 1.05

<sup>a</sup> N.D.: not detected; <sup>b</sup> Calculated by difference; <sup>c</sup> TOC: total organic carbon; <sup>d</sup> CV: calorific value

**Table 6:** Proximate and ultimate characterization of waste office paper and its microwave-assisted pyrolysis products

	Waste office paper	Organic phase bio-oil	Aqueous phase bio-oil	Bio-char
<b>Proximate analysis (wt.%)</b>				
<b>Moisture</b>	4.5	---	---	1.1
<b>Volatile matter</b>	71.9	---	---	44.0
<b>Fixed carbon</b>	10.8	---	---	21.1
<b>Ash</b>	12.8	1.2	8.3	33.8
<b>Ultimate analysis</b>				
<b>C (%)</b>	$34.56 \pm 0.16$	$49.88 \pm 0.15$	$16.89 \pm 0.21$	$38.89 \pm 0.26$
<b>H (%)</b>	$4.30 \pm 0.03$	$5.84 \pm 0.04$	$4.22 \pm 0.03$	$4.01 \pm 0.03$
<b>N (%)</b>	N.D. <sup>a</sup>	N.D.	N.D.	N.D.
<b>S (%)</b>	$0.091 \pm 0.003$	$0.043 \pm 0.005$	$0.032 \pm 0.004$	$0.171 \pm 0.003$
<b>O (%)<sup>b</sup></b>	$48.25 \pm 0.19$	$44.24 \pm 0.19$	$78.86 \pm 0.24$	$23.14 \pm 0.29$
<b>Water content (%)</b>	---	$2.6 \pm 0.3$	---	---
<b>TOC (mg L<sup>-1</sup>)<sup>c</sup></b>	---	---	180,000	---
<b>CV (MJ kg<sup>-1</sup>)<sup>d</sup></b>	$13.6 \pm 1.5$	$21.8 \pm 1.2$	---	$11.7 \pm 1.6$

<sup>a</sup> N.D.: not detected; <sup>b</sup> Calculated by difference; <sup>c</sup> TOC: total organic carbon; <sup>d</sup> CV: calorific value

**Table 7:** Ultimate characterization of DIR and its microwave-assisted pyrolysis products

	<b>DIR raw material</b>	<b>Organic phase bio-oil</b>	<b>Aqueous phase bio-oil</b>	<b>Microwave residue</b>
<b>C (%)</b>	24.08 ± 0.32	55.40 ± 0.22	16.55 ± 0.18	13.48 ± 0.25
<b>H (%)</b>	2.14 ± 0.05	7.10 ± 0.03	9.07 ± 0.02	0.36 ± 0.02
<b>N (%)</b>	N.D. <sup>a</sup>	N.D.	N.D.	N.D.
<b>S (%)</b>	0.110 ± 0.002	0.102 ± 0.005	0.051 ± 0.003	0.132 ± 0.003
<b>Other (%)<sup>b</sup></b>	73.67 ± 0.37	37.40 ± 0.25	74.33 ± 0.20	86.03 ± 0.27
<b>Water content (%)</b>	<1.0	2.3 ± 0.2	---	<1.0
<b>TOC (mg L<sup>-1</sup>)<sup>c</sup></b>	---	---	170,000	---
<b>CV (MJ kg<sup>-1</sup>)<sup>d</sup></b>	5.71 ± 0.56	26.26 ± 0.65	---	1.38 ± 0.16

<sup>a</sup> N.D.: not detected; <sup>b</sup> Calculated by difference; <sup>c</sup> TOC: total organic carbon; <sup>d</sup> CV: calorific value

#### 2.4.2 Mineral content analysis

The metal contents of spruce wood chips, waste office paper and DIR were determined using inductively coupled plasma–mass spectrometry (ICP-MS). Instrumentation and detailed experimental procedures for sample preparation and ICP-MS analysis are illustrated in section 4.2.7 in chapter 4. Table 8, 9 and 10 summarize the metal contents of raw materials and their relative microwave-assisted low-temperature (<200 °C) pyrolysis products (except incondensable gaseous products) for spruce wood chips, waste office paper and DIR, respectively. The ICP-MS data for waste office paper (Table 9) and DIR (Table 10) and their relative pyrolysis products show very high levels of calcium in the bio-char and/or microwave residue. The high abundance of calcium in waste office paper, DIR as well as their pyrolysis products is due to the presence of calcium carbonate which is added during paper manufacturing processes.<sup>174</sup> Also, significant high amounts of silica/silicon were present in waste office paper, DIR and their pyrolysis products compared with those of spruce wood chips (Table 8). The high silica/silicon content most likely originates from kaolinite (aluminosilicate), water-soluble silica-based sizing agents and potential organosilane sizing agents that are added during manufacturing of high-quality coated paper.<sup>175, 176</sup>

**Table 8:** Mineral contents of spruce wood chips and their relative low-temperature microwave-assisted pyrolysis products as determined by ICP-MS

Element (ppm <sup>a</sup> )	Spruce wood chips	Organic phase bio-oil (21 wt.%)	Aqueous phase bio-oil (32 wt.%)	Bio-char (34 wt.%)
<b>Na</b>	11.81	8.42	3.51	9.53
<b>Mg</b>	3.52	4.01	4.23	10.04
<b>Al</b>	108.82	84.31	N.D. <sup>b</sup>	178.21
<b>Si</b>	5877.41	26187.22	19130.82	2636.31
<b>K</b>	9.22	1.21	1.62	21.61
<b>Ca</b>	16.81	4.43	4.43	89.24
<b>Cr</b>	190.91	1.82	2.11	153.41
<b>Mn</b>	65.73	0.62	1.01	305.62
<b>Fe</b>	352.12	15.63	17.31	521.33
<b>Cu</b>	6.71	2.32	3.42	7.71
<b>Zn</b>	39.12	14.01	16.43	67.02
<b>As</b>	1.62	0.51	0.06	1.86
<b>Nb</b>	0.23	0.17	0.13	0.37
<b>Pd</b>	0.27	0.11	0.08	0.53
<b>Sn</b>	3.27	0.18	0.56	3.66
<b>Ir</b>	0.12	0.02	N.D.	0.17
<b>Pt</b>	0.03	0.03	0.02	0.05
<b>Au</b>	0.86	0.05	0.01	1.13
<b>Pb</b>	0.41	0.09	0.72	0.93

<sup>a</sup> ppm refers to parts per million in mass; <sup>b</sup> N.D. = not detected

**Table 9:** Mineral contents of waste office paper and its relative low-temperature microwave-assisted pyrolysis products as determined by ICP-MS

Element (ppm <sup>a</sup> )	Waste office paper	Organic phase bio-oil (19 wt.%)	Aqueous phase bio-oil (23 wt.%)	Bio-char (43 wt.%)
<b>Na</b>	2463.83	194.33	123.36	3790.26
<b>Mg</b>	919.61	2.90	12.49	2414.23
<b>Al</b>	328.49	3.56	8.76	532.93
<b>Si</b>	27168.06	20668.25	23239.69	4956.24
<b>K</b>	1102.36	199.48	131.59	539.56
<b>Ca</b>	92877.53	712.27	411.83	243719.67
<b>Cr</b>	12.73	0.29	0.57	7.35
<b>Mn</b>	20.89	N.D. <sup>b</sup>	N.D.	46.56
<b>Fe</b>	936.27	1.10	4.03	929.95
<b>Cu</b>	10.81	0.25	0.26	21.63
<b>Zn</b>	7.74	12.31	N.D.	13.86
<b>As</b>	4.64	6.01	2.51	11.32
<b>Nb</b>	0.45	0.04	0.52	0.05
<b>Pd</b>	0.31	0.02	0.11	0.63
<b>Sn</b>	1.13	18.84	1.69	16.53
<b>Ir</b>	0.16	0.03	0.05	0.04
<b>Pt</b>	0.05	0.03	0.05	0.06
<b>Au</b>	5.52	0.49	0.25	3.88
<b>Pb</b>	0.22	0.02	0.07	1.17

<sup>a</sup> ppm refers to parts per million in mass; <sup>b</sup> N.D. = not detected

**Table 10:** Mineral contents of DIR and its relative low-temperature microwave-assisted pyrolysis products as determined by ICP-MS

Element (ppm <sup>a</sup> )	DIR	Organic phase bio-oil (6 wt.%)	Aqueous phase bio-oil (8 wt.%)	Microwave residue (78 wt.%)
<b>Na</b>	957.81	101.92	99.23	763.13
<b>Mg</b>	2818.52	9.71	2.14	3264.41
<b>Al</b>	1328.70	14.14	2.41	5405.83
<b>Si</b>	75666.82	281761.72	249630.93	235726.54
<b>K</b>	148.34	215.80	75.32	N.D. <sup>b</sup>
<b>Ca</b>	281806.52	669.81	545.24	327603.54
<b>Cr</b>	4.72	0.23	0.51	5.61
<b>Mn</b>	77.20	N.D.	N.D.	85.83
<b>Fe</b>	924.81	1.82	3.94	1351.81
<b>Cu</b>	52.92	0.91	0.23	58.22
<b>Zn</b>	84.80	2.41	N.D.	102.62
<b>As</b>	2.14	3.31	1.74	1.93
<b>Nb</b>	0.23	0.31	0.62	0.18
<b>Pd</b>	0.56	0.09	0.09	0.63
<b>Sn</b>	51.3	0.82	0.33	65.6
<b>Ir</b>	0.18	0.03	0.04	0.12
<b>Pt</b>	0.07	0.02	0.06	0.08
<b>Au</b>	3.65	0.22	0.21	3.61
<b>Pb</b>	2.84	N.D.	0.04	4.63

<sup>a</sup> ppm refers to parts per million in mass; <sup>b</sup> N.D. = not detected

## **2.5 ATR-IR Characterization of feedstocks and their microwave-assisted pyrolysis products**

Fourier transform-infrared spectroscopy in attenuated total reflectance (ATR) mode was employed to characterize the chemical composition of raw materials (spruce wood chips, waste office paper and DIR) and to study the structural changes in functional groups occurred during the microwave-assisted low-temperature pyrolysis processes. The experimental details for ATR-IR characterization are described in section 4.2.8 in chapter 4.

In this study, the ATR-IR spectra of spruce wood chips, waste office paper, DIR as well as their relative pyrolysis products (except incondensable gaseous products) were recorded directly after the pyrolysis processes, to avoid any interferences of impurities during transferring of pyrolysis products. The ATR-IR spectra of spruce wood chips, waste office paper, DIR and their low-temperature (<200 °C) microwave-assisted pyrolysis products are analyzed and discussed in the subsections 2.5.1, 2.5.2 and 2.5.3, respectively.

### **2.5.1 ATR-IR characterization of spruce wood chips and their pyrolysis products**

The ATR-IR spectra of original spruce wood chips, the derived organic and aqueous phases of bio-oils and bio-char are illustrated in Figure 21. From the infrared spectrum of spruce wood chips, strong hydrogen bonded (O-H) stretching vibration and prominent C-H stretching vibration absorption bands are observed in the 3700 cm<sup>-1</sup> – 3000 cm<sup>-1</sup> region and 3000 cm<sup>-1</sup> – 2800 cm<sup>-1</sup> region, respectively. The intense, broad O-H stretching vibration band between 3700 cm<sup>-1</sup> and 3000 cm<sup>-1</sup> is mainly attributed to the intra- and intermolecular hydrogen bonded hydroxyl groups associated with residual moisture, cellulosic matter and lignin in spruce wood chips. Characteristic lignin absorption bands due to a variety of aromatic skeletal vibrations are observed at 1607 cm<sup>-1</sup>, 1595 cm<sup>-1</sup>, 1510 cm<sup>-1</sup>, 1427 cm<sup>-1</sup> and 1265 cm<sup>-1</sup>.<sup>177</sup> The small, broad absorption band centred at around 1640 cm<sup>-1</sup> is originated by absorbed water and/or moisture, but may also be due to cellulosic matter. The absorption bands at 1735 cm<sup>-1</sup>, 1372 cm<sup>-1</sup>, 1240 cm<sup>-1</sup>, 1160 cm<sup>-1</sup>, 1035 cm<sup>-1</sup> are typical C=O, C-H, C-O-C, C-O deformation and/or stretching

vibrations associated with carbohydrates (mainly cellulose and hemicellulose).<sup>177, 178</sup> The absorption band at 1735 cm<sup>-1</sup> is attributed to the C=O stretching vibrations in unconjugated carbonyl compounds, primarily originating from uronic acids of xylans.<sup>178</sup> Hence this band is also a characteristic absorption band of hemicellulose. The C-H deformation vibration in cellulose is observed at 897 cm<sup>-1</sup>.<sup>178</sup>

By comparing the ATR-IR spectra of pyrolysis products (*i.e.* organic phase bio-oil, aqueous phase bio-oil and bio-char) with that of spruce wood chips raw material, many significant changes could be observed. This suggests dramatic changes in chemical compositions had occurred during the microwave-assisted low-temperature pyrolysis process.

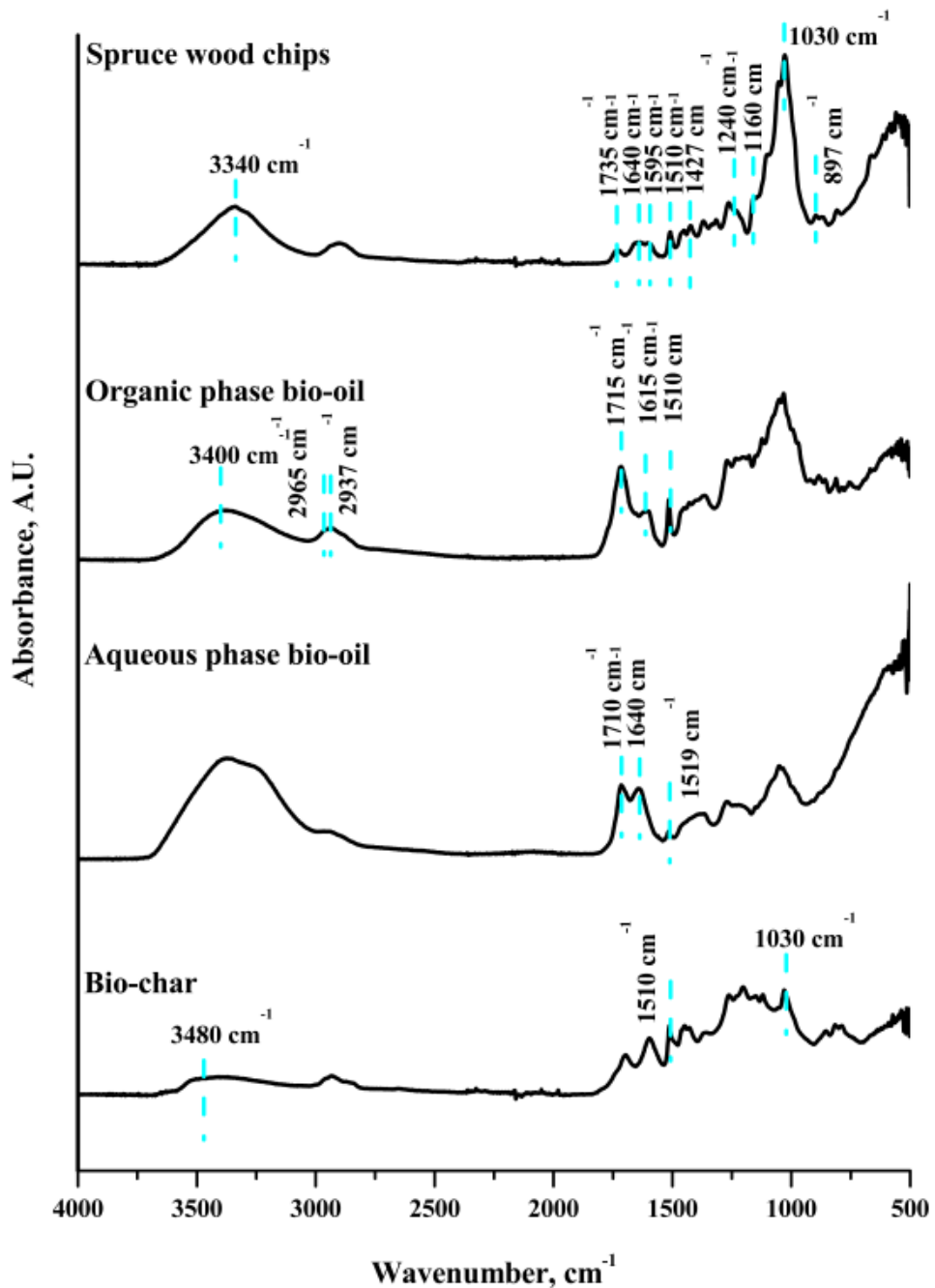


**Figure 21:** ATR-IR spectra of spruce wood chips and the products generated from microwave-assisted pyrolysis process (except gas fraction): organic fraction bio-oil, aqueous fraction bio-oil and microwave residue. (Originally in colour)

From the ATR-IR spectrum of spruce wood chips derived organic phase bio-oil, the broad O-H stretching vibration band between  $3700\text{ cm}^{-1}$  and  $3020\text{ cm}^{-1}$  indicates the possible presence of phenols, alcohols, carboxylic acids, and residual water. Compared with the O-H stretching band of spruce wood raw materials, the O-H stretching band of the organic phase bio-oil drifts to a

higher wavenumber (from about  $3340\text{ cm}^{-1}$  to  $3400\text{ cm}^{-1}$ ), suggesting a reduction in hydrogen bonding. The symmetrical and asymmetrical C-H stretching vibrations are observed at  $2937\text{ cm}^{-1}$  and  $2965\text{ cm}^{-1}$ , respectively. This indicates the presence of alkyl structures, which is further evidenced by the small C-H deformation vibration band at around  $1456\text{ cm}^{-1}$ . The most significant change compared with the spruce wood chips raw material is the appearance of a medium intensity carbonyl ( $\text{C=O}$ ) absorption band centred at  $1715\text{ cm}^{-1}$ . This carbonyl stretching vibration band corresponds to ketone, aldehyde and carboxylic acid compounds present within the organic phase bio-oil. In addition, the absorption band centred at  $1615\text{ cm}^{-1}$  is assigned to the  $\text{C=C}$  stretching of alkene, furans and aromatic compounds, indicating the presence of aromatic compounds. However, this absorption band may also correspond to residual water in the organic phase bio-oil. The region between  $1630\text{ cm}^{-1}$  and  $1450\text{ cm}^{-1}$  is a typical region where aromatic skeletal vibrations are observed. The absorption bands in this region indicate the presence of aromatic compounds in the organic phase bio-oil. Despite the bands are significantly overlapped due to the complex chemical composition of bio-oil, the characteristic absorption band for aromatic skeletal vibrations at around  $1510\text{ cm}^{-1}$  is clearly visible in the ATR-IR spectrum of organic phase bio-oil.<sup>177</sup> The weak absorbances observed below  $1000\text{ cm}^{-1}$  are mainly attributed to C-H out of plane bending vibrations of (substituted) aromatic compounds. The ATR-IR spectrum of organic phase bio-oil also shows many differences in this region compared with that of the spruce wood chips.

The ATR-IR spectrum of the aqueous phase bio-oil reveals a significantly different chemical composition in comparison with the organic phase bio-oil. The presence of possible carboxylic acids is indicated by the broad O-H stretching vibration ( $3700\text{ cm}^{-1}$  to  $3000\text{ cm}^{-1}$ ) and the high-intensity carbonyl stretching vibration band centred at  $1715\text{ cm}^{-1}$ . The absorption band at around  $1640\text{ cm}^{-1}$  further suggests the aqueous phase bio-oil contains high amounts of water. The aqueous phase bio-oil also contains organic matter as evidenced by the vast number of absorption bands in the range between  $1750\text{ cm}^{-1}$  and  $750\text{ cm}^{-1}$ . It is noteworthy that aromatic compounds were also trapped into this phase of bio-oil as evidenced by the small absorption band centred at  $1519\text{ cm}^{-1}$ , which is attributed to skeletal vibrations in aromatic compounds.<sup>177</sup> Probably due to the presence of large amounts of inorganic matter (*e.g.*, water, carboxylic acids),

this absorption band of aqueous phase bio-oil ( $1519\text{ cm}^{-1}$ ) drifts slightly to a higher wavenumber compared with that of the organic phase bio-oil (at  $1510\text{ cm}^{-1}$ ).

The ATR-IR spectrum of the bio-char (residues in the rotating microwave vessel after pyrolysis) indicates many significant structural changes occurred during the pyrolysis process. The intensity of the O-H stretching vibration band significantly decreased. Also, this band of bio-char drifts significantly to a higher wavenumber ( $3480\text{ cm}^{-1}$ ) compared to that of the spruce wood chips ( $3340\text{ cm}^{-1}$ ), indicating a dramatic reduction in hydrogen bonding. In addition, the intensity of the C-O vibration band centred at  $1030\text{ cm}^{-1}$  decreased dramatically as a result of the decomposition of the spruce wood chips during pyrolysis. The absorption bands between  $1600\text{ cm}^{-1}$  and  $1000\text{ cm}^{-1}$  are possibly due to the residual lignin and carbohydrates.<sup>177, 178</sup> Compared with the ATR-IR spectrum of spruce wood chips, many changes could be observed in this region, suggesting the formation of new chemical bonds during pyrolysis. This is largely due to increased aromatisation and rearrangement of chemical bonds in the bio-char. The aromatisation of bio-char is further evidenced by the changes of absorption bands in the typical aromatic C-H out of plane bending region ( $950\text{ cm}^{-1}$  to  $600\text{ cm}^{-1}$ ).

## 2.5.2 ATR-IR characterization of waste office paper and its pyrolysis products

The ATR-IR spectral analysis of the virgin milled office paper and subsequent pyrolysis products are shown in Figure 22. As can be seen in the spectrum of milled waste office paper (Figure 22 A), the broad absorbance band between  $3600\text{ cm}^{-1}$  and  $3200\text{ cm}^{-1}$  is attributed to the O-H stretching vibration associated with residual water, cellulosic matter and sugars. Bands between  $3000\text{ cm}^{-1}$  and  $2800\text{ cm}^{-1}$  originated by C-H stretching vibrations are associated with saturated or aliphatic structures. A very weak but slightly broad absorption band centred at  $1630\text{ cm}^{-1}$  is due to the O-H deformation most likely from residual water or cellulosic matter. The very broad, strong band ranging from  $1500\text{ cm}^{-1}$  to  $1250\text{ cm}^{-1}$  is a complex mixture of many absorbances: the C-H deformation ( $1370\text{ cm}^{-1}$ ); the C-OH stretch ( $1315\text{ cm}^{-1}$ ); and the C-O-C stretch ( $1245\text{ cm}^{-1}$ ), but is mainly due to  $\text{CaCO}_3$  vibrations seen centred at  $1415\text{ cm}^{-1}$ .<sup>173</sup> The C-O-C vibrations are further evidenced at  $1160\text{ cm}^{-1}$  and  $1100\text{ cm}^{-1}$ . The sharp band at  $870\text{ cm}^{-1}$

also evidences the presence of  $\text{CaCO}_3$ , the content of which can be up to 8% in office paper.<sup>173</sup>

<sup>174</sup> The band at  $870\text{ cm}^{-1}$  may also corresponds to torsional vibrations of methylene groups.<sup>179</sup>

A vast number of structural changes during the pyrolysis process can be seen from the spectra of the waste office paper derived two phases of bio-oil. From the spectrum of the organic phase bio-oil (Figure 22 B), the most significant change with respect to milled waste office paper is the appearance of a medium intensity band centred at  $1715\text{ cm}^{-1}$  corresponding to the  $\text{C=O}$  stretching vibration, indicating the presence of carbonyls. Also, the  $\text{O-H}$  stretching vibration drifts upward to a higher wavenumber ( $3400\text{ cm}^{-1}$ ) when compared with that of the raw material ( $3320\text{ cm}^{-1}$ ), indicating a reduction in hydrogen bonding. The absorption band at  $1623\text{ cm}^{-1}$  is due to the  $\text{C=C}$  stretching of alkene or aromatic compounds, but may also be associated with residual water. Figure 22 C shows the IR spectrum of the waste office paper derived aqueous phase bio-oil. The intense, broad  $\text{O-H}$  stretching vibration band between  $3700\text{ cm}^{-1}$  and  $3000\text{ cm}^{-1}$ , together with the intense carbonyl stretching vibration band (centred at  $1715\text{ cm}^{-1}$ ), suggests the presence of carboxylic acids. The band at  $1640\text{ cm}^{-1}$  and the broad  $\text{O-H}$  stretching band confirm the presence of water. The aqueous phase bio-oil may also contain trace amounts of sugars and other compounds from the various bands in the region from  $1500\text{ cm}^{-1}$  to  $800\text{ cm}^{-1}$ .

Compared with the IR spectrum of milled waste office paper, significant changes can be observed in the spectrum of bio-char (Figure 22 D). The broad  $\text{O-H}$  stretching band between  $3500\text{ cm}^{-1}$  and  $3200\text{ cm}^{-1}$  has almost disappeared, indicating that the oxygen in the parent materials was removed during the pyrolysis process and any acidic structures were cracked to leave a carbonaceous solid product. The intense band at  $1410\text{ cm}^{-1}$  and the narrow band at  $870\text{ cm}^{-1}$  and  $710\text{ cm}^{-1}$  were assigned to  $\text{CaCO}_3$ .<sup>166, 173</sup> As carbon is formed during the pyrolysis process, once the char gets dark in colour, it acts as a black body and absorbs radiation over all frequencies, making most bands appear relatively weak. The presence of remaining organics is still evidenced by bands at  $1700\text{ cm}^{-1}$ ,  $1580\text{ cm}^{-1}$  and  $1035\text{ cm}^{-1}$ .

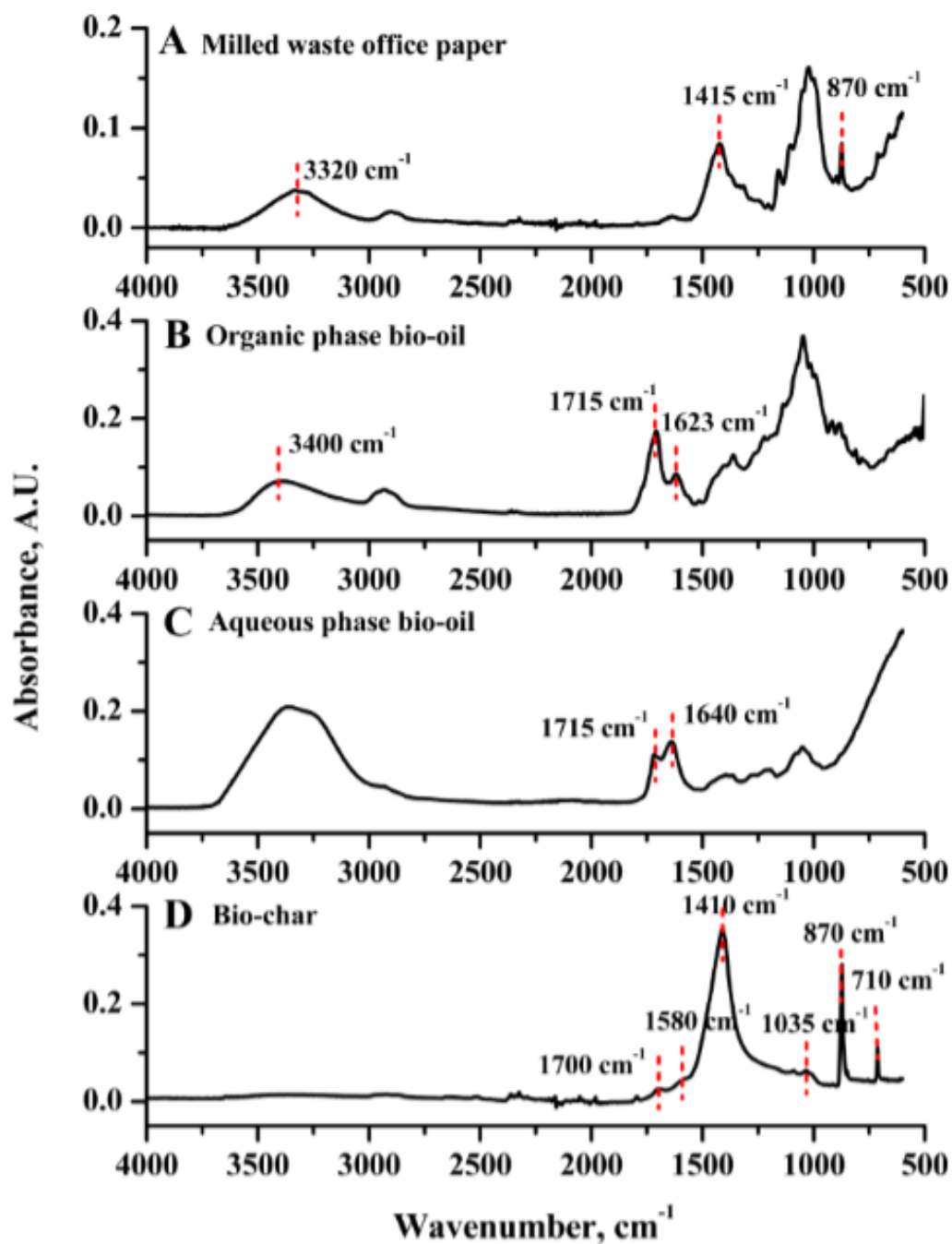


**Figure 22:** ATR-IR spectra of waste office paper and the products generated from microwave-assisted pyrolysis process (except gas fraction): organic fraction bio-oil, aqueous fraction bio-oil and bio-char. (Originally in colour)

### 2.5.3 ATR-IR characterization of DIR and its pyrolysis products

Figure 23 shows the ATR-IR spectra of DIR raw material, organic and aqueous phase bio-oil and microwave residue, as well as those of commercial calcium carbonate (calcite) and kaolinite to allow a better evaluation of the inorganic content of DIR and its pyrolysis products. From the

spectrum of DIR raw material, characteristic absorption bands of inorganic mineral matter that generally added as fillers during paper manufacturing can be observed. For example, the two small bands centered at  $3693\text{ cm}^{-1}$  and  $3619\text{ cm}^{-1}$  are characteristic O-H stretching absorption bands for kaolinite (a clay mineral);<sup>180</sup> while the broad, strong absorption band centered at around  $1400\text{ cm}^{-1}$ , together with the two sharp bands at  $870\text{ cm}^{-1}$  and  $710\text{ cm}^{-1}$ , are attributed to calcium carbonate ( $\text{CaCO}_3$ ).<sup>166, 173</sup> Also, characteristic absorption bands for organic matter (mainly cellulose) could be observed.<sup>181</sup> The broad medium intensity band from  $3600\text{ cm}^{-1}$  to  $3100\text{ cm}^{-1}$  is due to O-H stretching vibration mainly associated with cellulose; while the weak band at  $1645\text{ cm}^{-1}$  is attributed to O-H deformation vibration from either cellulose or residual water. The alkyl stretching vibrations are observed between  $3000\text{ cm}^{-1}$  and  $2800\text{ cm}^{-1}$ . The presence of cellulosic matter is also evidenced by the bands at  $1160\text{ cm}^{-1}$  and  $1110\text{ cm}^{-1}$ , which are assigned to C-O-C vibrations of cellulose bands.

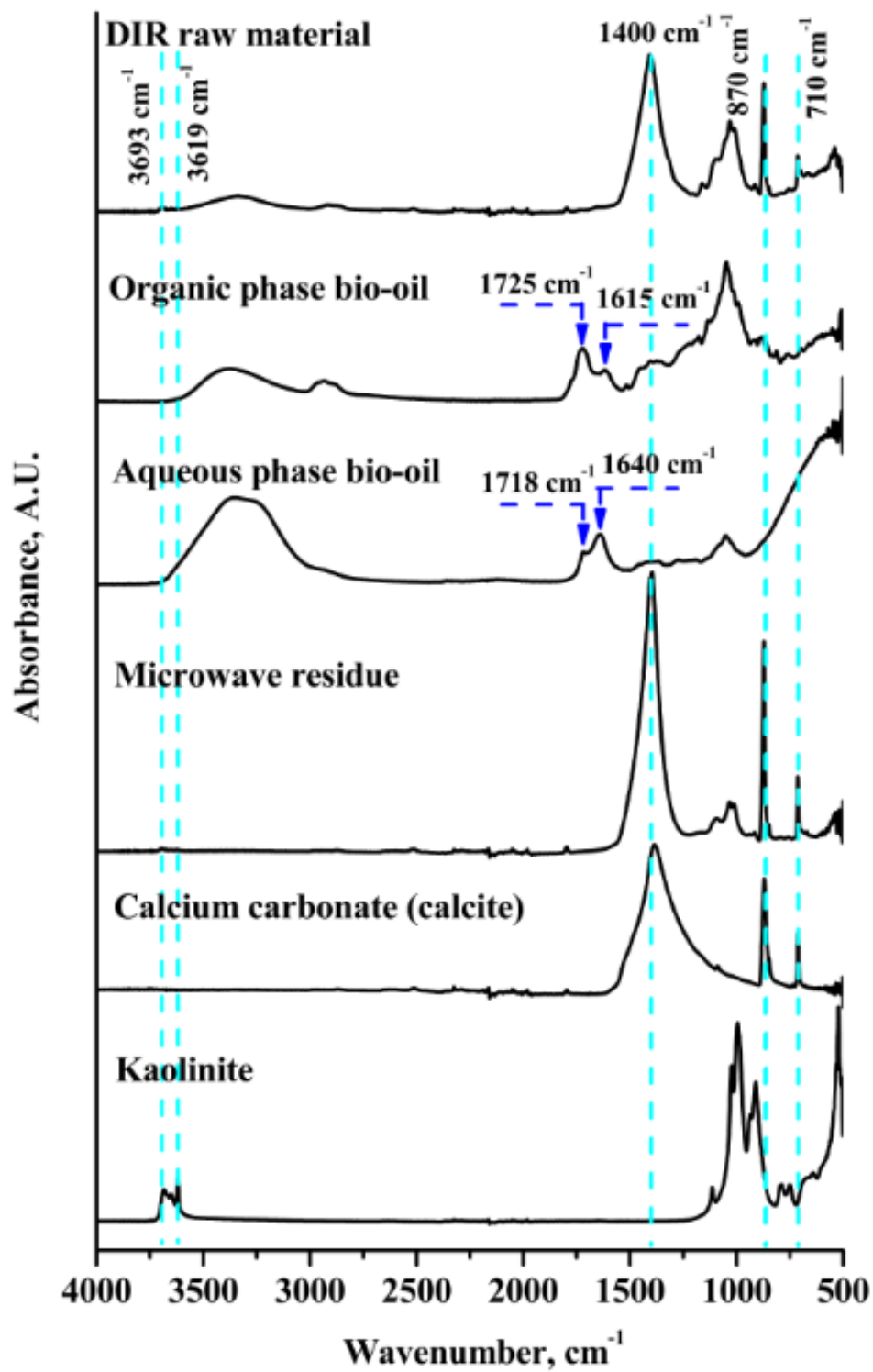


**Figure 23:** ATR-IR spectra of DIR raw material and the products generated from microwave-assisted pyrolysis of DIR (except gas fraction): organic phase bio-oil, aqueous phase bio-oil and microwave residue, together with those of calcium carbonate (calcite) and kaolinite.

As evidenced by the ATR-IR spectra of pyrolysis products, dramatic structural changes occurred during the pyrolysis of DIR. A medium intensity absorption band appears at  $1725\text{ cm}^{-1}$  in the spectrum of organic phase bio-oil, corresponding to C=O stretching vibrations. The presence of this band confirms the presence of carbonyl containing molecules in the organic phase bio-oil, such as aldehydes, ketones and carboxylic acids. Also, a new absorption band could be observed at  $1615\text{ cm}^{-1}$ , which is due to the C=C bond stretching of alkenes and/or aromatics/furans, but might also relate to residual water in this phase of bio-oil. Bands between  $900\text{ cm}^{-1}$  and  $700\text{ cm}^{-1}$  are assigned to C-H out of plane bending vibrations of aromatics. The presence of aromatics is also evidenced by bands between  $1630\text{ cm}^{-1}$  and  $1450\text{ cm}^{-1}$ , which are mainly due to skeletal vibrations of aromatic rings.

From the spectrum of aqueous phase bio-oil, it is obvious that the composition of this phase is significantly different from that of organic phase bio-oil. The very broad O-H stretching vibration ranging from  $3650\text{ cm}^{-1}$  to  $2700\text{ cm}^{-1}$ , together with the band at  $1718\text{ cm}^{-1}$  (carbonyl stretching), suggests the presence of large amounts of carboxylic acids. Also, most generated water was trapped into the aqueous phase bio-oil, which is evidenced by the broad O-H stretching vibration band and the medium intensity band at  $1640\text{ cm}^{-1}$ .

The most significant absorption bands for the microwave residue are the broad, strong band at  $1400\text{ cm}^{-1}$ , and the two sharp bands at  $870\text{ cm}^{-1}$  and  $710\text{ cm}^{-1}$ . These bands are characteristic for  $\text{CaCO}_3$ . Two small bands are still present at  $3693\text{ cm}^{-1}$  and  $3619\text{ cm}^{-1}$ , but of slightly lower intensities than those of the DIR raw material, which are attributed to kaolinite. Bands between  $1200\text{ cm}^{-1}$  and  $950\text{ cm}^{-1}$  probably resulted from small amounts of residual organic matter and also relate to kaolinite.

#### **2.5.4 Summary of the ATR-IR characterization**

The ATR-IR spectroscopy analysis of feedstocks for the low-temperature ( $<200\text{ }^{\circ}\text{C}$ ) microwave-assisted pyrolysis processes (*i.e.* spruce wood chips, waste office paper and DIR) and their relative pyrolysis products (*i.e.* organic and aqueous phase bio-oil, bio-char/microwave residue) was conducted. The results reveal that a significant number of chemical reactions

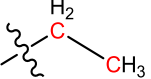
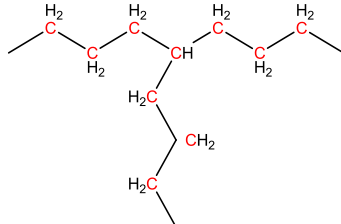
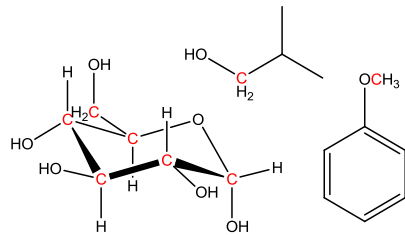
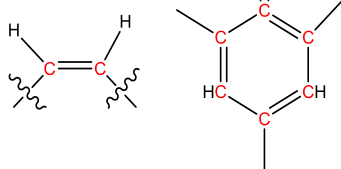
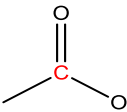
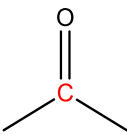
occurred during the pyrolysis process. The high molecular weight biomass raw materials were degraded during pyrolysis and decomposed into smaller molecules, which were trapped into the organic and aqueous phase bio-oil. The ATR-IR spectroscopy characterization suggests that most water and possible carboxylic acids were collected into the aqueous phase bio-oil, although it also contains small amounts of organic matter. Most organic biomass decomposition products were condensed into the organic phase bio-oil including possible sugars, furans, aldehydes, ketones, aromatic compounds and carboxylic acids. The bio-char derived from microwave-assisted pyrolysis of spruce wood chips shows increased aromatisation compared with the raw material. For waste office paper and DIR, the inorganic components of raw materials (*e.g.*, calcium carbonate, kaolinite) remain in the bio-char and/or microwave residue.

## 2.6 NMR Characterization of bio-oils

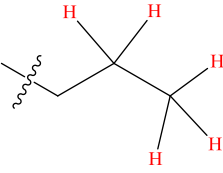
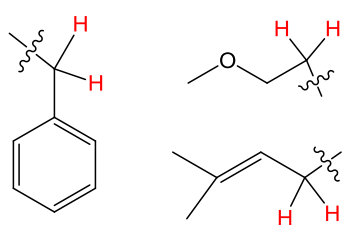
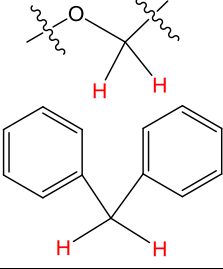
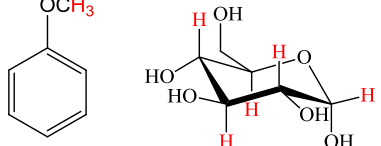
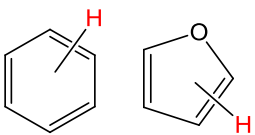
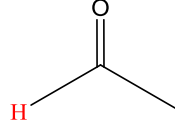
Due to the complex chemical nature of bio-oils, exact characterization of compositions of bio-oils was always a challenging task. Among the various spectroscopic and chromatographic characterization approaches, nuclear magnetic resonance (NMR) spectroscopy is a particularly useful technique for analysing bio-oil due to its great potential to characterize bio-oil in a nearly entire and intact way.<sup>182</sup> Several other commonly employed characterization techniques such as gas chromatography (GC), gas chromatography mass spectrometry (GC-MS), high-performance liquid chromatography (HPLC), gas permeation chromatography (GPC) *etc.* also allow detailed characterization of bio-oil. However, unlike NMR, these techniques could only identify and characterize partial selected fractions of bio-oil.<sup>182</sup> For instance, GC and GC-MS analysis is generally employed to identify and/or quantify individual components of bio-oil. However, since a large fraction of bio-oil comprises oligomers of carbohydrates and lignin which are not volatile enough to be detected by GC, only around 25 – 40% of bio-oil components could be detected by these methods.<sup>182 - 184</sup> Only water-soluble compounds could be identified and quantified by HPLC. While infrared (IR) spectroscopy could also give significant insights into functional groups of bio-oils, intensive overlapping of IR bands renders it ineffective for accurate assignment and identification of absorption bands.<sup>185</sup>

The liquid-state NMR characterization of bio-oils was carried out according to the procedure described in experimental section 4.2.9 in chapter 4. In order to obtain comprehensive structural information, both organic and aqueous phases of bio-oils produced from the low-temperature microwave-assisted pyrolysis processing of spruce wood chips, waste office paper and DIR were dissolved in dimethyl sulfoxide-d<sub>6</sub> (DMSO-d<sub>6</sub>) and subjected to <sup>13</sup>C and <sup>1</sup>H Nuclear Magnetic Resonance (NMR) spectroscopy characterization. Due to the complex chemical composition of bio-oils, vast numbers of resonance signals were detected in both phases of bio-oils. For ease of analysis, both the carbon and hydrogen resonance signals were broadly categorized into several groups according to literature.<sup>182</sup> Table 11 and Table 12 summarize the carbon and hydrogen assignments with respect to ranges of chemical shifts. Section 2.6.1, 2.6.2, 2.6.3 further discusses the liquid-state NMR analysis of bio-oils yielded from low-temperature microwave-assisted pyrolysis of spruce wood chips, waste office paper and DIR, respectively.

**Table 11:** Classification of bio-oil carbon contents in accordance with the chemical shift range<sup>182</sup>

Chemical shift (ppm)	Carbon assignments	Structure
<b>0 - 28</b>	Short aliphatic structures	
<b>28 - 55</b>	Long, branched aliphatic structures	
<b>55 - 105</b>	Carbohydrate sugars, alcohols, ethers	
<b>105 - 165</b>	Aromatics, olefins	
<b>165 - 180</b>	Carboxylic acids, esters	
<b>180 - 220</b>	Aldehydes, ketones	

**Table 12:** Classification of bio-oil hydrogen contents in accordance with the chemical shift range<sup>182</sup>

Chemical shift (ppm)	Carbon assignments	Structure
<b>0.5 – 1.5</b>	Alkanes	
<b>1.5 – 3.0</b>	Aliphatics $\alpha$ -to heteroatom or unsaturation	
<b>3.0 – 4.4</b>	Alcohols, Methylene-dibenzene	
<b>4.4 – 6.0</b>	Methoxy, carbohydrates	
<b>6.0 – 8.5</b>	(Hetero-) aromatics	
<b>9.5 – 10.1</b>	Aldehydes	

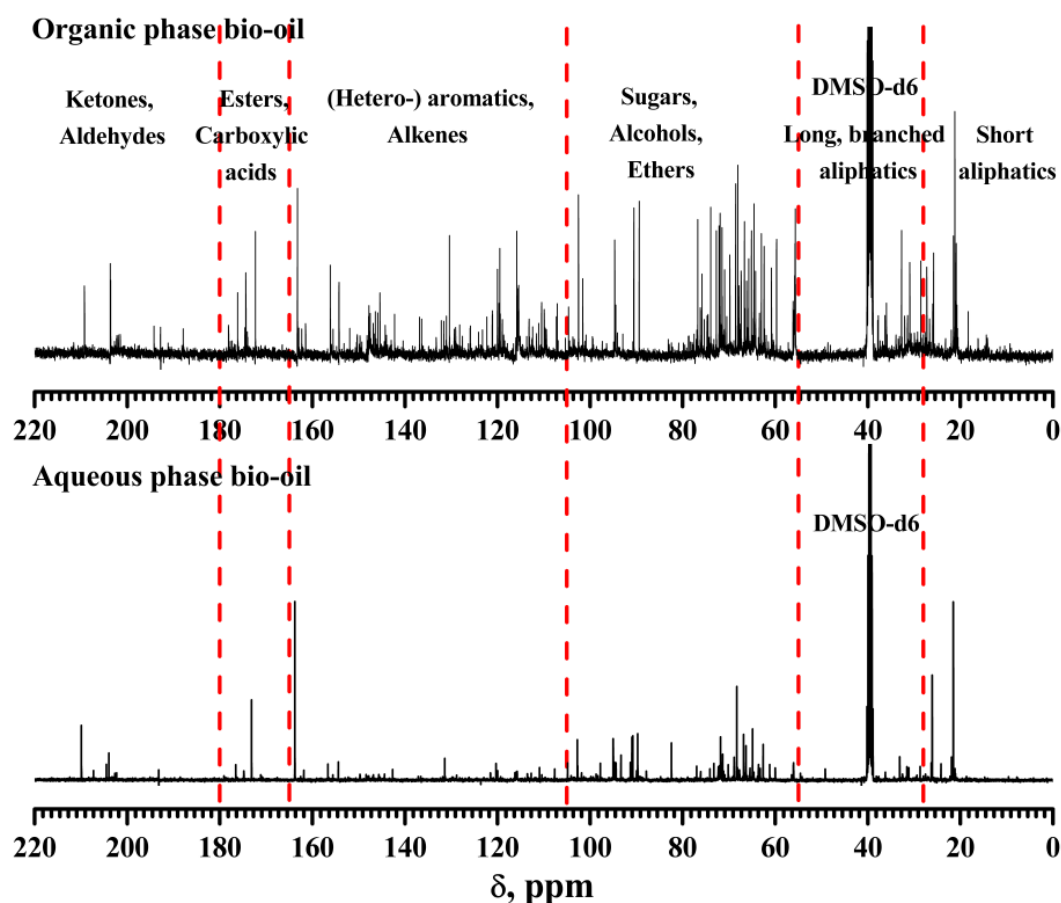
## **2.6.1 NMR characterization of spruce wood chips derived organic and aqueous phase bio-oils**

Figure 24 and 25 demonstrate the  $^{13}\text{C}$  and  $^1\text{H}$  NMR spectra of spruce wood chips derived organic and aqueous phase bio-oil, respectively. The complex chemical compositions of both the organic and aqueous phase bio-oils render it difficult to determine their exact compositions. However, the abundance of specific groups of compounds is clearly illustrated. From the liquid-state NMR spectra, it is evident that there are many differences in the overall chemical makeup of the spruce wood chips derived organic and aqueous phase bio-oils.

For the  $^{13}\text{C}$  NMR spectra of bio-oils (Figure 24), the central resonance of DMSO-d<sub>6</sub> ( $\delta\text{C}$ , 39.52 ppm) was used as the internal reference. Most carbohydrate sugars and their derivatives (*e.g.*, levoglucosan, levoglucosenone) generated from thermal degradation of cellulose and hemicellulose are present in the organic phase bio-oil, as indicated by the many complex signals in the typical sugar region (55 – 105 ppm). Compared with the  $^{13}\text{C}$  NMR spectrum of the organic phase bio-oil, that of the aqueous phase bio-oil contains fewer and much simpler signals in this region. Also, the intensities of these resonance signals in the  $^{13}\text{C}$  NMR spectrum of aqueous phase bio-oil are much lower, suggesting only small amounts of carbohydrate sugars and their derivatives were trapped in the aqueous phase bio-oil. The vast numbers of resonance signals in this region also indicate the possible presence of alcohols and ethers which contain carbon atoms adjacent to an oxygen atom. The high-intensity and sharp resonance signal observed at around 55 ppm in the  $^{13}\text{C}$  NMR spectrum of organic phase bio-oil is attributed to the carbon atoms in methoxy groups on phenolics such as guaiacol and syringol derivatives, which are common pyrolysis products of lignin.

The region between 105 ppm and 165 ppm in the  $^{13}\text{C}$  NMR spectra represents carbon atoms in (hetero-) aromatic structures. By assessing the  $^{13}\text{C}$  NMR spectra of these two phases of bio-oils, it is obvious that the organic phase bio-oil contains much more and higher amounts of (hetero-) aromatic components than the aqueous phase bio-oil. Also, most furan compounds are present in the organic phase bio-oil, as indicated by the resonance signals between 145 ppm and 165 ppm in the organic phase bio-oil. Similar trends can be observed in other regions of the  $^{13}\text{C}$

NMR spectra, indicating that the chemical composition of the organic phase bio-oil is much more complicated than that of the aqueous phase bio-oil.



**Figure 24:**  $^{13}\text{C}$  NMR spectra of organic and aqueous phase bio-oil generated from microwave-assisted processing of spruce wood chips. All spectra used the central resonance of DMSO-d<sub>6</sub> ( $\delta\text{C}$ , 39.52 ppm) as internal reference. (Originally in colour)

The  $^1\text{H}$  NMR spectra of spruce wood chips derived organic and aqueous phase bio-oil (Figure 25) also indicates that the organic phase bio-oil has a much more complex chemical composition profile than the aqueous phase bio-oil. The presence of aromatic compounds in the organic phase bio-oil is evidenced by the complex signals between 6.0 ppm and 8.5 ppm. The signals in this region not only represent hydrogen atoms in benzenoids, but also those in hetero aromatic compounds which contain oxygen atoms. Compared with the  $^1\text{H}$  NMR spectrum of organic phase bio-oil, few signals were detected in the aromatic region (6.0 ppm – 8.5 ppm) of

the  $^1\text{H}$  NMR spectrum of aqueous phase bio-oil. This observation further confirms that most (hetero-) aromatic compounds were condensed in the organic phase bio-oil).

The resonance signals of the aromatic ether protons presenting in guaiacol and syringol derivatives (lignin degradation products) are observed between 4.4 ppm and 6.0 ppm. This is in good agreement with the  $^{13}\text{C}$  NMR analysis of the organic phase bio-oil discussed above. Resonance signals in this region also represent many of the hydrogen atoms in carbohydrate sugars and their derivatives. Due to the high amounts of carbohydrates produced from thermal degradation of cellulose and hemicellulose during pyrolysis, this region (4.4 ppm – 6.0 ppm) is the most populated and complex region in the  $^1\text{H}$  NMR spectrum of the bio-oils.

High amounts of water were generated and collected in the aqueous phase bio-oil during the microwave-assisted pyrolysis process, resulting in a broad resonance signal centred around 4.20 ppm in the  $^1\text{H}$  NMR spectrum of the spruce wood chips derived aqueous phase bio-oil. In contrast, water content of the organic phase bio-oil is very low (only around 2 wt.%). Hence the  $^1\text{H}$  NMR spectrum of the organic phase bio-oil does not contain an obvious water resonance signal. Resonance signals in the region between 3.0 and 4.4 ppm suggest the possible presence of alcohols and ethers. In addition, this region also represents protons in methylene groups that join two aromatic rings. These moieties may exist in partially degraded lignin oligomers. The resonance signals in the most downfield region (9.5 ppm – 10 ppm) of the  $^1\text{H}$  NMR spectra indicate the presence of aldehydes and also possible trace amounts of carboxylic acids. The intensities of these signals in the spectrum of the aqueous phase bio-oil are lower than those of the signals in the spectrum of the organic phase bio-oil.

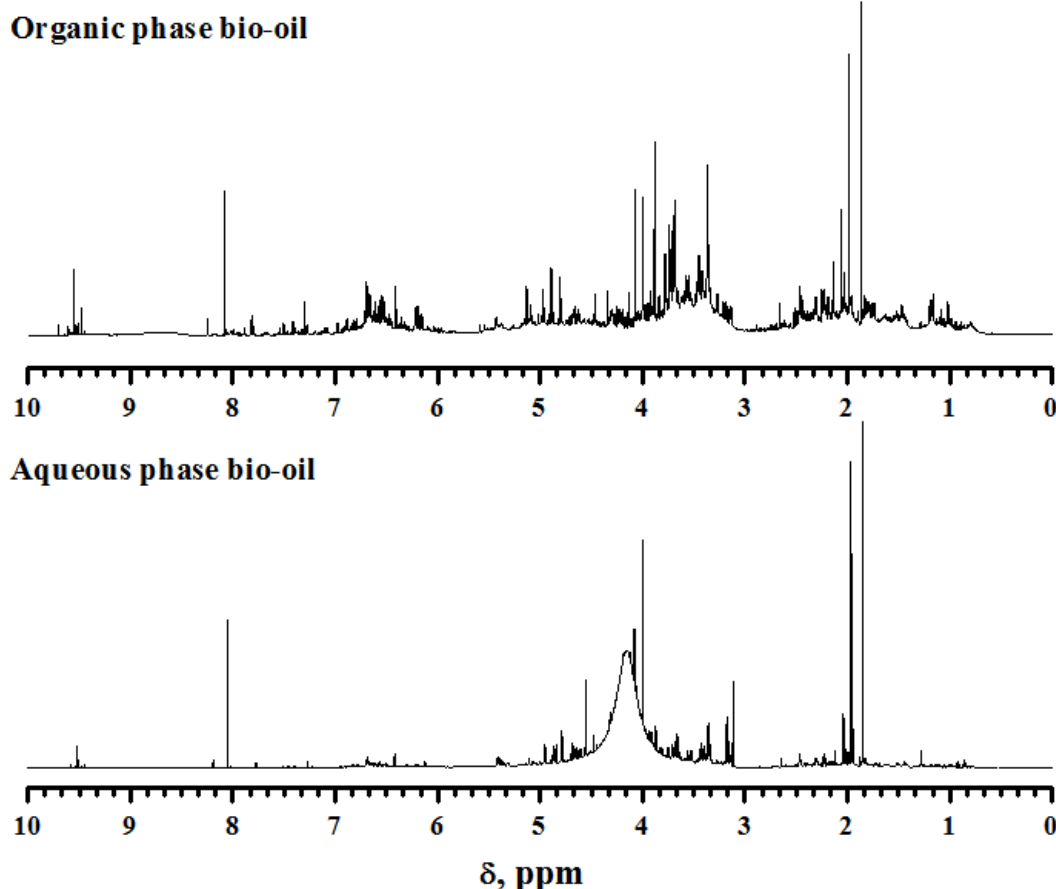


**Figure 25:**  $^1\text{H}$  NMR spectra of organic and aqueous phase bio-oil generated from microwave-assisted processing of spruce wood chips. (Originally in colour)

### 2.6.2 NMR characterization of waste office paper derived organic and aqueous phase bio-oils

Figure 26 illustrates the  $^{13}\text{C}$  NMR spectra of organic and aqueous phase bio-oils yielded from microwave-assisted low-temperature ( $<200\text{ }^\circ\text{C}$ ) pyrolysis of waste office paper. The spectrum of organic phase bio-oil shows more signals and was of greater intensity than that of the aqueous phase bio-oil between 55 and 105 ppm, suggesting more carbohydrates and their derivatives (*e.g.*, levoglucosan, levoglucosenone) were trapped in the organic phase bio-oil. A similar trend was observed in the (hetero-) aromatic region (110 – 165 ppm), which implies the organic phase bio-oil contains more (hetero-) aromatic compounds than the aqueous phase bio-oil. Although the true identify has not been ascertained, possible compounds in this region could include 5-(hydroxyl-methyl)-2-furaldehyde (HMF) and phenolic compounds. It is well documented in the literature that simple phenols are present in bio-oils obtained from pyrolysis of cellulose and

hemicelluloses.<sup>186, 187</sup> These relatively small amounts of phenolics may come either from gas phase polymerization of small molecular weight unsaturated species<sup>187</sup> or from hydrothermolysis of HMF or other furan derivatives.<sup>188</sup> Luijkx *et al.* studied the reaction pathway for hydrothermal transition of HMF to 1, 2, 4-trihydroxybenzene, which may also be present in the organic phase bio-oil.<sup>188</sup> A small portion of signals in this region may also be attributed to phenolics derived from lignin pyrolysis, as lignin content in office paper is up to 6%, but this is yet to be fully ascertained.<sup>174</sup>

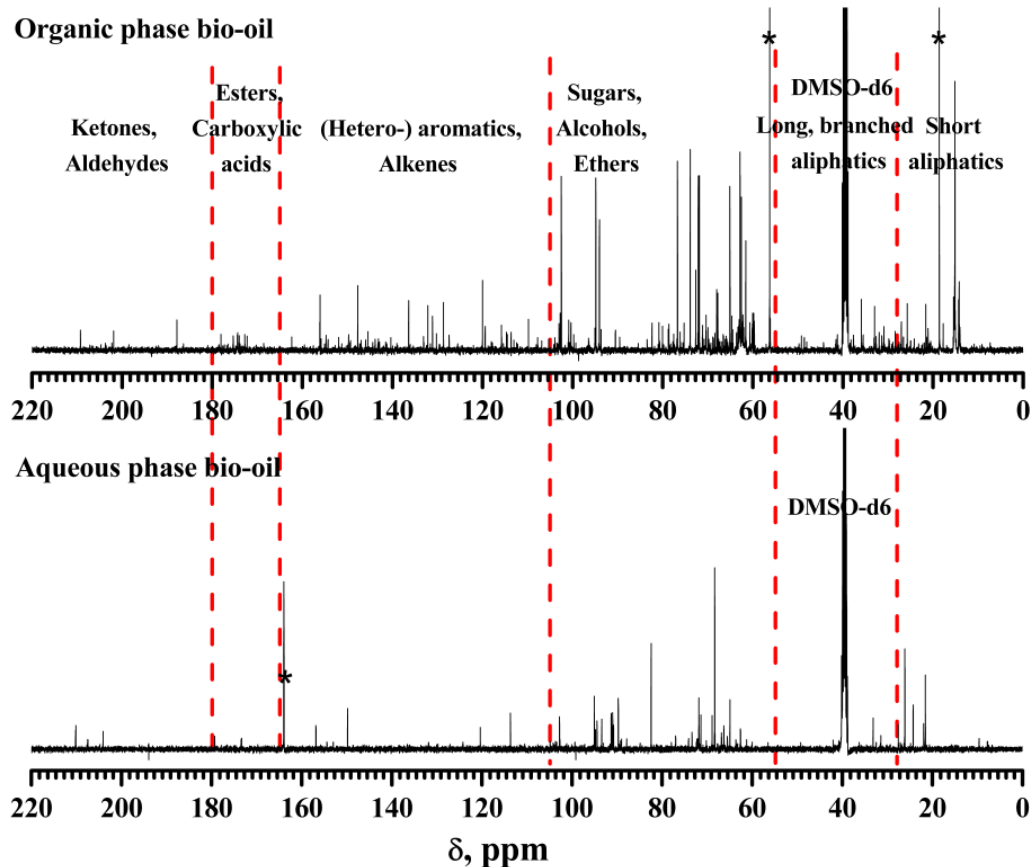


**Figure 26:**  $^{13}\text{C}$  NMR spectra of organic and aqueous phase bio-oil generated from microwave-assisted processing of waste office paper. All spectra used the central resonance of DMSO-d<sub>6</sub> ( $\delta\text{C}$ , 39.52 ppm) as internal reference. (Originally in colour)

Both the organic and aqueous phase bio-oils produced from microwave-assisted low-temperature (<200 °C) pyrolysis of waste office paper contain carbonyl carbons: carboxylic acids and esters (165 – 180 ppm); ketones and aldehydes (180 – 215 ppm). The types of

carbonyl carbons in the organic phase bio-oil are more various and complex than those of the aqueous phase bio-oil. Among these, levulinic acid (4-oxopentanoic acid) is a common acid derived from HMF during pyrolysis of biomass. Signals between 0 and 55 ppm are attributed to aliphatic structures within the bio-oil.

The  $^1\text{H}$  NMR spectra of waste office paper derived organic and aqueous phase bio-oils are illustrated in Figure 27. The presence of (hetero-) aromatic compounds in the organic phase bio-oil is further evidenced by the many resonance signals in the (hetero-) aromatic region of the spectrum (6.0 ppm – 8.5 ppm), although the intensities of these signals are not high. In contrast, the  $^1\text{H}$  NMR spectrum of the aqueous phase bio-oil contains few signals in this region, indicating almost all the (hetero-) aromatic compounds were collected into the organic phase bio-oil. In addition, the  $^1\text{H}$  NMR spectrum of the organic phase bio-oil shows much more and complex resonance signals and is of greater intensity in other regions compared with that of the aqueous phase bio-oil. This is in good consistency with the  $^{13}\text{C}$  NMR analysis that most carbohydrate sugars and their derivatives, alcohols, ethers, furans *etc.* generated from microwave-assisted pyrolysis of waste office paper were condensed into the organic phase bio-oil. The  $^1\text{H}$  NMR spectrum of the aqueous phase bio-oil shows an intense and broad resonance signal in the range between 3.10 ppm and 3.90 ppm. This resonance signal is attributed to high amounts of water present in this phase of bio-oil. The chemical shift of water may vary significantly depending on its amounts and chemical environment.

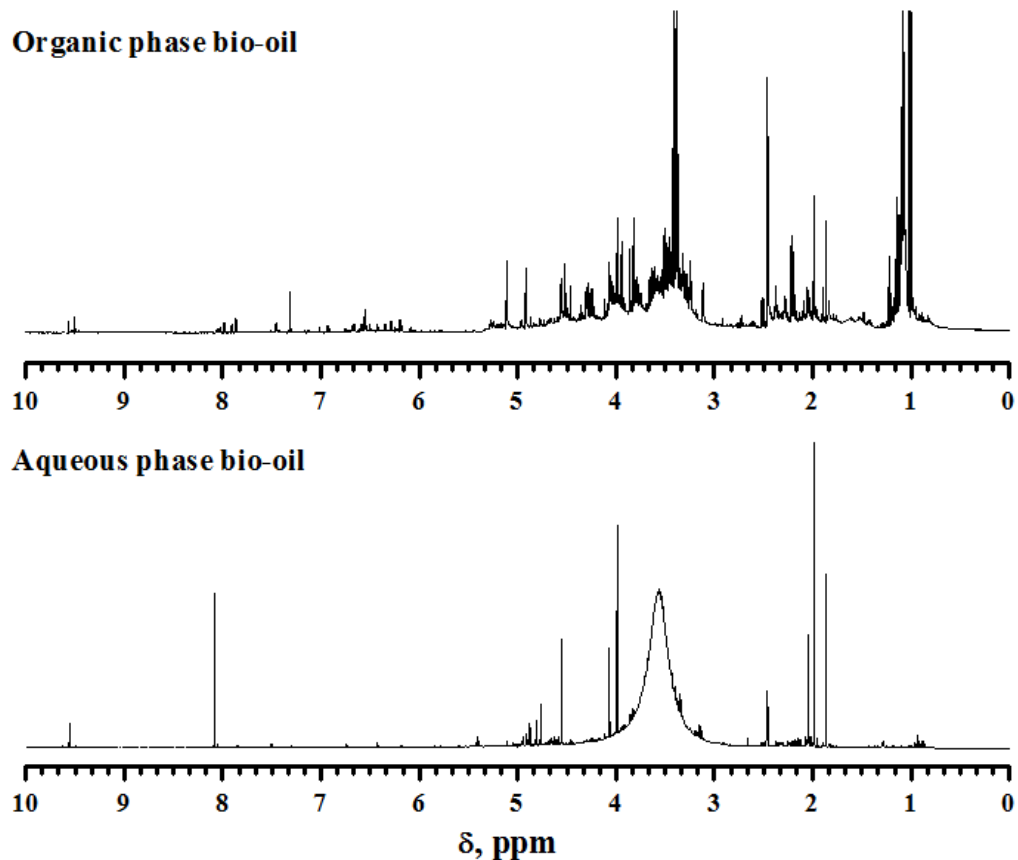


**Figure 27:**  $^1\text{H}$  NMR spectra of organic and aqueous phase bio-oil generated from microwave-assisted processing of waste office paper.

### 2.6.3 NMR characterization of DIR derived organic and aqueous phase bio-oils

Figure 28 and 29 demonstrate the  $^{13}\text{C}$  and  $^1\text{H}$  NMR spectra of DIR derived organic and aqueous phase bio-oils. Similar to the  $^{13}\text{C}$  and  $^1\text{H}$  NMR spectra of organic and aqueous phase bio-oils produced from microwave-assisted low-temperature ( $<200\text{ }^\circ\text{C}$ ) pyrolysis of spruce wood chips and waste office paper, there are significant differences in the overall chemical composition of the two bio-oil phases.

It is obvious that most carbohydrate sugars and their derivatives were condensed into the organic phase bio-oil, as the typical sugar region (55 – 105 ppm) contains many more and complicated signals in the spectrum of the DIR organic phase bio-oil compared with that of the DIR aqueous phase bio-oil. For example, levoglucosan is a common partially dehydrated sugar derivative resulting from pyrolysis of cellulosic matter. Signals in this region may also come

from carbons that are adjacent to an oxygen atom in ethers or alcohols. A similar trend can be observed between 105 and 165 ppm, where most carbon atoms in (hetero-) aromatic and alkene compounds resonate. Furan compounds were also present in both the DIR organic and aqueous phase bio-oils as several signals were detected between 145 and 165 ppm, in which region typical furan components resonate. The signals between 165 and 180 ppm are assigned to carbonyl carbon atoms of carboxylic acids and esters, while those between 180 and 220 ppm are due to carbonyl carbons of ketones and aldehydes. Resonance signals for aliphatic structures are observed from 0 to 55 ppm: short chain aliphatics (0 – 28 ppm) and branched long chain aliphatics (28 – 55 ppm). This region is very complicated with signals originating not only from aliphatics in the bio-oil, but also alkyl structures associated with sugar derivatives, aromatics, furans, ketones, esters, ethers, aldehydes and carboxylic acids.

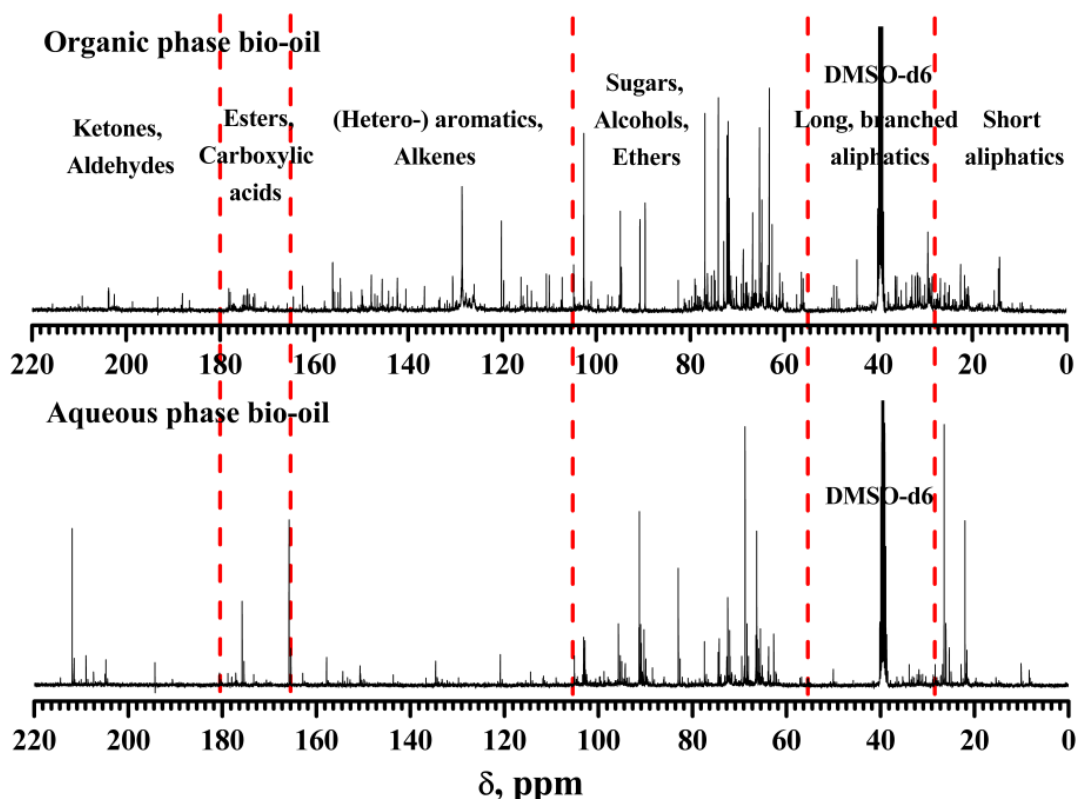


**Figure 28:**  $^{13}\text{C}$  NMR spectra of organic and aqueous phase bio-oil generated from microwave-assisted processing of DIR. All spectra used the central resonance of DMSO-d<sub>6</sub> ( $\delta\text{C}$ , 39.52 ppm) as internal reference. (Originally in colour)

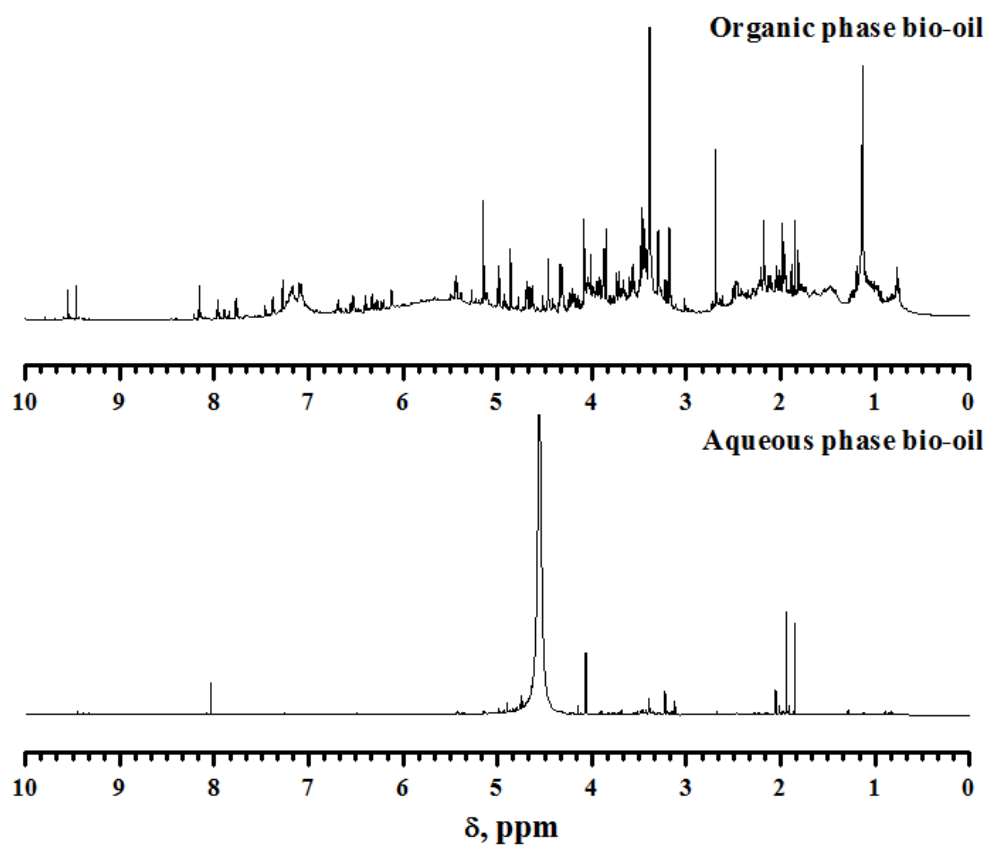


**Figure 29:**  $^1\text{H}$  NMR spectra of organic and aqueous phase bio-oil generated from microwave-assisted processing of DIR.

Similar to the discussions for NMR analysis of bio-oils derived from spruce wood chips (section 2.6.1) and waste office paper (section 2.6.2), the  $^1\text{H}$  NMR spectra of the DIR derived organic and aqueous phase bio-oil also show significant differences in their chemical compositions. For instance, (hetero-) aromatic compounds are present in the organic phase bio-oil, whereas the  $^1\text{H}$  NMR spectrum of the DIR aqueous phase bio-oil is almost clean in the aromatic region (6.0 ppm – 8.5 ppm). Also, a similar trend could be observed in other regions of the  $^1\text{H}$  NMR spectra. In contrast to the organic phase bio-oil, the aqueous phase bio-oil mainly contains water as evidenced by the broad and intense resonance signal at around 4.60 ppm and trace amounts of other chemical components.

#### 2.6.4 Summary of liquid-state $^1\text{H}$ and $^{13}\text{C}$ NMR characterization of bio-oils

Overall, the  $^1\text{H}$  and  $^{13}\text{C}$  NMR characterization of both organic and aqueous phase bio-oils derived from microwave-assisted low-temperature ( $<200$  °C) pyrolysis of spruce wood chips,

waste office paper and DIR provides a holistic overview of their chemical compositions. In consistence with infrared spectroscopy characterization, the NMR analysis further proves the efficiency of the separating system employed in the pyrolysis experiments. Most organic biomass decomposition products including carbohydrate sugars and their derivatives, aromatic compounds, furans, aldehydes, ketones, esters, aliphatic compounds *etc.* were trapped into the organic phases. The aqueous bio-oil phases essentially contain high amounts of water mainly generated from dehydration reactions of biomass compounds during pyrolysis processes, together with small amounts of organic compounds.

By comparing the  $^{13}\text{C}$  NMR spectra of organic phases of bio-oils generated from microwave-assisted pyrolysis of spruce wood chips (Figure 24), waste office paper (Figure 26) and DIR (Figure 28), especially in the range between 105 ppm and 165 ppm where most aromatic and alkene carbons resonate, it is noteworthy that both the amounts and intensities of carbon resonance signals for the spruce wood chips derived organic phase bio-oil are greater. This is attributed to the higher lignin content of spruce wood chips compared with that of waste office paper and DIR.

## 2.7 GC-MS characterization of bio-oils

Gas chromatography-mass spectrometry (GC-MS) characterization was performed to identify the compounds obtained in the organic and aqueous phases of bio-oils produced from the microwave-assisted low-temperature ( $<200\ ^\circ\text{C}$ ) pyrolysis of spruce wood chips, waste office paper and DIR. The qualitative GC-MS characterization of bio-oils was conducted according to the procedure described in the experimental section 4.2.10 in chapter 4. Qualification analysis of chemical compositions of bio-oils was carried out by comparison with the National Institute of Standards and Technology 2008 mass spectral library (NIST 2008 library). The NIST library is a database of mass spectra allowing for the prediction of chemical structures of different components by the mass fragmentation. For the identification of chromatographic peaks, the NIST 2008 mass spectral library was employed in this study to search for the best possible match mass spectra.

Due to the complex chemical compositions of both organic and aqueous phase bio-oils, many chromatographic peaks were detected in the gas chromatography (GC) traces for both phases of bio-oils, even though generally only a relatively small fraction (around 25%) of bio-oil compounds can be observed by GC, as most lignin and carbohydrate oligomers have insufficient volatility under the operating conditions of the instrument.<sup>182 - 184</sup> As a result, complete and accurate identification of chromatographic peaks in GC traces is very difficult and only those separated products in considerable amounts were qualified. The GC-MS analysis of organic and aqueous phase bio-oils derived from spruce wood chips, waste office paper and DIR are discussed in section 2.7.1, section 2.7.2 and section 2.7.3, respectively.

### **2.7.1 GC-MS characterization of spruce wood chips derived bio-oils**

Figure 30 demonstrates the GC traces of spruce wood chips derived organic (Figure 30 A) and aqueous phase bio-oil (Figure 30 B). The major identified compounds according to the NIST 2008 mass spectral library in the organic and aqueous phase bio-oils are summarized in Table 13 and Table 14, respectively.

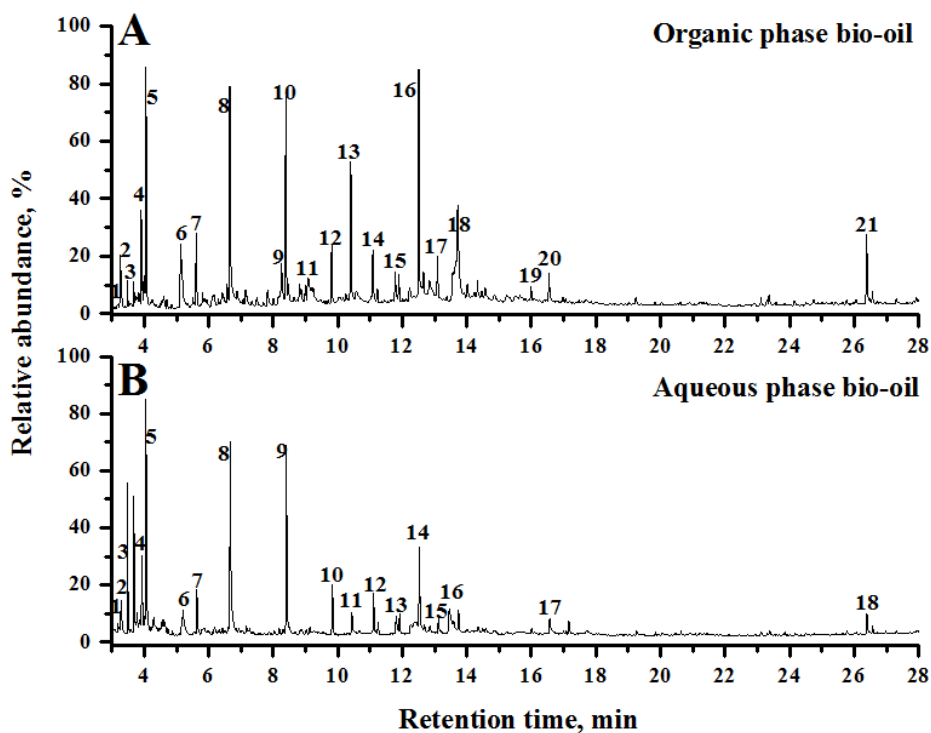


**Figure 30:** GC-MS spectra of (A) organic and (B) aqueous phase bio-oils derived from microwave-assisted pyrolysis of spruce wood chips.

**Table 13:** Major identified compounds in spruce wood chips derived organic phase bio-oil<sup>a</sup>

<b>Peak number</b>	<b>Retention time (min)</b>	<b>Identified compound</b>
1	3.18	Acetic acid
2	3.28	Furfural
3	3.48	Tetrahydro-2,5-dimethoxyfuran
4	3.91	2(5 <i>H</i> )-Furanone
5	4.05	2-Hydroxycyclopent-2-en-1-one
6	5.17	1-Hydroxy-2-pentanone
7	5.61	3-Methyl-1,2-cyclopentanedione
8	6.65	2-Methoxyphenol (Guaiacol)
9	8.18	Levoglucosenone
10	8.39	2-Methoxy-4-methylphenol
11	9.07	1,2-Benzenediol (Catechol)
12	9.81	4-Ethyl-2-methoxyphenol
13	10.40	2-Methoxy-4-vinylphenol
14	11.09	3-Allyl-6-methoxyphenol
15	11.78	5-(Hydroxymethyl)-2-furaldehyde (HMF)
16	12.51	2-Methoxy-4-(1-propenyl)phenol
17	13.09	1-(4-Hydroxy-3-methoxyphenyl)ethanone
18	13.72	Levoglucosan
19	15.99	4-Hydroxy-3-methoxy-phenylacetyl formic acid
20	16.54	4-Hydroxy-2-methoxycinnamaldehyde
21	26.39	10,11-Dihydro-10-hydroxy-2,3-dimethoxydibenz(b,f)oxepin

<sup>a</sup>According to the NIST 2008 database.

**Table 14:** Major identified compounds in spruce wood chips derived aqueous phase bio-oil<sup>a</sup>

Peak number	Retention time (min)	Identified compound
1	3.18	Acetic acid
2	3.28	Furfural
3	3.48	Tetrahydro-2,5-dimethoxyfuran
4	3.92	2(5H)-Furanone
5	4.06	2-Hydroxycyclopent-2-en-1-one
6	5.20	1-Hydroxy-2-pentanone
7	5.62	3-Methyl-1,2-cyclopentanedione
8	6.66	2-Methoxyphenol (Guaiacol)
9	8.40	2-Methoxy-4-methylphenol
10	9.83	4-Ethyl-2-methoxyphenol
11	10.43	2-Methoxy-4-vinylphenol
12	11.11	3-Allyl-6-methoxyphenol
13	11.81	5-(Hydroxymethyl)-2-furaldehyde (HMF)
14	12.53	2-Methoxy-4-(1-propenyl)phenol
15	13.10	1-(4-Hydroxy-3-methoxyphenyl)ethanone
16	13.75	Levoglucosan
17	16.56	4-Hydroxy-2-methoxycinnamaldehyde
18	26.38	10,11-Dihydro-10-hydroxy-2,3-dimethoxydibenz(b,f)oxepin

<sup>a</sup>According to the NIST 2008 database.

Carboxylic acids such as acetic acid were detected in both phases of bio-oils (Peak marked ‘1’ in Figure 30 A and B), the compounds identified between three and seven minutes mainly include furans and their derivatives such as furfural (peak marked ‘2’ Figure 30 A and B) and tetrahydro-2, 5-dimethoxyfuran (peak marked ‘3’ in Figure 30 A and B), together with several small polar molecules. 5-(Hydroxymethyl)-2-furaldehyde (HMF) was also observed at around 11.78 min in both phases of bio-oils (peak marked ‘15’ in Figure 30 A and peak marked ‘13’ in Figure 30 B). The high-intensity chromatographic peaks observed between 6 and 13 minutes in

both GC traces of the two phases of bio-oils are mainly assigned to phenolic compounds. Compounds identified in this region (about 6 – 13 min) essentially comprise 2-methoxyphenol (guaiacol, peak marked ‘8’ in Figure 30 A and B), 2-methoxy-4-methylphenol (creosol, peak marked ‘10’ in Figure 30 A and peak marked ‘9’ in Figure 30 B), 4-ethyl-2-methoxyphenol (4-ethylguaiacol, peak marked ‘12’ in Figure 30 A and peak marked ‘10’ in Figure 30 B), 2-methoxy-4-vinylphenol (peak marked ‘13’ in Figure 30 A and peak marked ‘11’ in Figure 2.17 B), 2-methoxy-4-(1-propenyl)phenol (peak marked ‘16’ in Figure 30 A and peak marked ‘14’ in Figure 30 B). Also, 1, 2-benzenediol (catechol) is present in the organic phase bio-oil (peak marked ‘11’ in Figure 30 A). The many (substituted) phenolic compounds detected in both bio-oil phases indicate significant breakdown/decomposition of the lignin content of spruce wood chips during the microwave-assisted low-temperature (<200 °C) pyrolysis process. In addition, it is obvious that many more chromatographic peaks (also of greater intensities) appear in the GC trace of organic phase bio-oil (Figure 30 A) compared to that of the aqueous phase bio-oil (Figure 30 B) in the region between 6 – 13 minutes. This suggests that the chemical composition of the volatile fraction of the organic phase bio-oil is much more complex than that of the aqueous phase bio-oil, and the concentrations of these organic compounds are probably higher in the organic phase bio-oil. The chemical structures of several above mentioned typical phenolic compounds generated from thermolysis of lignin are illustrated in Figure 31.

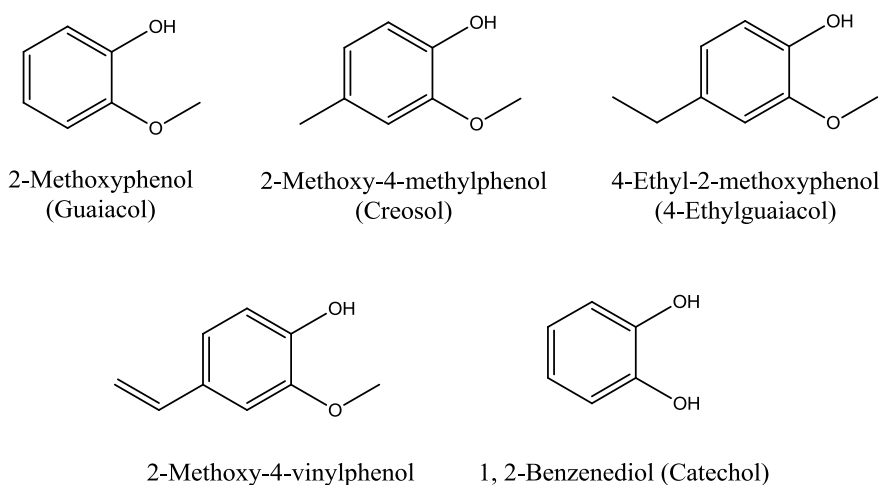


**Figure 31:** Chemical structures of several representative aromatic compounds derived from thermal degradation of lignin.

In addition, sugars such as levoglucosan and levoglucosenone are observed in the GC trace of organic phase bio-oil (peak marked ‘18’ for levoglucosan and peak marked ‘9’ for levoglucosenone in Figure 30 A). These carbohydrate derivatives were generated from thermal decomposition of cellulosic matter of spruce wood chips. Interestingly, trace amounts of levoglucosan was also trapped into the aqueous phase bio-oil (peak marked ‘16’ in Figure 30 B). The chromatographic peak for levoglucosan in the GC trace of aqueous phase bio-oil (Figure 30 B) is significantly smaller than that in the GC trace of organic phase bio-oil (Figure 30 A), indicating most of carbohydrate sugar derivatives were condensed into the organic phase bio-oil. Levoglucosenone was not detected in the aqueous phase bio-oil. The chemical structures for levoglucosan and levoglucosenone are shown in Figure 32.

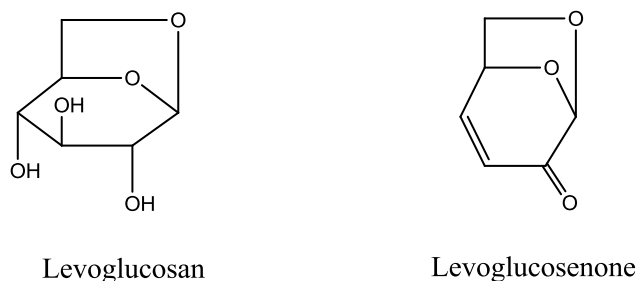


**Figure 32:** Chemical structures of levoglucosan and levoglucosenone.

The chromatographic peak shown at around 26.3 min in the GC traces of both organic (peak marked ‘21’ in Figure 30 A) and aqueous phase bio-oil (peak marked ‘18’ in Figure 30 B) at around 26.4 min is assigned to a poly-aromatic compound named 10, 11-dihydro-10-hydroxy-2,3-dimethoxydibenz(b,f)oxepin, which is probably an oligomer derived from lignin. The same compound was observed before by Liu and Zhang in their study about liquefaction of biomass for the production of fuels and chemical feedstocks.<sup>189</sup> The size of this chromatographic peak in the GC trace of organic phase bio-oil (Figure 30 A) is significantly larger than that in the GC trace of aqueous phase bio-oil (Figure 30 B). Similarly, this also confirms that most organic pyrolysis products were collected in the organic phase bio-oil despite few amounts of organic matter was also trapped into the aqueous phase bio-oil during the pyrolysis process.

## 2.7.2 GC-MS characterization of waste office paper derived bio-oils

Figure 33 illustrates the GC traces of organic (Figure 33 A) and aqueous phase bio-oil (Figure 33 B) derived from waste office paper. The major identified compounds in the waste office paper derived organic and aqueous phase bio-oil are summarized in Table 15 and Table 16, respectively.

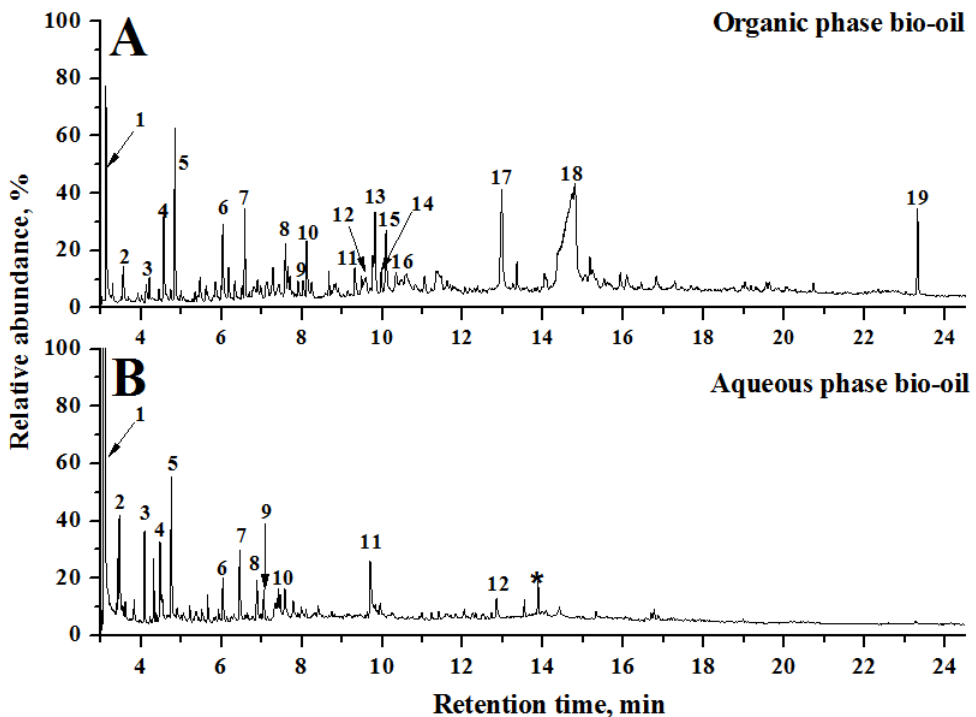


**Figure 33:** GC-MS spectra of (A) organic and (B) aqueous phase bio-oils derived from microwave-assisted pyrolysis of milled waste office paper. \*Possible artefacts

The main difference between the organic phase bio-oil and the aqueous phase bio-oil is the absence of levoglucosan (peak marked '18' in Figure 33 A) in the latter. The compounds identified in the organic phase bio-oil can be broadly categorized into several groups: carbohydrate and their derivatives such as 1,4:3,6-dianhydro- $\pi$ D-glucopyranose (peak marked '13' in Figure 33 A), 3,4-anhydro-D-galactosan (peak marked '14' in Figure 33 A) and levoglucosan; possible phenolic compounds such as guaiacol (peak marked '8' in Figure 33 A), benzenetriol (peak marked '10' in Figure 33 A) and 1,2-benzenediol (catechol, peak marked '12' in Figure 33 A) but their true identity is still to be ascertained; furanic structures such as furfural (peak marked '2' in Figure 33 A), tetrahydro-2,5-dimethoxyfuran (peak marked '3' in Figure 33 A).

A) and 5-(hydroxymethyl)-2-furaldehyde (HMF, peak marked ‘16’ in Figure 33 A). The organic phase bio-oil also contains acetic acid (peak marked ‘1’ in Figure 33 A) and 4, 4’-(1-methylethylidene) bisphenol (bisphenol A, peak marked ‘19’ in Figure 33 A) which is a common additive in paper products added during the manufacture of paper.<sup>190</sup> The aqueous phase bio-oil (Figure 33 B and Table 16) comprises a similar compositional profile in the range 3–10 min albeit with fewer components. Water soluble acids are noted together with polar small molecules. Using the vacuum pump in the microwave-assisted low-temperature (<200 °C) pyrolysis experiments as described in section 2.3.1, these smaller molecules together with most water were transferred across the tube fitted between the two round-bottom flasks and condensed into the aqueous phase bio-oil.

**Table 15:** Major identified compounds in waste office paper derived organic phase bio-oil<sup>a</sup>

<b>Peak number</b>	<b>Retention time (min)</b>	<b>Identified compound</b>
1	3.13	Acetic acid
2	3.56	Furfural
3	4.15	Tetrahydro-2,5-dimethoxyfuran
4	4.57	2(5H)-Furanone
5	4.85	1,2-Cyclopentanedione
6	6.04	1-Hydroxy-2-pentanone
7	6.58	3-Methyl-1,2-cyclopentanedione
8	7.59	2-Methoxyphenol (Guaiacol) <sup>b</sup>
9	8.03	Levoglucosenone
10	8.12	Benzeneetriol <sup>b</sup>
11	9.31	2-Furanmethanol
12	9.76	1,2-Benzenediol (Catechol) <sup>b</sup>
13	9.82	1,4:3,6-Dianhydro- $\pi$ d-glucopyranose
14	10.09	3,4-Anhydro-d-galactosan
15	10.34	3-Methylbenzaldehyde
16	10.6	5-(Hydroxymethyl)-2-furaldehyde (HMF)
17	12.96	5-Hydroxy-9-oxabicyclo[3.3.1]nonan-2-one
18	14.7	Levoglucosan
19	23.3	4,4'-(1-Methylethylidene)bisphenol

<sup>a</sup>According to the NIST 2008 database. <sup>b</sup>Tentative assignment.

**Table 16:** Major identified compounds in waste office paper derived aqueous phase bio-oil<sup>a</sup>

Peak number	Retention time (min)	Identified compound
1	3.13	Acetic acid
2	3.46	Furfural
3	4.09	Tetrahydro-2,5-dimethoxyfuran
4	4.49	2(5H)-Furanone
5	4.76	1,2-Cyclopentanedione
6	6.04	1-Hydroxy-2-pentanone
7	6.46	3-Methyl-1,2-cyclopentanedione
8	6.88	1,2,3-Butanetriol
9	7.05	2,2-Dimethyl-acetoacetic acid ethyl ester
10	7.46	2,5-Dimethyl-4-hydroxy-3(2H)-furanone
11	9.69	1,4:3,6-Dianhydro- $\pi$ D-glucopyranose
12	12.95	5-Hydroxy-9-oxabicyclo[3.3.1]nonan-2-one

<sup>a</sup>According to the NIST 2008 database.

### 2.7.3 GC-MS characterization of DIR derived bio-oils

Figure 34 demonstrates the GC traces of organic (Figure 34 A) and aqueous phase bio-oil (Figure 34 B) generated from microwave-assisted pyrolysis of DIR. The major identified compounds in the DIR derived organic and aqueous phase bio-oil are summarized in Table 17 and Table 18, respectively.

Similar to the bio-oils derived from spruce wood chips and waste office paper, the chemical composition of DIR derived organic phase bio-oil is very complex as indicated by the many chromatographic peaks shown in Figure 34 A. Carbohydrate sugars and their derivatives such as levoglucosan (peak marked as ‘22’ in Figure 34 A), 1,4:3,6-dianhydro- $\pi$ -D-glucopyranose (peak marked as ‘18’ in Figure 34 A), 3,4-anhydro-D-galactosan (peak marked as ‘19’ in Figure 34 A) and levoglucosenone (peak marked as ‘12’ in Figure 34 A) were identified in the DIR derived organic phase bio-oil. Furans and their derivatives including 5-(hydroxymethyl)-2-furaldehyde

(HMF, peak marked as ‘20’ in Figure 34 A) also present in this phase of bio-oil, together with many smaller polar molecules such as acetic acid and ketones.

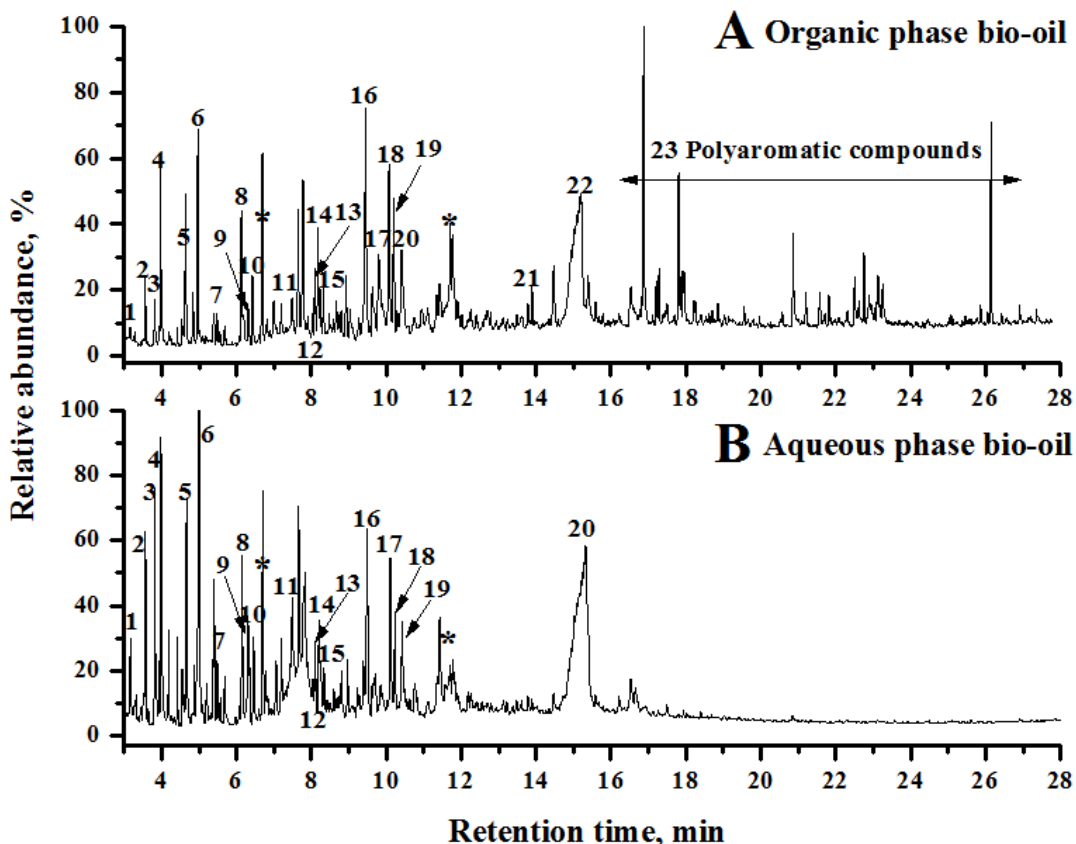


**Figure 34:** GC-MS spectra of (A) organic and (B) aqueous phase bio-oils derived from microwave-assisted pyrolysis of DIR. \*Possible artefacts

The compositional profile of the DIR derived aqueous phase bio-oil is very similar to that of the organic phase bio-oil in the region between 3 and 16 minutes. Levoglucosan was also trapped into the aqueous phase bio-oil during microwave-assisted pyrolysis of DIR (peak marked ‘20’ in Figure 34 B). In comparison with the GC traces of bio-oils derived from spruce wood chips and waste office paper, it is noteworthy that the GC traces of DIR derived bio-oil show much more chromatographic peaks in the region between 3 and 16 min. This indicates that the DIR derived bio-oils contain much many smaller molecules than the bio-oils produced from spruce wood chips and waste office paper. This effect probably arises from the much higher inorganic mineral content of DIR compared with spruce wood chips and waste office paper. It is possible

that the metals within DIR catalysed the thermal decomposition of DIR and even initiated many other chemical reactions between pyrolysis products.

**Table 17:** Major identified compounds in DIR derived organic phase bio-oil<sup>a</sup>

Peak number	Retention time (min)	Identified compound
1	3.16	Acetic acid
2	3.57	Furfural
3	3.81	Tetrahydro-2,5-dimethoxyfuran
4	3.97	2-Furanmethanol
5	4.64	2(5H)-Furanone
6	4.97	1,2-Cyclopentanedione
7	5.46	5-Methyl-2-furancarboxaldehyde
8	6.13	3-Methyl-1,2-cyclopentanedione
9	6.31	Phenol
10	6.42	2-Methoxyphenol (Guaiacol)
11	7.65	2,5-Dimethyl-4-hydroxy-3(2H)-furanone
12	8.09	Levoglucosenone
13	8.17	3-Hydroxy-2-methyl-4H-pyran-4-one (Maltol)
14	8.23	2(3H)-Furanone, dihydro-5-pentyl-
15	8.32	3-Ethyl-2-hydroxy-2-Cyclopenten-1-one
16	9.62	2-Methoxy-4-methylphenol
17	9.8	Butanoic acid, propyl ester
18	10.07	1,4:3,6-Dianhydro- $\pi$ D-glucopyranose
19	10.20	3,4-Anhydro-D-galactosan
20	10.41	5-(Hydroxymethyl)-2-furaldehyde (HMF)
21	13.89	2-Methoxy-4-(1-propenyl)phenol
22	15.18	Levoglucosan
23	16 - 28	Polyaromatic compounds

<sup>a</sup>According to the NIST 2008 database.

**Table 18:** Major identified compounds in DIR derived aqueous phase bio-oil<sup>a</sup>

<b>Peak number</b>	<b>Retention time (min)</b>	<b>Identified compound</b>
1	3.17	Acetic acid
2	3.57	Furfural
3	3.81	Tetrahydro-2,5-dimethoxyfuran
4	3.97	2-Furanmethanol
5	4.67	2(5 <i>H</i> )-Furanone
6	5.01	1,2-Cyclopentanedione
7	5.48	5-Methyl-2-furancarboxaldehyde
8	6.15	3-Methyl-1,2-cyclopentanedione
9	6.32	Phenol
10	6.45	2-Methoxyphenol (Guaiacol)
11	7.66	2,5-Dimethyl-4-hydroxy-3(2 <i>H</i> )-furanone
12	8.10	Levoglucosenone
13	8.20	3-Hydroxy-2-methyl-4 <i>H</i> -pyran-4-one (Maltol)
14	8.25	2(3 <i>H</i> )-Furanone, dihydro-5-pentyl-
15	8.35	3-Ethyl-2-hydroxy-2-Cyclopenten-1-one
16	9.63	2-Methoxy-4-methylphenol
17	10.11	1,4:3,6-Dianhydro- $\pi$ D-glucopyranose
18	10.23	3,4-Anhydro-d-galactosan
19	10.42	5-(Hydroxymethyl)-2-furaldehyde (HMF)
20	15.25	Levoglucosan

<sup>a</sup>According to the NIST 2008 database.

The major differences between the GC traces of DIR derived organic and aqueous phase bio-oil is the appearance of many chromatographic peaks after 16 min in the former. According to the NIST library, these chromatographic peaks are mainly assigned to polycyclic aromatic hydrocarbons (PAHs) such as 1,1'-(1,3-propanediyl) bis-benzene, 2,6-diisopropylnaphthalene and 1,1'-(3-methyl-1-propene-1,3-diyl) bis-benzene. The presence of PAHs in bio-oils generated from pyrolysis of paper deinking residue was also observed by Lou *et al.* previously in their study about pyrolysis of deinking residue in a static tubular furnace<sup>162</sup> and Beauchamp *et al.*<sup>191</sup>. These materials maybe resulted from the additives added during paper manufacturing processes, ink particles, coatings and chemicals used in deinking processes.<sup>162, 191</sup>

In addition, the organic phase bio-oil generated from microwave-assisted low-temperature (<200 °C) pyrolysis of DIR was subjected to an external service for both qualitative and quantitative GC-MS characterization. Detailed instrumentation and experimental procedure are described in section 4.2.11 in chapter 4. This GC-MS characterization further reveals that the DIR derived organic phase bio-oil is a complex mixture of many compounds, mainly including carbohydrate sugars (around 20%), nonaromatic compounds such as acids, esters, alcohols, and aldehydes (in total around 15%), and heterocyclic compounds such as furans and pyrans (8%). Moreover, it reveals that aromatic compounds contribute to around 2.4% of DIR derived organic phase bio-oil, comprising benzenes, guaiacols, syringols, which were derived from remaining lignin within DIR. A comprehensive and detailed list of identified compounds, together with the GC-MS traces, is provided in the Appendix A (Table 26 and 27, Figure 112 - 116).

#### 2.7.4 Summary of GC-MS characterization of bio-oils

In this section, both the organic and aqueous phase bio-oils generated from microwave-assisted low-temperature (<200 °C) pyrolysis of spruce wood chips, waste office paper and DIR were qualitatively characterized using GC-MS. The results are consistent with the ATR-IR and liquid-state NMR analysis. Most organic compounds were trapped into the organic phase bio-oils mainly including carbohydrate sugars and their derivatives (*e.g.*, levoglucosan, levoglucosenone, 1,4:3,6-dianhydro- $\pi$ D-glucopyranose *etc.*), furans (*e.g.*, furfural, HMF *etc.*),

aromatic compounds, ketones, aldehydes, carboxylic acids *etc.* The chemical compositions of bio-oils are directly related to that of the feedstock. For instance, the spruce wood chips derived bio-oils contain prominently high amounts of substituted aromatic compounds (mainly methoxyphenols) such as guaiacol, creosol *etc.* as well as catechol due to the high lignin content of spruce wood chips. Except the “common” pyrolysis products, the DIR derived organic phase bio-oil contains polycyclic aromatic compounds that may come from paper additives, coatings, ink particles and/or other chemicals employed in the deinking processes.

## 2.8 Adhesion properties of organic phase bio-oils

It was pointed out previously in the literature that bio-oils generated from pyrolysis of biomass could be used for adhesive applications.<sup>192, 193</sup> Indeed, several publications mentioned the use of the phenolic fraction of bio-oil, which derived mainly from lignin, as a replacement for the phenol needed in the phenol/formaldehyde resin formulations, used to produce oriented strand board (OSB) and plywood.<sup>194, 195</sup> However, no literature was found about the adhesive properties of bio-oil themselves. Herein, the crude organic phase bio-oils produced from microwave-assisted low-temperature (<200 °C) pyrolysis of spruce wood chips, waste office paper and DIR were applied directly as adhesives for aluminium – aluminium (Al – Al) bonding. The adhesive properties of organic phase bio-oils were investigated by measuring the tensile strengths of bio-oil adhered Al plates, which were cured at various temperatures and time in a lab oven (section 2.8.1 and 2.8.2). Scrapings of formed bio-oil polymers at the Al – bio-oil – Al interfaces were subjected to ATR-IR spectroscopy (section 2.8.3) and solid-state CP/MAS <sup>13</sup>C NMR characterization (section 2.8.4). In addition, the scrapings were also characterized with solid-state CP/MAS <sup>13</sup>C NMR with dipolar dephasing as an attempt to obtain a holistic overview of the chemical structures of cured bio-oil polymers.

### 2.8.1 Adhesion tests of organic phase bio-oils

Figure 35 demonstrates the procedure followed for the curing experiments and subsequent adhesion tests for the application of bio-oil as an adhesive for Al – Al bonding. More detailed

information is illustrated in experimental section 4.2.12 in chapter 4. Basically, the curing experiments and adhesion tests were conducted following the steps summarized below:

**Step 1:** Organic phase bio-oil (70 mg) was homogeneously applied to the surface of one Al plate (50 mm x 50 mm). A glass rod was used to guarantee homogeneous spreading of bio-oil on the Al surfaces, the weight of bio-oil on Al surfaces were accurately measured by weighing the Al plate before and after applying the bio-oil.

**Step 2:** The Al plate, which has bio-oil on its surface, was pressed together with another Al plate of the same surface size using light pressure (finger-strength), weighed down with a stainless steel metal block (350 g) to mimic constant pressure.

**Step 3:** The specimens prepared in step 2 were subjected to heating for curing in a lab oven. The stainless steel metal block still stays at the top of the two Al plates to guarantee homogeneous pressure during curing. Samples were cured at various temperatures: 120 °C, 140 °C, 160 °C and 180 °C for 4 and 8 h curing to investigate the influences of curing temperature and time on the adhesion properties of bio-oil.

**Step 4:** After curing, the bio-oil adhered Al plates were removed from the oven and cooled to room temperature naturally (around 25 °C), followed by gluing the cured Al plates to two stainless steel metal blocks (50 mm × 50 mm) with commercial ‘Superglue’ purchased from B&Q at York, UK.

**Step 5:** The tensile strengths of the adhesive bonds formed between the two Al plates post cure was measured using an Instron 3367 universal testing machine (and accompanying software) fitted with a 3000 N capacity load cell, at a cross-head speed of 5 mm min<sup>-1</sup> (as shown in Figure 36).

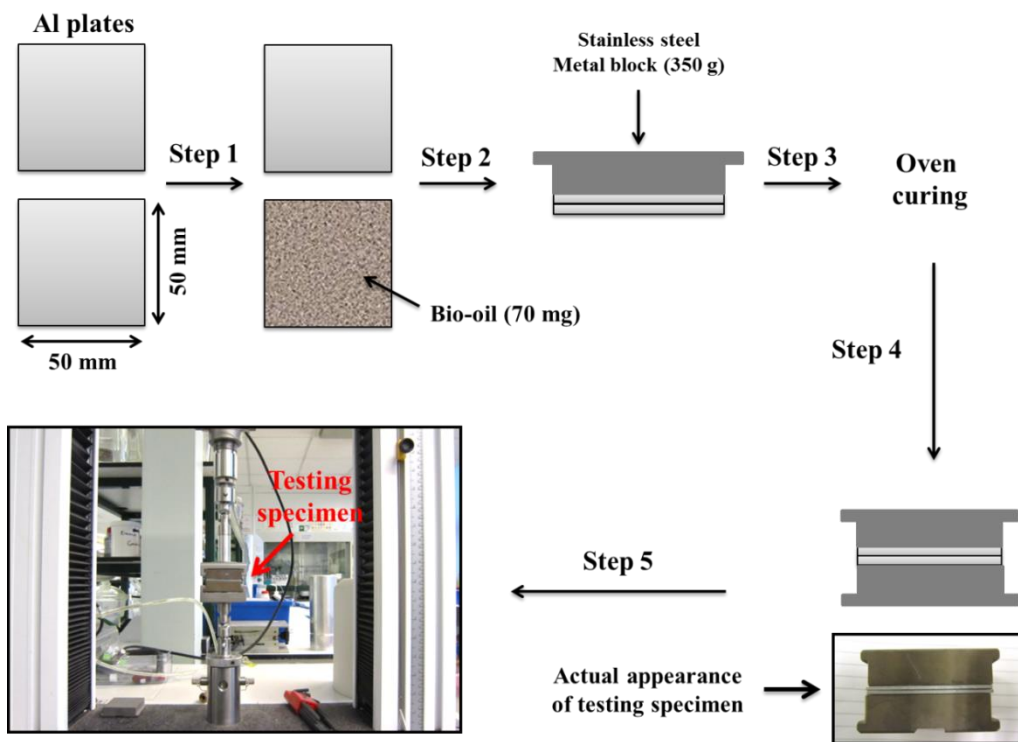


**Figure 35:** Curing procedures for the application of bio-oil as an adhesive for Al – Al bonding.  
(Originally in colour)

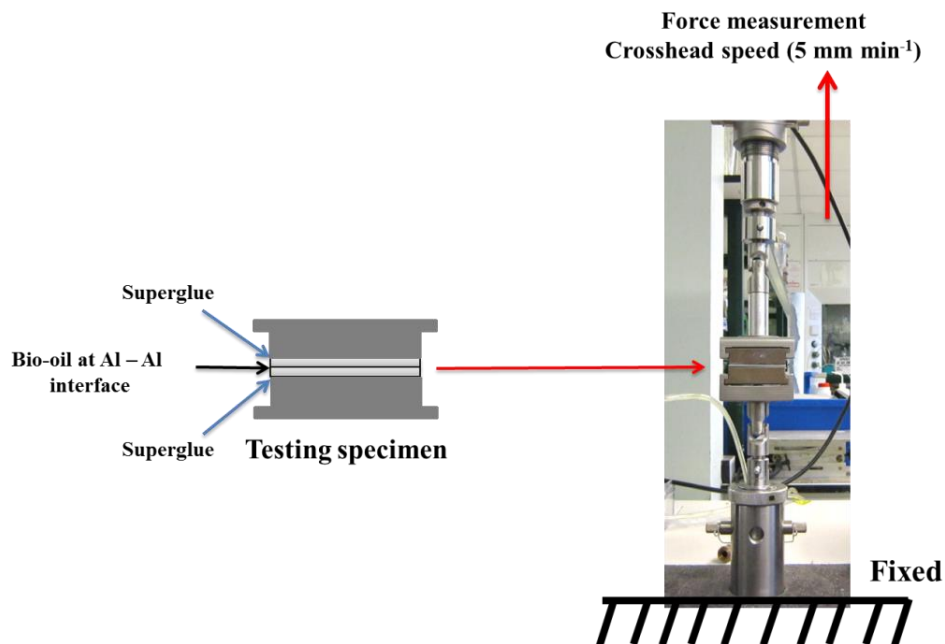


**Figure 36:** Illustration of tensile strength tests of bio-oil cured Al plates using an Instron 3367 universal testing machine, at a crosshead speed of  $5 \text{ mm min}^{-1}$ . (Originally in colour)

During tensile tests, the bio-oil cured Al plates were pulled apart at a fixed crosshead speed until the testing specimen failed and an extension – load (tensile strength) curve for the test was generated by the accompanying software. A representative extension – load (tensile strength) curve for bio-oil cured Al plates is shown in Figure 37. The load (tensile strength) continuously increases with extension distance until the testing specimen fails, which indicates that the cured bio-oil polymers at the interface of Al – Al plates undergo continual deformation prior to failure. The maximum load at breaking (*i.e.* maximum tensile strength) is one important parameter for determining the adhesive properties of bio-oils. In the following discussions, the average values of maximum tensile strengths for four measurements for each organic phase bio-oil sample are reported with error bars.

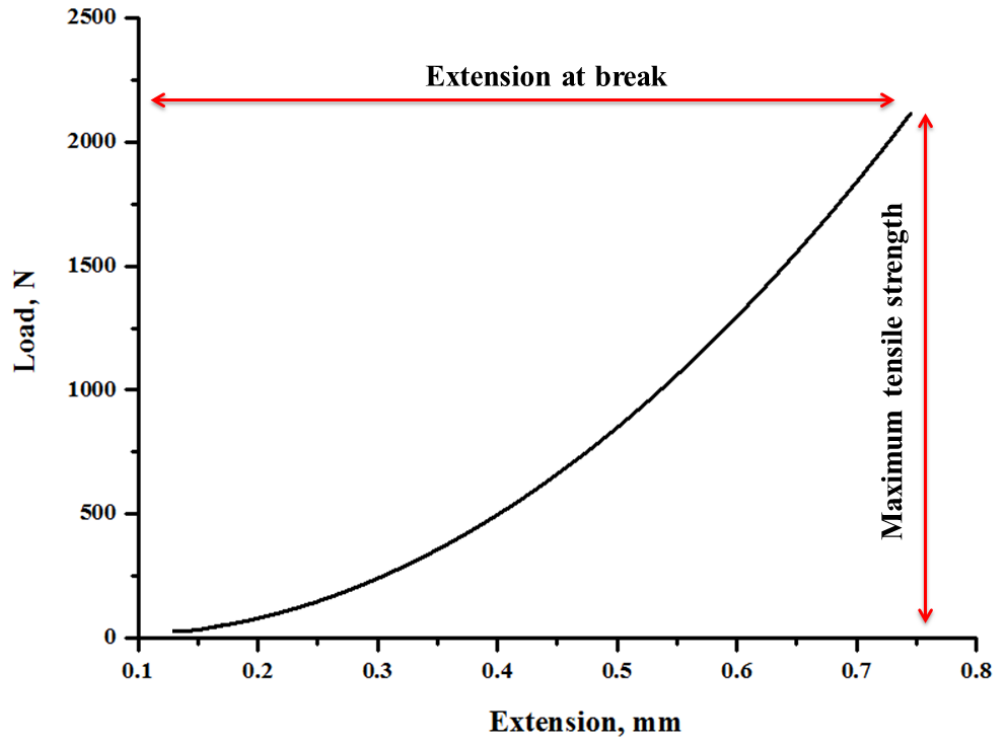


**Figure 37:** A general extension – load curve generated by the accompanying software of Instron 3367 universal testing machine for bio-oil cured Al plates. (Originally in colour)

## 2.8.2 Adhesion strengths of organic phase bio-oils

The appearances of the Al – bio-oil – Al interfaces post tensile strength tests for specimens oven cured by the organic phases of bio-oils generated from microwave-assisted low-temperature

(<200 °C) pyrolysis of spruce wood chips, waste office paper and DIR are shown in Figure 38, 39 and 40, respectively.

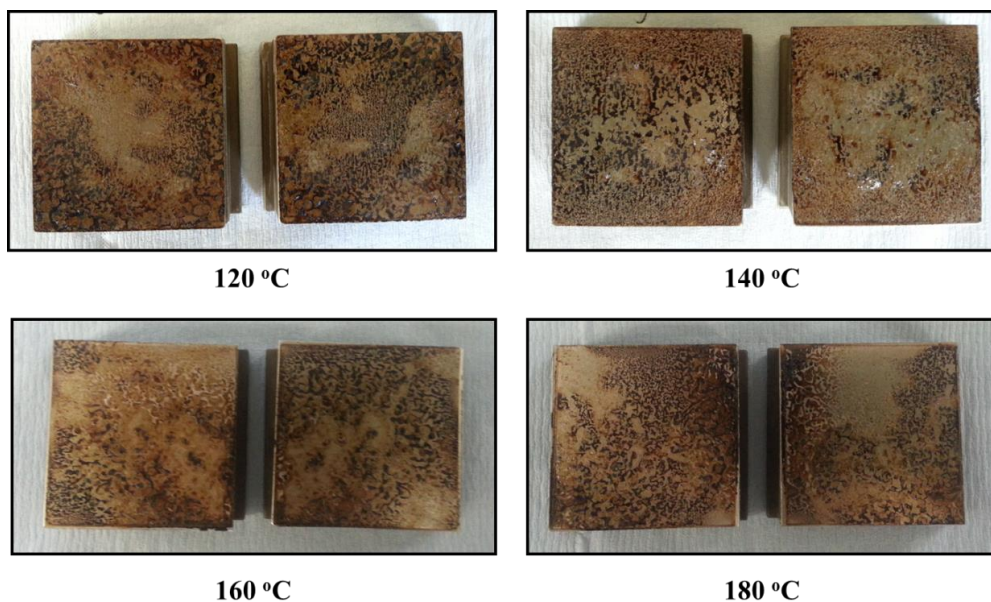


**Figure 38:** Appearances of the Al – bio-oil –Al interfaces of Al plates oven cured by the spruce wood chips derived organic phase bio-oil at various temperatures for 8 h. (Originally in colour)

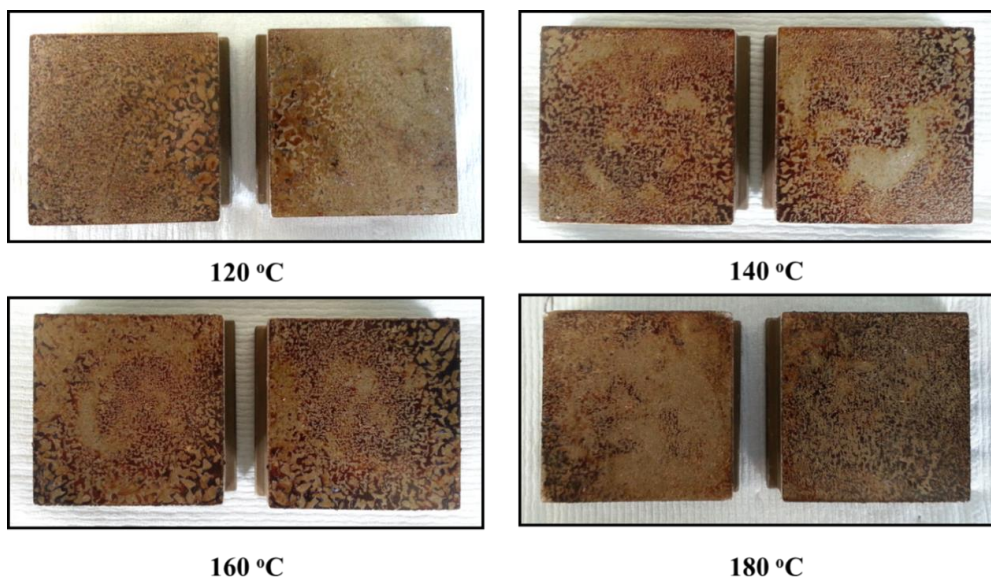


**Figure 39:** Appearances of the Al – bio-oil –Al interfaces of Al plates oven cured by the waste office paper derived organic phase bio-oil at various temperatures for 8 h. (Originally in colour)

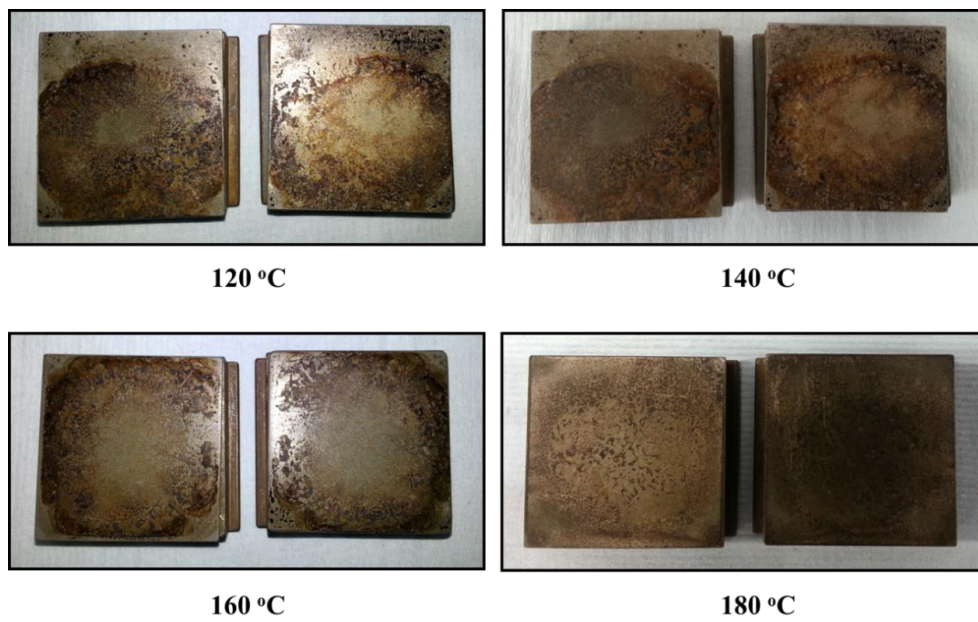


**Figure 40:** Appearances of the Al – bio-oil –Al interfaces of Al plates oven cured by the DIR derived organic phase bio-oil at various temperatures for 8 h. (Originally in colour)

It can be observed that all the bio-oil adhesives derived from different feedstocks were polymerized during curing in oven at various temperatures and time. It is prominent that all the bio-oil adhered Al plates were broken cohesively rather than adhesively during tensile tests. More specifically, with increasing tensile strengths applied on the bio-oil cured Al plates, the interfaces of Al–bio-oil–Al undergo continual deformation until failure occurs. For all the Al plates adhered together with organic phases of bio-oils derived from spruce wood chips, waste office paper and DIR, bond failure occurred within the bio-oil polymer formed between the two Al plates, rather than at the interfaces between the adhesive (organic phase bio-oil) and the substrate (Al plates). Hence, the fractured bio-oil polymers are observed at both surfaces of the two substrates (Al plates) in Figures 38, 39 and 40. Adhesion and cohesion are two important properties of adhesive materials.<sup>196</sup> Basically, as described by von Fraunhofer, adhesion is any attractions between dissimilar molecular species (*i.e.* the adhesive and substrates) and cohesion refers to any attractions between similar molecules (*i.e.* within the adhesive).<sup>196</sup> Cohesion primarily originates from chemical bonds formed between the individual adhesive components, hence cohesive describes the internal strengths of adhesives resulting from various interactions

within adhesive materials.<sup>196</sup> Figure 41 illustrates the basic principles of adhesion and cohesion, as well as the differences between adhesive and cohesive failure patterns of cured systems.

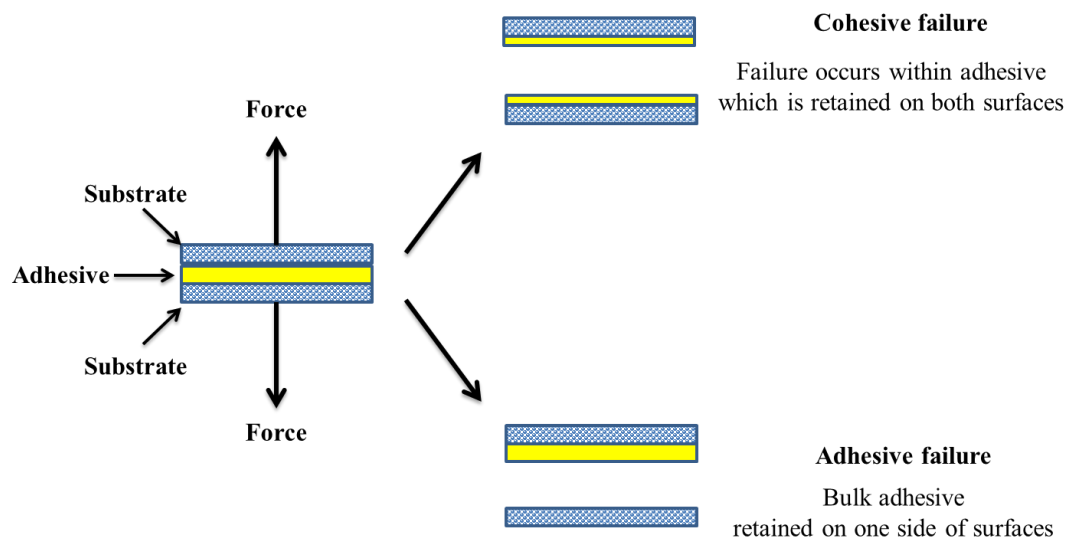


**Figure 41:** Illustration of principles of adhesion and cohesion, together with differences between adhesive and cohesive joint failure patterns, adapted from reference 196. (Originally in colour)

The average tensile strengths of the bonds between Al plates adhered together by the organic phase bio-oil derived from spruce wood chips, waste office paper and DIR are shown in Figure 42, 43 and 44, respectively. Samples were cured at 120 °C, 140 °C, 160 °C and 180 °C for 4 and 8 h. In general, the bio-oil adhesives derived from spruce wood chips and waste office paper could bond the two Al plates with acceptable bond strengths at all curing temperatures and time periods.

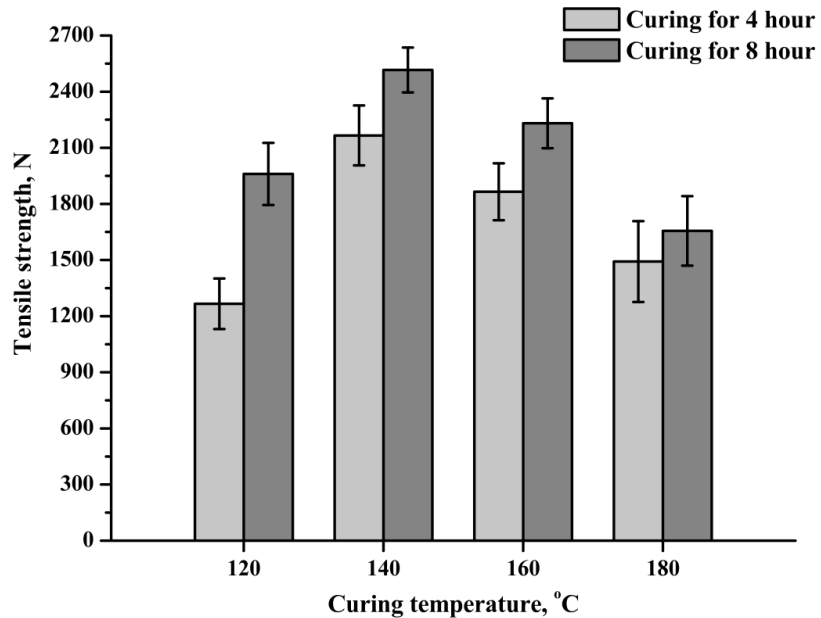


**Figure 42:** Tensile strengths of spruce wood chips derived organic phase bio-oil (70 mg) cured Al plates

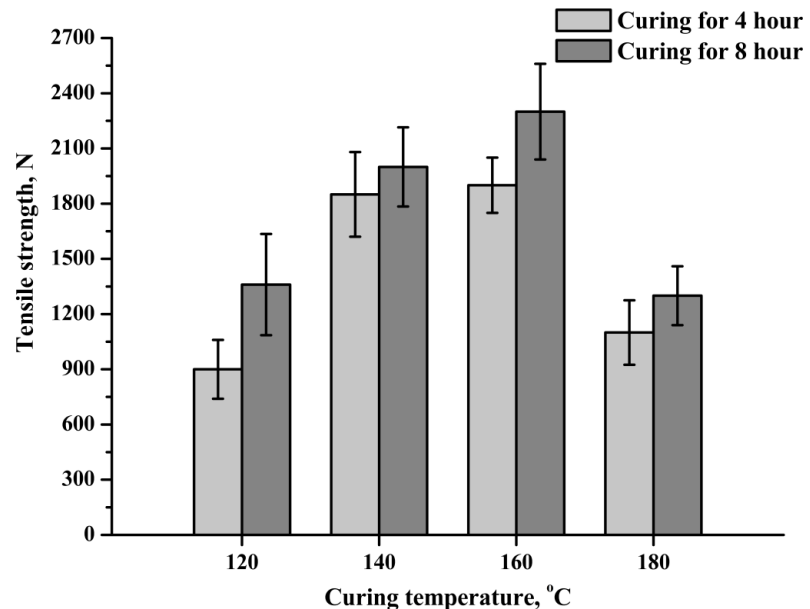


**Figure 43:** Tensile strengths of waste office paper derived organic phase bio-oil (70 mg) cured Al plates. (Originally in colour)

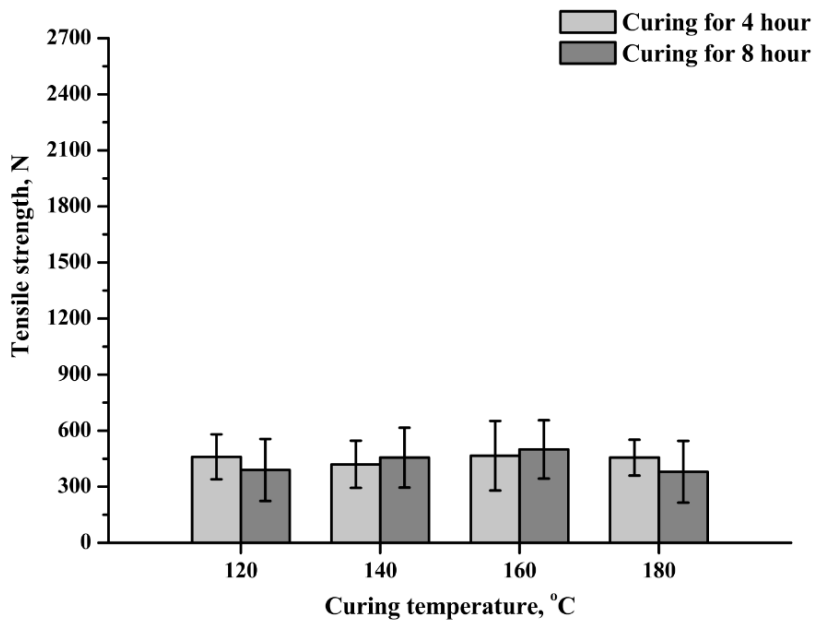


**Figure 44:** Tensile strengths of DIR derived organic phase bio-oil (70 mg) cured Al plates.

For the Al plates cured by spruce wood chips derived organic phase bio-oil (Figure 42), the maximum tensile strengths were obtained when cured at 140 °C for 8 h, reaching around 2520 N. The minimum tensile strengths are around 1250 N for specimens cured at 120 °C for 4 h. When the curing temperature increased from 120 °C to 140 °C, tensile strengths of cured samples increased. This phenomenon is more prominent for shorter curing time. For instance, the average tensile strength significantly increased from around 1250 N (120 °C for 4 h) to around 2160 N (140 °C for 4 h). The average tensile strength of samples cured at 120 °C and 140 °C for 8 h only increased about 560 N from 1960 N (120 °C for 8 h) to 2520 N (140 °C for 8 h). For samples cured at temperatures above 140 °C, the tensile strengths decrease with increasing of curing temperature, higher curing temperatures result in lower tensile strengths. In addition, it is obvious that the average tensile strength increases with curing time, regardless of curing temperatures. This effect is more significant at lower curing temperatures. For example, the average tensile strength increased from approximate 1250 N (120 °C, 4h) to 1960 N (120 °C, 8 h). For samples cured at 140 °C, the increase is less significant: from about 2160 N (140 °C, 4 h) to 2520 N (140 °C, 8 h).

A similar trend could be observed for Al plates cured by the waste office paper derived organic phase bio-oil at various curing temperatures (120 °C, 140 °C, 160 °C and 180 °C) for 4 and 8 h (Figure 43). Although maximum tensile strengths were obtained at a slightly higher curing temperature: around 2300 N at 160 °C for 8 h curing. The minimum tensile strengths (around 900 N) were obtained when cured at 120 °C for 4 h. Also, the longer the curing time, the higher the Al–bio-oil–Al bond tensile strengths. Similar to the spruce wood chips derived organic phase bio-oil, this effect is more significant when cured at lower temperatures. For example, when cured at 120 °C, the tensile strength increased by ~50% to 1360 N (for 8 h cure) from around 900 N (for 4 h cure). However, at higher temperatures, the increase of tensile strength was only around 15%.

In contrast to the organic phase bio-oils generated from microwave-assisted pyrolysis of spruce wood chips and waste office paper, the DIR derived organic phase bio-oil shows very poor adhesion properties. The tensile strengths of the Al plates bonded by the DIR derived organic phase bio-oil are much lower than those obtained with the organic phase bio-oils derived from spruce wood chips and waste office paper. As demonstrated in Figure 44, tensile strengths of Al plates cured by the DIR derived organic phase bio-oil were only around 400 N for all the specimens, regardless of curing temperatures and time. It was observed that the polymer formed at the Al–bio-oil–Al interfaces of DIR bio-oil cured Al plates was very soft and easy to scratch off. In contrast, the formed polymers at the interfaces of spruce wood chips and waste office paper derived organic phase bio-oil cured specimens were stiffer and more difficult to scratch off. The reason for this effect is uncertain but maybe due to the presence of polycyclic aromatic hydrocarbons (PAHs) in the DIR derived organic phase bio-oil, as revealed by the GC-MS analysis (section 2.7.3).

The mass loss of bio-oil adhesive during oven curing was monitored and calculated by weighing the total weight of applied bio-oil (70 mg) plus two Al plates before and after curing. Figure 45 and 46 demonstrate the mass loss in weight percentage (wt.%) of the organic phase of bio-oils derived from spruce wood chips, waste office paper and DIR during curing the Al substrates at various temperatures for 4 and 8 h curing, respectively. It is obvious that the mass loss of bio-oil

increased with curing temperature. For example, the mass loss (wt.%) of spruce wood chips derived organic phase bio-oil increased from 31.6 wt.% (120 °C) to 41.8 wt.% (180 °C) for 4 h curing (Figure 45). Similar trends are observed for the organic phase bio-oils derived from waste office paper and DIR. By comparing the mass loss for samples cured for 4 h (Figure 45) and 8 h (Figure 46) at various temperatures, it is noteworthy that the mass loss of bio-oil also increased with curing temperature. For instance, the weight loss of spruce wood chips derived organic phase bio-oil increased from 33.9 wt.% (140 °C, for 4 h curing) to 38.6 wt.% (140 °C for 8 h curing). In general, about 30 - 50 wt.% of the applied bio-oil adhesive (70 mg) was lost during curing in oven, the exact mass loss depends on curing temperatures and time. The mass loss of bio-oil during curing is probably due to the evaporation of small amounts of water (around 2 wt.%), carboxylic acids, other volatile compounds within bio-oil as well as compounds generated from the various polymerization reactions of bio-oil (*e.g.*, water). The exact composition of released chemicals during curing needs further investigation.

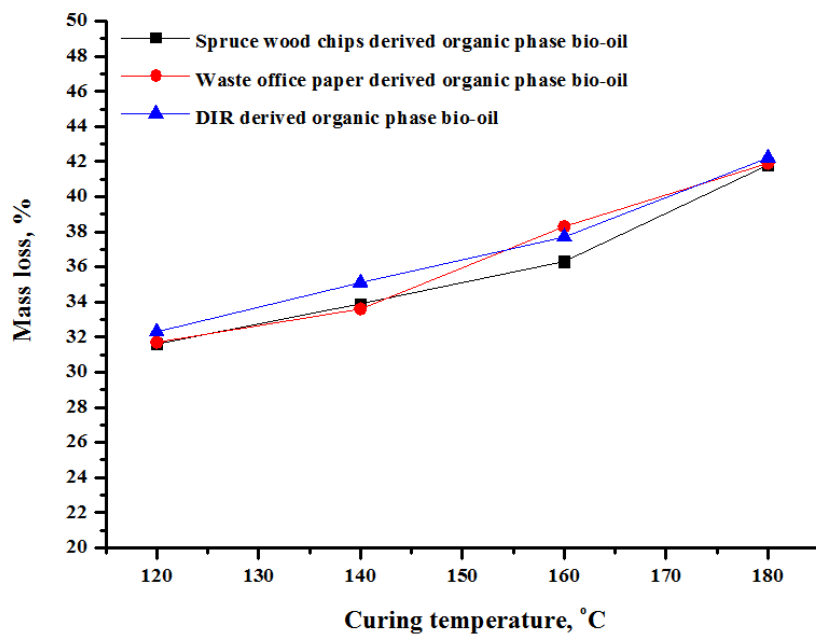


**Figure 45:** Mass loss (wt.%) of spruce wood chips, waste office paper and DIR derived organic phase bio-oil during curing Al in oven at various temperatures for 4 h curing. (Originally in colour)

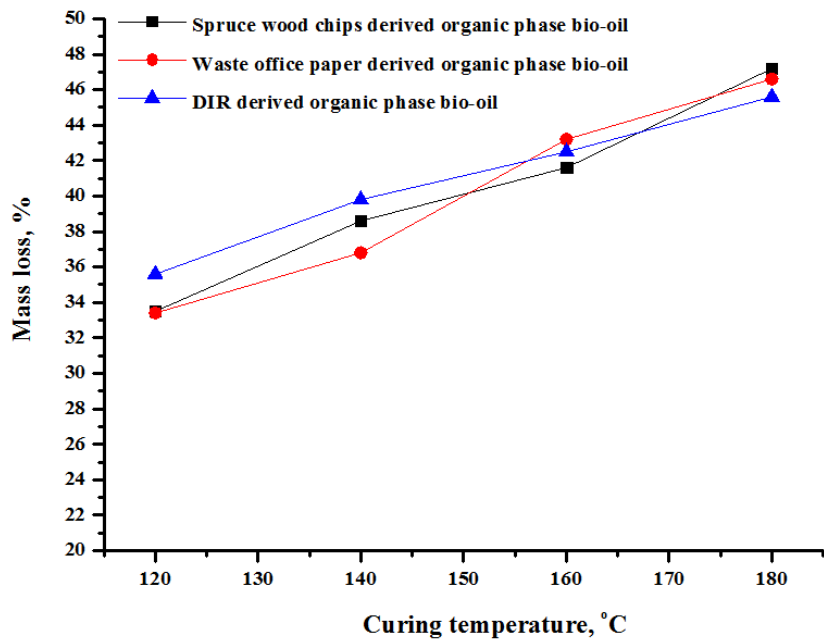


**Figure 46:** Mass loss (wt.%) of spruce wood chips, waste office paper and DIR derived organic phase bio-oil during curing Al in oven at various temperatures for 8 h curing. (Originally in colour)

To allow a direct evaluation of the strengths of bio-oil adhesive, as shown in Figure 47, the crude organic phase bio-oil (except the one derived from DIR) is strong enough to lift an adult (around 95 kg) without failure. The specimen used for this test is Al plates cured by the waste office paper derived organic phase bio-oil at 160 °C for 8 h curing.



**Figure 47:** Adhesion strength test of the waste office paper derived organic phase bio-oil. The tested specimen is Al plates adhered by the crude, waste office paper derived organic phase bio-oil at 160 °C for 8 h curing. (Originally in colour)

### 2.8.3 ATR-IR characterization of scrapings of cured bio-oil polymers

To get more structural information, the ATR-IR spectra of the spruce wood chips, waste office paper and DIR derived organic phase bio-oils and their scrapings from the organic/Al interface were recorded and compared. However, it is acknowledged that characterization of the scrapings of cured bio-oil polymers using Diffuse Reflectance Infrared Fourier Transform spectroscopy (DRIFT) could provide more holistic structural information, as the colour of the scrapings are generally dark brown/black. The scrapings were scratched off from the Al–bio-oil–Al interfaces of specimens directly after tensile tests. In both cases, many significant changes of functional groups occurred before and after curing.

Figure 48 compares the ATR-IR spectra of the crude spruce wood chips derived organic phase bio-oil and the scrapings of the formed bio-oil polymers after curing Al plates in oven at 140 °C for 4 and 8 h (at which temperature maximum tensile strengths were obtained). To clearly see the subtle changes of functional groups in the fingerprint region, the ATR-IR spectra between 2000 cm<sup>-1</sup> and 500 cm<sup>-1</sup> are highlighted in Figure 49. From Figure 48 and 49, it is obvious that many changes of functional groups had occurred before and after curing in oven. The carbonyl stretching vibration (C=O) at around 1718 cm<sup>-1</sup> in the spectrum of spruce wood chips derived organic phase bio-oil drifts slightly to a lower wavenumber (around 1705 cm<sup>-1</sup>) in the spectrum of bio-oil polymers. The absorption band centred at around 1615 cm<sup>-1</sup> attributed to C=C stretching of alkenes, furans and aromatic compounds *etc.* became much sharper after curing. In addition, the intensity of this band significantly increased after curing, suggesting the formation of new conjugated and/or aromatic structures. The characteristic absorption band for aromatic skeletal vibrations at around 1510 cm<sup>-1</sup> presents in both the ATR-IR spectra of spruce wood chips derived organic phase bio-oil and the scrapings of cured polymers. The formation of new aromatic structures during curing is also evidenced by many subtle changes in region below 1000 cm<sup>-1</sup>, which is mainly attributed to C-H out of plane bending vibrations of olefinic and aromatic structures. Many structural changes could also be observed between 1500 cm<sup>-1</sup> and 1000 cm<sup>-1</sup>, suggesting the involvement of many different compounds in the polymerization of bio-oil.

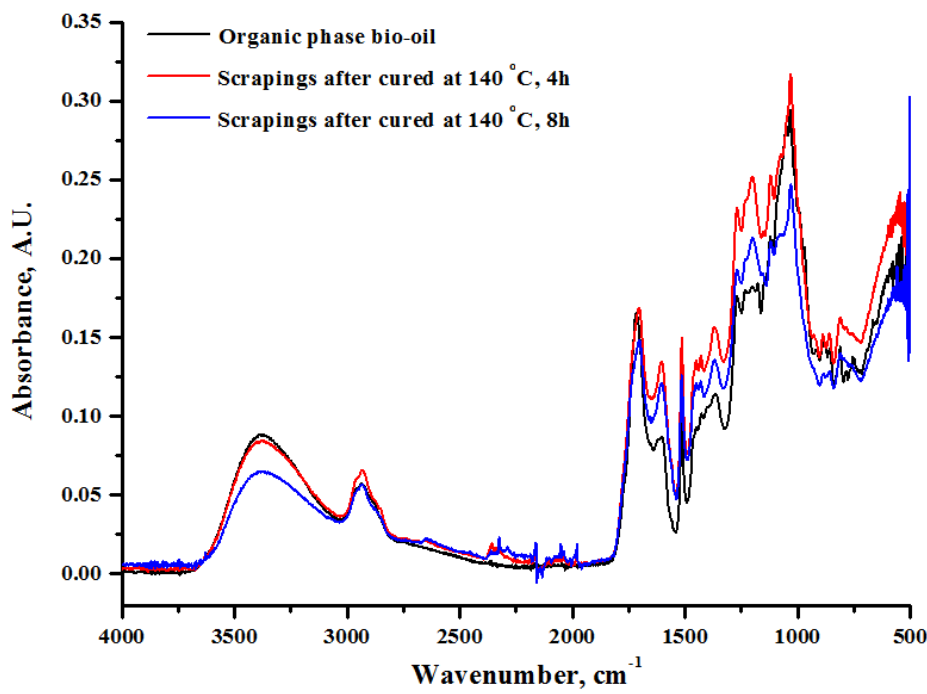


**Figure 48:** ATR-IR spectra of spruce wood chips derived organic phase bio-oil, scrapings of the Al-bio-oil-Al interface polymer formed at 140 °C for 4 and 8 h curing (between 4000  $\text{cm}^{-1}$  and 500  $\text{cm}^{-1}$ ). (Originally in colour)

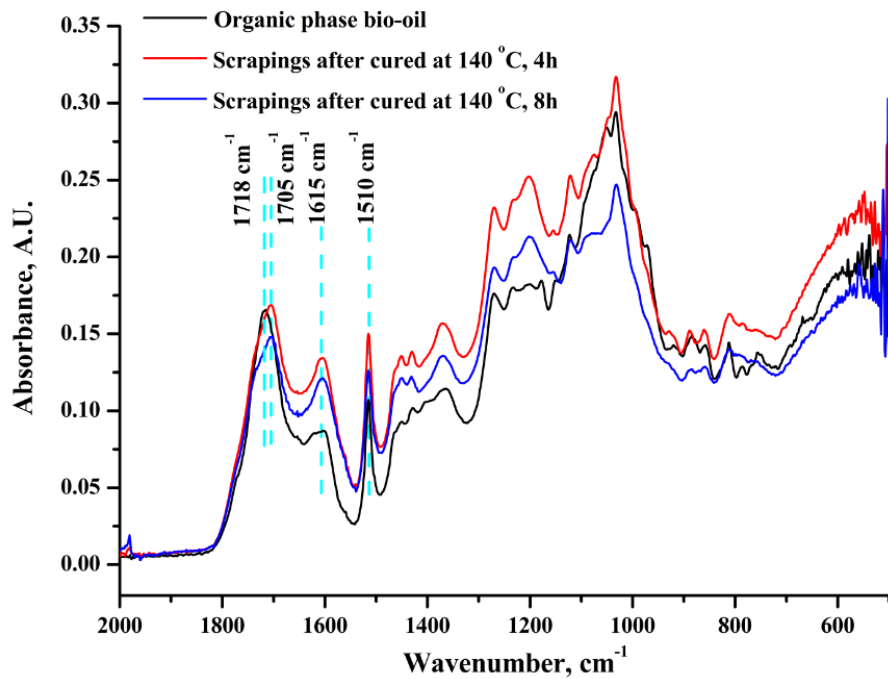


**Figure 49:** ATR-IR spectra of spruce wood chips derived organic phase bio-oil, scrapings of the Al-bio-oil-Al interface polymer formed at 140 °C for 4 and 8 h curing (between 2000  $\text{cm}^{-1}$  and 500  $\text{cm}^{-1}$ ). (Originally in colour)

Highest tensile strengths of Al plates cured by the waste office paper derived organic phase bio-oil were obtained at 160 °C. The ATR-IR spectra of waste office paper derived organic phase bio-oil and the scrapings of bio-oil polymers formed at 160 °C for 4 and 8 h curing are shown in Figure 50 (4000 cm<sup>-1</sup> to 500 cm<sup>-1</sup>) and Figure 51 (2000 cm<sup>-1</sup> to 500 cm<sup>-1</sup>)

Compared with the crude organic phase bio-oil derived from waste office paper, the cured bio-oil polymer is characterized by a lower C=O:C=C ratio, suggesting polymerization occurred in carbonyl groups. Also, the C=C stretching frequency at 1617 cm<sup>-1</sup> is characteristic of olefinic double bonds in five membered rings. The intensity of this peak increased after curing of the organic phase bio-oil on the Al surface, suggesting the formation of conjugated/aromatic structures. This effect is also evidenced by a significant number of changes between 800 cm<sup>-1</sup> and 900 cm<sup>-1</sup>, which represents the C–H out of plane bending vibrations in substituted alkenes and aromatics. This may be caused by changes in the substitution patterns of such molecules during polymerization.

Another significant change is observed in the C–O stretching region (900 cm<sup>-1</sup> – 1200 cm<sup>-1</sup>): the intensity of this band dramatically decreased, and many subtle changes occurred after curing. However, for bands centred at 1443 cm<sup>-1</sup>, 1184 cm<sup>-1</sup>, 1138 cm<sup>-1</sup>, 1075 cm<sup>-1</sup>, 1012 cm<sup>-1</sup>, 918 cm<sup>-1</sup>, 890 cm<sup>-1</sup> and 856 cm<sup>-1</sup>, they are either remaining or becoming more obvious in the spectra of scrapings. These bands are characteristic absorptions for levoglucosan, which is a common sugar derivative generated from pyrolysis of biomass. So it is possible that carbohydrate sugars were not significantly involved in the polymerization reactions during curing. This hypothesis is further investigated in the following discussions.

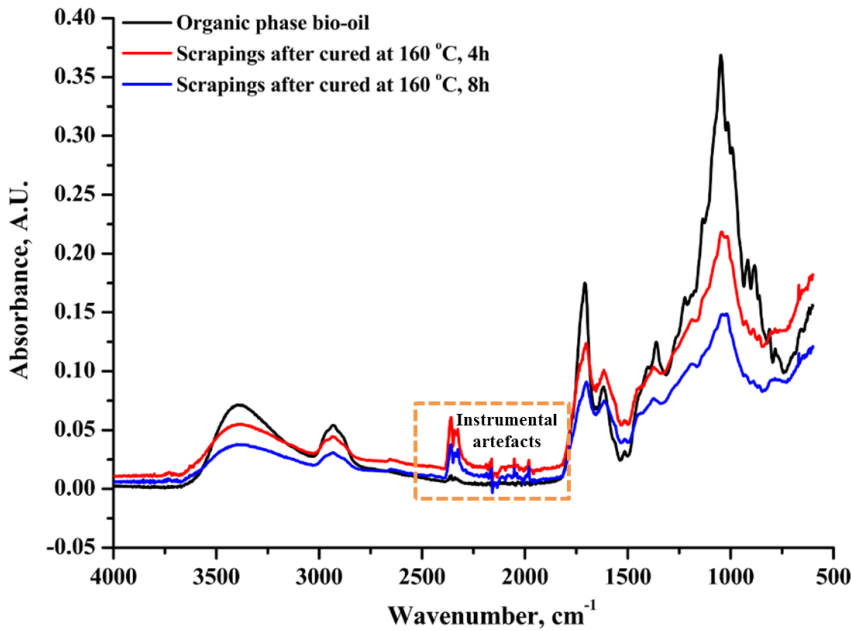


**Figure 50:** ATR-IR spectra of waste office paper derived organic phase bio-oil, scrapings of the Al-bio-oil-Al interface polymer formed at 160 °C for 4 and 8 h curing. (Originally in colour)

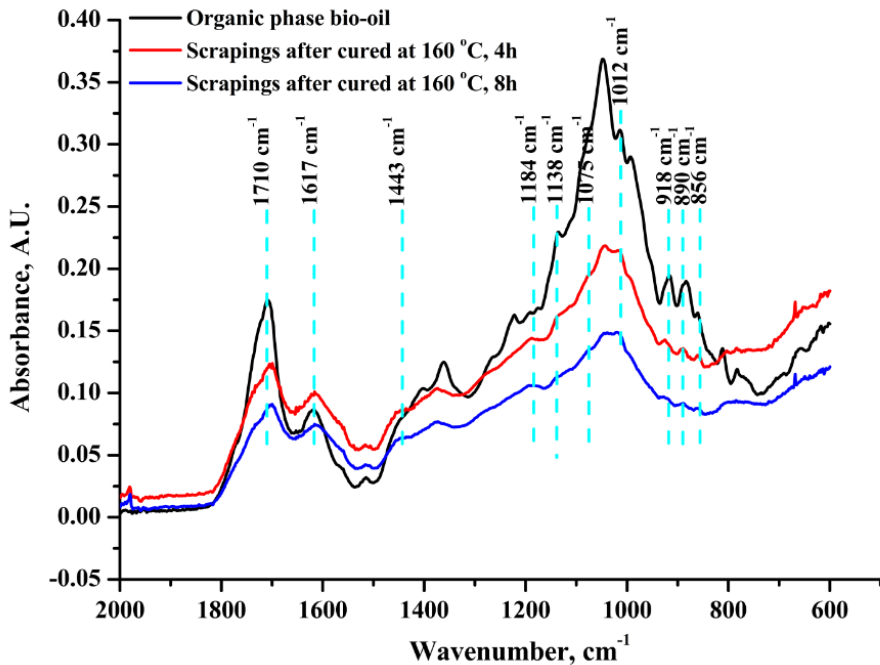


**Figure 51:** ATR-IR spectra of waste office paper derived organic phase bio-oil, scrapings of the Al-bio-oil-Al interface polymer formed at 160 °C for 4 and 8 h curing (between 2000 cm⁻¹ and 500 cm⁻¹). (Originally in colour)

The ATR-IR spectra of DIR derived organic phase bio-oil and the scrapings of polymers formed at 160 °C for 4 and 8 h curing are illustrated in Figure 52 (4000 cm<sup>-1</sup> to 500 cm<sup>-1</sup>) and Figure 53 (2000 cm<sup>-1</sup> to 500 cm<sup>-1</sup>). In comparison with the ATR-IR spectrum of DIR derived organic phase bio-oil, the absorption band characteristic for O-H stretching vibration (3700 cm<sup>-1</sup> to 3100 cm<sup>-1</sup>) slightly drifts to a higher wavenumber, and the intensity of this band decreased. The absorption bands attributed to symmetrical and asymmetrical C-H stretching vibrations (3000 cm<sup>-1</sup> and 2800 cm<sup>-1</sup>) became much sharper after curing. The intensities of these bands also increased significantly. Similar to the spruce wood chips and waste office paper derived organic phase bio-oil, the carbonyl stretching absorption band of DIR derived organic phase bio-oil also drifts to a lower wavenumber (from around 1725 cm<sup>-1</sup> to 1705 cm<sup>-1</sup>). Intensity of this band also decreased after curing. However, the absorption band characteristic for C=C stretching vibration became very broad (between 1670 cm<sup>-1</sup> and 1540 cm<sup>-1</sup>) and the intensity of this band significantly increased after curing, even surpassing that of the carbonyl stretching absorption band. This effect might be resulted from the formation of new conjugated and/or aromatic structures during curing, but may also due to the presence of polycyclic aromatic hydrocarbons (PAHs) in the DIR derived organic phase bio-oil as revealed by the GC-MS characterization of the DIR derived bio-oils in section 2.7.3.

Similar to the waste office paper derived organic phase bio-oil and its scrapings, characteristic absorption bands for levoglucosan centred around 1184 cm<sup>-1</sup>, 1138 cm<sup>-1</sup>, 1075 cm<sup>-1</sup>, 1012 cm<sup>-1</sup>, 918 cm<sup>-1</sup>, 890 cm<sup>-1</sup> and 856 cm<sup>-1</sup> could also be observed in the ATR-IR spectra of DIR derived organic phase bio-oil and its scrapings after curing. The characteristic absorption bands for levoglucosan in the fingerprint region are also highlighted in Figure 53 with dashed lines.

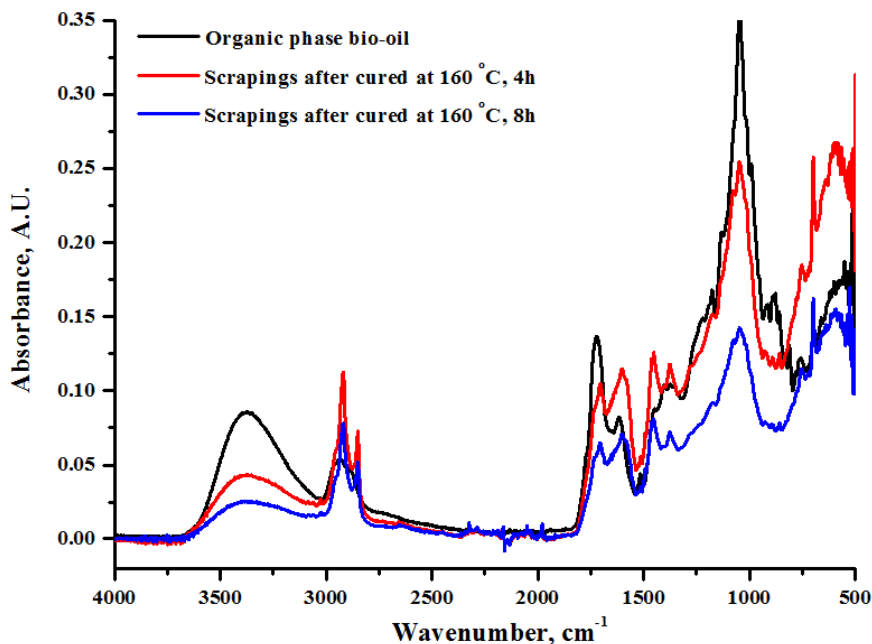


**Figure 52:** ATR-IR spectra of DIR derived organic phase bio-oil, scrapings of the Al-bio-oil-Al interface polymer formed at 160 °C for 4 and 8 h curing (between 4000  $\text{cm}^{-1}$  and 500  $\text{cm}^{-1}$ ).  
 (Originally in colour)

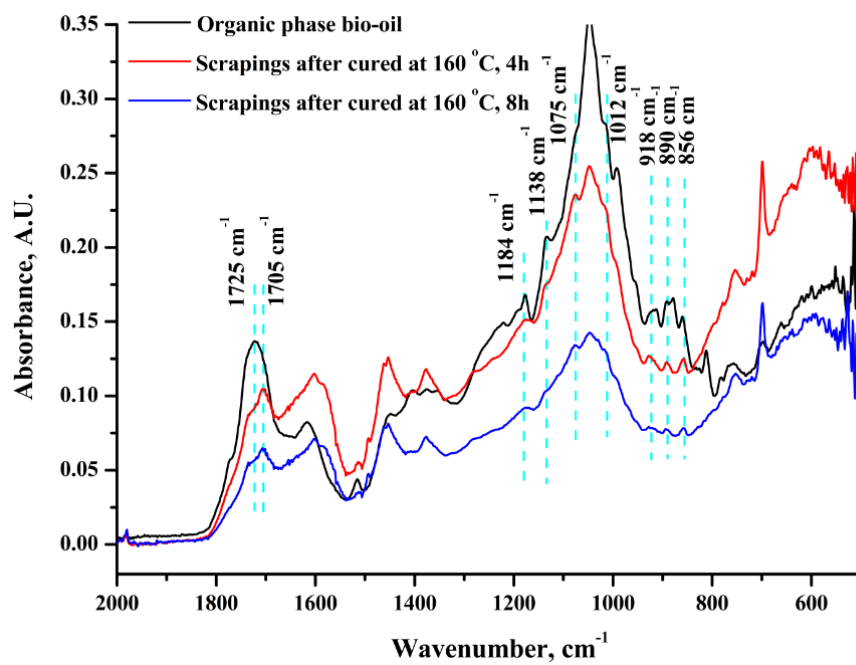


**Figure 53:** ATR-IR spectra of DIR derived organic phase bio-oil, scrapings of the Al-bio-oil-Al interface polymer formed at 160 °C for 4 and 8 h curing (between 2000  $\text{cm}^{-1}$  and 500  $\text{cm}^{-1}$ ).  
 (Originally in colour)

## 2.8.4 Solid-state CP/MAS $^{13}\text{C}$ NMR characterization of scrapings of cured bio-oil polymers

The scrapings from the Al – bio-oil – Al interfaces of Al plates cured by spruce wood chips, waste office paper and DIR derived organic phase bio-oil post tensile tests were further characterized with cross-polarization/magic angle spinning (CP/MAS) solid-state  $^{13}\text{C}$  NMR. In addition, a solid-state  $^{13}\text{C}$  NMR with dipolar dephasing (DD) spectrum was recorded for each sample to allow better assignment of resonance bands. The experimental details for solid-state  $^{13}\text{C}$  CP/MAS NMR with and without dipolar dephasing (DD) are described in section 4.2.13 in chapter 4. In the dipolar dephasing experiments, immobile carbons with directly attached hydrogens were significantly attenuated, so the spectrum will largely consist of the quaternary carbons and mobile carbons such as methyl groups.

Figure 54 illustrates the  $^{13}\text{C}$  CP/MAS NMR spectra with and without dipolar dephasing of the scrapings from Al plates cured by spruce wood chips derived organic phase bio-oil at 140 °C for 8 h. Similarly, the  $^{13}\text{C}$  CP/MAS NMR spectra with and without dipolar dephasing of the bio-oil polymer scrapings derived from waste office paper and DIR are shown in Figure 55 and 56, respectively. The scrapings for waste office paper and DIR derived bio-oil polymers are those cured at 160 °C for 8 h (*i.e.* same samples used for ATR-IR characterization in section 2.8.3). In both cases the solid-state  $^{13}\text{C}$  NMR spectra are overlapped with the liquid-state  $^{13}\text{C}$  NMR spectrum of the crude organic phase bio-oil derived from spruce wood chips, waste office paper and DIR, respectively.

Comparing the solid-state  $^{13}\text{C}$  NMR spectra of the scrapings derived from spruce wood chips (Figure 54), waste office paper (Figure 55) and DIR (Figure 56), it is noteworthy that the solid-state  $^{13}\text{C}$  NMR spectrum of the scrapings of the spruce wood chips derived bio-oil polymer contains a sharp, high-intensity signal between 52 and 59 ppm. This sharp signal also exists in the  $^{13}\text{C}$  NMR spectrum with dipolar dephasing in Figure 54. As discussed previously in section 2.6.1, the sharp signal at around 55 ppm in the liquid-state  $^{13}\text{C}$  NMR spectrum of the spruce wood chips derived organic phase bio-oil is a characteristic resonance signal for the carbon atoms in methoxy groups on phenolic compounds such as guaiacol and syringol. These

phenolic compounds were generated from thermal degradation of lignin. Since the lignin content of spruce wood chips is significantly higher than the lignin contents of waste office paper and DIR, this signal is not prominent (even missing) in the solid-state  $^{13}\text{C}$  CP/MAS NMR spectra of the bio-oil polymer scrapings derived from waste office paper (Figure 55) and DIR (Figure 56). Despite the carbon atoms in these methoxy groups have three hydrogen atoms attached, they are not immobile carbons. Hence, this resonance signal still exists in the  $^{13}\text{C}$  NMR spectrum with dipolar dephasing.

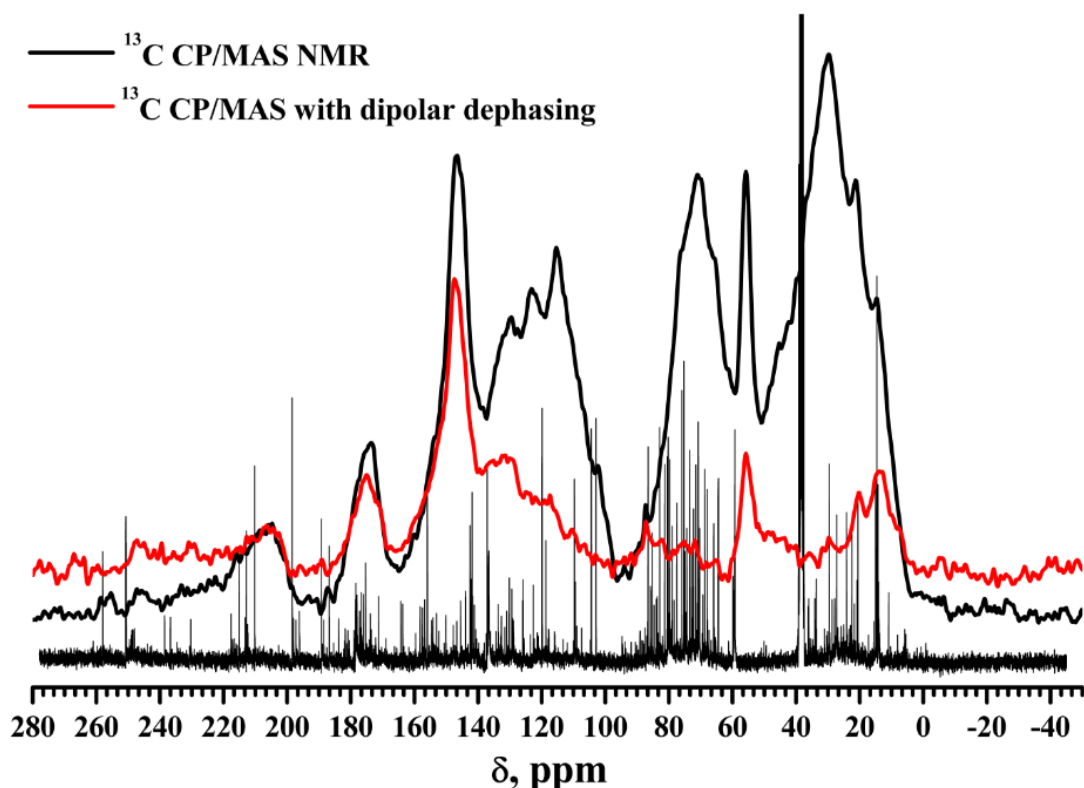


**Figure 54:** Solid-state  $^{13}\text{C}$  CP/MAS NMR spectrum of spruce wood chips derived bio-oil / Al scraping (black) and  $^{13}\text{C}$  CP/MAS NMR spectrum of spruce wood chips derived bio-oil / Al scraping with dipolar dephasing (red), overlapped with the liquid-state  $^{13}\text{C}$  NMR spectrum of organic phase bio-oil from spruce wood chips. (Originally in colour)

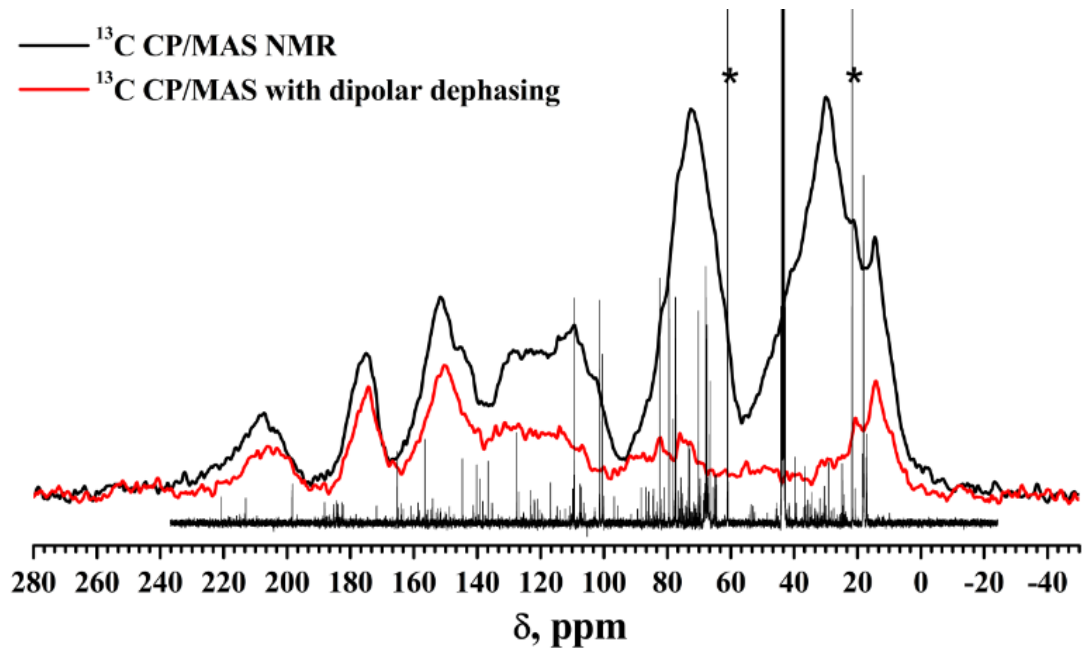


**Figure 55:** Solid-state  $^{13}\text{C}$  CP/MAS NMR spectrum of waste office paper derived bio-oil / Al scraping (black) and  $^{13}\text{C}$  CP/MAS NMR spectrum of waste office paper derived bio-oil / Al scraping with dipolar dephasing (red), overlapped with the liquid-state  $^{13}\text{C}$  NMR spectrum of organic phase bio-oil (\*possible artefacts). (Originally in colour)

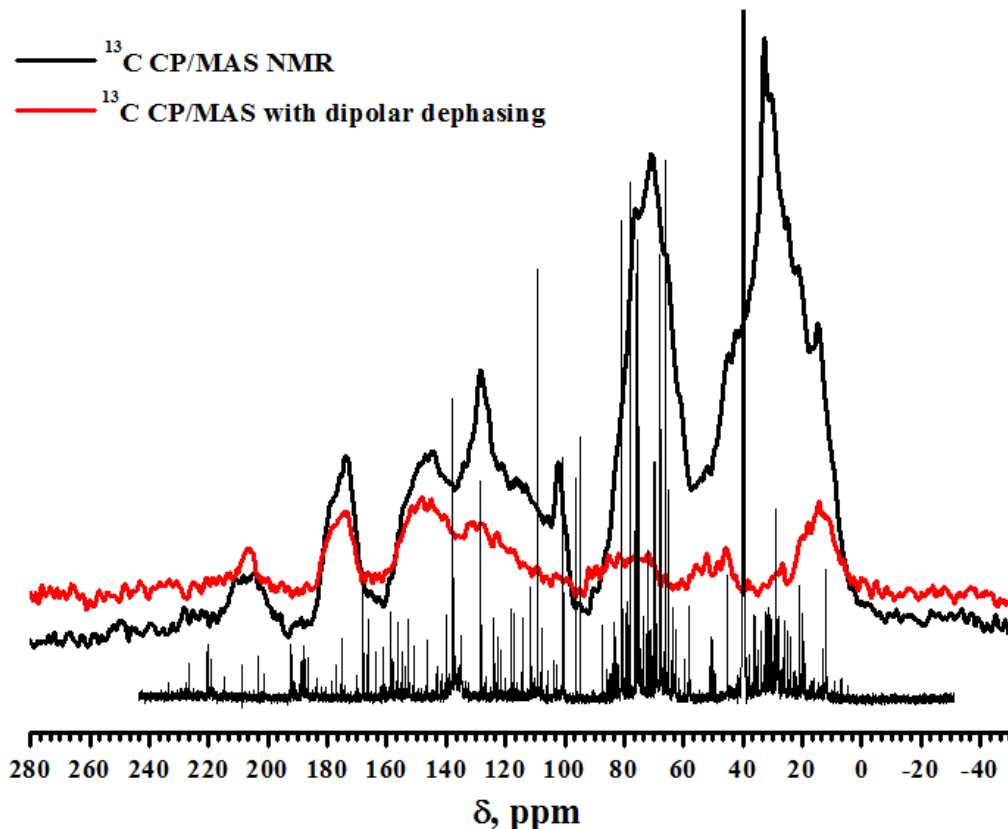


**Figure 56:** Solid-state  $^{13}\text{C}$  CP/MAS NMR spectrum of DIR derived bio-oil / Al scraping (black) and  $^{13}\text{C}$  CP/MAS NMR spectrum of DIR derived bio-oil / Al scraping with dipolar dephasing (red), overlapped with the liquid-state  $^{13}\text{C}$  NMR spectrum of organic phase bio-oil from DIR. (Originally in colour)

The solid-state  $^{13}\text{C}$  CP/MAS NMR spectra with and without dipolar dephasing of the bio-oil polymer scrapings derived from spruce wood chips (Figure 54), waste office paper (Figure 55) and DIR (Figure 56) show similar trends in other resonance regions. For the solid-state  $^{13}\text{C}$  CP/MAS NMR spectra, the broad intense band between 59 ppm and 100 ppm in Figure 54, and those between 50 ppm and 100 ppm in Figure 55 and 56 are assigned to sugar carbons, which were almost not observed in the  $^{13}\text{C}$  NMR spectra with dipolar dephasing. This is because the carbon atoms in carbohydrate sugars and their derivatives generally have at least one hydrogen atom attached. Hence, these carbons were significantly attenuated in dipolar dephasing experiments. The various resonance bands between 105 ppm and 165 ppm verify the presence of complicated aromatic structures. Broadly, the resonance bands between 140 ppm and 160

ppm are attributed to quaternary aromatic carbons, which still exist in the dipolar dephasing  $^{13}\text{C}$  NMR spectra of bio-oil polymer scrapings. Resonance bands between 105 ppm and around 140 ppm are attributed to aromatic carbons with a hydrogen atom attached, so the intensities of these bands decreased in the  $^{13}\text{C}$  dipolar dephasing spectra. The band between 100 ppm and 105 ppm in the  $^{13}\text{C}$  solid-state CP/MAS NMR spectra is a characteristic resonance band for anomeric carbons in carbohydrate compounds. The scrapings of bio-oil polymers derived from spruce wood chips, waste office paper and DIR also contain various carbonyl structures as proved by resonance bands centred at around 210 ppm and 175 ppm. In both cases these bands still remain in the spectra of  $^{13}\text{C}$  NMR with dipolar dephasing, suggesting that they are mainly ketone (210 ppm) and ester (175 ppm) structures. Alkyl groups are also present in the scrapings: methyl groups (0 ppm to 20 ppm) and  $\text{CH}_2$  structures (20 ppm to 50 ppm). The mobile carbons in methyl groups ( $\text{CH}_3$ ) are not attenuated, whereas the  $\text{CH}_2$  structures were significantly attenuated in the solid-state  $^{13}\text{C}$  NMR with dipolar dephasing experiments.

The assignments of carbon resonance bands according to chemical shifts in the solid-state  $^{13}\text{C}$  CP/MAS NMR spectra with and without dipolar dephasing are summarized in Table 19. The fact that there is no significant change seen in the spectra of the post-cure scrapings in all the Figures (Figure 54, 55 and 56) is indicative of little or no decomposition of the main structural units, *i.e.*, the aromatic and sugar moieties largely remain intact, thus undergoing possible homo- and cross-coupling polymerisation reactions that help adhesion.

**Table 19:** Assignments of carbon resonance signals in the solid-state  $^{13}\text{C}$  CP/MAS NMR spectra with and without dipolar dephasing in accordance with the chemical shift range

Chemical shifts (ppm)	Carbon assignments	Solid-state $^{13}\text{C}$ CP/MAS NMR spectra	
		Without dipolar dephasing	With dipolar dephasing
0 – 20	Methyl groups ( $\text{CH}_3$ )	✓	✓
20 – 50	$\text{CH}_2$ structures	✓	
52 – 59	Carbons in methoxy groups of methoxyphenols	✓	✓
50 – 100	Carbons in carbohydrates	✓	
100 – 105	Anomeric carbons in carbohydrates	✓	
105 – 140	Aromatic carbons with hydrogen atom attached	✓	
140 – 160	Quaternary aromatic carbons	✓	✓
160 – 195	esters	✓	✓
195 – 220	ketones	✓	✓

✓Resonance signals observed in the spectrum

## 2.9 Liquid-liquid fractionation of waste office paper derived organic phase bio-oil and the adhesive properties of different bio-oil fractions

As characterized by the ATR-IR spectroscopy (section 2.5), liquid-state  $^1\text{H}$  and  $^{13}\text{C}$  NMR spectroscopy (section 2.6) and GC-MS (section 2.7), the organic phase bio-oils generated from microwave-assisted low-temperature (<200 °C) pyrolysis of the spruce wood chips, waste office paper and DIR are mainly complex mixtures of many different kinds of organic compounds. The organic compounds within organic phase bio-oils mainly contain sugar and its derivatives, (hetero-) aromatics, hydrocarbons and carbonyl containing compounds. In order to gain some understanding of the bonding behaviour of the organic phase bio-oils, the waste office paper derived organic phase bio-oil was subjected to a liquid-liquid fractionation process. In the

literature, extensive efforts have been devoted to upgrade crude bio-oil by separating with different solvents/liquids, mainly with the aim to recover valuable aromatic compounds and carbohydrate sugars *etc.*<sup>197 - 201</sup>

Herein, the different fractions of bio-oil obtained from liquid-liquid fractionation of the waste office paper derived organic phase bio-oil were characterized with ATR-IR spectroscopy, liquid-state <sup>13</sup>C NMR spectroscopy and GC-MS. The mechanical strengths (*i.e.* tensile strengths) of Al plates cured by these different bio-oil fractions were investigated using the same method which was employed for testing the crude organic phase bio-oil cured Al plates (as described in section 2.8.1 in this chapter and section 4.2.12 in chapter 4). The Al plates were adhered together using the different bio-oil fractions at 160 °C for 4 h curing. The curing temperature (160 °C) was selected because this is the temperature at which maximum tensile strengths were obtained for the Al plates cured by crude organic phase bio-oil generated from microwave-assisted pyrolysis of waste office paper (as described in section 2.8.2 in this chapter). The scrapings of the formed polymers at the Al–bio-oil–Al interfaces post tensile tests were characterized using ATR-IR spectroscopy.

### **2.9.1 Liquid-liquid fractionation of the crude organic phase bio-oil derived from waste office paper**

The organic phase bio-oil (10 g) generated from microwave-assisted low-temperature (<200 °C) pyrolysis of waste office paper was subjected to liquid-liquid fractionation using alkali (aqueous sodium hydroxide) and organic solvent (ethyl acetate), from which three different bio-oil fractions (i. “neutral” ethyl acetate fraction, ii., “acidic” ethyl acetate fraction, *i.e.*, acidified aqueous sodium hydroxide layer extracted with ethyl acetate, and iii., aqueous fraction) were obtained. The employed procedure was modified and adapted from the method reported by Amen-Chen *et al.*<sup>201</sup> The experimental procedure is described in section 4.2.14 in chapter 4. Herein, a scheme for the liquid-liquid fractionation of waste office paper derived organic phase bio-oil is illustrated in Figure 57.

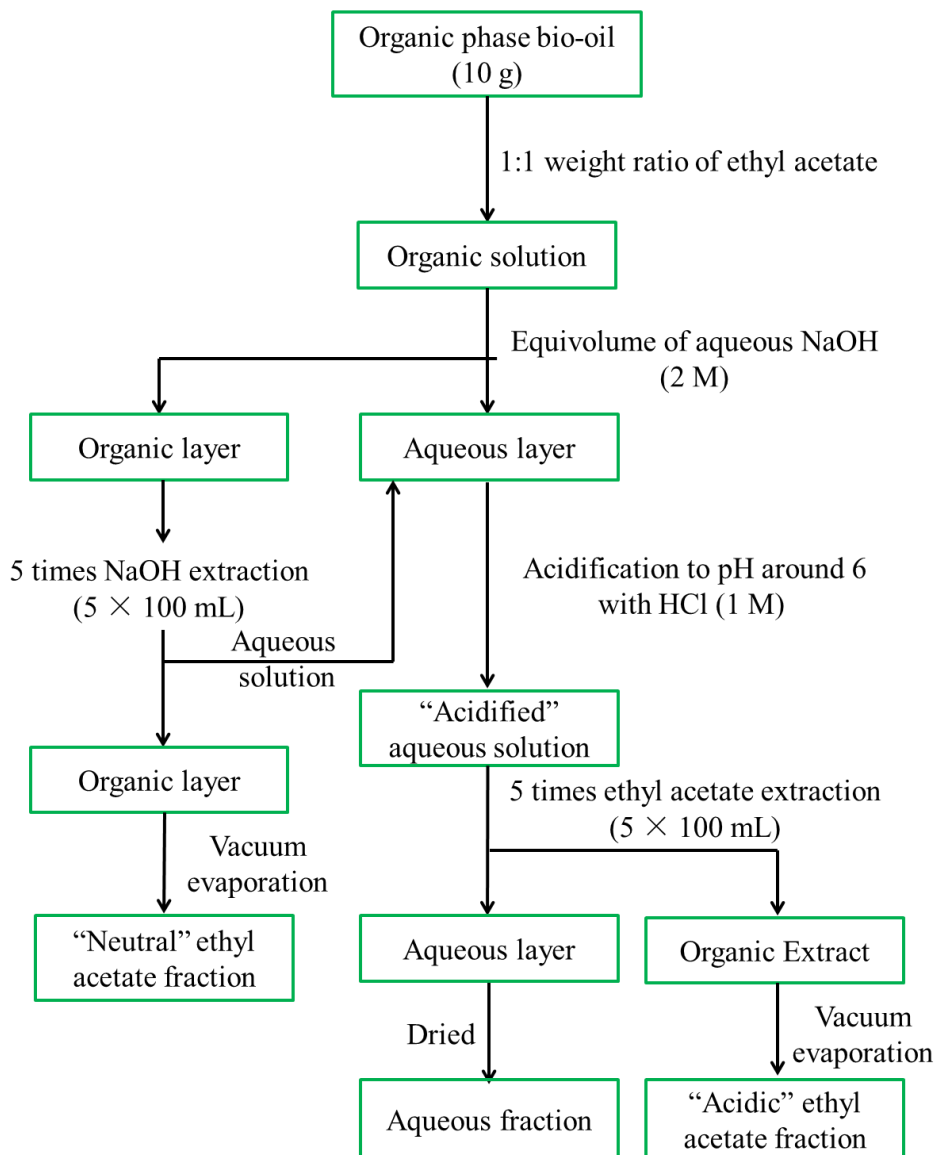


**Figure 57:** Liquid-liquid fractionation of the waste office paper derived organic phase bio-oil.

(Originally in colour)

Basically, the liquid-liquid fractionation procedure comprises five main steps:

**Step 1:** The waste office paper derived organic phase bio-oil (10 g) was dissolved in ethyl acetate at a 1 : 1 weight ratio and transferred to a separating funnel containing an Equivolume of aqueous sodium hydroxide solution (2 M). The mixture was mixed by shaking the separating funnel and settled until two separate layers were formed.

**Step 2:** The aqueous layer was set aside whilst the organic layer (ethyl acetate layer) was further extracted with aqueous 2 M sodium hydroxide solution for five times ( $5 \times 100$  mL).

**Step 3:** The remaining organic layer after five times extraction with aqueous sodium hydroxide in step 2 was isolated, dried and the solvent removed *in vacuo* to give the “neutral” ethyl acetate fraction as red-brown oil (1.9 g).

**Step 4:** The combined aqueous extracts (aqueous layer in step 1 and the aqueous layers extracted in step 2) were acidified with HCl (1 M) until the pH of the solution dropped to around 6.

**Step 5:** Thus obtained “acidified” aqueous solution was extracted with ethyl acetate ( $5 \times 100$  mL), dried and the solvent (*i.e.* ethyl acetate) removed *in vacuo* to afford the “acidic” ethyl acetate fraction as red-brown oil (2.5 g). The water in the aqueous layer was removed to yield the aqueous fraction bio-oil which mainly contains solid matter.

Figure 58 shows the appearances of the “neutral” ethyl acetate fraction, “acidic” ethyl acetate fraction and aqueous fraction bio-oil generated from the liquid-liquid fractionation of the waste office paper derived organic phase bio-oil. As illustrated in Figure 59. The yields for the “neutral” and “acidic” ethyl acetate fractions are 19% and 25%, respectively. For the aqueous fraction, as sodium chloride was generated during the acidification process, the yield for this fraction (56%) was calculated by mass difference.

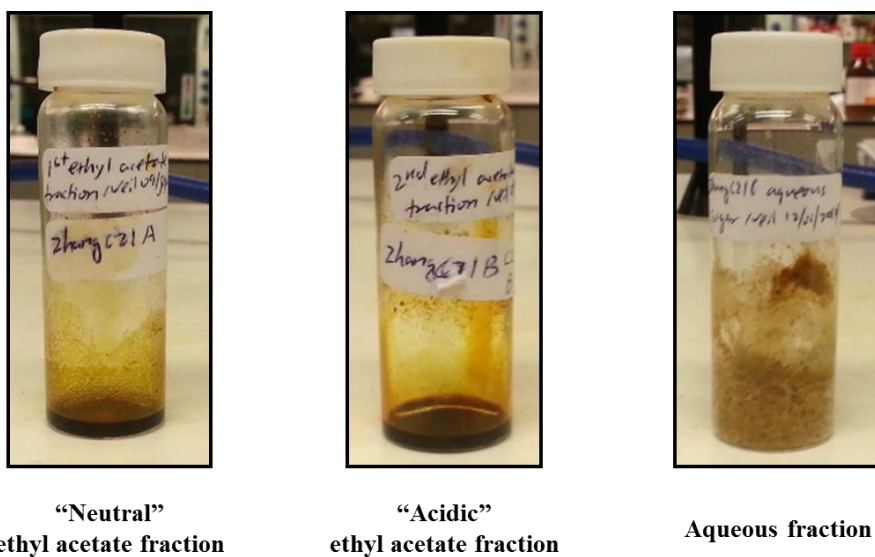


**Figure 58:** Appearances of the “neutral” ethyl acetate fraction, “acidic” ethyl acetate fraction and aqueous fraction bio-oil. (Originally in colour)

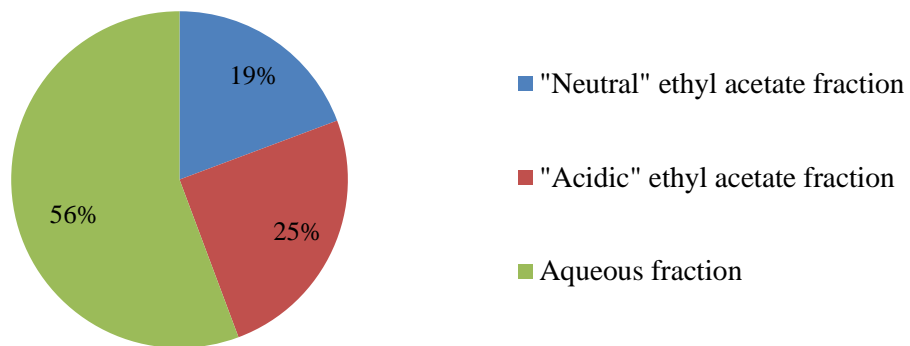


**Figure 59:** Yield of liquid-liquid fractionation of waste office paper derived organic phase bio-oil. (Originally in colour)

### 2.9.2 $^{13}\text{C}$ NMR analysis of different bio-oil fractions

The three bio-oil fractions obtained from liquid-liquid fractionation of the waste office paper derived organic phase bio-oil were dissolved in DMSO-d<sub>6</sub> and characterized with liquid-state  $^{13}\text{C}$  NMR spectroscopy. The analysis method is similar to the one used for liquid-state  $^{13}\text{C}$  NMR characterization of the crude organic phase bio-oils, as described in experimental section 4.2.9 in chapter 4. Figure 60 illustrates the  $^{13}\text{C}$  NMR spectra of “neutral” ethyl acetate fraction,

“acidic” ethyl acetate fraction and aqueous fraction bio-oil. For all the  $^{13}\text{C}$  NMR spectra, the central resonance of DMSO-d<sub>6</sub> ( $\delta\text{C}$ , 39.52 ppm) was used as internal reference.

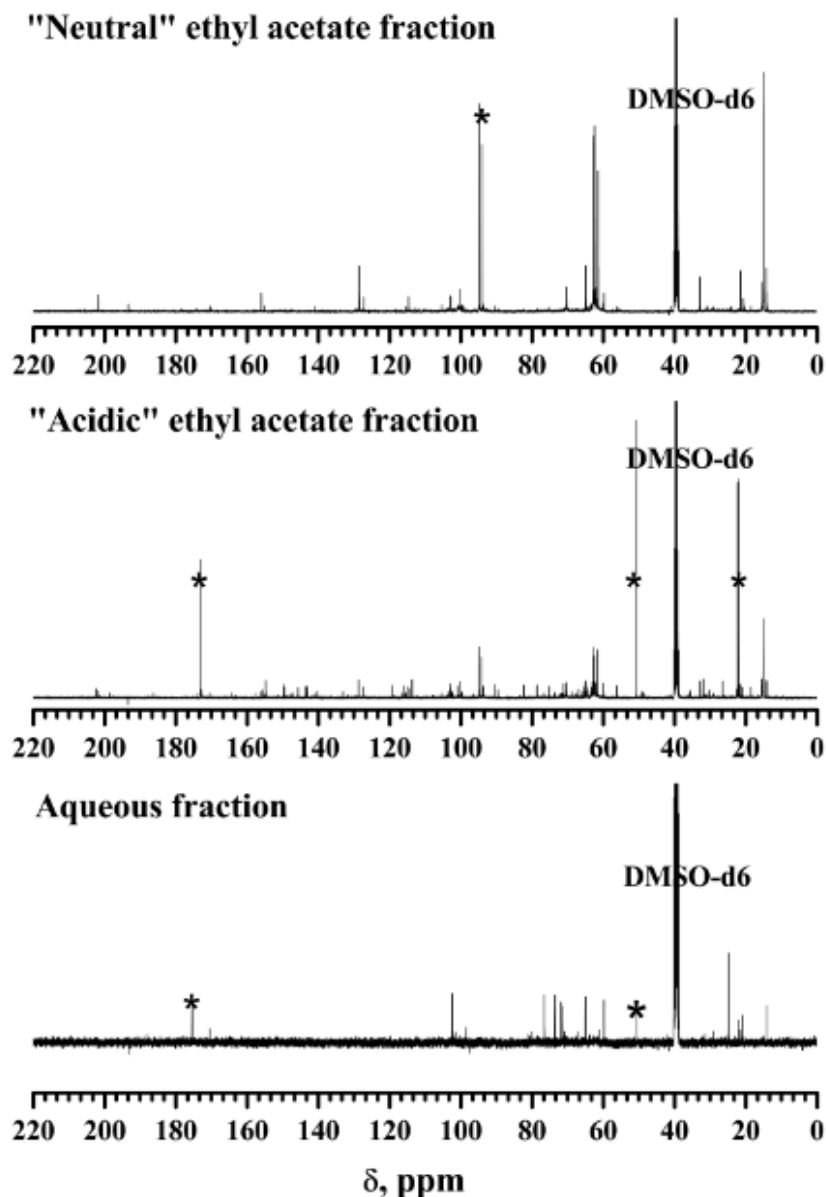


**Figure 60:**  $^{13}\text{C}$  NMR spectra of “neutral” ethyl acetate fraction, “acidic” ethyl acetate fraction and aqueous fraction bio-oil yielded from liquid-liquid fractionation of waste office paper derived organic phase bio-oil (all spectra used the central resonance of DMSO-d<sub>6</sub> ( $\delta\text{C}$ , 39.52 ppm) as internal reference). \*possible artefacts.

Due to the complex chemical composition of the waste office paper derived original organic phase bio-oil, it was very hard to achieve complete separation. Basically, a relatively large percentage of (hetero-) aromatic compounds were separated into the “acidic” ethyl acetate fraction, with many peaks detected in the (hetero-) aromatic portion of the spectrum of “acidic” ethyl acetate fraction bio-oil, ranging from 110 to 165 ppm. The sharp signals (centred at 94 ppm, 62 ppm and 15 ppm) shown in the spectrum of “neutral” ethyl acetate fraction bio-oil were also detected in the “acidic” ethyl acetate fraction bio-oil, but with lower intensities in the spectrum of the “acidic” ethyl acetate fraction. These peaks are possibly due to ethers with relatively short carbon chains. It is noteworthy that the  $^{13}\text{C}$  NMR spectrum of aqueous fraction bio-oil is almost “clean” in the aromatic portion (105 – 165 ppm), with most peaks detected between 55 and 105 ppm (mostly carbohydrate sugars and their derivatives).

### 2.9.3 GC-MS characterization of different bio-oil fractions

The GC traces for the “neutral” ethyl acetate fraction, “acidic” ethyl acetate fraction and aqueous fraction bio-oil resulting from liquid-liquid fractionation of waste office paper derived organic phase bio-oil are shown in Figure 61. The instrumentation and methodology for GC-MS characterization of the three bio-oil fractions are similar to those applied for crude organic phase bio-oils generated from the microwave-assisted pyrolysis experiments, as described in the experimental section 4.2.10 in chapter 4.

It is noteworthy that compared with the GC trace of aqueous fraction bio-oil, carbohydrate sugars were not detected in both the “neutral” ethyl acetate and “acidic” ethyl acetate bio-oil fractions, suggesting most carbohydrate sugars and their derivatives were remaining in the aqueous fraction. Most furans and acidic compounds were separated into the “acidic” ethyl acetate fraction; while some furans and acidic compounds were also detected in the “neutral” ethyl acetate fraction.

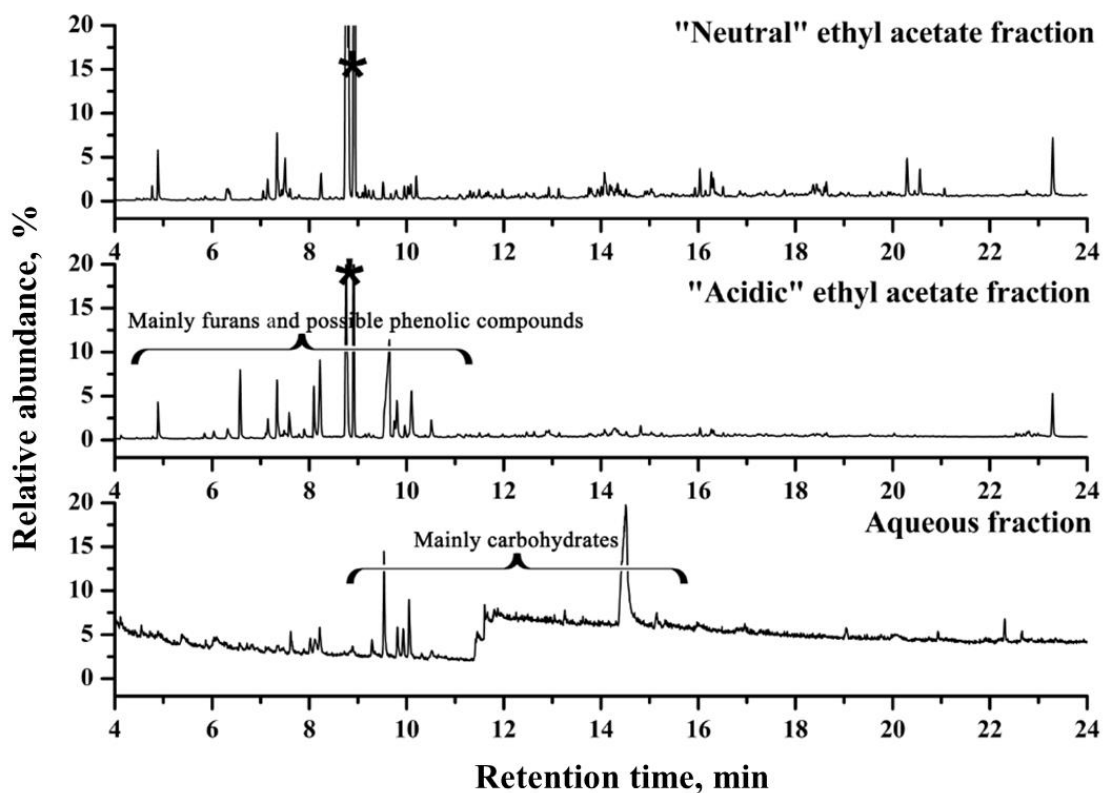


**Figure 61:** GC-MS spectra of “neutral” ethyl acetate fraction, “acidic” ethyl acetate fraction and aqueous fraction bio-oil generated from liquid-liquid separation of waste office paper derived organic phase bio-oil. \*possible artefacts. (Originally in colour)

#### 2.9.4 Adhesive strengths of different bio-oil fractions

To investigate the adhesive properties of the three fractions of bio-oil generated from liquid-liquid separation of the waste office paper derived organic phase bio-oil, they were used as adhesives for Al – Al bonding. The same procedure which was applied for tests of the crude organic phase bio-oils was followed for the bonding and tensile strength tests of the Al plates cured by these three bio-oil fractions.

The tensile strengths of the waste office paper derived organic phase bio-oil, and the subsequently fractionated “neutral” ethyl acetate fraction bio-oil, “acidic” ethyl acetate fraction bio-oil, aqueous fraction bio-oil, as well as the mixture of the two ethyl acetate fraction bio-oil cured Al plates are demonstrated in Figure 62. Specimens were cured in oven at 160 °C for 4 h (the temperature at which maximum tensile strengths were obtained for the Al plates cured by the waste office paper derived organic phase bio-oil).

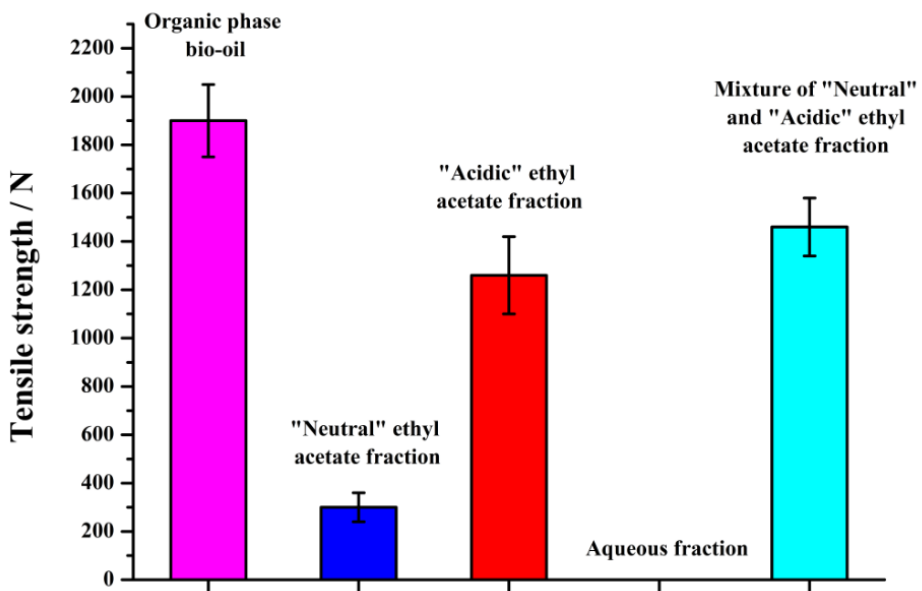


**Figure 62:** Tensile strengths of waste office paper derived organic phase bio-oil, “neutral” and “acidic” ethyl acetate and aqueous fraction bio-oil, and a mixture of the “neutral” and “acidic” ethyl acetate fraction bio-oil cured Al plates (Specimens cured at 160 °C for 4 h. (Originally in colour)

The tensile strengths obtained with different fractions of bio-oil are all lower than that obtained with original organic phase bio-oil generated from low-temperature (<200 °C) microwave-assisted pyrolysis of waste office paper. The tensile strength of the Al-“acidic” ethyl acetate fraction bio-oil-Al bond was about 1260 N, while the “neutral” ethyl acetate fraction bio-oil could also bond the two Al plates but with very weak tensile strength (around 300 N). For the solids obtained from the aqueous fraction bio-oil (water removed), they cannot bond the Al plates at all. As these solids are probably composed of carbohydrates mainly, it is obvious that the carbohydrate sugars by themselves could not bond the Al substrates. An interesting observation is that when the “neutral” ethyl acetate fraction bio-oil and the “acidic” ethyl acetate fraction bio-oil were mixed by a weight ratio of 1 : 1.25 (the same ratio as in the organic phase bio-oil prior fractionation), the tensile strengths of this mixture bonded Al plates (around 1460 N) were higher than those when bonded separately, but still lower than that of organic phase bio-oil (around 1990 N). So it is possible that there is a *co-operative* or *synergistic* effect between the compounds from “neutral” and “acidic” ethyl acetate bio-oil fractions and those from aqueous fraction that is responsible for the bonding properties of the original organic

phase bio-oil, with the aromatic (mainly furanic) and acidic compounds mainly from “acidic” ethyl acetate fraction contributing more towards bonding. Bonding may be similar to phenol-formaldehyde cross-linking and this is further investigated with a model compound study using catechol, HMF and levoglucosan.

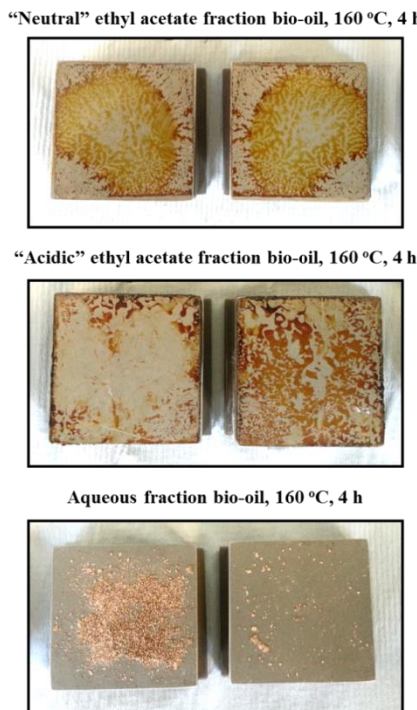


**Figure 63:** Appearances of the Al – bio-oil –Al interfaces of Al plates oven cured by the “neutral” ethyl acetate fraction, “acidic” ethyl acetate fraction and aqueous fraction bio-oil at 160 °C for 4 h. (Originally in colour)

The appearances of the Al–bio-oil–Al interfaces post tensile tests of the Al plates cured by the three bio-oil fractions (*i.e.* “neutral” ethyl acetate fraction, “acidic” ethyl acetate fraction and aqueous fraction bio-oil) are shown in Figure 63. For the specimen cured by “neutral” ethyl acetate fraction bio-oil, similar to the specimens cured by the crude organic phase bio-oils (described in section 2.8.2 in this chapter), the adhesive bonds were broken cohesively. Fractured bio-oil polymers present on both sides of Al plates. Interestingly, the failure pattern of the “acidic” ethyl acetate fraction bio-oil adhered Al plates were broken both cohesively and adhesively (more significant). The reason for this effect needs further investigation. The aqueous fraction bio-oil cannot cure the two Al plates, the residues stayed at the surface of the

Al plate. Figure 64 illustrates the mass loss (wt.%) of the three bio-oil fractions during curing Al plates in oven at 160 °C for 4 h. For comparison, the mass loss of the crude, waste office paper derived organic phase bio-oil (around 38.3 wt.%) under the same curing conditions is also shown in Figure 64. It is obvious that the compounds released during curing were mainly those consisted in the two ethyl acetate bio-oil fractions. The mass loss of the “neutral” and “acidic” ethyl acetate fraction bio-oil during curing is similar: around 41.8 wt.% for the “neutral” ethyl acetate fraction and 42.6 wt.% for the “acidic” ethyl acetate fraction bio-oil. As discussed previously in section 2.8.2, the compounds released during curing probably comprises residual water, small volatile organic compounds and the substances generated from various polymerization reactions occurred during curing. However, the exact chemical composition of the released compounds needs to be further investigated.

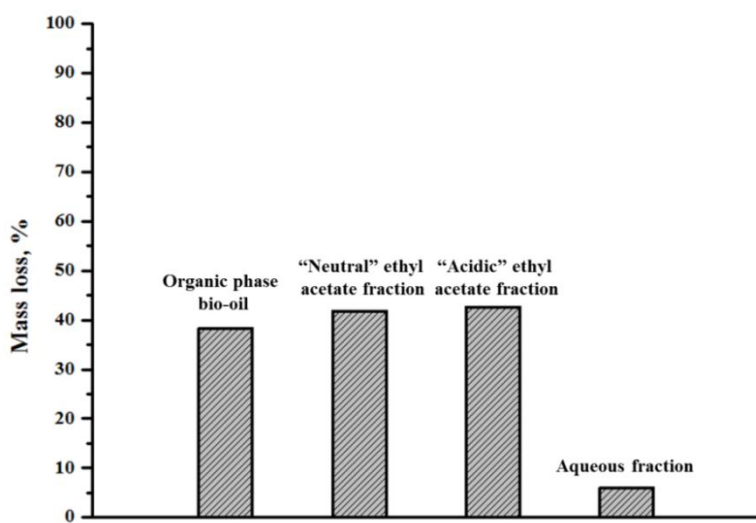


**Figure 64:** Mass loss (wt.%) of waste office paper derived organic phase bio-oil, “neutral” ethyl acetate fraction, “acidic” ethyl acetate fraction and aqueous phase fraction bio-oil during curing Al plates in oven at 160 °C for 4 h curing. (Originally in colour)

## 2.9.5 ATR-IR characterization of scrapings from cured different bio-oil fractions

The hypothesis that the (hetero-) aromatic and acidic compounds consisted in the “acidic” ethyl acetate fraction bio-oil contribute more towards bonding is further proved by the ATR-IR characterization of the bio-oil polymer scrapings. Figure 65 compares the ATR-IR spectra of the “neutral” and “acidic” ethyl acetate fraction bio-oil with the scrapings of formed polymers after

curing Al plates in oven at 160 °C for 4 h. The polymer of the cured “neutral” ethyl acetate fraction bio-oil shows little structural changes before and after curing (Figure 65 A), while the polymer of cured “acidic” ethyl acetate fraction bio-oil shows dramatically significant changes after curing (Figure 65 B). Similar to the waste office paper derived organic phase bio-oil, the intensity of the carbonyl absorption band at 1710 cm<sup>-1</sup> decreased dramatically due to polymerization on the carbonyl bonds. The intensity of the C=C stretching vibration band increased dramatically, and this stretching vibration band slightly shifts to a lower wavenumber (1625 cm<sup>-1</sup> to 1617 cm<sup>-1</sup>). Also, significant structural changes and formation of new chemical bonds can be observed between 1630 cm<sup>-1</sup> and 1450 cm<sup>-1</sup>, which is characteristic of skeletal vibrations of aromatic rings, suggesting the formation of new aromatic structures during curing. The formation of the significant shoulder peak between 1670 cm<sup>-1</sup> and 1530 cm<sup>-1</sup>, together with the dramatic intensity increase of the C=C stretching band at 1617 cm<sup>-1</sup>, probably implies the formation of conjugated aromatic structures during curing. This is also confirmed by the changes in the alkene/aromatic C-H out of the plane bending region (800 cm<sup>-1</sup> to 900 cm<sup>-1</sup>). For the “acidic” ethyl acetate fraction bio-oil, after curing between Al plates, the O-H stretching band drifts to higher wavenumbers, and the carbonyl stretching peak at 1710 cm<sup>-1</sup> slightly drifts to lower wavenumbers, suggesting a reduction of hydrogen bonding.

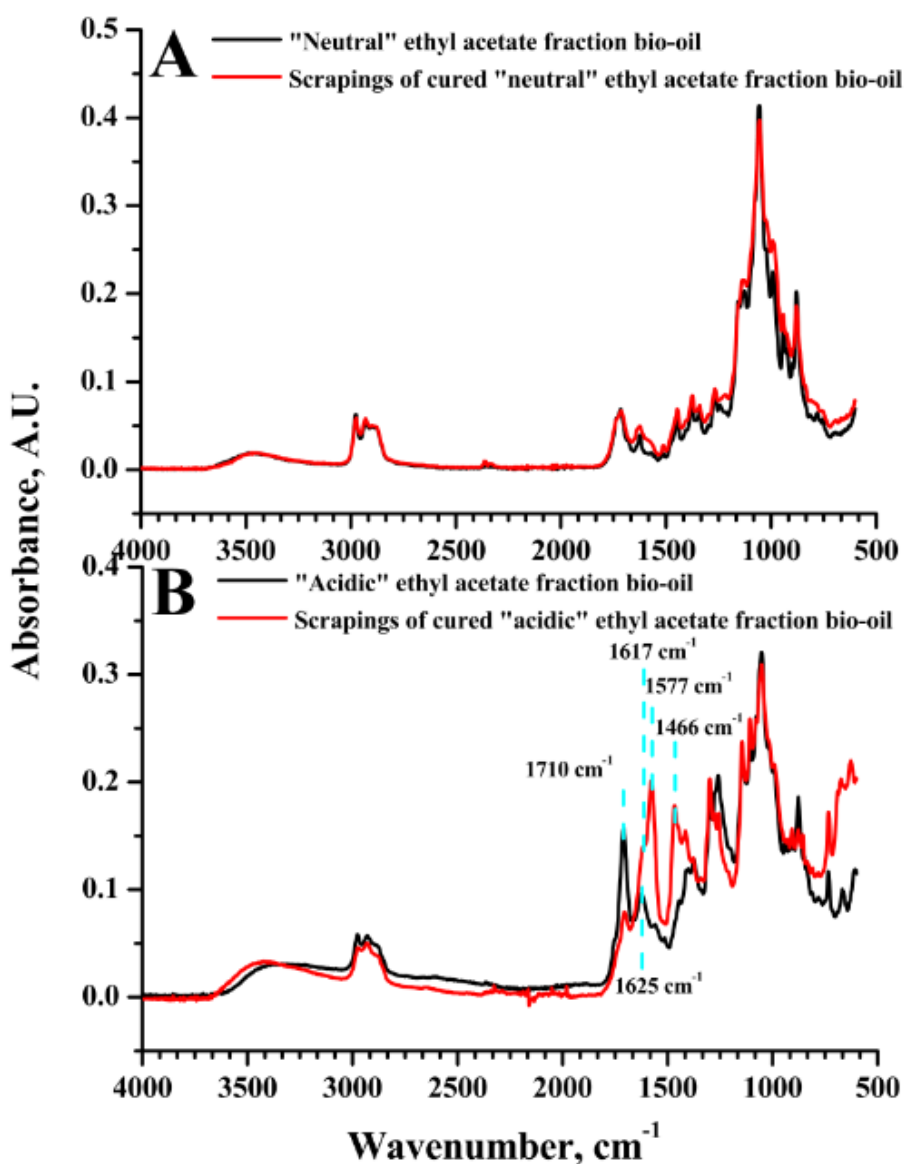


**Figure 65:** ATR-IR spectra of (A) “neutral” ethyl acetate fraction bio-oil and scrapings of cured polymer of this fraction (B) “acidic” ethyl acetate fraction bio-oil and scrapings of cured polymer of this fraction (specimens cured at 160 °C for 4 h). (Originally in colour)

## 2.10 Model compound study of adhesive properties of organic phase bio-oils

From the previous discussions in this chapter, it is revealed that the crude organic phase bio-oils produced from the microwave-assisted low-temperature (<200 °C) pyrolysis of biorenewable feedstocks (*i.e.* spruce wood chips, waste office paper and DIR) are very complicated mixtures

of a wide variety of oxygenated compounds. These compounds are essentially thermal decomposition products of cellulose, hemicellulose and lignin, even though the amounts of these compounds vary significantly depending on the feedstock. Also, it was found that the spruce wood chips and waste office paper derived organic phase bio-oils could efficiently bond two Al plates, with relatively high tensile strengths. As an attempt to gain some understanding of the bonding behaviours and adhesive properties of the complex bio-oils, a model compound study was conducted. Model compound study has been widely used to study particular reactions of bio-oil.<sup>202–205</sup> Hu *et al.* also investigated the polymerization reactions on heating up of bio-oil using model compound study.<sup>206</sup>

Oxygen-containing functional groups (*e.g.*, hydroxyls, carbonyls) present in most chemical compounds in bio-oil. These functional groups activate the compounds, making the reactions between these compounds very complex.<sup>206</sup> Herein, three model compounds (levoglucosan, HMF and catechol) were selected representing carbohydrate sugars, sugar derivatives and aromatics found in bio-oil, to study their contributions towards bonding. More specifically, levoglucosan as a common anhydrate sugar which is generally found in high abundance in bio-oils represents carbohydrate sugars. HMF represents sugar derivatives in bio-oil and catechol is selected to represent aromatic compounds. The chemical structures of these three model compounds are illustrated in Figure 66.

The adhesive properties of these model compounds towards Al bonding was studied by bonding Al plates using single model compound (section 2.10.1), mixtures of each two model compounds with various molar ratios (section 2.10.2) as well as mixtures of the three model compounds with various molar ratios (section 2.10.3). The tensile strengths of adhered Al plates were tested, following the procedure described in experimental section 4.2.12 in chapter 4. The polymers and/or residues on the Al plates post tensile tests were characterized by ATR-IR spectroscopy.

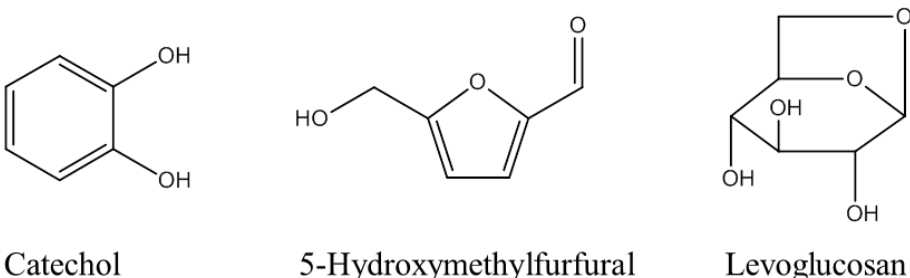


**Figure 66:** Chemical structures of the three selected model chemical compounds (catechol, HMF and levoglucosan).

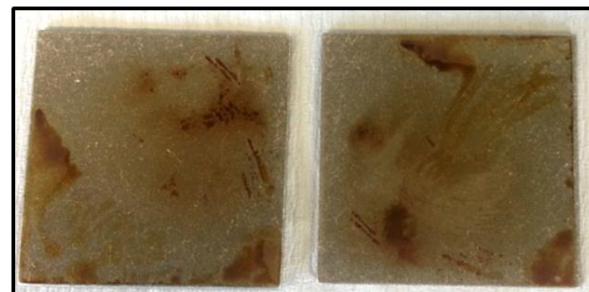
### 2.10.1 Adhesion properties of single model compounds

Each component (70 mg) was applied homogeneously between two Al plates with surface sizes 50 mm × 50 mm. The two Al plates were placed in a lab oven with a stainless steel metal block (around 350 g) on top to mimic a constant pressure at 140 °C for 4 h. After curing in oven, no bonding was achieved for all the specimens, suggesting individual compounds cannot bond Al plates at all. The appearances of the Al– single compound–Al interfaces after heating are shown in Figure 67. The residual material at the Al–HMF–Al interface is a brown colour liquid and the residual solids at the Al–catechol–Al and Al–levoglucosan–Al interfaces are mainly white powders.

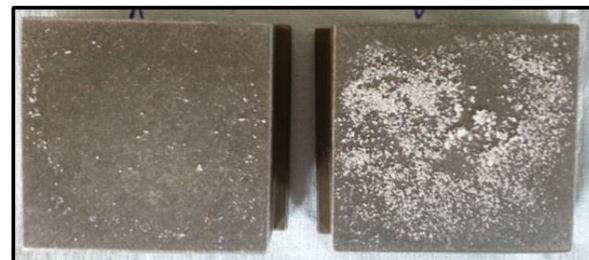
Figure 68, 69 and 70 compares the ATR-IR spectra of the single model compound and the residual matter at the Al – individual compound – Al interfaces post heating in oven for HMF, catechol and levoglucosan, respectively. Many structural changes could be seen in the ATR-IR spectra of HMF and the residual matter at the Al – HMF – Al interface (Figure 68). For example, the O-H stretching vibration band became very broad compared with that of HMF prior heating. Also, a significant number of changes could be seen in the fingerprint region, especially between 1500 cm<sup>-1</sup> and 500 cm<sup>-1</sup>. These structural changes suggest some reactions such as (partial) oxidation occurred during heating. For the ATR-IR spectra of catechol and the residual matter at the Al – catechol – Al interface (Figure 69), there are no significant changes in the bands for catechol before and after heating. A slight change could be observed around 1000

$\text{cm}^{-1}$ . This indicates that catechol might be polymerized slightly during heating through the formation of new C-C and/or C-O-C bonds. For the ATR-IR spectra of levoglucosan and the residual matter at the interface of Al–levoglucosan–Al (Figure 70), the absorption bands for levoglucosan remain the same after heating, suggesting no change occurred.

**HMF, after curing**



**Levoglucosan, after curing**



**Catechol, after curing**

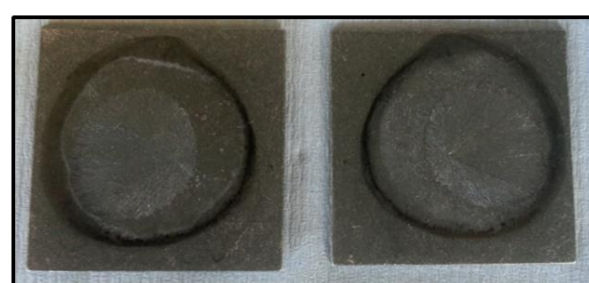


**Figure 67:** Appearances of the Al – single compound –Al interfaces of Al plates oven cured by single model compound (70 mg) at 140 °C for 4 h. (Originally in colour)

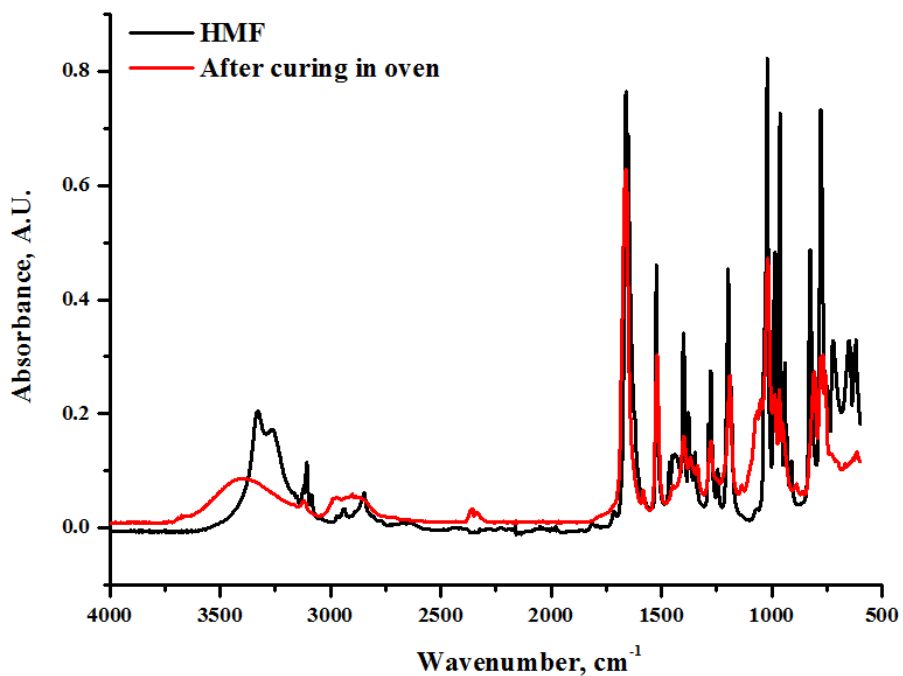


**Figure 68:** ATR-IR spectra of HMF and the residue at the Al-HMF-Al interface after curing at 140 °C for 4 h. (Originally in colour)

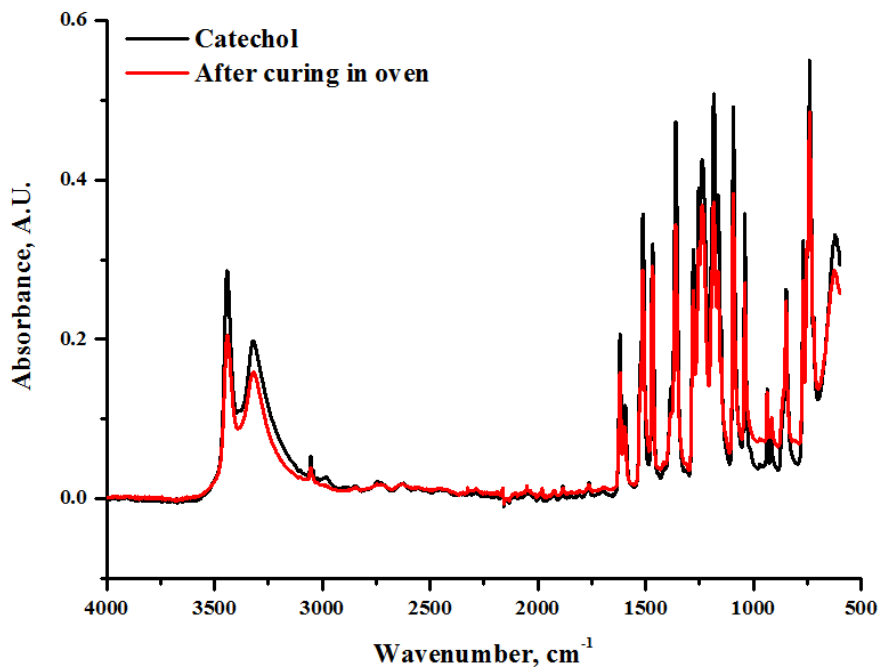


**Figure 69:** ATR-IR spectra of catechol and the residue at the Al-catechol-Al interface after curing at 140 °C for 4 h. (Originally in colour)

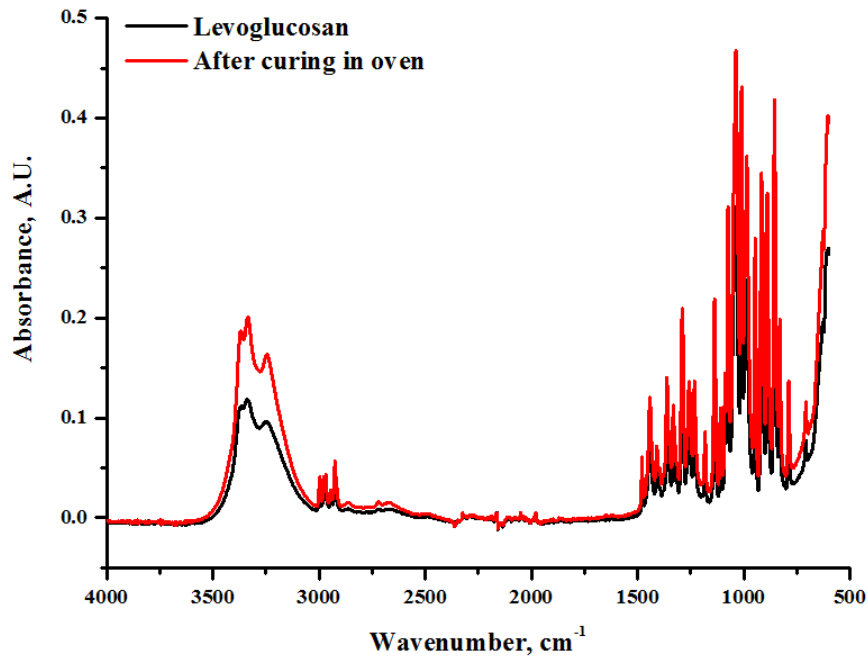


**Figure 70:** ATR-IR spectra of levoglucosan and the residue at the Al-levoglucosan-Al interface after curing at 140 °C for 4 h. (Originally in colour)

### 2.10.2 Adhesion properties of mixtures of two model compounds

Initially, mixtures of each two of the model compounds (70 mg) with various molar ratios (*i.e.* mixture of HMF and levoglucosan with molar ratio 5 : 5, mixture of catechol and HMF with molar ratio 1 : 9 and mixture of catechol and levoglucosan with molar ratio 1 : 9) were applied as adhesives for the bonding of two Al plates. Table 20 summarizes the tensile strengths of the Al plates cured by these mixtures. Basically, the mixture of HMF and levoglucosan (molar ratio 5 : 5) and that of catechol and levoglucosan (molar ratio 1 : 9) show very poor adhesion properties. The tensile strengths of Al plates cured by these two mixtures are very low: around 59 N for the mixture of HMF and levoglucosan, less than 50 N (failure occurred at the start of tensile tests) for the mixture of catechol and levoglucosan. The specimen cured by the mixture of catechol and HMF with molar ratio 1 : 9 has highest tensile strength (around 1734 N). These results indicate that the (hetero-) aromatic and other acidic compounds are of great importance towards good bonding.

**Table 20:** Tensile strengths of Al plates cured by mixtures of each two model compounds (70 mg) with various molar ratios

Mixture	Molar ratio	Tensile strengths (N) <sup>a</sup>
HMF and levoglucosan	5 : 5	59
Catechol and HMF	1 : 9	1734
Catechol and levoglucosan	1 : 9	<50

<sup>a</sup> The reported tensile strengths are averages of four times measurements

The appearances of the Al–mixture (two model compounds)–Al interfaces post tensile tests are illustrated in Figure 71. The residual material remaining on the Al–mixture–Al interfaces for the mixture of HMF and levoglucosan (molar ratio 5 : 5) and that of catechol and levoglucosan (molar ratio 1 : 9) are essentially semisolids. On the contrast, the residue at the Al–mixture–Al interface for the mixture of catechol and HMF (molar ratio 1 : 9) is a polymer adhering on the surfaces of cured Al plates.

**HMF and levoglucosan, after curing**



**HMF and catechol, after curing**



**Levoglucosan and catechol, after curing**

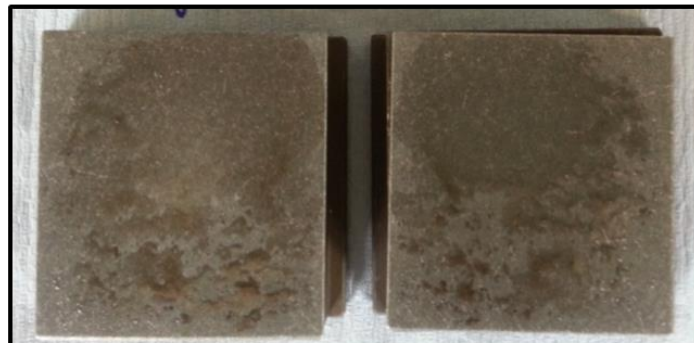


**Figure 71:** Appearances of the Al–mixture–Al interfaces of Al plates oven cured by mixtures of two model compounds (70 mg) at 140 °C for 4 h. (Originally in colour)

It is noteworthy that the failure pattern of the Al plates cured by the mixture of catechol and HMF (molar ratio 1 : 9) is mainly cohesive, although some parts seem to be broken adhesively. According to McBride and Wesselink, catechol and other aromatic compounds as weak acids could be efficiently chemisorbed and bound on Al surfaces.<sup>207</sup> Hence, higher tensile strengths could be potentially achieved with Al plates cured by mixtures containing (hetero-) aromatic compounds.

The high tensile strength of Al plates cured by mixture of catechol and HMF (molar ratio 1 : 9) is mainly attributed to the significant polymerization reactions between these two model compounds. Phenolic compounds contain conjugated  $\pi$  bonds, which could be easily targeted by electrophilic reagents. Hence, phenolic compounds (*e.g.*, catechol) could directly react with other compounds within bio-oil such as furans to form a polymer.<sup>206</sup> In addition, during curing Al plates with bio-oil in oven, phenolic compounds could act as catalysts for the acid-catalyzed polymerization reactions. The organic phase bio-oils generated from microwave-assisted low-temperature (<200 °C) pyrolysis of spruce wood chips, waste office paper and DIR also contain small amounts of carboxylic acids including acetic acid. These acids could also act as catalysts for acid-catalyzed polymerization reactions. Due to the higher acidity of these carboxylic acids, they are much more efficient than phenolic compounds as catalysts.<sup>206</sup>

Furthermore, Hu *et al.* have pointed out that among the various carbohydrate sugar derivatives, furans (*e.g.*, furfural, HMF) present the highest tendency towards polymerization.<sup>206</sup> This is mainly attributed to the presence of conjugated  $\pi$  bonds in furan rings and the carbonyl groups containing in many furan derivatives such as HMF. Figure 72 shows a possible reaction pathway for phenolic compounds and furans in the presence of acid catalysts (*e.g.*, carboxylic acids, phenolic compounds).

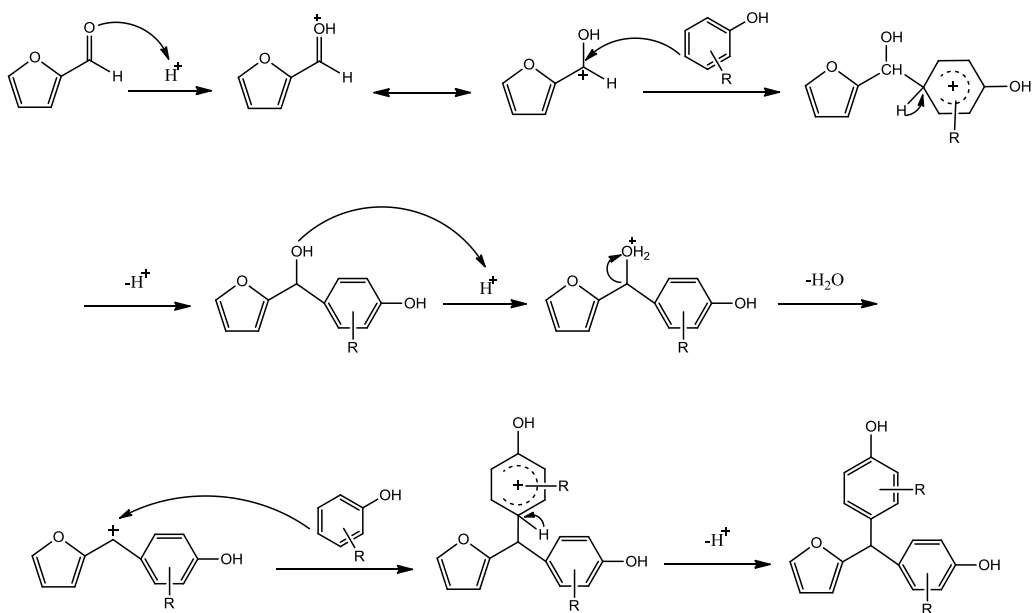


**Figure 72:** Illustration of a potential reaction pathway for phenolic compounds and furans in the presence of acid catalysts (*e.g.*, carboxylic acids, phenolic compounds)

Figure 73, 74 and 75 demonstrate the ATR-IR spectra of the residual materials at the Al–mixture–Al interfaces post tensile tests and those of the mixture of HMF and levoglucosan with molar ratio 5 : 5 (Figure 73), mixture of catechol and HMF with molar ratio 1 : 9 (Figure 74) and mixture of catechol and levoglucosan with molar ratio 1 : 9 (Figure 75). The ATR-IR spectra of the mixture of HMF and levoglucosan (molar ratio: 5 : 5) in Figure 73 shows a much broader absorption band between  $3700\text{ cm}^{-1}$  and  $3000\text{ cm}^{-1}$ , compared with the absorption bands in this region in the ATR-IR spectra of single HMF (Figure 68) and levoglucosan (Figure 70). This is probably due to the formation of various hydrogen bonds between the hydroxyl groups of HMF and levoglucosan during mixing. Significant structural changes occurred during curing Al plates in oven with the mixture of HMF and levoglucosan (molar ratio: 5 : 5). The intensity of the carbonyl stretching vibration band centred at around  $1662\text{ cm}^{-1}$  significantly decreased, along with many structural changes in the fingerprint region between  $1500\text{ cm}^{-1}$  and  $500\text{ cm}^{-1}$ . Also, the shape of the absorption band characteristic for O-H stretching vibration has changed dramatically. All these changes in the ATR-IR spectra of this mixture before and after curing suggest various reactions occurred between HMF and levoglucosan. Reactions between the HMF molecules also led to the significant changes observed in the ATR-IR spectra.

However, these reactions did not contribute to bonding, the tensile strength of Al plates cured by the mixture of HMF and levoglucosan is only around 59 N.

Polymerization between HMF and catechol during curing is evidenced by the many structures changes as can be seen from the ATR-IR spectra of the mixture of these two compounds before and after curing (Figure 74). The differences in the region between  $3000\text{ cm}^{-1}$  and  $2800\text{ cm}^{-1}$  indicate that the C-H structures in the polymer are significantly different from the original mixtures. Various changes in the region between  $2000\text{ cm}^{-1}$  and  $500\text{ cm}^{-1}$  indicate the formation of new structures such as C-C, C-O and C-O-C etc. No significant differences could be observed from the ATR-IR spectra of the mixture of catechol and levoglucosan with molar ratio 1 : 9 before and after curing (Figure 75). A slightly broad, low-intensity absorption band appears at around  $1636\text{ cm}^{-1}$  in the ATR-IR spectrum of the residual materials at the interface of Al-mixture (catechol and levoglucosan)-Al interface. The appearance of this band is probably due to water, suggesting dehydration reactions between catechol and levoglucosan might occur during curing Al plates in oven.

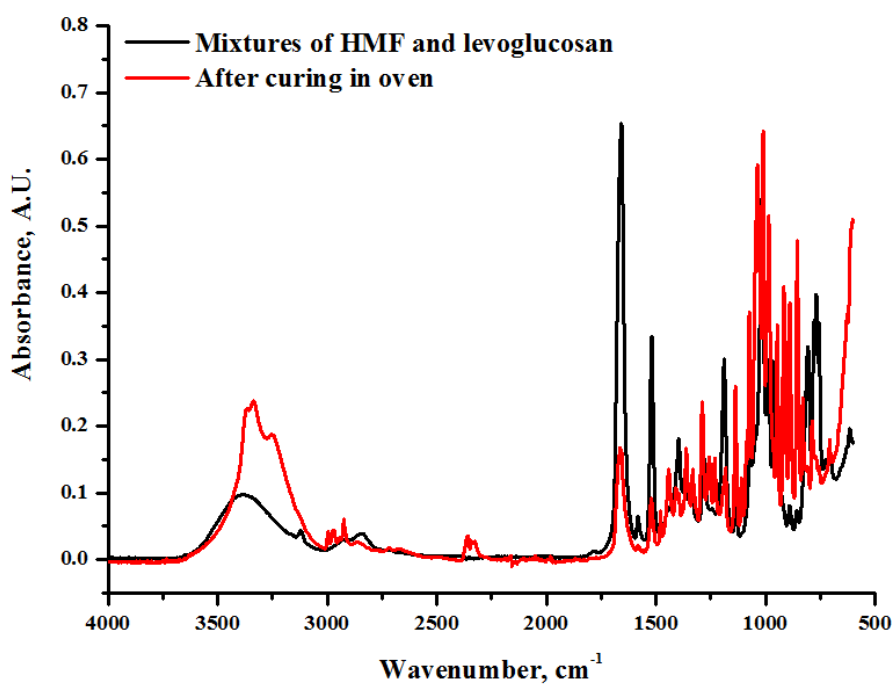


**Figure 73:** ATR-IR spectra of mixtures of HMF and levoglucosan with molar ratio 5 : 5 and the residue at the Al-mixture-Al interface after curing at  $140\text{ }^{\circ}\text{C}$  for 4 h. (Originally in colour)

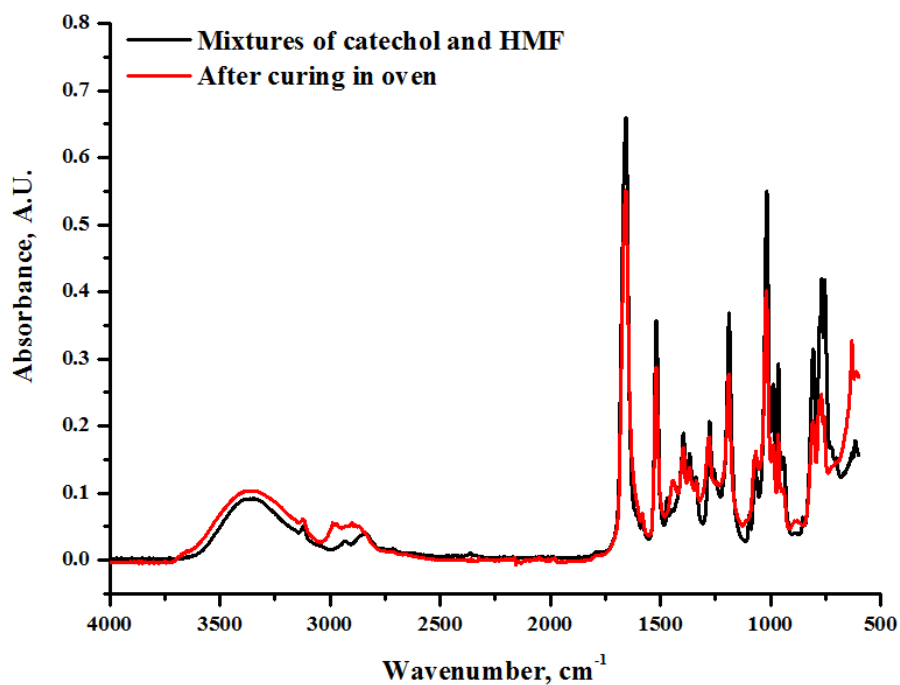


**Figure 74:** ATR-IR spectra of mixtures of catechol and HMF with molar ratio 1 : 9 and the residue at the Al–mixture–Al interface after curing at 140 °C for 4 h. (Originally in colour)

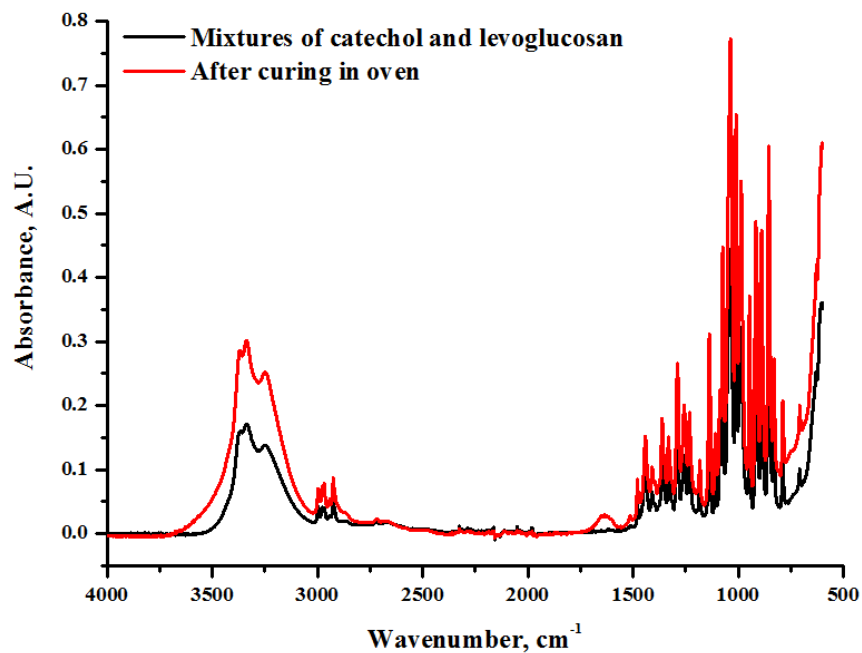


**Figure 75:** ATR-IR spectra of mixtures of catechol and levoglucosan with molar ratio 1 : 9 and the residue at the Al–mixture–Al interface after curing at 140 °C for 4 h. (Originally in colour)

For the Al plates adhered with mixtures of each two model compounds with various molar ratios (70 mg), the highest tensile strength (around 1734 N) of adhered Al plates was obtained with the mixture of catechol and HMF (molar ratio 1 : 9). To further investigate the influence of the amount of phenolic compounds on the tensile strengths of adhered Al plates, mixtures of catechol and HMF with molar ratio 3 : 7 and 5 : 5 were prepared and applied as adhesives for Al bonding. These specimens were also cured in oven at 140 °C for 4 h. Figure 76 illustrates the average tensile strengths of Al plates cured by mixtures of catechol and HMF with various molar ratios: 1 : 9, 3 : 7, and 5 : 5. It is obvious that the tensile strengths of adhered Al plates increase with the amounts of catechol significantly. The average tensile strength of Al plates cured by the mixture of catechol and HMF with molar ratio 3 : 7 is 3785 N, almost doubled the average tensile strength obtained with the mixture of catechol and HMF with molar ratio 1 : 9 (1734 N). For Al plates cured with the mixture of catechol and HMF with molar ratio 5 : 5, the specimens could not be pulled apart during tensile tests and the tests were stopped manually when the tensile strength reached around 6000 N.

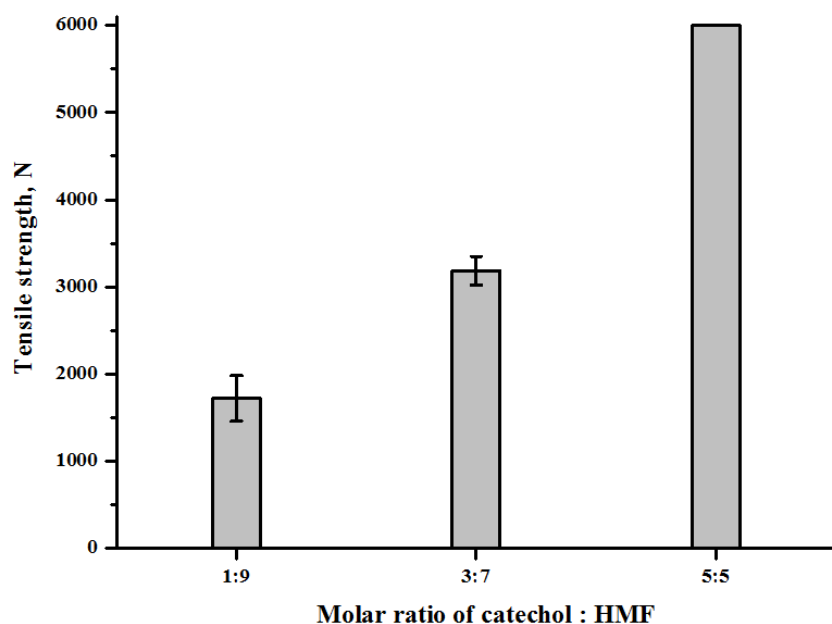


**Figure 76:** Tensile strengths of Al plates cured by catechol and HMF mixtures with various molar ratios (1 : 1, 3 : 7 and 5 : 5), specimens cured at 140 °C for 4 h. (Originally in colour)

### 2.10.3 Adhesion properties of mixtures of three model compounds

From the discussions above, it is clear that the presence of (hetero-) aromatic compounds (*e.g.*, furanics) in the bio-oil is of pivotal importance to achieve high tensile strengths. The polymerization reactions between aromatic compounds and furans probably contribute most towards good adhesion. In this section, the adhesive properties of mixtures of the three compounds were investigated, with emphasis on studying the influences of the amount of catechol on the mixtures' adhesive properties. For preparing the mixtures of three model compounds, the molar ratio of catechol increased from 4% to 40% while that of HMF and levoglucosan remaining the same. Each mixture (70 mg) was applied as adhesives for Al bonding and the specimens were cured in oven at 140 °C for 4 h, following the experimental procedure described in section 4.2.12 in chapter 4.

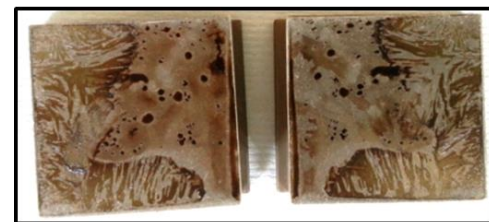
Figure 77 shows the exact molar ratios of the three compounds in each mixture and the appearances of the Al–mixture (three model compounds)–Al interfaces post tensile tests. The tensile strengths of Al plates cured with the mixtures of catechol, HMF and levoglucosan at various molar ratios are illustrated in Figure 78. For Al plates cured by the mixtures with a relatively low catechol content (*i.e.* mixtures of catechol, HMF and levoglucosan with molar ratio 4 : 48 : 48 and 8 : 42 : 42), the residual materials at the Al–mixture–Al interface were mainly liquids. Hence, the tensile strengths of Al plates cured with these two mixtures were very low: less than 50 N (failure occurred at the start of tensile tests). With the increasing of molar ratio of catechol in the mixture, the tensile strengths of Al plates cured by the mixtures of three model compounds increased. This is also reflected by the morphology of the fractured polymers at the Al–mixture–Al interfaces (Figure 77). For example, the residual materials at the Al–mixture–Al interfaces for the specimens cured with mixtures of catechol, HMF and levoglucosan with molar ratios 12 : 44 : 44 and 16 : 42 : 42 were polymers, rather than liquids. However, these fractured polymers were still wet. On the contrast, the fractured polymers at the Al–mixture–Al interfaces for the specimens adhered by mixtures of catechol, HMF and levoglucosan with molar ratios 20 : 40 : 40 and 24 : 38 : 38 were dry and stiff.

Maximum tensile strengths (around 5266 N) were obtained with the Al plates cured by mixture of catechol, HMF and levoglucosan with molar ratio 28 : 36 :36. After that, the tensile strengths dropped with increasing of the molar ratio of catechol (Figure 78). Significant differences in the morphology of fractured polymers at the Al– mixture–Al interfaces for specimens cured with mixtures which have very high catechol contents could be observed (Figure 77). For instance, the fractured polymers at the Al – mixture – Al interfaces of specimens cured with mixtures of catechol, HMF and levoglucosan with molar ratio 36 : 32 :32 and 40 : 20 : 20 were more brittle compared with those of other specimens. In addition, it is noteworthy that both cohesive and adhesive failure occurred for the Al plates cured with mixtures of catechol, HMF and levoglucosan with molar ratio 36 : 32 :32 and 40 : 20 : 20. The failure patterns of other specimens cured by mixtures with lower molar ratios of catechol were essentially cohesive, except the one cured with mixture of catechol, HMF and levoglucosan with molar ratio 4 : 48 :48 (surface was liquid).

**C : H : L = 4 : 48 : 48**



**C : H : L = 8 : 46 : 46**



**C : H : L = 12 : 44 : 44**



**C : H : L = 16 : 42 : 42**



**C : H : L = 20 : 40 : 40**



**C : H : L = 24 : 38 : 38**



**C : H : L = 28 : 36 : 36**



**C : H : L = 32 : 34 : 34**



**C : H : L = 36 : 32 : 32**



**C : H : L = 40 : 30 : 30**

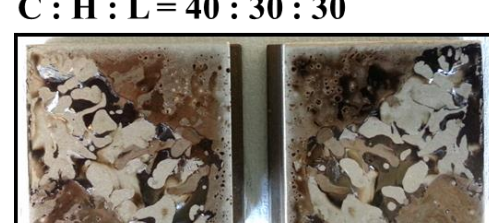


**Figure 77:** Appearances of the Al – mixture –Al interfaces of Al plates oven cured by mixtures of three model compounds (70 mg) with various molar ratios at 140 °C for 4 h. C: catechol; H: HMF; L: levoglucosan. (Originally in colour)

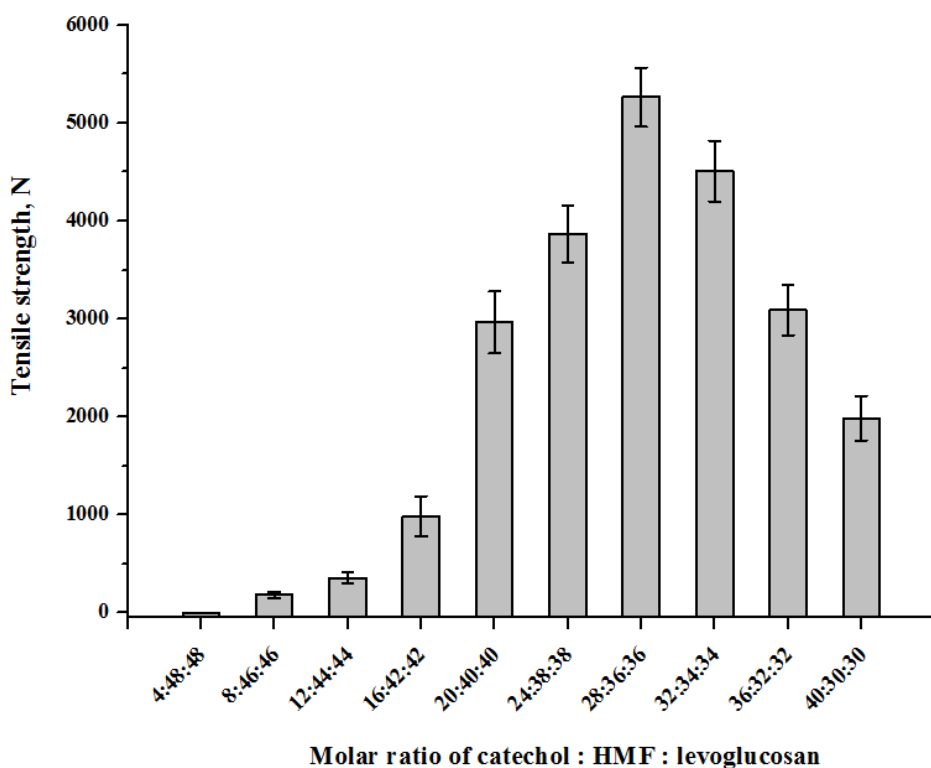


**Figure 78:** Tensile strengths of catechol, HMF and levoglucosan mixtures with variable molar ratios cured Al plates, samples cured at 160 °C for 4 h. (Originally in colour)

The specimens cured with the mixture of catechol, HMF and levoglucosan with molar ratio 28 : 36 : 36 showed the highest tensile strengths (around 5266 N) among the specimens cured by mixtures of three model compounds. The ATR-IR spectra of this mixture and the fractured polymer at the Al–mixture–Al interface of the specimen cured by this mixture are shown in Figure 79. A vast number of structural changes due to polymerization reactions occurred during curing in oven can be seen from the ATR-IR spectra. The shape of the O-H stretching vibration band between 3600 cm<sup>-1</sup> and 3000 cm<sup>-1</sup> changed significantly. It is noteworthy that the small absorption band centred at around 3120 cm<sup>-1</sup> which is a characteristic absorption band for the C-H stretching vibrations of aromatic compounds and/or =C-H stretching vibrations of alkenes completely disappeared after curing. The formation of new C-H structures during polymerization is evidenced by the significant changes between 3000 cm<sup>-1</sup> and 2800 cm<sup>-1</sup>. A similar trend was observed in the ATR-IR spectra of mixture of catechol and HMF with molar ratio 1 : 9 before and after curing in section 2.10.2, Figure 74. The intensity of the carbonyl stretching vibration centred at around 1659 cm<sup>-1</sup> decreased significantly, suggesting

polymerization on the carbonyl groups in HMF. The polymerization reactions occurred during curing in oven also led to the formation of many new structures such as C-C, C-O and C-O-C, as evidenced by the vast number of changes in the fingerprint region between  $1500\text{ cm}^{-1}$  and  $2000\text{ cm}^{-1}$ .

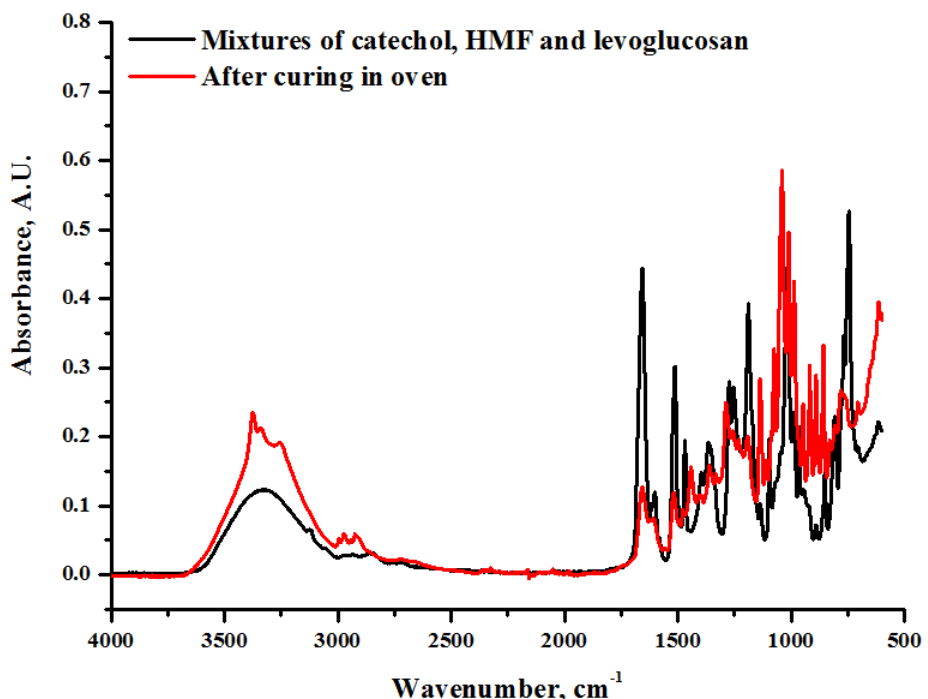


**Figure 79:** ATR-IR spectra of mixture of catechol, HMF and levoglucosan with molar ratio 28 : 36 : 36 and the residue at the Al-mixture-Al interface after curing at  $160\text{ }^{\circ}\text{C}$  for 4 h. (Originally in colour)

## 2.11 Characterization of DIR derived microwave residue

The microwave residue represents the largest fraction (78%) of products generated from microwave-assisted low-temperature ( $<200\text{ }^{\circ}\text{C}$ ) pyrolysis of DIR. From the results presented above in section 2.3, it was found that the microwave-assisted pyrolysis process is very efficient in terms of simultaneously efficient fast separation and recovery of DIR's organic content (as bio-oils) and inorganic content (microwave residue), at relatively low temperatures and within 15 min. The ATR-IR characterization of DIR and its pyrolysis products (section 2.5.3) further

reveals that the microwave-residue essentially contains inorganic matter mainly including calcium carbonate, kaolinite *etc.*

To gain a holistic understanding of the microwave residue, it was further characterized with a variety of analytical techniques in this section. The as-received DIR raw material and the microwave residue were characterized with solid-state CP/MAS  $^{13}\text{C}$  NMR (section 2.11.1). In addition, the morphology of DIR and its microwave residue, together with the TG ashes of DIR obtained from thermogravimetric analysis of DIR in both nitrogen and air atmosphere, were studied with scanning electron microscope (SEM) in section 2.11.2. These materials were also characterized by ATR-IR spectroscopy (section 2.11.3), ICP-MS analysis (section 2.11.4), powder X-ray diffraction (section 2.11.5) as well as solid-state Bloch-decay  $^{13}\text{C}$  NMR spectroscopy (section 2.11.6).

### **2.11.1 Solid-state CP/MAS $^{13}\text{C}$ NMR characterization of DIR and its microwave-residue**

The simultaneously complete separation of organic matter from inorganic content of DIR was also proved by the solid-state CP/MAS  $^{13}\text{C}$  NMR characterization. The instrumentation and methodology for the solid-state CP/MAS  $^{13}\text{C}$  NMR analysis are described in section 4.2.15 in chapter 4.

Figure 80 demonstrates the solid-state CP/MAS  $^{13}\text{C}$  NMR spectra of the DIR raw material and its microwave residue. The major resonance bands of DIR raw material were characterized to be cellulose: C-1 (98 – 110 ppm), C-4 (80 – 92 ppm), C-2, -3, and -5 (70 – 80 ppm), and C-6 (58 – 68 ppm).<sup>208 – 210</sup> Furthermore, similar to naturally occurring cellulose, the DIR containing cellulose also comprises a crystalline phase and a disordered noncrystalline phase. This is evidenced by the two signals between 80 and 92 ppm (C-4). It is well-documented that the band between 86 and 92 ppm is derived from the crystalline region of cellulose and the signal from 80 to 86 ppm may either result from the disordered noncrystalline phase or the crystal surfaces of cellulose.<sup>208 – 211</sup> This is further proved by the shoulder band between 58 and 68 ppm which is assigned to C-6. The signals for the C-6 carbons within the crystalline phase of cellulose are

around 64 ppm, while those for the carbons contained in the disordered noncrystalline phase or crystal surface of cellulose are at about 62 ppm.<sup>208, 209</sup> The <sup>13</sup>C CP/MAS NMR spectra of the microwave residue suggest it contains very little organic material (very low signal-to-noise ratio), indicating that most organic matter of DIR was converted to bio-oil and gaseous products during microwave-assisted pyrolysis.

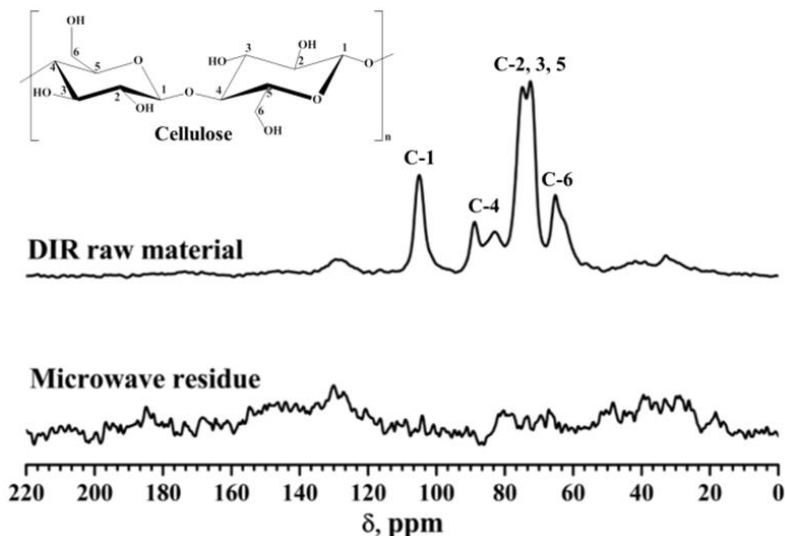


**Figure 80:** Solid-state CP/MAS <sup>13</sup>C NMR spectra of DIR raw material (upper) and its microwave residue (lower).

### 2.11.2 SEM morphology of DIR, microwave residue and TG ashes

The morphologies of DIR, its microwave residue and TG ashes of DIR obtained in both nitrogen and air atmosphere were studied with SEM. Figure 81 and 82 show the representative SEM micrographs of these materials on 100 µm and 10 µm scale, respectively.

The SEM micrographs of the DIR raw material show it contains irregular cracked short fibers and aggregates of inorganic mineral particles, which is a typical morphology of this kind of waste material (Figure 81 A).<sup>173</sup> After thermo-treatment, the amount of short cellulosic fibers significantly decreased. Small amounts of residual fibrous material can be observed in the micrographs of microwave residue (Figure 81 B) and TG ash of DIR obtained in nitrogen atmosphere (Figure 81 C), but not in the micrograph of TG ash of DIR obtained in air

atmosphere (Figure 81 D), as all the organic matter within DIR was burned off when the sample was heated in air to 625 °C.

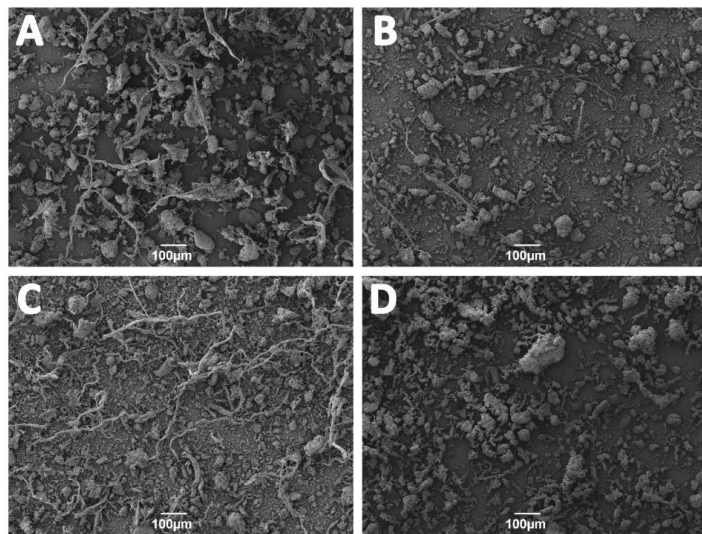


**Figure 81:** Representative SEM micrographs of (A) DIR raw material, (B) microwave residue, (C) TG ash of DIR (in N<sub>2</sub>), (D) TG ash of DIR (in air) on 100 μm scale. (Originally in colour)

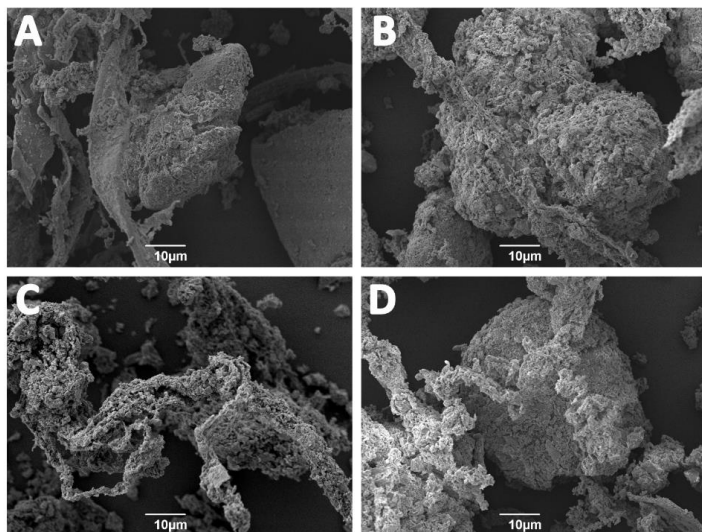


**Figure 82:** Representative SEM micrographs of (A) DIR raw material, (B) microwave residue, (C) TG ash of DIR (in N<sub>2</sub>), (D) TG ash of DIR (in air) on 10 μm scale. (Originally in colour)

### **2.11.3 ATR-IR characterization of DIR, microwave residue and TG ashes**

From the ATR-IR spectra of DIR raw material, microwave residue, and TG ashes of DIR obtained in nitrogen and air atmosphere (Figure 83), it is clear that the O–H stretching vibration (between  $3200\text{ cm}^{-1}$  and  $3600\text{ cm}^{-1}$ ) associated with organic matter (mainly cellulosic fibers) in DIR is not visible in the spectra of microwave residue and TG ashes, indicating most organic matter were converted to other products after thermo-treatment. This is also evidenced by a similar trend in the region between  $3000\text{ cm}^{-1}$  and  $2800\text{ cm}^{-1}$  associated with alkyl stretching vibrations. All of the samples show characteristic absorption bands of calcium carbonate: a strong and broad band at  $1400\text{ cm}^{-1}$  and two sharp bands at  $870\text{ cm}^{-1}$  and  $710\text{ cm}^{-1}$ . Characteristic bands for kaolinite at  $3693\text{ cm}^{-1}$  and  $3619\text{ cm}^{-1}$  can be observed in the spectra of DIR raw material and microwave residue, but not in the spectra of TG ashes, as the kaolinite dehydration and/or dehydroxylation reactions generally take place above  $300\text{ }^{\circ}\text{C}$ . Absorption bands between  $1200\text{ cm}^{-1}$  and  $900\text{ cm}^{-1}$  originate from both kaolinite and residual organic matter. The intensity of absorption bands in this region significantly decreased in the spectra of TG ashes, especially in the spectrum of TG ash of DIR obtained in air atmosphere, as in this case all of the organic matter within DIR was burned off and kaolinite was decomposed. The ICP-MS analysis also confirms calcium is the most predominant metal element in all of these samples, which will be further discussed in section 2.11.4.

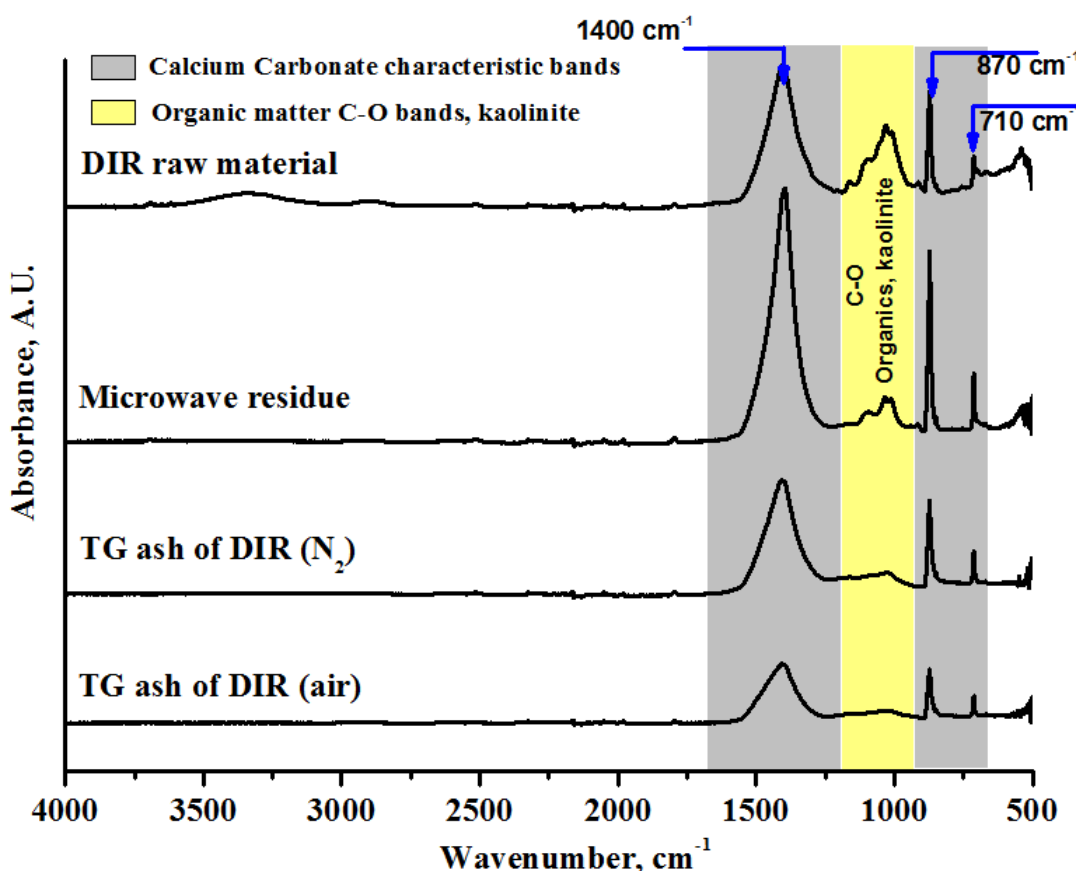


**Figure 83:** ATR-IR spectra of DIR raw material, microwave residue, TG ashes of DIR obtained in  $N_2$  and air atmosphere. (Originally in colour)

#### 2.11.4 ICP-MS analysis of DIR, its microwave residue and TG ashes

The mineral contents of DIR, microwave-residue and the TG ashes obtained from TG analysis of DIR in both nitrogen and air atmosphere are illustrated in Table 21. The ICP-MS characterization of these solid materials was carried out following the experimental procedure described in section 4.2.7 in chapter 4. The ICP-MS analysis further confirms calcium is the most predominant metal element in all of the samples, and all the products obtained after thermo-treatment show an elevated concentration of calcium. In general, the (trace) metal content of TG ash of DIR obtained in air atmosphere is highest among the three samples after thermo-treatment, because all the organic matter and fixed carbons within DIR were burned off completely in air when heated to  $625\text{ }^{\circ}\text{C}$ .

**Table 21:** Mineral contents of DIR raw material, microwave residue, TG ashes of DIR obtained in nitrogen and air atmosphere as determined by ICP-MS

Element (ppm <sup>a</sup> )	DIR raw material	Microwave residue	TG ash of DIR in N <sub>2</sub>	TG ash of DIR in air
<b>Na</b>	957.8	763.1	1110.3	1288.5
<b>Mg</b>	2818.5	3264.4	3479.9	4607
<b>Al</b>	1328.7	5405.8	13037.4	17771.8
<b>Si</b>	75666.8	235726.5	273506.3	297260.5
<b>K</b>	148.3	N.D. <sup>b</sup>	N.D.	234.3
<b>Ca</b>	281806.5	327603.5	328085.6	431019.5
<b>Cr</b>	4.7	5.6	9.7	12.3
<b>Mn</b>	77.2	85.8	85.9	113
<b>Fe</b>	924.8	1351.8	1469.7	1883.8
<b>Cu</b>	52.9	58.2	369.5	265.3
<b>Zn</b>	84.8	102.6	102.2	126.4
<b>As</b>	2.1	1.9	3.0	2.4
<b>Nb</b>	0.23	0.18	0.42	0.56
<b>Pd</b>	0.56	0.63	0.89	0.95
<b>Sn</b>	51.3	65.6	82.1	93.5
<b>Ir</b>	0.18	0.12	0.27	0.35
<b>Pt</b>	0.07	0.08	0.26	0.39
<b>Au</b>	3.65	3.61	4.92	6.73
<b>Pb</b>	2.8	4.6	5.8	7.7
<b>Co</b>	3.4	3.7	4.4	6.1
<b>Ni</b>	2.7	3.8	10.3	5.1
<b>Cd</b>	0.6	0.2	0.2	0.4

<sup>a</sup> ppm refers to parts per million in mass; <sup>b</sup> N.D. = not detected

## **2.11.5 Powder XRD characterization of DIR, microwave residue and TG ashes**

The powder X-ray diffraction patterns of DIR raw material, microwave residue, and TG ashes of DIR obtained in nitrogen and air atmosphere are shown in Figure 84 together with those of commercial calcium carbonate (calcite) and microcrystalline cellulose. The organic content of DIR raw material is mainly cellulose as further confirmed by the band between  $21.3$  and  $22.6^\circ 2\theta$ ,<sup>212, 213</sup> and the inorganic mineral content is predominantly composed of calcite and kaolinite. The cellulose bands are weak mainly due to the low cellulose content in DIR and cellulose degradation reactions that took place during the paper recycling process.<sup>173</sup> After thermo-treatment, cellulose bands are visible neither in the XRD spectra of microwave residue nor in the spectra of DIR TG ashes obtained in nitrogen or air atmosphere, elucidating the conversion of organic matter to other products during thermo-treatment. Also, all of the XRD spectra show the characteristic diffraction pattern of calcite. Calcite is the most thermally stable form of the three forms of calcium carbonate, calcite, aragonite, and vaterite, and is characterized by the predominant band centered at  $2\theta = 29.35^\circ$ .<sup>214</sup> Kaolinite was detected in DIR raw material and microwave residue but not in the TG ashes of DIR. This is probably due to the dehydration and/or dehydroxylation reactions associated with kaolinite when heated to above  $300^\circ \text{C}$ . The maximum sample temperature reached during microwave-assisted pyrolysis of DIR is around  $190^\circ \text{C}$ , which is not high enough for such reactions to take place.

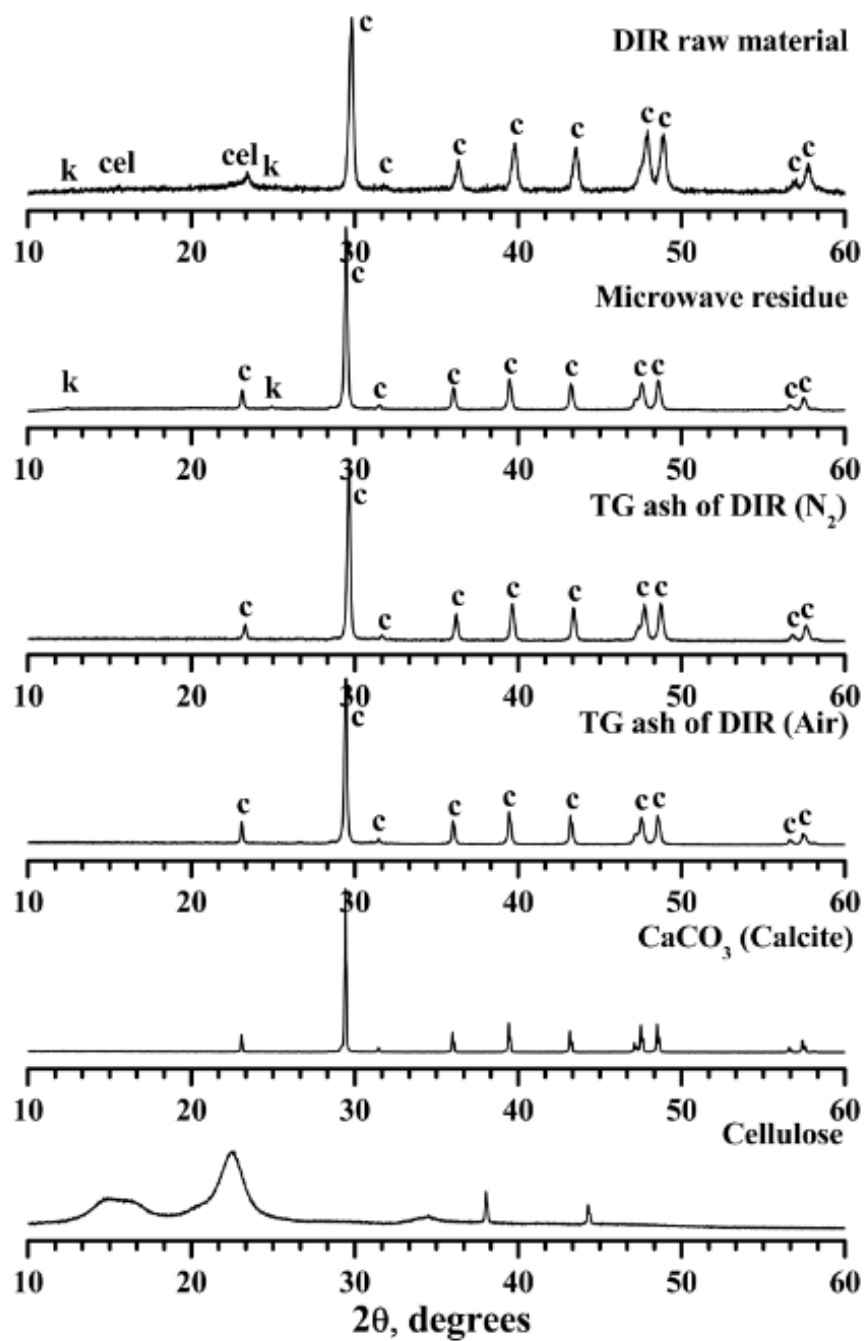


**Figure 84:** Powder XRD patterns of DIR raw material, microwave residue, TG ashes of DIR obtained in  $N_2$  and air atmosphere together with commercial  $CaCO_3$  (calcite) and kaolinite (k: kaolinite; cel: cellulose; c: calcite).

## **2.11.6 Solid-state Bloch-decay $^{13}\text{C}$ NMR characterization of DIR microwave residue**

To further characterize the inorganic content of the solid materials, DIR raw material, microwave residue and TG ashes of DIR obtained in nitrogen and air atmosphere, together with commercial calcium carbonate (calcite), were characterized with solid-state Bloch-decay  $^{13}\text{C}$  NMR spectroscopy (Figure 85). All of these samples show a very strong resonance signal at 168.6 ppm, which is a characteristic resonance signal for the most stable polymorph of calcium carbonate (calcite).<sup>215</sup> The fwhh (full width at half-height) values of the resonance signals are also indicated in Figure 85. Compared with the resonance signal of commercial  $\text{CaCO}_3$  (calcite), the signals for other samples are slightly broader. For example, the fwhh for commercial  $\text{CaCO}_3$  (calcite) is 0.27 ppm, and those for the other samples are around 0.5 ppm. This effect results from and reflects slightly poorer crystallinity of the  $\text{CaCO}_3$  in DIR raw material and its relative products after thermo-treatment.<sup>215</sup>

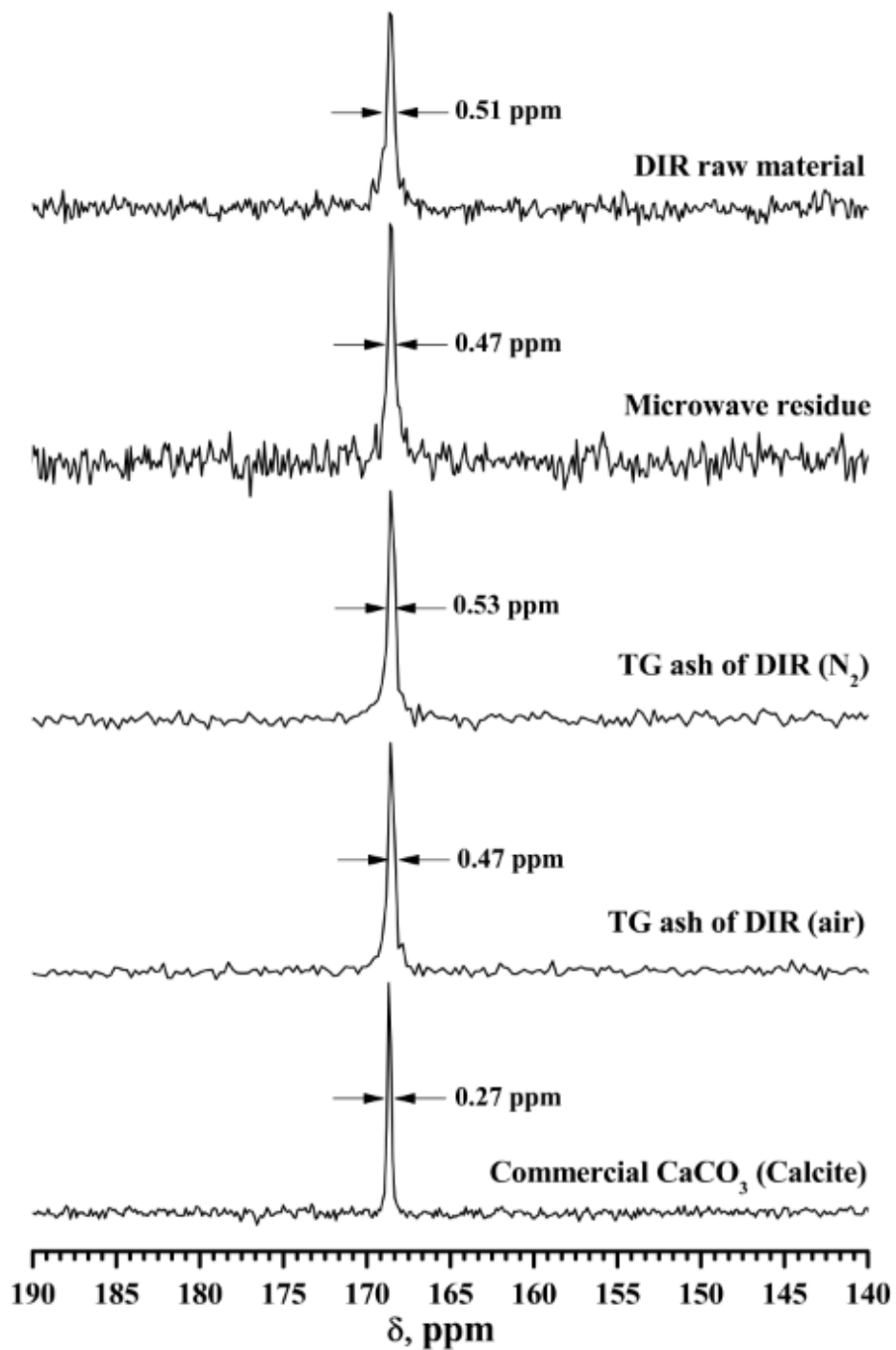


**Figure 85:**  $^{13}\text{C}$  Bloch-decay solid-state NMR spectra of DIR raw material, microwave residue resulting from microwave-assisted pyrolysis of DIR, TG ash of DIR ( $\text{N}_2$ ), TG ash of DIR (air) and commercial  $\text{CaCO}_3$  (calcite), with full width at half height (FWHH) of each signal indicated (background corrected).

## 2.12 Conclusions and future work

It has been demonstrated in this chapter that the microwave-assisted low-temperature ( $<200\text{ }^{\circ}\text{C}$ ) pyrolysis offers great potential for valorisation of biorenewable waste streams by converting these low-value under-utilised materials into value-added products, which could have many innovative applications. As demonstrated in Figure 86, three kinds of biorenewable waste streams including spruce wood chips, waste office paper (printed and/or photocopied), and paper deinking residue (DIR) have been successfully converted into two phases (organic phase and aqueous phase) of bio-oils, bio-char (microwave residue) and gas at relatively low temperatures ( $<200\text{ }^{\circ}\text{C}$ ) within about 15 min.

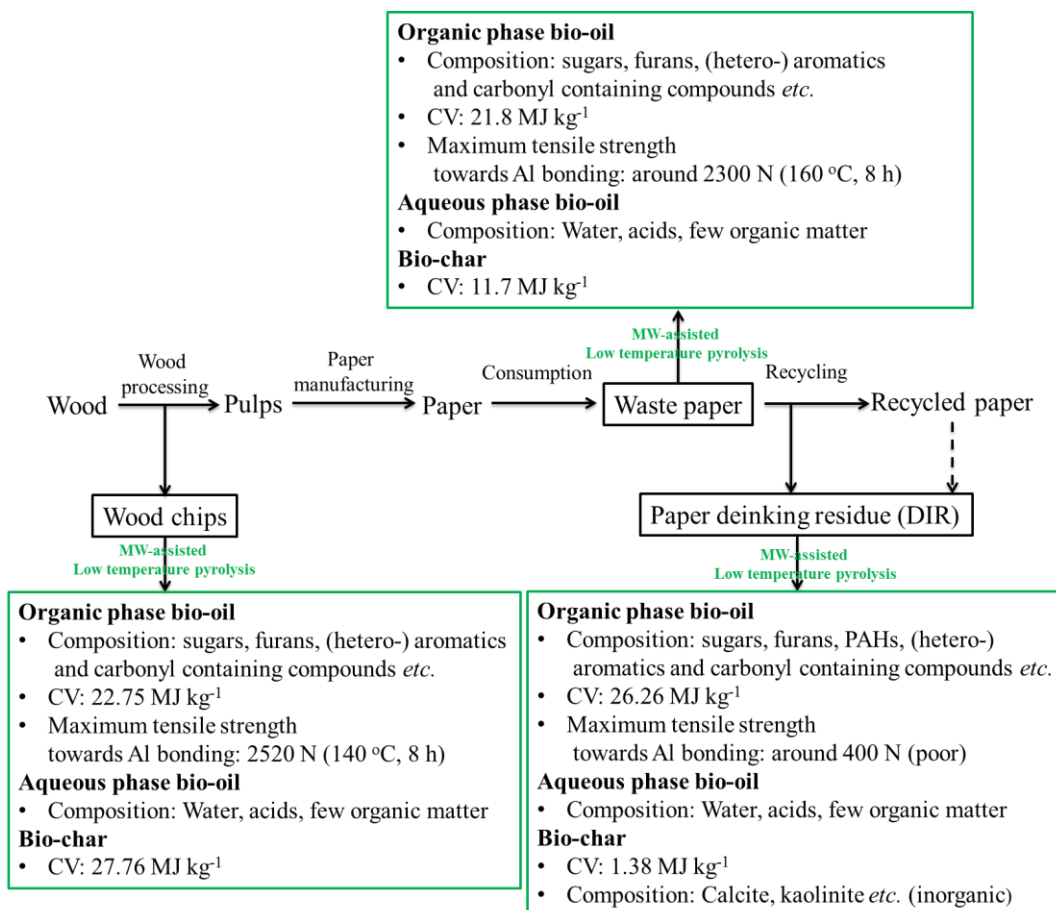


**Figure 86:** Summary of microwave-assisted low-temperature ( $<200\text{ }^{\circ}\text{C}$ ) pyrolysis of three biorenewable waste streams. (Originally in colour)

Using the efficient separation system, the organic phase bio-oils generated from the microwave-assisted processes are energy densified. In other words, the calorific values of the organic phase bio-oils derived from the three biorenewable waste streams are all higher than those of their relative parent material. This effect is most prominent for DIR, the calorific value of DIR derived organic phase bio-oil ( $26.26 \text{ MJ kg}^{-1}$ ) was almost five times higher than that of DIR ( $5.71 \text{ MJ kg}^{-1}$ ). The ICP-MS characterization of the mineral contents of spruce wood chips, waste office paper and DIR and their relative pyrolysis products (organic and aqueous phase bio-oil, bio-char or microwave residue) revealed that the waste office paper, DIR and their pyrolysis products contain significantly higher levels of calcium and silica/silicon, in comparison with those of the spruce wood chips and relative pyrolysis products. This is mainly attributed to the additives including calcium carbonate, kaolinite and silica based and/or potential organosilane sizing agents added to paper products during paper manufacturing processes. From the ATR-IR,  $^1\text{H}$  and  $^{13}\text{C}$  NMR and GC-MS characterization of the organic and aqueous phases of bio-oils derived from the three biorenewable waste streams, it was found that the aqueous phase bio-oils mainly contains water generated from various dehydration reactions occurred during pyrolysis, carboxylic acids and traces amounts of organic matter. On the contrast, the organic phase bio-oils have complex but valuable chemical compositions, with trace amounts of water (less than 2%). The organic phase bio-oils are complex mixtures of broad categories of compounds, mainly including carbohydrate sugars and their derivatives such as levoglucosan and levoglucosenone, furans such as furfural and HMF, (hetero-) aromatic compounds, carbonyl-containing moieties such as aldehydes, ketones and carboxylic acids *etc.* The exact compositions of bio-oils are directly related to their parent material. For instance, due to the high lignin content of spruce wood chips, the organic phase bio-oil generated from microwave-assisted low-temperature ( $<200 \text{ }^\circ\text{C}$ ) pyrolysis of spruce wood chips contains prominently higher amounts of methoxyphenols including guaiacol, creosol *etc.* GC-MS characterization of the DIR derived organic phase bio-oil indicates the presence of polycyclic aromatic hydrocarbons (PAHs) in this phase of bio-oil. These compounds were probably originated from paper additives, coatings, ink particles and/or other chemicals used during deinking processes.

It was found that the organic phase bio-oils generated from microwave-assisted low-temperature (<200 °C) pyrolysis of spruce wood chips and waste office paper hold great potential to be directly used as adhesives for Al – Al bonding. Application of small amounts of spruce wood chips derived organic phase bio-oil (70 mg) to two Al plates followed by curing in oven at various temperatures (120 °C, 140 °C, 160 °C and 180 °C) and time (4 and 8 h), maximum tensile strengths around approximately 2520 N could be reached. The waste office paper derived organic phase bio-oil could also bond Al substrates with high tensile strengths. The highest tensile strengths around 2300 N were obtained for specimens cured at 160 °C for 8 h. It is noteworthy that small amounts of spruce wood chips and waste office paper derived organic phase bio-oils (70 mg) could adhere Al plates with acceptable strengths (>900 N) under all these curing conditions. Also, the tensile strengths increase with curing time. This effect is more prominent at lower curing temperatures (*e.g.*, 120 °C). However, tensile strengths decreased if the curing temperature is too high (*e.g.*, 180 °C), the reason for this phenomenon needs to be further investigated. On the contrast, the tensile strengths of Al plates cured by the DIR derived organic phase bio-oil were only around 400 N, regardless of curing temperature and time. The polymers formed from DIR derived organic phase bio-oil were more “soft” and easier to scratch off compared with those formed from spruce wood chips and waste office paper derived organic phase bio-oils, this is probably due to the presence of polycyclic aromatic hydrocarbons (PAHs) in this phase of bio-oil.

The mass loss of bio-oil during curing in oven varies with curing temperature and time, generally ranging from 30 wt.% to 50 wt.%. Also, the mass loss of bio-oil increases with curing temperature and time, which is probably attributed to evaporation of water, carboxylic acids and/or other volatile compounds within bio-oil and those generated from various polymerization reactions of bio-oil. The true chemical compositions of released compounds also require further investigation. By comparing the ATR-IR and solid-state CP/MAS <sup>13</sup>C NMR (with and without dipolar dephasing) spectra of crude organic phase bio-oils and the scrapings of the formed polymers at the Al – bio-oil – Al interfaces, it was found that there is little or no decomposition of the main structural units including carbohydrate sugars and aromatics. This effect suggests that the possible homo- and cross-coupling polymerisation reactions of bio-oil contribute to

adhesion. The ATR-IR characterization of scrapings also indicates polymerisation reactions occurred on carbonyl groups, and new conjugated and/or aromatic structures were formed during curing.

Liquid-liquid fractionation of the waste office paper derived organic phase bio-oil using alkali and organic solvent (ethyl acetate) was carried out to investigate the influences of different categories of compounds towards bonding. This study further reveals there is a *synergistic* and/or *co-operative* effect between various compounds within bio-oil, while “acidic” compounds such as furans and (hetero-) aromatics contribute most towards good adhesion.

The adhesive properties of bio-oils were further investigated using a model compound study with HMF, catechol and levoglucosan. It was revealed that the presence of furans and aromatic compounds (even trace amounts) is of paramount importance for good adhesion. This result is in agreement with the liquid-liquid fractionation study of the waste office paper derived organic phase bio-oil. It is well documented in the literature that furans such as furfural and HMF have the highest tendency towards polymerization. The aromatic compounds could directly react with furans to form a polymer and could also act as catalysts for the acid-catalyzed polymerisation reactions. In addition, it was pointed out in the literature that the (hetero-) aromatic compounds could be effectively chemisorbed and bound on Al surfaces. The presence of small amounts of carboxylic acids might also catalyze the various polymerisation reactions of bio-oil, as their acidity is much higher than that of phenolic compounds. Future work should also include the study of the effects of carboxylic acids towards bonding.

From the microwave-assisted low-temperature (<200 °C) pyrolysis of DIR, it was found that this process allows for simultaneously efficient fast separation and recovery of the organic and inorganic content of DIR at relatively low temperature and within 15 min. The organic content of DIR was converted to bio-oils and gas while the inorganic content (mainly calcium carbonate and kaolinite) remaining as microwave residue during pyrolysis. The microwave residue represents the largest fraction of products (78%) and is almost free from organic matter as evidenced by TG analysis, SEM, ATR-IR characterization. In addition, the microwave residue

was comprehensively characterized with solid-state CP/MAS  $^{13}\text{C}$  NMR, XRD, ICP-MS and solid-state Bloch-decay  $^{13}\text{C}$  NMR. The results further revealed that the microwave residue contained calcium carbonate is calcite, which is the most thermally stable form among the three forms of calcium carbonate. The fact that the microwave residue predominantly comprises calcite and kaolinite and is free from organic matter potentially allows its reuse in the paper recycling process to produce new paper/cardboard products. Thus, it should be industrially favorable. Notably, this study on microwave-assisted low-temperature ( $<200\text{ }^{\circ}\text{C}$ ) pyrolysis of DIR is the first highly detailed account of the use of microwave-assisted pyrolysis at low temperatures to effect this change. Also, as illustrated in Figure 87, this study demonstrates a potential route for valorisation of DIR in the concept of biorefinery using a low-environmental-impact technology.

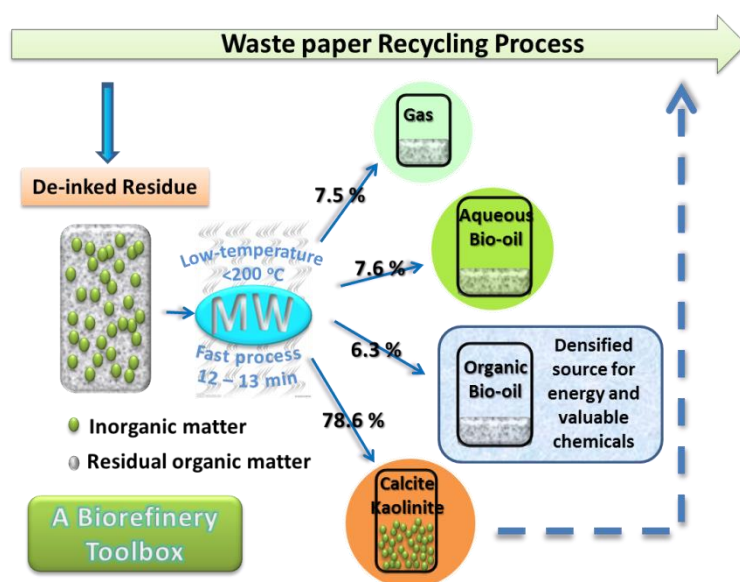


**Figure 87:** Illustration of a potential route for valorisation of DIR in the concept of biorefinery.  
(Originally in colour)

# Chapter 3

## *Valorisation of waste starch and the application of expanded starch and its esters in hot melt adhesives*

Aspect of work described in this chapter has been published in:

Z. Zhang, D. J. Macquarrie, J. H. Clark and A. S. Matharu, *RSC Advances*,  
2014, **4**, 41947-41955.



### **3.1 Summary**

The application of expanded high amylose corn starch (HACS) and its propionate derivatives with differing degrees of substitution (DS) in a formulation comprising polyvinyl alcohol (PVOH) and glycerol to afford potentially biodegradable hot melt adhesives is studied. Esterification of expanded starch was conducted to increase the stability and hydrophobicity of starch. The effects of amounts of esterifying reagent (propionic anhydride) and reaction time on DS of starch propionates were investigated. Native HACS was expanded (BET surface area,  $176\text{ m}^2\text{ g}^{-1}$ ; DS, 0) and derived propionate esters were studied by ATR-IR, TGA, solid-state  $^{13}\text{C}$  CP/MAS NMR,  $^1\text{H}$  NMR and titrimetric methods. The HMAs, irrespective of DS, displayed a glass transition temperature ( $T_g$ ) at approximately  $0\text{ }^\circ\text{C}$ , melting ( $T_{\text{peak}}$ ) at approximately  $160\text{ }^\circ\text{C}$  and crystallisation (on cooling) at approximately  $115\text{ }^\circ\text{C}$ . The adhesive properties (tensile strength) with respect to DS of expanded high amylose corn starch and its propionate esters show a distinct structure–property relationship. Expanded high amylose corn starch (DS, 0) gives the strongest adhesion, outperforming native (non-expanded) starch. The expansion process is beneficial in promoting adhesion which may be linked to the increased availability of hydroxyl moieties promoting better non-covalent interactions and mixing with PVOH and glycerol. Adhesion strengths decrease with increasing DS of base polymer and those of starch propionates with DS in the range 1.46 – 1.82 are comparable to that of non-expanded HACS based HMA.

### **3.2 Introduction**

#### **3.2.1 Hot melt adhesives**

In 2013, the total global market for adhesives and sealants reached about €34 billion, representing a global demand for over 13 million tonnes of adhesives.<sup>216</sup> Among these, hot melt adhesives (HMAs) represent the most dynamically developing area because of a need within the industry to move away from solvent-based adhesives.<sup>217</sup> Actually, since firstly introduced to the market in the 1950s, hot melt adhesives (HMAs) have become increasingly important and now occupy a special place in the adhesive family, reaching 15 – 21% of the global volume of

production and consumption of adhesives around the world.<sup>217</sup> More importantly, the total average annual growth rate of the consumption of HMAs is 1.5 – 2 times higher than that for other types of adhesives.<sup>217</sup> It has been estimated by several analytical and consulting agencies that the global hot melt adhesives market will grow significantly in the foreseeable future, despite their predicted market values are different.<sup>218, 219</sup> The Frost & Sullivan announced that the global hot melt adhesives market will grow from about \$3.56 billion in 2012 to \$ 5.01 billion in 2019 at a compound annual growth rate (CAGR) of around 5.0% in its 2013 report entitled *Global analysis of the hot melt adhesives market*.<sup>218</sup> At the same time, another analytical agency MarketsandMarkets released its market research report about hot melt adhesives, in which it is predicted that the global hot melt adhesives market will be worth \$7 billion by 2018.<sup>219</sup> In both reports, they pointed out that the Asia-Pacific market will be the fastest growing hot melt adhesives market in next several years, although the contribution of this market is currently meagre compared to other regions in the world.<sup>218, 219</sup>

Importantly, according to the market investigation report published by MarketsandMarkets in September, 2013, there is a gradual but clear shift from traditional solvent based adhesives towards reactive and/or hot melt adhesives in terms of global demand for high performance adhesives.<sup>219</sup> This shift in the adhesive portfolio has nurtured the globally fast growing market for HMAs. Also, this trend will be maintained and stimulated by the constant pressure from regulatory authorities such as EPA (Environmental Protection Agency) and the REACH (Registration, Evaluation, Authorisation and Restriction of Chemicals, implemented in the UK since April, 2007).<sup>219</sup> The increasingly stringent regulations will probably limit the use of solvent-borne adhesives in order to reduce and/or eliminate the associated negative environmental impacts, which will in turn boost the global hot melt adhesives market.

Hot melt adhesives are solvent-free thermoplastic materials. Specifically, they are solid materials at low-temperatures (<80 °C) and can melt to liquid or viscous-flow state at elevated temperatures, in which form they are applied on the surface of substrates.<sup>220 - 224</sup> The application temperature of hot melt adhesive depends on the application and the materials that are to be adhered. They regain their solid form and cohesive strength during cooling by solidification

and/or crystallisation, thus adhering two substrates together.<sup>224</sup> A typical temperature – time curve for hot melt adhesive is demonstrated in Figure 88. After application onto substrates in liquid state, the hot melt adhesives transfer to plastic state and then solidified to achieve bonding. The time between application of the hot melt adhesive and the beginning of the plastic state refers to “open time”, which means the second substrate must be applied during this time period to get acceptable bond.<sup>225, 226</sup>

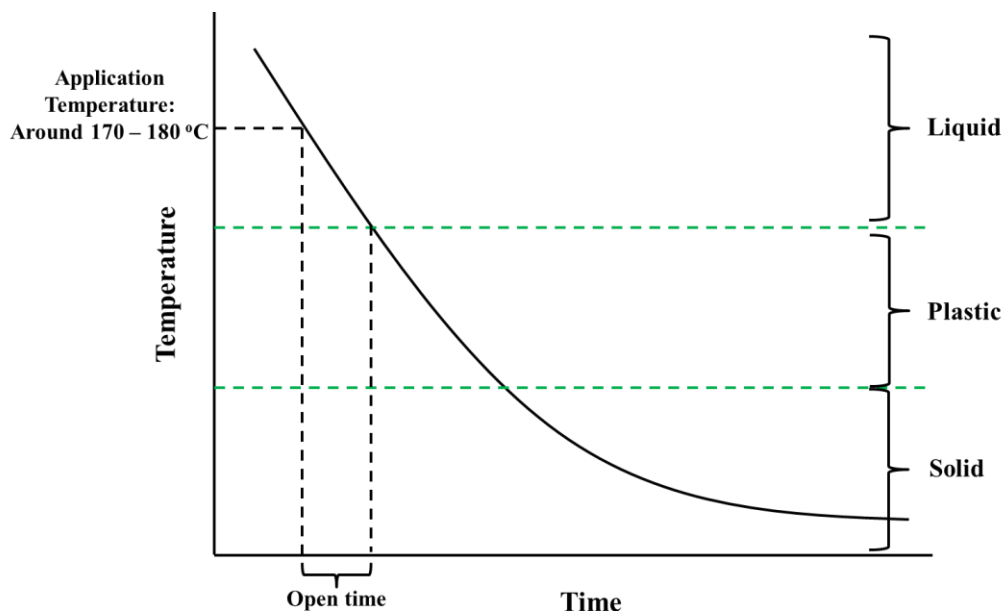


**Figure 88:** Illustration of a typical temperature – time curve for hot melt adhesive, adapted from reference 225 and 226. (Originally in colour)

Compared with conventional solvent-based adhesives which generally involve evaporation and/or removal of solvents or polymerization to bond substrates together, hot melt adhesives show significant advantages. For example, the elimination of a carrier fluid or solvent in HMA formulations not only overcomes the hazards associated with solvent usage and emissions of volatile organic compounds (VOCs), but also allows for faster production speeds and lower costs.<sup>226</sup> Also, their properties could be relatively easily modified to meet different application requirements. Since HMAs are 100% solid materials, they could be produced in various forms such as pellets, slugs, blocks, sticks and continuous rope forms for either bulk application or small-scale applications using heated gun.<sup>219</sup> In addition, HMAs could also “fill the gaps”

between the surfaces of substrates to be adhered because they are applied in liquid state. Last but not least, they are clean and easy to handle.<sup>226</sup>

On the other hand, due to the thermoplastic nature of HMAs, these materials also have several drawbacks, which may limit their use in certain applications.<sup>220, 227</sup> For instance, the bonds may lose strength at elevated temperatures and/or even low temperatures since some HMAs might become brittle if the service temperature is too low. HMAs may be sensitive to certain chemicals and/or solvents and have the tendency to creep and fail with time. The high application temperatures of HMAs could also limit the widespread application of HMAs since the substrates and/or components of a substrate may be sensitive to high temperatures. For HMAs that are highly viscous, sophisticated application equipment may be required.<sup>220, 221</sup>

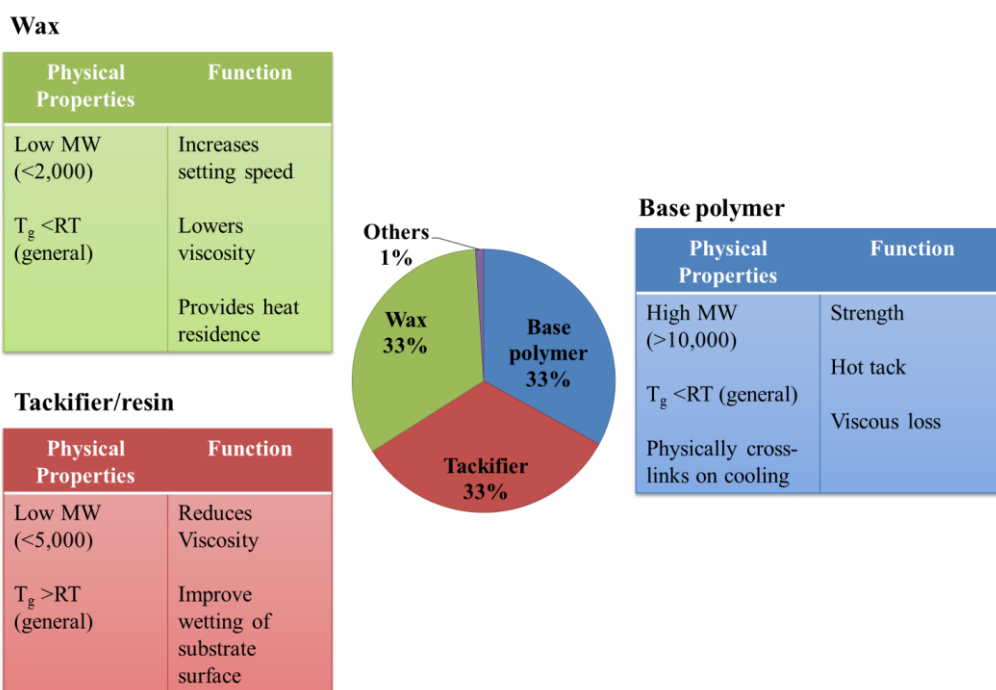


**Figure 89:** Primary constituents of a typical hot melt adhesive and the general properties and functions of each constituent, according to references 225 - 228. (Originally in colour)

In general, HMAs are provided in various forms of complex formulas, and consisting of four main components: polymers (around 33%), tackifiers/resins (around 33%), wax (around 33%) and antioxidants (around 1%).<sup>225 – 228</sup> Some HMAs may have more complicated compositions comprising up to 10 components to meet certain application requirements.<sup>218</sup> Figure 89

demonstrates the primary ingredients of a typical hot melt adhesive, together with the general properties and functions of each ingredient.

Currently, almost all the base and/or major polymers for HMAs on the market are primarily derived from petroleum resources, such as ethylene vinyl acetate (EVA), block copolymers of styrene and butadiene (SBS) or isoprene (SIS), polyesters, polyamides, polyurethanes and polyolefins.<sup>229 - 232</sup> To this, a variety of tackifiers, plasticizers, waxes, and antioxidants are incorporated to meet special application requirements.<sup>226, 232</sup> However, such compositions are derived from depleting petroleum resources, and there are concerns over their degradation ability. Concerns of bio-degradation abilities are not only about the adhesive themselves, but also the substrates bonded with them, especially in the paper and pulp industry.<sup>226, 233</sup>

### **3.2.2 The development of biodegradable “green” hot melt adhesives**

To reduce the environmental impacts associated with substrate recycling and to overcome the shortcomings associated with traditional petroleum resource based HMAs and meet the global growing demand for HMAs, it is imperative and necessary to develop natural product based HMAs. The utilisation of naturally abundant and renewable feedstocks in HMAs will not only contribute to the reduction of negative environmental impacts of currently widely used petroleum based HMAs, but also add value to the agricultural and or forest products.<sup>234 - 239</sup> Thus derived hot melt formulations are generally considered to be renewable, biodegradable and “green”.<sup>226</sup> The benefits of using hot melt adhesives and potential benefits of the development of bio-based hot melt adhesives are highlighted in Table 22.

**Table 22:** Current benefits of hot melt adhesives and potential benefits of bio-based hot melt adhesives, reproduced from reference 240.

Current benefits of HMAs	Potential benefits of bio-based HMAs
<ul style="list-style-type: none"> <li>• Absence of carrier fluids or solvents</li> <li>• No need for drying and/or evaporation</li> <li>• Quicker production line speed</li> <li>• No hazardous VOCs</li> <li>• Simple operation for various substrates</li> <li>• Clean and easy to handle</li> </ul>	<ul style="list-style-type: none"> <li>• Disconnect from petroleum</li> <li>• Reduce green house gas emissions</li> <li>• Reduce energy inputs</li> <li>• Biodegradability</li> <li>• Easy disassembly and disposal</li> <li>• Add value to agricultural products</li> <li>• Potential improved properties</li> </ul>

Actually, the development of natural product based adhesives dates back to early 1920s when soybean meal-based glue was firstly produced.<sup>241, 242</sup> However, the availability of petrochemical based products at low costs and the better performances of these materials soon render it ineffective for using natural products in adhesive formulations.<sup>226</sup> After about 50 years, it has been realized the importance and significance for using naturally renewable products instead of petrochemicals due to a number of factors: negative environmental impacts and safety concerns over petrochemical derived adhesives, rapid increasing of the prices of petrochemical products, advances in polymer sciences *etc.*<sup>226</sup> Agricultural- and/or forest derived natural products hold great potential to be incorporated in adhesive formulations due to their high levels of inherent functionality, renewability, biodegradability and wide abundance.<sup>226, 234</sup>

During the past several years, the development of HMAs using naturally abundant biorenewable materials has attracted increasing attention from both academia and industry. For example, Choi *et al.* developed a biodegradable hot melt adhesive formulation using poly- $\epsilon$ -caprolactone and soy protein isolate for uses in food packaging systems.<sup>243</sup> The lap shear strength of the developed hot melt adhesive could reach about 1.9 MPa. Viljanmaa *et al.* also produced hot melt adhesives for packaging applications using biodegradable lactic acid based polymers.<sup>244 - 246</sup>

Ke and Sun investigated the mechanical properties of blends of starch, polylactic acid (PLA) and polyvinyl alcohol (PVOH).<sup>247</sup> Inkkinen *et al.* studied the stabilities of blends of a lactic acid-base hot melt adhesive and starch.<sup>248</sup> Among the various bio-polymers, starch has attracted much attention for its applications in thermoplastic materials due to its abundant and guaranteed supply, low cost, renewability and biodegradability.<sup>249 - 252</sup> There are a number of US patents with regard to the application of starch and its derivatives, especially starch esters, in potentially 100% biodegradable hot melt adhesive formulations.<sup>253 - 257</sup> For instance, Billmers *et al.* reported several HMA formulations comprising selected modified starch esters with ester component of about 2 to 18 carbons with DS varying from around 0.3 to 3.0.<sup>254</sup>

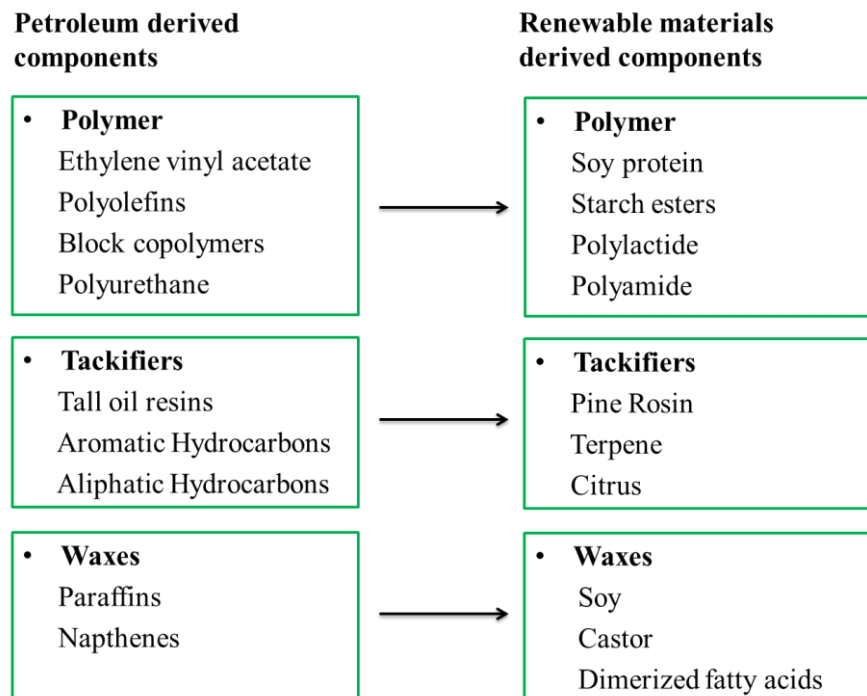


**Figure 90:** The shift from petrochemical derived materials to biorenewable materials derived products in hot melt adhesive formulations, adapted from references 240 and 258. (Originally in colour)

In the context of developing bio-based HMAs, Li *et al.* reviewed the current research and development status and prospect of HMAs, in which they also reviewed the new challenges and trends in terms of developing so-called “environmentally friendly” and/or “green” HMAs.<sup>226</sup> Petrie also provided a holistic review of the current status and trends of incorporating bio-based

components into hot melt adhesive formulations.<sup>240</sup> The trend for using products derived from biorenewable materials to substitute their petrochemical derived counterparts in hot melt adhesive formulations is illustrated in Figure 90.<sup>240, 258</sup>

### 3.2.3 Expansion of starch

As mentioned above in section 3.2.2, starch as one of the most abundant and widely available natural polymers, together with its derivatives, has attracted significant attention for its utilisation in bio-degradable hot melt adhesives. However, natural starches are water/moisture unstable and mechanical properties of starches are poorer than those of synthetic polymers, something which hampers more wide-spread use of these materials in modern industry.<sup>259, 260</sup> Native starches are generally chemically and/or physically modified to overcome the limitations associated with starch and to improve its performance as an adhesive. Esterification of starch has been intensively studied and employed due to the large number of hydroxyl groups within starch molecules.<sup>261</sup> However, access to these hydroxyl groups is significantly hindered due to the dense packing of polysaccharide chains within starch granules.<sup>262</sup> Harsh pre-treatments and chemical modification conditions are required to obtain desired starch derivatives. Expansion of starch has been proposed as an effective method to increase the accessibility of hydroxyl groups by increasing the surface area of native starch ( $<5\text{ m}^2\text{ g}^{-1}$ ) to around  $180\text{ m}^2\text{ g}^{-1}$ .<sup>263, 264</sup> After expansion of starch, chemical modification including esterification could take place under relatively mild conditions. This is of pivotal importance, especially when mild, environmentally friendly process conditions are desired.

Glenn *et al.* initially developed the method of expansion of starch for preparation of starch-based microcellular foams (expanded starch) which were characterized as low density, high pore volume and surface area.<sup>265, 266</sup> The microcellular foams (expanded starch) were prepared by gelatinising starch in water, followed by retrogradation in a fridge at 5 °C. The formed aqua gel was then solvent exchanged with ethanol and dried to yield expanded starch.

The gelatinisation and retrogradation of various types of starches have been extensively studied previously. As illustrated in Figure 91, gelatinisation of starch generally occurs when starch

granules are heated in excess of water and can be described as a phase transition from an ordered to a disordered state of starch.<sup>267, 268</sup> During gelatinisation, starch granules are heated above their critical temperatures and swell simultaneously. Gelatinisation of starch could also be achieved at lower temperatures and even room temperature (RT) in some other solvents such as liquid ammonia and dimethyl sulfoxide, and/or by mechanical milling.<sup>269, 270</sup> This process could open up the dense packing of starch granules and thus enables more effective chemical modifications of starch, resulting in high degree of substitutions (DS) of starch derivatives.<sup>271</sup> The process of starch gelatinisation has been directly observed by Atkin *et al.* using a variety of microscopic techniques.<sup>272</sup> In their study, they observed both radical and tangential expansion of dry starch granules in the presence of excess of water due to hydration reactions. The volume of dry starch granules could increase to around 6 times of its original volume at ambient temperature. About 25 times of its original volume could be achieved when temperature increases to around 65 – 75 °C, depending on the types of starch.<sup>272</sup> Simultaneous to the swelling of starch granules during gelatinisation, the linear amylose diffuses out of the swollen granules and forms an aqua gel matrix surrounding the granules.<sup>268</sup> It has been reported that after gelatinisation, starch granules lose their birefringence when visualised under crossed polarisation lenses, indicating the loss of crystallinity of starch granules and the transition from an ordered to a disordered structure of starch during gelatinisation.<sup>273</sup>

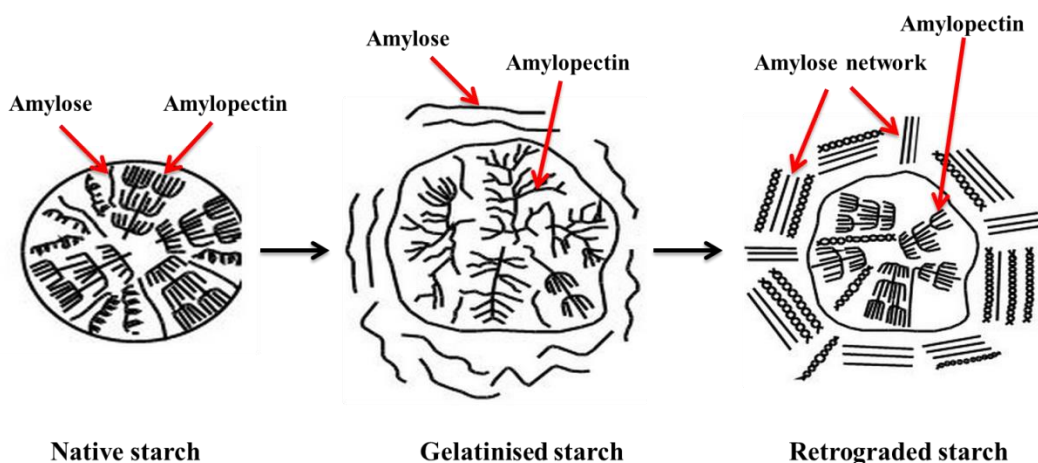


**Figure 91:** Illustration of gelatinisation and retrogradation of starch granules, adapted from reference 274. (Originally in colour)

The association and/or recrystallization of polysaccharide chains at relatively low temperatures (*e.g.*, around 5 °C) in gelatinised starch are known as retrogradation.<sup>268, 275</sup> During retrogradation, the aqua gel formed from the gelatinisation of starch changes from an amorphous state to a more ordered crystalline state through polysaccharide chain aggregation and/or recrystallization, resulting in precipitation, gelation and changes in the consistency and opacity of the starch aqua gel.<sup>268</sup>

Due to the high surface tension of water, if water containing in the retrograded starch aqua gel is directly removed (*e.g.*, through filtration) and/or evaporated off, then the capillary forces pull starch polymer blocks together and affect the starch porous structures, causing the expanded gel structures to collapse.<sup>276</sup> This effect is highlighted in Figure 92. The surface area of collapsed starch when water is removed is less than  $1 \text{ m}^2 \text{ g}^{-1}$ .<sup>276</sup> Hence, solvent exchange of water using other solvents which have lower surface tensions compared with water, such as ethanol, is of pivotal importance to preserve the porous structures and high surface areas of expanded starch.<sup>276, 277</sup> At this stage the solvents could be filtered and/or evaporated off. Then the residual starch material could be dried in vacuum oven at 50 °C for about 24 h, yielding white powers (*i.e.*, expanded starch) with significantly high surface area around  $180 \text{ m}^2 \text{ g}^{-1}$ .<sup>278</sup> In comparison, the surface area of original non-expanded starch is less than  $5 \text{ m}^2 \text{ g}^{-1}$  as determined by nitrogen porosimetry.

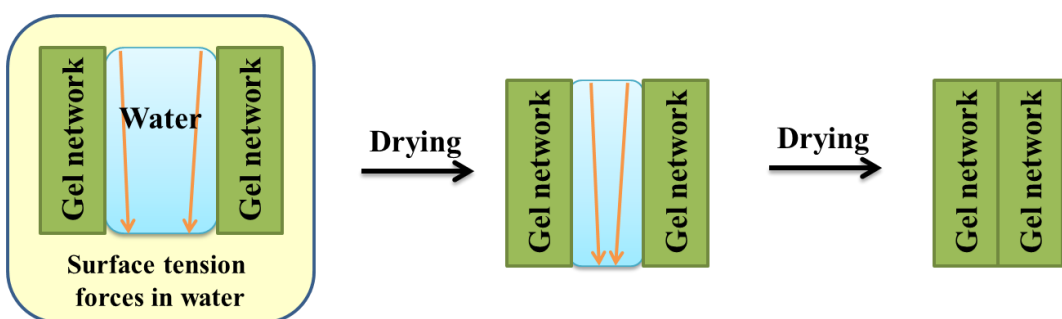


**Figure 92:** Illustration of collapsing of starch porous structures if water is directly removed from the aqua gel matrix without solvent exchange, adapted from reference 276. (Originally in colour)

Except for using as base materials for other modifications (*e.g.*, esterification) as described in the proceeding discussions, expanded starch has also found its uses in a wide variety of applications. Recent advances for applications of expanded starch mainly include support media in catalysis,<sup>271, 279</sup> chromatographic techniques,<sup>280</sup> adsorption media,<sup>281</sup> thermosetting resins<sup>282</sup> and adhesives (solvent-based)<sup>283</sup>.

### 3.2.4 Esterification of starch

To address the drawbacks associated with native starches as mentioned in section 3.2.3, chemical modification, including esterification, has been intensively studied to modify the properties of starch polymers.<sup>284 - 286</sup> Due to the presence of abundant hydroxyl groups in starch molecules, a wide variety of reactions such as esterification, etherification and oxidation reactions could take place conveniently to yield a variety of chemically modified starch derivatives. Each anhydroglucose unit contains three hydroxyl groups on C-2, -3, -6 (*i.e.*, OH – 2, -3, -6), hence in general a maximum degree of substitution (DS) of three could be attained. However, theoretically a DS slightly higher than three could be achieved if end group modification is taken into consideration. The three hydroxyl groups (OH – 2, -3, -6) present in anhydroglucose units have different availabilities in terms of introducing new moieties onto these groups. The primary hydroxyl group located at C-6 (OH-6) is more readily available than the other two located at the secondary C-2 and C-3 (OH-2, -3) due to steric hindrance.<sup>287</sup> In addition, the primary hydroxyl group (OH-6) is readily available at the exterior of the starch polymer surface compared with the other two secondary hydroxyl groups (OH-2, -3), which are located at the interior and associated with hydrogen bonding to neighbouring anhydroglucose units.

The properties of starch derivatives are different from those of non-modified native starch and vary significantly depending on the degree of substitution and substituents. There is a large body of existing literature on the topic of preparation of various types of starch esters using different starting materials and the properties of derived starch esters.<sup>284 - 291</sup> One of the most intensively investigated esterification methods of starch is acetylation. This is primarily due to the significant commercial interest of starch acetates for both food and non-food applications

such as adhesion, texturing paper coating and packaging *etc.*, as well as their ease of preparation. The DS of starch esters depends upon a number of factors such as starting material (types of starch), reaction media, reaction time and temperature as well as reactant concentrations *etc.* For acetylation of starch, starch acetates with low DS (0.01 – 0.2) are commonly achieved by esterification of native starch using acetic acid and/or acetic anhydride in aqueous medium (*e.g.*, dilute sodium hydroxide solution) with/without catalyst.<sup>292, 293</sup> In recent years, starch esters with higher DS (1.5 – 3) have attracted much attention due to their thermoplastic properties, solubility in acetone and chloroform and a much wider variety of applications such as hot melt adhesives, coatings, tablet binders and biodegradable packaging materials.<sup>292</sup> These starch esters with high DS could be prepared using strong polar solvents such as pyridine and dimethyl sulfoxide.<sup>287, 294</sup>

A standard laboratory method using acetic anhydride and pyridine for the preparation of starch acetates with various DS is widely employed, due to its versatility, ease of preparation, minimum degradation and the ability to alter the DS of derived starch acetates *via* control of reaction temperature, time and/or concentration of acetic anhydride.<sup>295</sup> Recently, Shuttleworth *et al.* have demonstrated that using acetic anhydride, toluene and 4-dimethylaminopyridine (DMAP) as a catalyst could be more efficient in terms of preparing starch acetates, especially for those with higher DS. They also reported that this method could potentially maintain or cause little damage to the porous structures and high surface areas of expanded starch if it is used as the base polymer.<sup>283</sup> Due to the electron donating effect of the 4-dimethylamino group, DMAP is a more efficient nucleophile than pyridine, and hence a more effective catalyst than pyridine.<sup>296</sup> In addition, it is documented in the literature that the efficiency of DMAP could be significantly improved if it is used with acid anhydrides instead of acids.<sup>296</sup> Since DMAP is a solid, it is potentially more convenient and easier to use but care needs to be taken because it is still derived from pyridine.

In this chapter, instead of preparing starch acetates, starch propionates with various DS were prepared using expanded starch, propionic anhydride (esterifying reagent) and DMAP as a catalyst. The incorporation of expanded starch and starch propionates with various DS into

potentially biodegradable hot melt adhesive formulations were studied subsequently (Figure 93). A possible reaction pathway for esterification of starch using propionic anhydride and DMAP is illustrated in Figure 94.

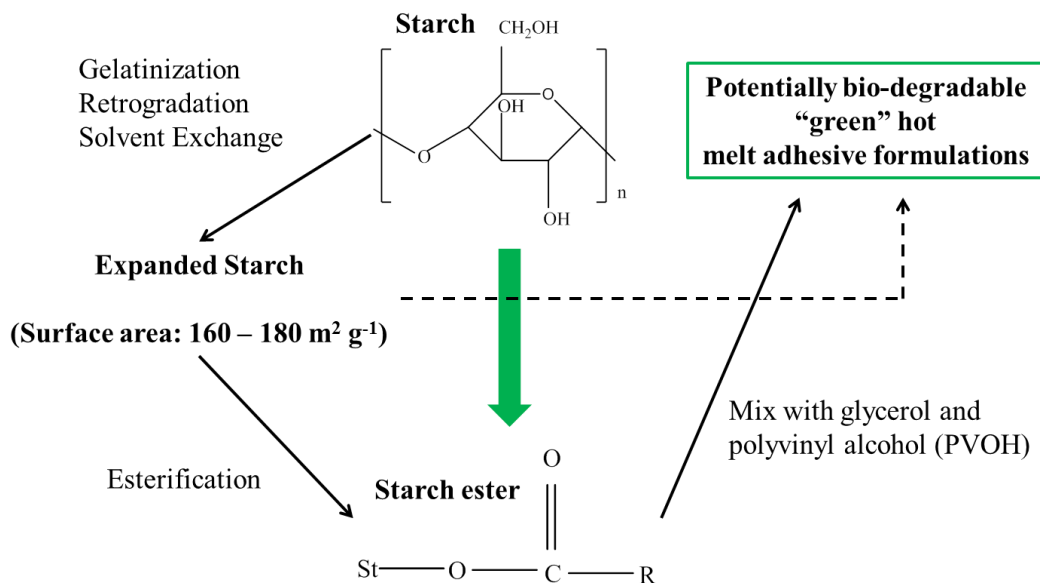


**Figure 93:** Illustration of the concept of the work within this chapter. (Originally in colour)

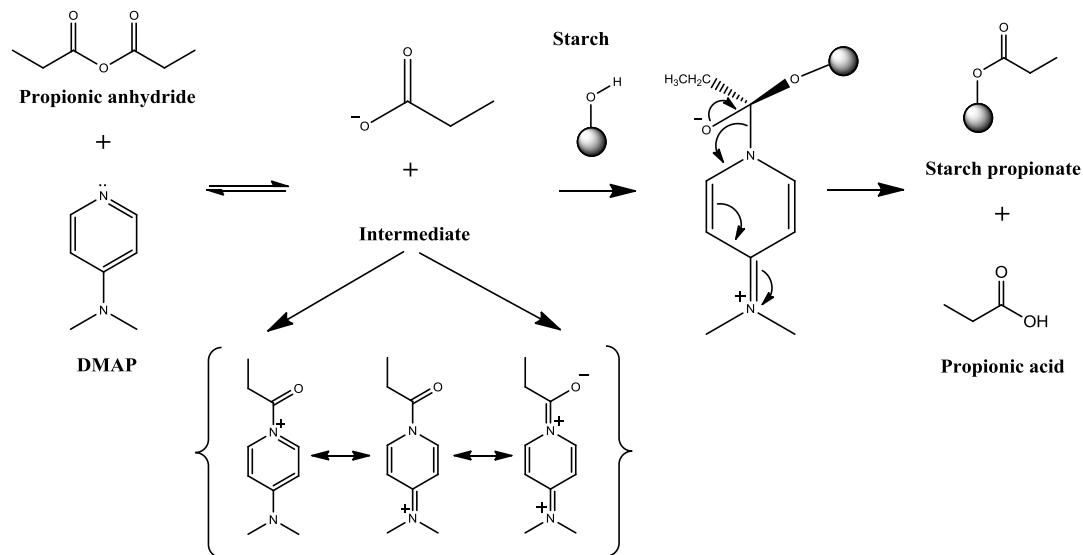


**Figure 94:** Mechanism for esterification of starch using propionic anhydride (esterifying reagent) and DMAP (catalyst). (Originally in colour)

### **3.3 Expansion and esterification of high amylose corn starch**

#### **3.3.1 Preparation of expanded high amylose corn starch and its propionate derivatives**

The employed method for expansion of HACS was developed from the work of Shuttleworth *et al.* with slight modifications.<sup>283</sup> Detailed experimental procedure for HACS expansion is described in section 4.3.1 in Chapter 4. Basically, HACS was gelatinized in hot water at 140 °C for 90 min and retrograded at 5 °C for 3 days. After that the formed matrix was solvent exchanged with less polar solvents (ethanol and toluene) followed by drying in vacuum oven to yield white powders, *i.e.* expanded HACS. The expanded HACS was characterized by much higher BET surface area ( $176 \text{ m}^2 \text{ g}^{-1}$ ) compared with that of non-expanded HACS ( $<5 \text{ m}^2 \text{ g}^{-1}$ ), as determined by nitrogen adsorption/desorption measurements (Experimental section 4.3.2 in chapter 4). The increased surface area of HACS could facilitate chemical modifications to take place under relatively milder conditions, as the accessibility of hydroxyl groups within starch molecules were dramatically increased.

In the current work, a series of starch propionates with various degree of substitution (DS) were prepared by changing the amount of esterifying reagent (propionic anhydride) and reaction time using 4-dimethylaminopyridine (DMAP) as catalyst. Detailed reaction conditions and procedure for esterification of expanded HACS are described in the experimental section 4.3.3 in chapter 4. Table 23 summarizes the reaction conditions and DS of yielded starch propionates. The DS of derived starch propionates was determined by titrimetric method, which involves complete basic hydrolysis of ester linkages in aqueous sodium hydroxide and back titration of excess alkaline using hydrochloric acid,<sup>292</sup> according to the experimental procedure described in section 4.3.4 in chapter 4. For 6 h reactions, with increasing amounts of propionic anhydride, the DS of starch propionates significantly increased from around 0.38 (5 g, 0.038 mol, propionic anhydride) to 1.91 (17.5 g, 0.134 mol, propionic anhydride). Thereafter, the reaction equilibrium was reached, as also highlighted in Figure 95, DS increased from around 1.91 (17.5 g, 0.134 mol, propionic anhydride) just to 2.05 (40 g, 0.307 mol, propionic anhydride). To

further increase the DS, one more experiment was conducted with propionic anhydride (40 g, 0.307 mol, propionic anhydride) for 12 h. By doubling reaction time, DS increased from 2.05 (6 h reaction) to 2.54 (12 h reaction).

For reference, the esterification of non-expanded HACS was conducted with propionic anhydride (10 g, 0.077 mol) and DMAP (0.4 g, 3.3 mmol) for 6 h. The DS of resulted starch propionate is only around 0.02, which is dramatically lower than that of the one obtained with expanded starch under the same reaction conditions (DS, 1.00).

**Table 23:** Esterification reaction conditions and degree of substitutions (DS) of resultant starch propionates.<sup>a</sup>

Propionic anhydride (g)	Propionic anhydride (mol)	Expanded HACS <sup>b</sup> (mol)	Reaction time (h)	DS
5.0	0.038	0.062	6	0.38 ± 0.03
7.5	0.058	0.062	6	0.78 ± 0.02
10.0	0.077	0.062	6	1.00 ± 0.02
12.5	0.096	0.062	6	1.46 ± 0.03
15.0	0.115	0.062	6	1.82 ± 0.03
17.5	0.134	0.062	6	1.91 ± 0.02
20.0	0.154	0.062	6	1.95 ± 0.02
30.0	0.231	0.062	6	1.99 ± 0.03
40.0	0.307	0.062	6	2.05 ± 0.02
40.0	0.307	0.062	12	2.54 ± 0.04

<sup>a</sup> For all the reactions, DMAP (0.4 g, 3.3 mmol) was added as catalyst. <sup>b</sup> Expanded HACS with surface area 176 m<sup>2</sup> g<sup>-1</sup> (10 g, 0.062 mol) was used as base polymer for esterification.

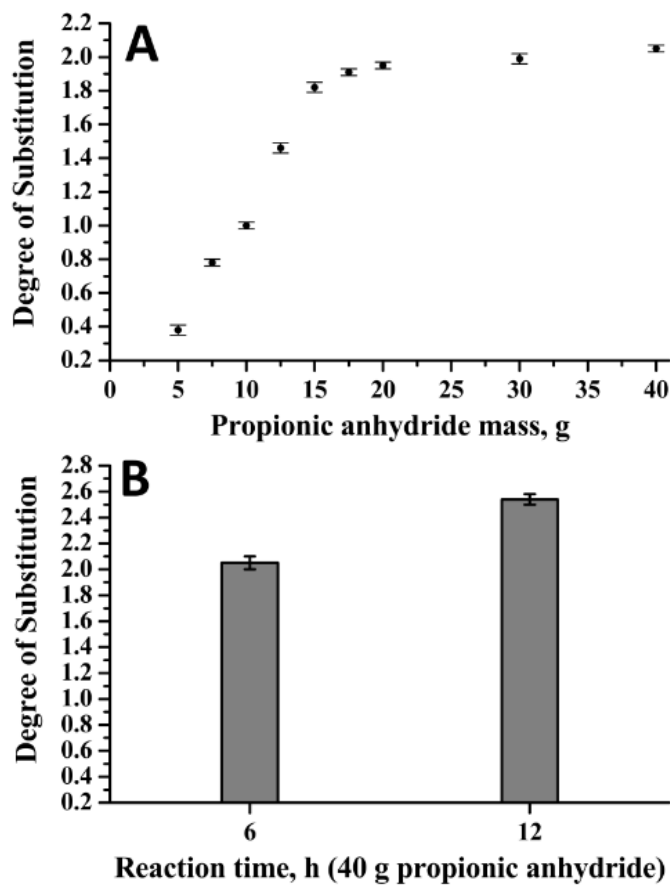


**Figure 95:** Effects of (A) amounts of esterifying reagent *i.e.* propionic anhydride for 6 h reaction and (B) reaction time on DS of starch propionates.

### 3.3.2 ATR-IR characterization of expanded HACS and its esters

Fourier transform-infrared spectroscopy (FT-IR) in attenuated total reflectance (ATR) mode was also used to characterize both the expanded HACS (surface area:  $176 \text{ m}^2 \text{ g}^{-1}$ ) and its propionate derivatives (DS varies between 0.38 and 2.54) in order to confirm the modification. Detailed instrumentation and testing procedure are described in section 4.3.5 in chapter 4.

Figure 96 illustrates the ATR-IR spectra of expanded HACS and its propionates. The key band changes with increasing DS were highlighted in Figure 96 with dashed lines and the assignment of these bands is summarized in Table 24. Esterification is confirmed by the carbonyl stretching vibration band centred at  $1745 \text{ cm}^{-1}$ . Intensity of this band increases and that of hydroxyl O - H stretching vibration band ( $3000 \text{ cm}^{-1}$  to  $3600 \text{ cm}^{-1}$ ) decreases with increasing DS, suggesting the conversion of hydroxyl groups to ester groups. This is further evidenced by the band at 1152

$\text{cm}^{-1}$  due to the ester C-O-C asymmetric stretching vibration, the intensity of which also increases with DS. The O-H stretching vibration band drifts to higher wavenumbers with increasing of DS, indicating a reduction in inter- and intra-molecular hydrogen bonding and increasing of hydrophobicity with DS. Increasing of hydrophobicity with DS is also indicated by the weak but slightly broad band at  $1648 \text{ cm}^{-1}$ , which is associated with tightly bound water. This band gradually diminishes up until a DS of 2.0, when it is no longer apparent. Furthermore, the esterification of expanded starch also imparts obvious changes in the fingerprint region. For example, new bands appeared at  $1456 \text{ cm}^{-1}$  and  $1360 \text{ cm}^{-1}$  and the intensities of these bands also increase with DS. These two bands are assigned to methyl asymmetric bending vibration and C-H deformation vibration, respectively.

In the spectrum of expanded HACS, some characteristic absorption bands for starch could be identified, such as bands centred at  $1079 \text{ cm}^{-1}$ ,  $1013 \text{ cm}^{-1}$  which are assigned to C – O bond stretching.<sup>292, 297</sup> Also, there are several additional characteristic absorption bands due to the entire anhydroglucose ring stretching vibrations, such as bands at  $929 \text{ cm}^{-1}$  and  $763 \text{ cm}^{-1}$ .<sup>292</sup> All these bands also exist in the ATR-IR spectra of starch propionates.

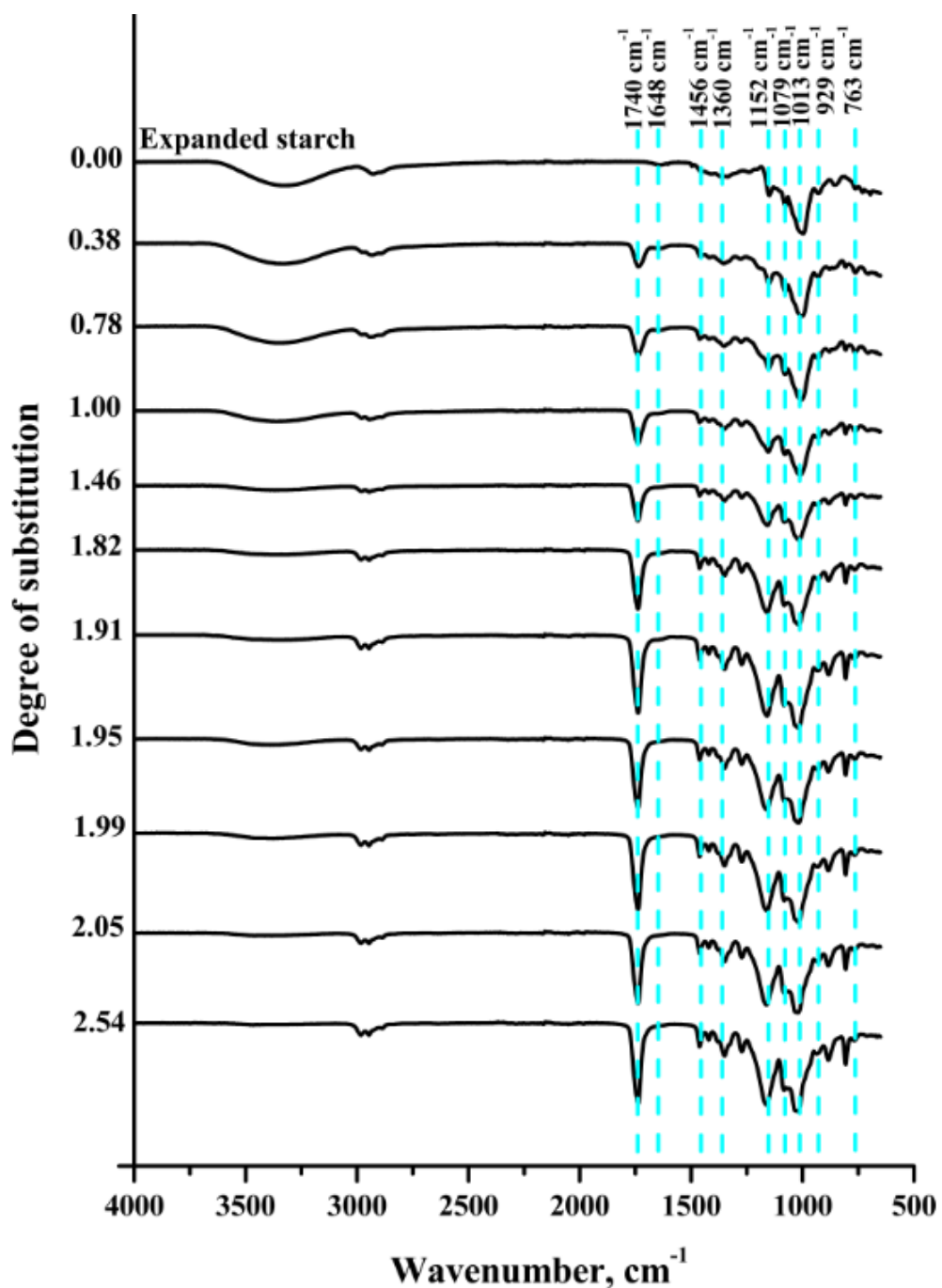


**Figure 96:** ATR-IR spectra of expanded HACS and its propionates. (Originally in colour)

**Table 24:** Summary of the assignments of major bands in the ATR-IR spectra of expanded HACS and its propionates

Wavenumber (cm <sup>-1</sup> )	Assignment
3600 - 3000	O-H stretching vibration
2960 - 2850	C-H vibrations
1745	C=O stretching vibration
1648	Tightly bound water
1456	CH <sub>3</sub> asymmetric bending vibration
1360	C-H deformation vibration
1152	Ester C-O-C asymmetric stretching
1079, 1013	C-O vibration (anhydroglucose ring)
929, 763	Anhydroglucose ring stretching vibration

### 3.3.3 Thermogravimetric characterization of expanded HACS and its esters

To investigate the thermal properties of expanded HACS and its propionates with various DS, these materials were subjected to a thermogravimetric (TG) analysis. Samples were heated from 30 °C to 625 °C at a heating rate of 10 °C min<sup>-1</sup> in nitrogen atmosphere (100 mL min<sup>-1</sup>). Detailed instrumentation and methodology for TG characterization of expanded HACS and its propionates are described in section 4.3.6 in chapter 4. The TG and dTG traces of these materials are shown in Figure 97 and Figure 98, respectively.

It is obvious that esterification considerably affects the thermal decomposition of starch. The first mass loss step for expanded HACS starts immediately as heat begins and finishes around 150 °C with around 5% mass loss, which is mainly attributed to the evaporation of water moisture. For starch propionates, the weight loss in this temperature range is much smaller than that of expanded HACS and decreases with increasing of DS. For example, the starch propionate (DS, 0.38) lost around 2.5% between 30 – 150 °C, while the starch propionate (DS, 2.54) shows almost no weight loss in this region. This results from increased hydrophobicity of starch propionates and is consistent with the ATR-IR analysis.

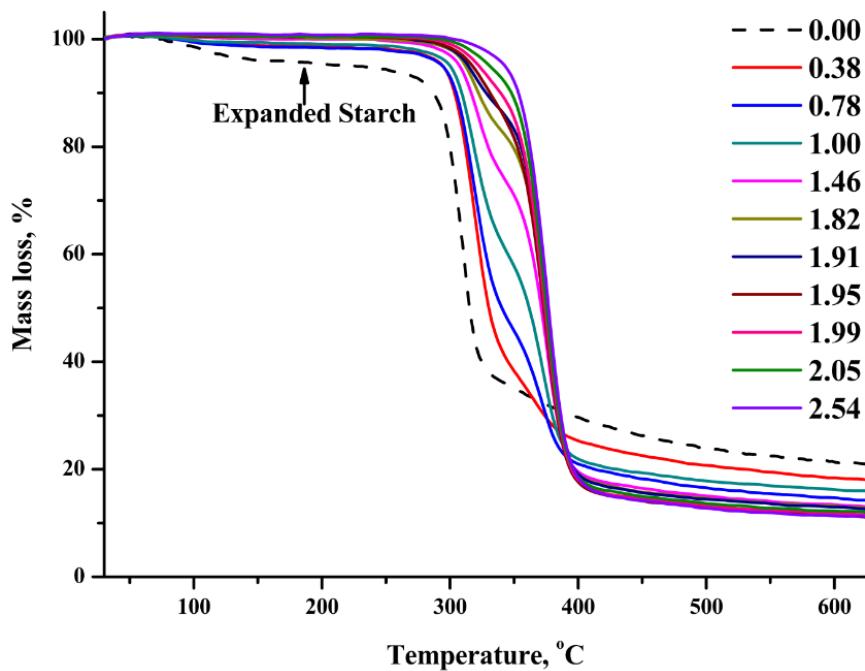


**Figure 97:** TGA traces for expanded HACS and its propionates, samples heated from 30 °C to 625 °C at a heating rate of 10 °C min<sup>-1</sup>. (Originally in colour)

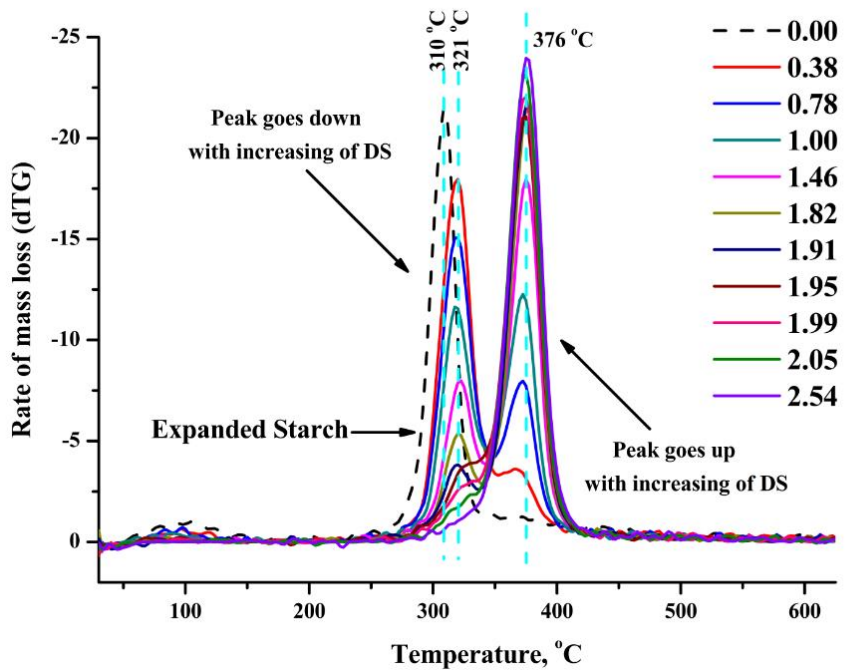


**Figure 98:** dTG traces for expanded HACS and its propionates, samples heated from 30 °C to 625 °C at a heating rate of 10 °C min<sup>-1</sup>. (Originally in colour)

Decomposition of expanded HACS starts at approximately 260 °C and is a one step process with peak decomposition temperature (dTG peak) at 310 °C. It is noteworthy that there is a clear shift towards higher decomposition temperatures with increasing of DS. For instance, the major peak decomposition temperature of starch propionate with DS 2.54 (376 °C) is much higher than that of expanded HACS, indicating the thermal stability increased with DS. With the increasing of DS, more hydroxyl groups on anhydroglucose units were converted to ester groups. As the thermal decomposition of starch is primarily due to inter- and/or intra-molecular dehydration reactions with water as a main product, the dehydration reactions became increasingly difficult and slow with increasing of DS.<sup>287, 298</sup> This effect finally results in higher thermal stabilities of the derived starch propionates.

Unlike expanded HACS, thermal decomposition of starch propionates mainly consists of two steps. From the dTG traces (Figure 98), it is obvious that the 1<sup>st</sup> and 2<sup>nd</sup> decomposition step of starch propionates show almost the same peak decomposition temperatures: around 321 °C for the 1<sup>st</sup> step and 376 °C for the 2<sup>nd</sup> decomposition step. Also, from the TGA traces (Figure 97), with increasing of DS, mass loss in the 1<sup>st</sup> decomposition step decreased from around 60% (DS, 0.38) to 3.6% (DS, 2.54). On the contrary, mass loss in the 2<sup>nd</sup> decomposition step increased from around 20% (DS, 0.38) to 82% (DS, 2.54). This phenomenon probably indicates that inter- or intra-molecular dehydration reactions primarily occur during the 1<sup>st</sup> decomposition step. As the amount of available hydroxyl groups reduce with increasing DS, mass loss of the 1<sup>st</sup> decomposition step decreases, while that of the 2<sup>nd</sup> decomposition step increases. For both expanded HACS and its propionates, approximately 15 + 5 wt.% remains after heating to above 600 °C.

### 3.3.4 NMR characterization of expanded HACS and its esters

Both expanded HACS and its propionates with various DS were further characterized by solid-state <sup>13</sup>C CP/MAS NMR spectroscopy and liquid-state <sup>1</sup>H NMR spectroscopy (using DMSO-d<sub>6</sub> as solvent). The instrumentation and methodology for the solid-state <sup>13</sup>C CP/MAS NMR and liquid-state <sup>1</sup>H NMR characterization are described in section 4.3.7 and 4.3.8 in chapter 4, respectively.

Figure 99 illustrates the solid-state  $^{13}\text{C}$  NMR spectra of expanded HACS (Figure 99 A) and starch propionate with DS of 1.00 (Figure 99 B). From the  $^{13}\text{C}$  NMR spectrum of expanded HACS, the corresponding signals for carbon atoms in the starch molecule are assigned in accordance with literature.<sup>299 - 301</sup> The signals between 106 and 92 ppm is attributed to the C-1 of the anhydroglucose units. Signals for the C-4 and C-6 are observed at 82 and 62 ppm, respectively. The large signal ranging from 70 to 76 ppm is attributed to C-2, C-3 and C-5 of the anhydroglucose units. From the  $^{13}\text{C}$  NMR spectrum of starch propionate with DS of 1.00 (Figure 99 B), the characteristic peak for the carbonyl carbon is observed at 174 ppm. Also, the characteristic signals for the methylene and methyl group are observed at approximately 28 and 9.8 ppm, respectively. These results are in good consistency with the ATR-IR analysis and further provide evidence for the success of esterification of expanded HACS.

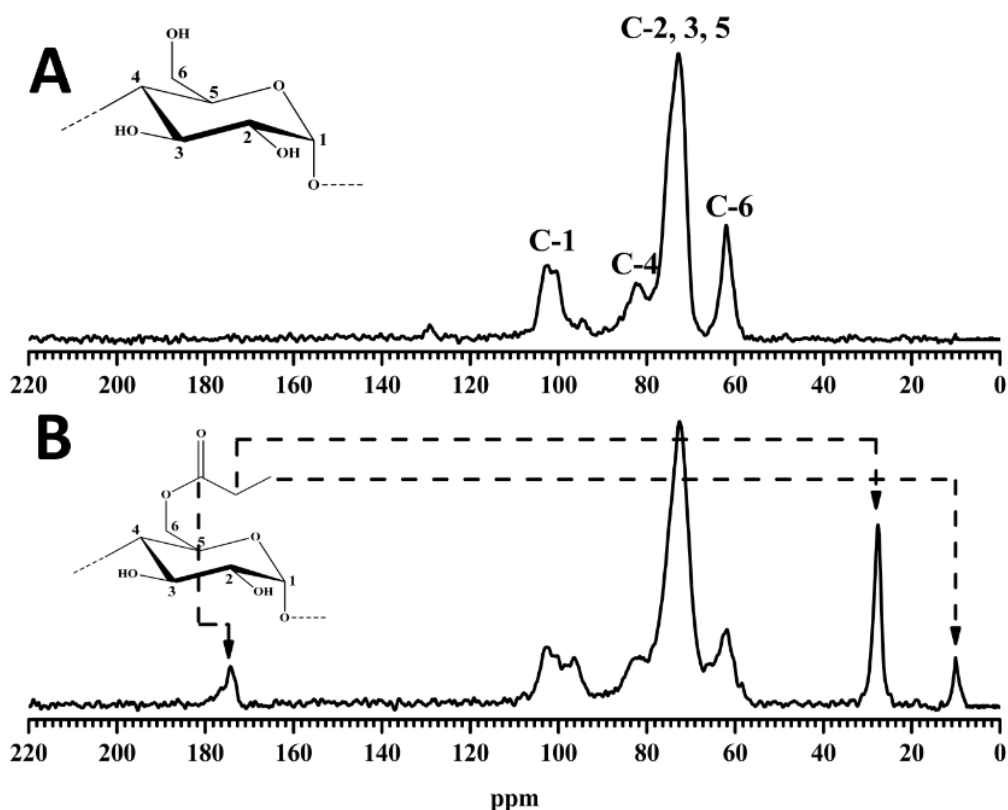


**Figure 99:** Solid-state  $^{13}\text{C}$  CP/MAS NMR spectra of (A) expanded HACS and (B) starch propionate (DS, 1.00). The repeating unit shown in Figure 99 B is with the ester group connected to the most probable C position (C - 6).<sup>287</sup>

The liquid-state  $^1\text{H}$  NMR spectra of expanded HACS and starch propionates with DS (0.38, 1.46, 1.99 and 2.54) are illustrated in Figure 100. These samples were dissolved in DMSO-d<sub>6</sub> and the  $^1\text{H}$  NMR spectra were recorded at 25 °C. The broad, strong signals ranging from 3.2 to 4.0 ppm are assigned to starch chain protons (H – 2, 3, 4, 5, 6), but is mainly attributed to residual water (centred at 3.30 ppm), because of the hygroscopic nature of starch and DMSO-d<sub>6</sub>.<sup>302</sup>

According to the literature, the resonance signals centred at 5.40 ppm, 5.50 ppm and 4.59 ppm are assigned to the three hydroxyl groups on C – 2, 3, 6 (OH – 2, 3, 6), respectively.<sup>292</sup> Also, resonance signal of the anomeric hydrogen atom (H – 1), which corresponding to the internal  $\alpha$  – 1, 4 linkages, is observed at 5.10 ppm.<sup>292, 302</sup>

During the esterification process, the propionate moieties were gradually introduced into starch molecules. From the  $^1\text{H}$  NMR spectra of starch propionates, the characteristic resonance bands of anhydroglucose units are still visible, even though the resolution of spectra decreased with increasing of the DS, which is probably due to the subsequent increased viscosity of the NMR solution. However, subtle changes of the resonance of protons on anhydroglucose units can be observed compared with that of expanded HACS, which is resulted from slightly changed chemical environments.

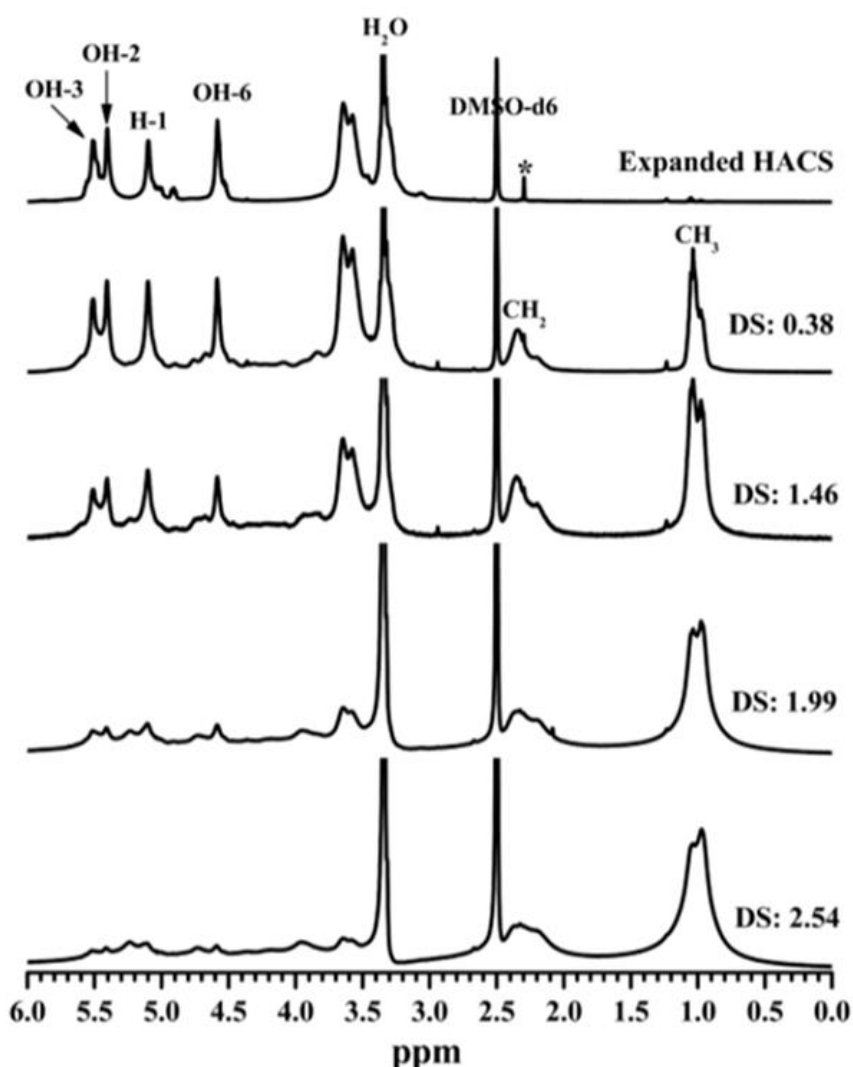


**Figure 100:**  $^1\text{H}$  NMR spectra of expanded HACS and its propionates (DS: 0.38, 1.46, 1.99 and 2.54) in  $\text{DMSO-d}_6$ . \* Possible artefact

With increasing DS, it is obvious that the resonance bands of OH – 2, –3, –6 (centred at 5.40 ppm, 5.50 ppm and 4.59 ppm) gradually diminish, referenced to the intensity of the anomeric hydrogen (H–1) band at 5.10 ppm. In all the spectra of starch propionates, the resonance signals for  $\text{CH}_2$  and  $\text{CH}_3$  groups of propionate moieties are found between 2.0 – 2.45 ppm and 0.6 – 1.3 ppm, respectively.

## 3.4 Preparation and characterization of hot melt adhesive formulations

### 3.4.1 Preparation of hot melt adhesive formulations

According to the experimental procedure described in section 4.3.9 in chapter 4, non-expanded HACS, expanded HACS and its propionates with various DS were incorporated into potentially biodegradable hot melt adhesive (HMA) formulations by mixing with glycerol and polyvinyl alcohol (PVOH) at the same weight ratio, as illustrated in Figure 101. This formulation comprising mixtures of starch, glycerol and PVOH was previously reported in an US patent.<sup>254</sup>

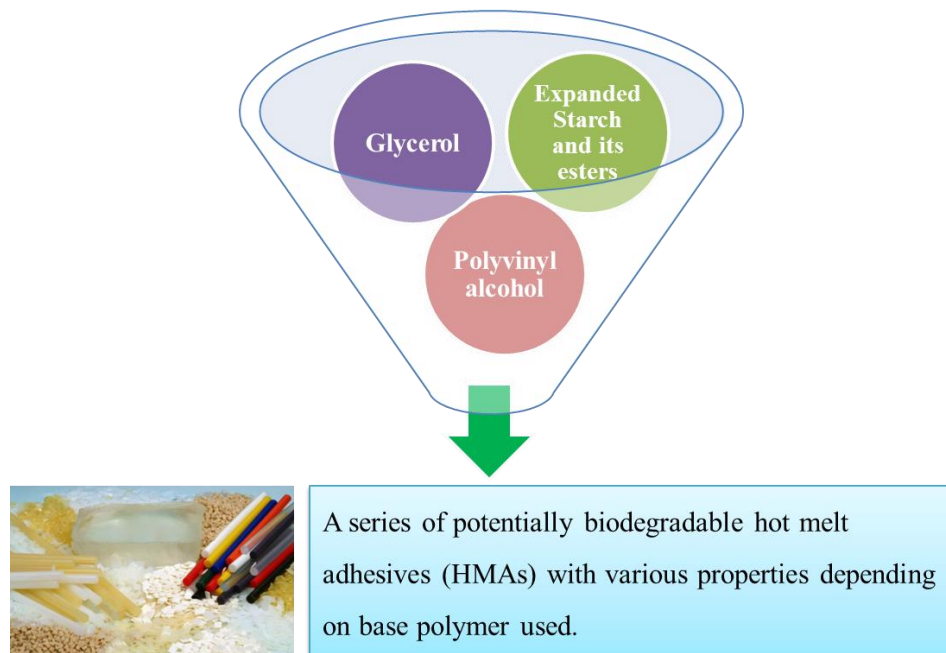


**Figure 101:** Illustration of the potentially biodegradable hot melt adhesive formulations.  
(Originally in colour)

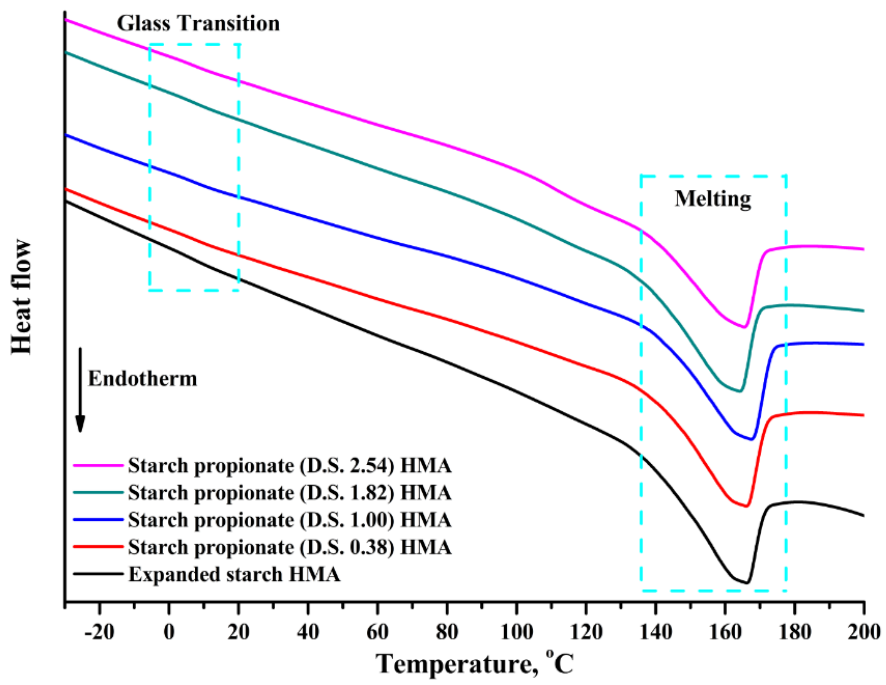
### 3.4.2 DSC Characterization of hot melt adhesive formulations

The prepared hot melt adhesives (HMAs) were characterized with differential scanning calorimetry (DSC) using a heat–cool–heat–cool method to mimic the real industrial application of HMAs. Instrumentation and methodology for DSC characterization of the formulated HMAs are described in section 4.3.10 in chapter 4. Before being subjected to DSC, the HMA formulations were equilibrated in a lab oven at 50 °C for 24 h. As the materials were mixed with

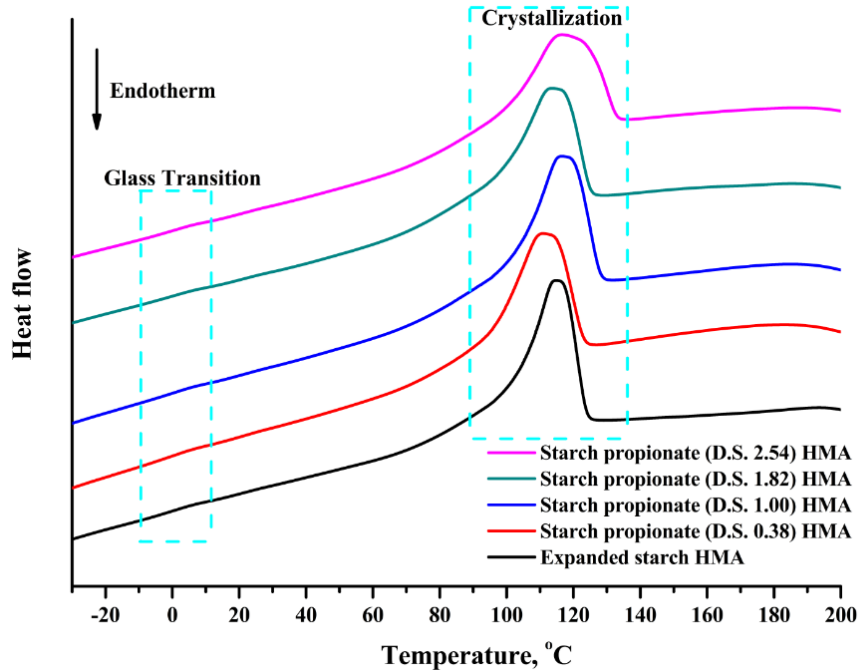
spatula in glass vials, the 2<sup>nd</sup> cycle of the heat–cool–heat–cool DSC traces is of more interest and allows better evaluation of the thermal properties of the formulated HMAs.

Figure 102 and Figure 103 show the 2<sup>nd</sup> heating and cooling DSC traces of expanded HACS and its propionates with DS of 0.38, 1.00, 1.82 and 2.54 based HMA formulations, respectively. The glass transition of the HMAs (approximately between -5 °C and 5 °C) is observed in both heating and cooling traces. From the heating traces shown in Figure 102, slightly endothermic transitions of the HMAs could be observed around 115 °C; however, a significant large endothermic peak is shown between 135 °C and 175 °C for all the traces, corresponding to the major melting of HMA formulations. From the cooling traces (Figure 103), all the samples show an exothermic crystallization peak between 130 °C and 90 °C. All these transitions are characteristic for HMA formulations. As the major endothermic melting transition for all the HMA formulations ends around 175 °C, a higher temperature (190 °C) was chosen for the application of such HMAs during the adhesion experiments.

In order to study the stability/reusability of the expanded HACS and its propionates based HMA formulations, the starch propionate (DS: 1.00) based HMA was characterized in DSC for more heat – cool cycles in accordance with the experimental procedure described in section 4.3.10 in chapter 4, which is similar to the heat – cool – heat – cool method mentioned above (just for more cycles). The DSC traces are demonstrated in Figure 104. Even though the peak temperatures of melting and crystallization shift slightly due to changes of the environment within sealed Tzero aluminium pans, characteristics of glass transitions, melting and crystallization transitions basically remain even after 5 heat – cool cycles, indicating high stability of the formulated HMAs.



**Figure 102:** DSC traces of the 2<sup>nd</sup> heating run of expanded HACS and starch propionates (DS: 0.38; 1.00; 1.82; 2.54) based HMAs. (Originally in colour)



**Figure 103:** DSC traces of the 2<sup>nd</sup> cooling run of expanded HACS and starch propionates (DS: 0.38; 1.00; 1.82; 2.54) based HMAs. (Originally in colour)

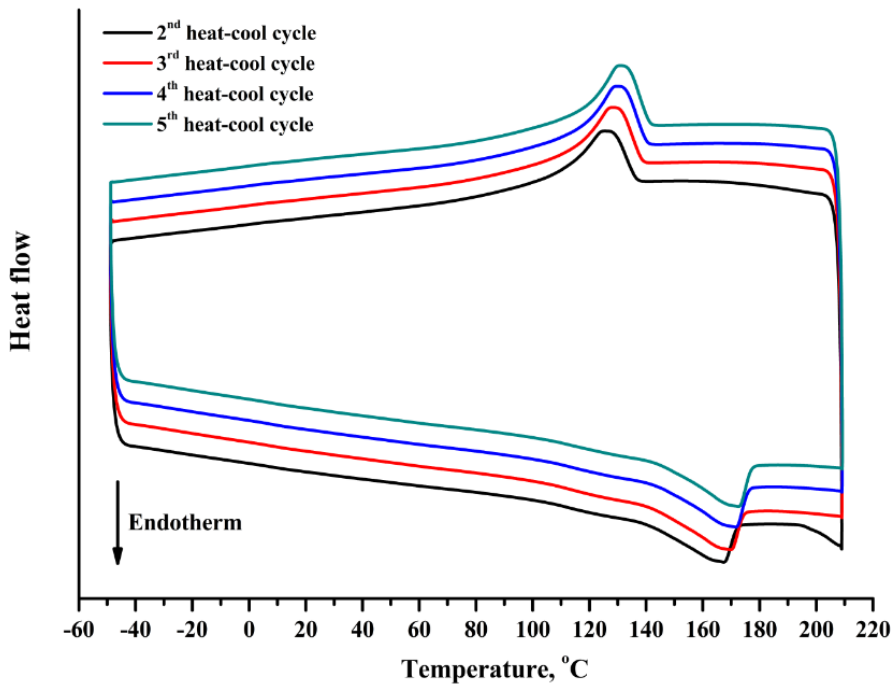


**Figure 104:** DSC traces of the 2<sup>nd</sup> to 5<sup>th</sup> heat – cool cycle of starch propionate (DS, 1.00) based HMA formulation. (Originally in colour)

### 3.4.3 ATR-IR Characterization of hot melt adhesive formulations

Stability of formulated HMAs was further proved by comparing the ATR-IR spectra of the base material, formulated HMA before and after DSC measurement. Figure 105 shows the ATR-IR spectra of expanded HACS, and expanded HACS based HMA before and after DSC measurement (Figure 105 A) and that of starch propionate (DS, 1.82), starch propionate (DS, 1.82) based HMA before and after DSC measurement (Figure 105 B). It is obvious that all the characteristic absorption bands of both expanded HACS and its propionate based HMA formulations are still remaining almost the same before and after heating and cooling in DSC, suggesting no thermal degradation and any non-reversible reactions occurred during heating and cooling.

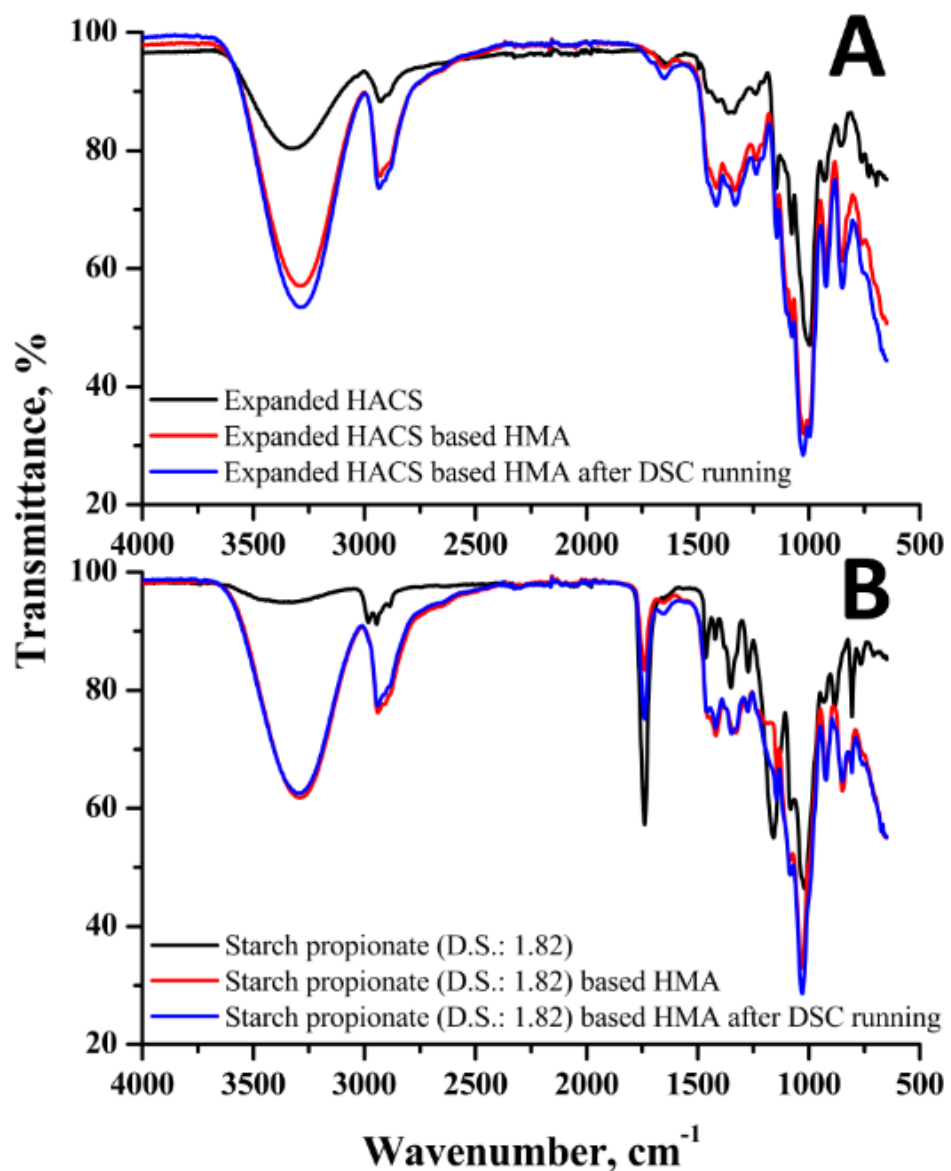


**Figure 105:** ATR-IR spectra of (A) expanded HACS, expanded HACS based HMA before and after DSC measurement, (B) starch propionate (DS, 1.82), starch propionate (DS, 1.82) based HMA before and after DSC measurement. (Originally in colour)

### 3.5 Adhesion testing of hot melt adhesives

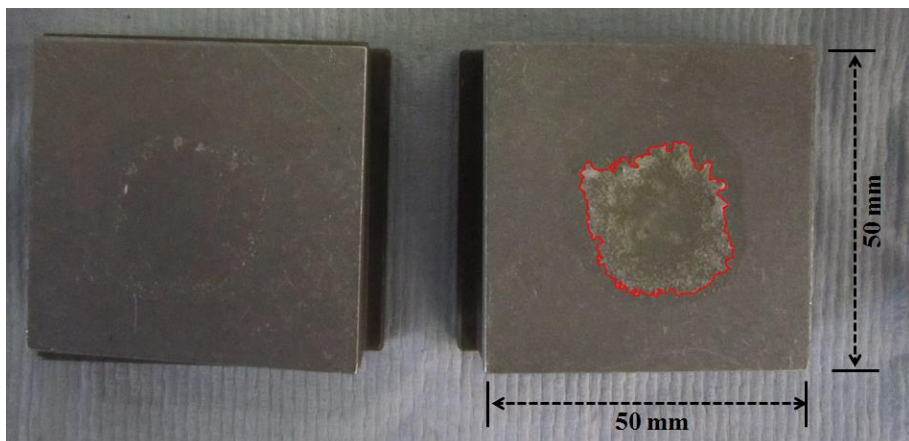
#### 3.5.1 Adhesion tests of hot melt adhesives

Non-expanded HACS, expanded HACS and derived starch propionates with various DS based HMA formulations (50 mg) were applied to bond Al plates (surface area, 50 mm × 50 mm). Specimens were bonded under pressure at 190 °C for 30 seconds using a hot press machine. The

tensile strengths of the Al – HMA – Al bond were measured using an Instron 3367 Dual Column System universal testing machine (and accompanying software) fitted with a 3000 N capacity load cell, at a crosshead speed of 5 mm min<sup>-1</sup>. Obtained results were normalized to effective tensile stress by calculating the effective bonding area using Adobe Photoshop CS6. Detailed experimental information is described in section 4.3.11 in chapter 4.

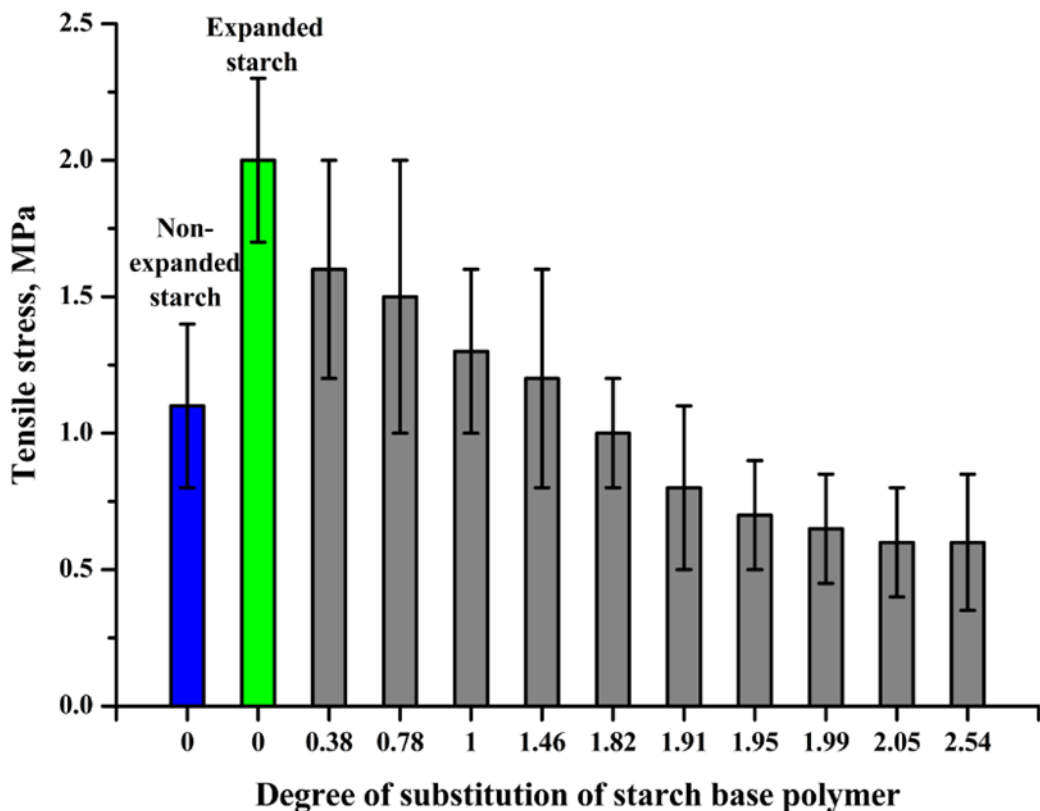
### 3.5.2 Tensile stress tests of hot melt adhesives

Figure 106 illustrates a typical failure pattern of the Al plates adhered with the formulated HMAs. All the other adhered specimens show a similar failure pattern and broken adhesively (failure occurred between the HMA – Al interface), suggesting the cohesive strengths of the HMA formulations are higher than adhesive strengths between HMA and Al substrates.



**Figure 106:** A typical failure pattern of formulated HMA bonded Al plates, sample shown is the Al – HMA – Al interface of expanded HACS based HMA cured Al plates. (Originally in colour)

To allow a better evaluation of the mechanical properties of the HMA formulations, measured tensile strengths were normalized to effective tensile stress by calculating the surface area of effective bonding area (circled by red lines, Figure 106). Figure 107 illustrates the normalized tensile stress of Al plates cured by the formulated HMAs. The reported values are average values of four specimens adhered by each kind of HMA formulation (50 mg).



**Figure 107:** Normalized tensile stress of non-expanded HACS, expanded HACS and its starch propionates based HMA formulations (50 mg) bonded Al plates. (Originally in colour)

It is significant that the tensile stress of expanded HACS based HMA (around 2.0 MPa) is dramatically higher than that of HMA based on non-expanded HACS (around 1.1 MPa). This effect might result from the significant increased surface area of expanded HACS and subsequent improved accessibility of hydroxyl groups within starch molecules. This effect probably leads to higher extent of interaction (non-covalent and/or cross-linking) between starch, glycerol and polyvinyl alcohol (PVOH), resulting in significant increase of tensile stress. For the starch propionates based HMA formulations, tensile stress decreased with increasing of DS. When DS increased from 0.38 to 2.54, the tensile stress of the starch propionate based HMAs dropped from about 1.6 MPa to 0.6 MPa. As more and more hydroxyl groups were converted to ester groups during esterification, the amounts of available “free” hydroxyl groups decreased. As a result, the cross-linking effect between the three HMA components deteriorated, leading to decreased tensile stress. Also, as hydrophobicity of starch propionates increases with DS, starch propionates with higher DS might sacrifice their abilities to be compatible with glycerol and

PVOH, which will also leads to decreased tensile stress. However, tensile stress of starch propionates (DS<1.5) based HMA formulations are still higher than that of non-expanded HACS based HMA formulation, despite lower than that of the one based on expanded HACS.

For reference, the tensile stress of commercial ethylene vinyl acetate (EVA) based LOCTITE hot melt glue (around 6 MPa, purchased from B & Q, York, UK) was tested under the same conditions. Due to the nature of the formulated potentially bio-degradable HMAs and the fact that they were not engineered, the maximum tensile stress of these HMA formulations is around 2.3 MPa obtained with expanded HACS based HMA. However, within this work, the great potential of application of expanded starch in potentially biodegradable “green” HMA formulations is demonstrated.

### 3.6 Conclusions and future work

Following the expansion (gelatinisation, retrogradation and solvent exchange) procedure, surface area of high amylose corn starch (HACS) was dramatically increased to around  $176\text{ m}^2\text{ g}^{-1}$  compared with that of non-expanded HACS (less than  $5\text{ m}^2\text{ g}^{-1}$ ). Thus the accessibility of the hydroxyl groups in starch molecules was significantly improved. This allows chemical modification of starch, including esterification, to take place at relatively milder conditions. To take advantage of this effect, esterification of expanded HACS was conducted with propionic anhydride (esterifying reagent) and DMAP (catalyst) in toluene. The DS of derived starch propionates were controlled through changing the amounts of propionic anhydride and reaction time. The results revealed that DS of derived starch propionates increases with increasing of the amounts of propionic anhydride used. For instance, DS increased almost linearly from around 0.38 (with 5 g, 0.038 mol, propionic anhydride) to 1.95 (with 20 g, 0.154 mol, propionic anhydride) for 6 h reaction. After that, the esterification reaction reaches equilibrium; DS remains around 2 even if the amounts of propionic anhydride increased to 40 g (0.307 mol). DS also increases with reaction time, for example, DS increased from about 2.05 (6 h) to 2.54 (12 h) with 40 g (0.307 mol) propionic anhydride.

The derived starch propionates with various DS were characterized by ATR-IR, TGA, solid state  $^{13}\text{C}$  CP/MAS NMR and liquid-state  $^1\text{H}$  NMR spectroscopy. The results confirmed the success of esterification of expanded HACS and further revealed that the properties of starch were changed significantly during esterification. For instance, the thermal stability and hydrophobicity of starch propionates increase with DS. This is because with increasing of DS, more and more hydroxyl groups within starch molecules were converted to ester groups, which renders it more and more difficult for inter- and/or intra- molecular dehydration reactions to take place.

The expanded HACS and starch propionates with various DS were incorporated into potentially bio-degradable HMA formulations by mixing them with glycerol and PVOH at the same weight ratio. The developed HMA formulations were characterized by DSC using a heat – cool – heat – cool method to mimic their real industrial applications. The glass transition generally occurs between -5 °C and 5 °C, and the major melting step occurs between 135 °C and 175 °C. During cooling, the hot melt adhesives recrystallize at temperatures between 130 °C and 90 °C. Both the DSC and ATR-IR characterization of the HMA formulations before and after DSC measurements revealed that no destructive and/or non-reversible reactions occurred during heating and cooling in DSC, suggesting high thermal stability of the formulated HMAs.

The adhesion properties of the HMA formulations were studied by applying each HMA formulation (50 mg) in the middle of two Al plates with surface area 50 mm × 50 mm, and specimens were adhered in a hot press machine for 30 seconds at 190 °C. Tensile stress of the Al – HMA – Al bond was measured and normalized by calculating the effective bonding area using Adobe Photoshop CS6. The tensile stress of expanded HACS based HMA (around 2.0 MPa) is dramatically higher than that of the one based on non-expanded HACS (around 1.1 MPa). For those based on starch propionates, tensile stress decreases with increasing of DS of the base polymer. However, tensile stress of starch propionates (DS<1.5) based HMAs are still higher than that of the one based on non-expanded HACS, even though lower than that of expanded HACS based HMA.

The properties of starch derivatives vary significantly depending upon the types of new functional groups introduced into the starch molecules during modification. In the context of esterification of starch, the types (*e.g.*, chain lengths) of the introduced ester moieties and also DS affect the properties of final products. Future work might include the investigation of the preparation of other starch esters from expanded starch and their applications into HMA formulations. In addition, the reported potentially biodegradable HMA formulations need to be improved, especially in terms of competing with commercial synthetic HMAs.

# **Chapter 4**

*Experimental*



## **4.1 Materials and reagents**

### **4.1.1 Biomass**

Spruce wood chips were harvested in southern Sweden in 2011. Since being collected, they were stored at room temperature at the Green Chemistry Centre of Excellence, University of York. Waste office papers (printed and/or photocopied) were obtained from the offices of Green Chemistry Centre of Excellence, University of York. Paper deinking residue (DIR) was kindly supplied by SalveTech UK and used as received. High amylose corn starch (HACS) under the trade name Hylon® VII with amylose content around 75% was obtained from National Starch & Chemical.

### **4.1.2 Chemical reagents**

Hydrochloric acid, sodium hydroxide, potassium hydroxide, ethanol, acetone, ethyl acetate and toluene were supplied by Fisher Scientific. Propionic anhydride, 4-dimethyl-aminopyridine (DMAP), calcium carbonate (calcite), microcrystalline cellulose, kaolinite and DMSO-d<sub>6</sub> used for NMR analysis (99.96% atom D) were purchased from Sigma-Aldrich, Gillingham, UK. All other standard laboratory reagents (purity>99.5%) were purchased from Sigma Aldrich, Gillingham, UK. All the chemicals were used directly without any further purification, unless specified otherwise. Oxygen free nitrogen gas (purity>99.5%) was used during thermogravimetric analysis (TGA) and supplied by BOC.

### **4.1.3 Other used materials**

Commercial LOCTITE Precision Superglue and ethylene vinyl acetate (EVA) based LOCTITE hot melt glue were purchased from B&Q, York, UK.

Aluminium plates used for adhesion tests were kindly provided and shot-blasted by the mechanical workshop of the Chemistry Department, University of York, UK.

## 4.2 Experimental details and instrumentation for chapter 2

### 4.2.1 Microwave-assisted low-temperature (<200 °C) pyrolysis of biorenewable waste streams

Microwave-assisted low-temperature (<200 °C) pyrolysis of spruce wood chips, waste office paper and paper deinking residue (DIR) was performed on a Milestone ROTO-SYNTH Rotative Solid Phase Microwave Reactor (Milestone Srl., Italy) fitted with a vacuum system, which allows for *in-situ* separation, condensation and collection of generated volatile compounds. The experimental set-up for the microwave-assisted pyrolysis experiments is demonstrated in Figure 108.

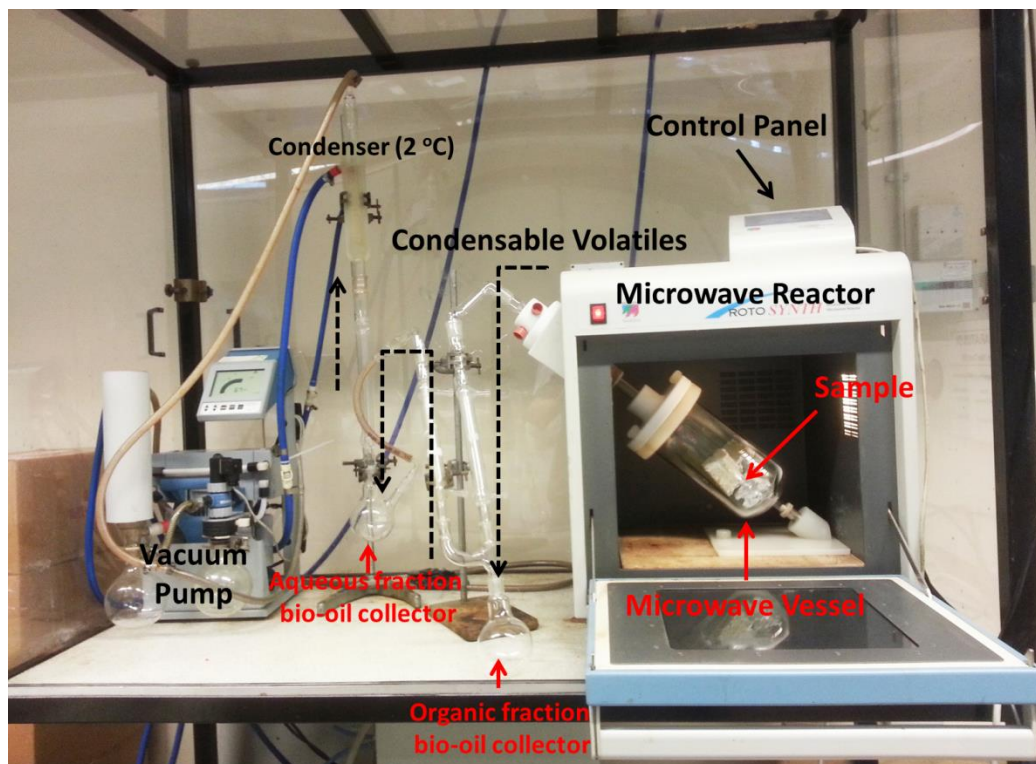


**Figure 108:** Illustration of the experimental set-up used for the microwave-assisted low-temperature (<200 °C) pyrolysis, sample shown in the microwave vessel is DIR. (Originally in colour)

Spruce wood chips (150 g per run, with particle sizes around 0.5 cm × 0.5 cm) were stored at room temperature and used directly without any pre-treatment. The collected waste office

papers (A4 printed and/or photocopied) were milled using a Farm Feed Solutions (UK) 12 KW hammer mill with 5 mm screen. Thereafter, milled office paper (150 g per run) was wet pressed into the microwave glass vessel and dried in an oven at 105 °C for 48 h until a fixed weight was reached (moisture content less than 3% with a density of around 0.3 g cm<sup>-3</sup>).

Fibrous DIR was wet-pressed with tap water using a lab-scale paper briquette press. The then formed DIR brick was dried in a laboratory oven at 90 °C for 24 h, yielding a dry DIR brick with density around 0.56 g cm<sup>-3</sup>. The DIR brick (400 g per run) was placed in the microwave vessel (2 L) and the pyrolysis was carried out under vacuum.

Samples (either spruce wood chips or waste office paper or DIR) were microwave irradiated at a fixed power (1200 W, 2.45 GHz). The process temperature gradually increased with reaction time and was monitored *via* on-line infrared temperature probes. The reaction was deemed complete after about 12-13 minutes irradiation based on no further release of volatiles and maximum temperature around 190 °C was achieved. Using the fitted vacuum system, two phases (organic and aqueous phase) of bio-oils and bio-char (microwave residue) were generated. In the current study the gas product was depleted from the system using the fitted vacuum pump and was not investigated further.

#### **4.2.2 Yield analysis of microwave-assisted low-temperature (<200 °C) pyrolysis of biorenewable waste streams**

For each feedstock (spruce wood chips, waste office paper and DIR), the pyrolysis process was conducted three times and the pyrolysis products (organic phase bio-oil, aqueous phase bio-oil and bio-char/microwave-residue) were combined together. The yield of organic phase bio-oil, aqueous phase bio-oil and bio-char/microwave-residue was determined by mass in relation to the total mass of raw materials (after pre-treatment for waste office paper and DIR) using the following equations.

**For organic phase bio-oil:**

$$Yield = \frac{\text{mass of recovered organic phase bio - oil (g)}}{\text{mass of raw material (g)}} \times 100\%$$

**For aqueous phase bio-oil:**

$$Yield = \frac{\text{mass of recovered aqueous phase bio - oil (g)}}{\text{mass of raw material (g)}} \times 100\%$$

**For bio-char/microwave-residue:**

$$Yield = \frac{\text{mass of recovered bio - char/microwave - residue (g)}}{\text{mass of raw material (g)}} \times 100\%$$

Since the incondensable gaseous products were depleted from the microwave-assisted pyrolysis system, the yields of gaseous products were calculated by difference.

#### **4.2.3 Thermogravimetric analysis of paper deinking residue (DIR)**

Thermogravimetric analysis (TGA) of the as-received DIR and its microwave-residue was conducted on a Netzsch 409 simultaneous thermal analyzer (STA). Each sample (100 mg) was heated from 30 °C to 625 °C at 10 °C min<sup>-1</sup> under nitrogen atmosphere with a flow rate of 100 mL min<sup>-1</sup>. TGA of DIR was also conducted in air (100 mL min<sup>-1</sup>) under the same heating program.

#### **4.2.4 Proximate and ultimate analysis of raw materials and their microwave-assisted pyrolysis products**

The proximate analysis of spruce wood chips, waste office paper and derived pyrolysis products was conducted to determine their moisture, volatile matter, fixed carbon and ash contents using a Netzsch 409 simultaneous thermal analyzer (STA). This method was adapted from the work of Donahue and Rais.<sup>303</sup> Samples (100 mg) were heated under nitrogen (100 mL min<sup>-1</sup>) and air atmosphere (100 mL min<sup>-1</sup>), respectively. The followed temperature programs are:

**Under nitrogen atmosphere ( $100 \text{ mL min}^{-1}$ ):**

- (1) Ramp from  $30^\circ\text{C}$  to  $105^\circ\text{C}$  at a heating rate of  $10^\circ\text{C min}^{-1}$
- (2) Isothermal at  $105^\circ\text{C}$  for 10 min
- (3) Ramp from  $105^\circ\text{C}$  to  $900^\circ\text{C}$  at a heating rate of  $50^\circ\text{C min}^{-1}$
- (4) Isothermal at  $900^\circ\text{C}$  for 1 hour

**Under air atmosphere ( $100 \text{ mL min}^{-1}$ )**

- (1) Ramp from  $30^\circ\text{C}$  to  $900^\circ\text{C}$  at a heating rate of  $50^\circ\text{C min}^{-1}$
- (2) Isothermal at  $900^\circ\text{C}$  for 1 hour

The moisture content corresponds to the mass loss in nitrogen atmosphere between  $30^\circ\text{C}$  and  $105^\circ\text{C}$ . The volatile matter content was determined by the mass loss between  $105^\circ\text{C}$  and  $900^\circ\text{C}$  under nitrogen atmosphere. Ash content was determined as the residual material after heating samples at  $900^\circ\text{C}$  for 1 h in air. Fixed carbon content represents the solid combustible material that remains after loss of moisture and volatile matter when heated in nitrogen but combusted in air. The proximate analysis of spruce wood chips is illustrated in Figure 109 as an example.

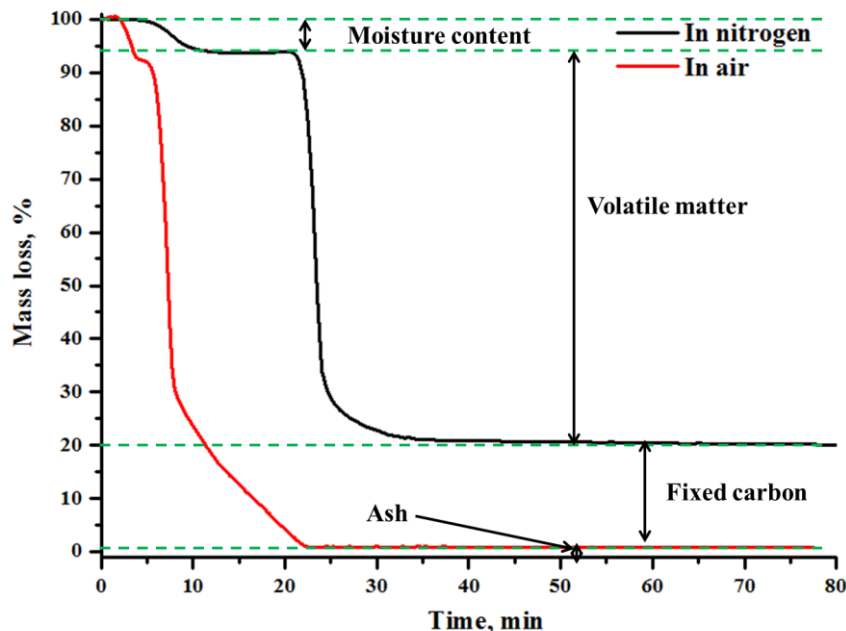


**Figure 109:** Proximate analysis (moisture content, volatile matter, fixed carbon and ash content) of spruce wood chips. (Originally in colour)

For ultimate characterization, elemental analysis (C, H, N and S) of spruce wood chips, waste office paper, DIR and their microwave-assisted pyrolysis products was conducted on an Exeter Analytical CE440 Elemental Analyzer. Sulfur contents of these materials, together with total organic carbon (TOC) of aqueous phase bio-oils were determined by Yara Analytical Services, York, UK. The oxygen contents of these materials were calculated by difference according to the following equation:

$$O (\%) = 100 \% - C (\%) - H (\%) - N (\%) - S (\%)$$

#### **4.2.5 Calorific value measurement**

The calorific values (CV) of spruce wood chips, waste office paper, DIR and their pyrolysis products were determined using a Parr 6200 bomb calorimeter (Parr Instrument Company, Moline, IL, USA). An exact known mass of each sample (around 1 g) was combusted in an oxygen-enriched atmosphere in the bomb calorimeter, and its caloric value ( $\text{MJ kg}^{-1}$ ) was determined. CV measurements were carried out in triplicate and mean values were reported.

#### **4.2.6 Karl Fischer Titration**

The Karl Fischer titration of organic phase bio-oils generated from microwave-assisted low-temperature ( $<200^\circ\text{C}$ ) pyrolysis of spruce wood chips, waste office paper and DIR was conducted on a GR Scientific Cou-Lo Aquamax Karl Fischer titrator to determine water content. HYDRANAL-Coulomat AK (anolyte solution) and HYDRANAL-Coulomat CG-K (catholyte solution) were used as coulometric reagents, to avoid any interference from ketones, amines, or aldehydes contained in the bio-oil.

#### **4.2.7 ICP-MS characterization**

Inductively coupled plasma-mass spectrometry (ICP-MS) of spruce wood chips, waste office paper, DIR and their microwave-assisted pyrolysis products were conducted on an Agilent 7700 $\times$  ICP-MS spectrometer to determine their metal contents. The TG ashes of DIR obtained in nitrogen and air atmosphere were also subjected to the ICP-MS analysis. Prior to analysis,

solid samples were acid digested in HCl and HNO<sub>3</sub> at a volume ratio of 3 : 1. Liquid samples (bio-oils) were diluted in acetone.

#### **4.2.8 ATR-IR characterization**

The Fourier-transform infrared (FT-IR) characterization of spruce wood chips, waste office paper, DIR and their pyrolysis products (except gaseous products) was performed on a Bruker Vertex 70 spectrometer in attenuated total reflectance (ATR) mode, with a resolution of 2 cm<sup>-1</sup> and 64 scans. In addition, the ATR-IR characterization of all the other samples mentioned in chapter 2 such as TG ashes of DIR, scrapings of bio-oil polymers and residual materials obtained after tensile tests, commercial model compounds *etc.* were conducted in the same manner described above.

#### **4.2.9 Liquid-state NMR characterization of bio-oils**

Both the organic and aqueous phase bio-oils produced from microwave-assisted low-temperature (<200 °C) pyrolysis of spruce wood chips, waste office paper and DIR were subjected to liquid-state Nuclear Magnetic Resonance (NMR) characterization. The <sup>13</sup>C NMR characterization of the three bio-oil fractions generated from liquid-liquid fractionation of the waste office paper derived organic phase bio-oil was conducted following the same procedure. <sup>13</sup>C and <sup>1</sup>H NMR spectra of bio-oils were recorded on a Jeol ECX-400 NMR spectrometer at 100 MHz (1024 scans) and 400 Hz (64 scans), respectively. Bio-oil (150 mg) was dissolved in deuterated dimethyl sulfoxide (DMSO-d<sub>6</sub>, 99.96% atom D). The measurements were conducted at 25 °C. For <sup>13</sup>C NMR analysis, the central resonance of DMSO-d<sub>6</sub> ( $\delta$ C, 39.52 ppm) was used as the internal reference.

#### **4.2.10 GC-MS characterization of bio-oils**

The GC-MS characterization of liquid products (bio-oils) was conducted on a Perkin Elmer Claus 500 gas chromatograph equipped with a Perkin Elmer Claus 560 s mass spectrometer. The column was a non-polar ZB-5HT (30 m × 0.25 mm id × 0.25 µm film thickness) from Phenomenex (UK). The oven temperature programme was maintained at 60 °C for 1 min, then ramped at 8 °C min<sup>-1</sup> to 360 °C and held for 1 min. The injection volume of sample is 1 µL. The

identification of chromatographic peaks was by comparison with the NIST 2008 library. In addition, the GC-MS characterization of the three bio-oil fractions generated from liquid-liquid fractionation of the waste office paper derived bio-oil were conducted using the same method.

#### **4.2.11 Qualitative and quantitative characterization of DIR derived organic phase bio-oil**

In addition to the qualitative analysis of the DIR derived organic phase bio-oil as mentioned in section 4.2.10. This phase of bio-oil was also sent for external validation to the Thunen Institute, University of Hamburg, Germany, for comprehensive qualitative and quantitative analysis. Detailed experimental procedure is:

About 60 mg of the DIR derived organic phase bio-oil was dissolved in 1 mL acetone, which contained a known amount of fluoranthene as internal standard for quantification. GC was performed using an Agilent 6890. Injector conditions: split/splitless injector, temperature 250 °C, split ratio 1:15, injection volume 1 µL.

Separation was carried out on a 60 m × 0.25 mm VF-1701MS (Varian) fused-silica column, containing 14% cyanopropyl-phenyl-methylpolysiloxane (0.25 µm film thickness). Oven programme was as follows: hold constant at 45 °C for 3 min, heat with 4 °C min<sup>-1</sup> to 280 °C and hold for 20 min. Helium was used as carrier gas with a constant flow of 2 mL min<sup>-1</sup>. The system was equipped with parallel FID & MS-detection. Electron impact mass spectra were obtained on a HP 5972 MS using 70 eV ionisation energy.

#### **4.2.12 Adhesion tests and tensile strength measurement**

The spruce wood chips, waste office paper and DIR derived organic phase bio-oils were applied as adhesives for Al – Al bonding. For the adhesion tests of other samples such as the three fractions of bio-oil generated from liquid-liquid fractionation of the organic phase bio-oil derived from waste office paper, and the (mixtures) of model compounds, they were performed in the same manner described below.

As mentioned in section 2.8.1, organic phase bio-oil (70 mg) was homogeneously applied to the surface of one Al plate (50 mm × 50 mm). The Al plates used throughout this project are blasted Al plates. Shot-blasting was carried out by the mechanical workshop of Chemistry Department, University of York, UK, to guarantee a fresh and homogeneous surface. Prior to adhesion tests, shot-blasted Al plates were washed with tap water and acetone to get rid of any impurities. A glass rod was used to guarantee homogeneous spreading of bio-oil on the Al surfaces, the weight of bio-oil on Al surfaces was accurately measured by weighing the Al plate before and after applying the bio-oil. The Al plate which has bio-oil on its surface was pressed together with another Al plate of the same surface size (50 mm × 50 mm) using light pressure (finger-strength), weighed down with a stainless steel metal block (350 g) to mimic constant pressure. After that, the specimens were subjected to heating for curing in a lab oven. The stainless steel metal block still stays at the top of the two Al plates to guarantee homogeneous pressure during curing. Samples were cured at various temperatures: 120 °C, 140 °C, 160 °C and 180 °C for 4 and 8 h curing. After curing, the bio-oil adhered Al plates were removed from the oven and cooled down to room temperature naturally (around 25 °C). Then the weight of the bio-oil cured Al plates was measured and the mass loss during curing was calculated by difference. Then cured Al plates were adhered to two stainless steel metal blocks (50 mm × 50 mm) with commercial ‘Superglue’ purchased from B&Q at York, UK.

The tensile strengths of the adhesive bonds formed between the two shot-blasted Al plates post cure were measured using an Instron 3367 Dual Column System universal testing machine (and accompanying software) fitted with a 3000 N capacity load cell, at a cross-head speed of 5 mm min<sup>-1</sup>. For each kind of organic phase bio-oil, the tensile strengths of four cured Al specimens were measured and the average values of four times measurements were reported in the main text.

#### **4.2.13 Solid-state CP/MAS <sup>13</sup>C NMR characterization of scrapings of cured bio-oil polymers**

The scrapings of cured bio-oil polymers post tensile tests were characterized using solid-state <sup>13</sup>C NMR with and without dipolar dephasing.

Solid-state  $^{13}\text{C}$  CP/MAS NMR spectra were acquired using a 400 MHz Bruker Avance III HD spectrometer equipped with a Bruker 4 mm H(F)/X/Y triple-resonance probe and a 9.4 T Ascend<sup>®</sup> superconducting magnet. The CP experiments employed a 1 ms linearly-ramped contact pulse, spinning rates of  $10\,000 \pm 2$  Hz, optimized recycle delay of 3 seconds, spinal-64 heteronuclear decoupling (at  $\nu_{\text{rf}} = 85$  kHz) and are a sum of 1024 co-added transients.

The dipolar dephasing experiments added a rotor-synchronized 180  $\mu\text{s}$  dephasing delay with a pi refocusing pulse to minimize baseline distortion. Chemical shifts are reported with respect to TMS, and were referenced using adamantane (29.5 ppm) as an external secondary reference.

#### **4.2.14 Liquid-liquid fractionation of waste office paper derived organic phase bio-oil**

The waste office paper derived organic phase bio-oil was subjected to liquid-liquid fractionation using alkali (aqueous sodium hydroxide) and organic solvent (ethyl acetate) to yield three sub-fractions of bio-oils: “neutral” ethyl acetate fraction, “acidic” ethyl acetate fraction, *i.e.*, acidified base layer extracted into ethyl acetate, and aqueous fraction bio-oil. This method was adapted from the procedure developed by Amen-Chen *et al.* with slight modifications.<sup>201</sup>

Initially, the waste office paper derived organic phase bio-oil (10 g) was dissolved in ethyl acetate (10 g) at a 1 : 1 weight ratio, followed by transferring into a separating funnel which contains an equivolume of aqueous sodium hydroxide (2 M). This mixture was mixed by shaking and left to settle until two separate layers were formed (about 1.5 h). The bottom layer (*i.e.* aqueous layer) was set aside and the upper layer (*i.e.* ethyl acetate layer) was further extracted (5x) using an equivolume of aqueous sodium hydroxide (2 M). The remaining organic layer (ethyl acetate layer) was isolated, dried and the solvent removed *in vacuo* using a Heidolph<sup>TM</sup> Hei-Vap<sup>TM</sup> rotary evaporator fitted with an ILMVAC pump to yield the “neutral” ethyl acetate fraction bio-oil (1.9 g, yield: 19%).

The combined basic aqueous extracts were transferred into a beaker, acidified with hydrochloric acid (1 M) to pH around 6, and was extracted with ethyl acetate ( $5 \times 100$  mL). The combined

organic extract was dried ( $\text{MgSO}_4$ ), filtered and concentrated *in vacuo* using a Heidolph<sup>TM</sup> Hei-Vap<sup>TM</sup> rotary evaporator fitted with an ILMVAC pump to generate the “acidic” ethyl acetate fraction bio-oil (2.5 g, yield: 25%). The aqueous layer (pH around 6) was removed to yield the aqueous fraction bio-oil which mainly contains solid matter (5.6 g, 56%). Figure 110 demonstrates the procedure employed for liquid-liquid fractionation of the waste office paper derived organic phase bio-oil and the appearances of samples at crucial separation stages.

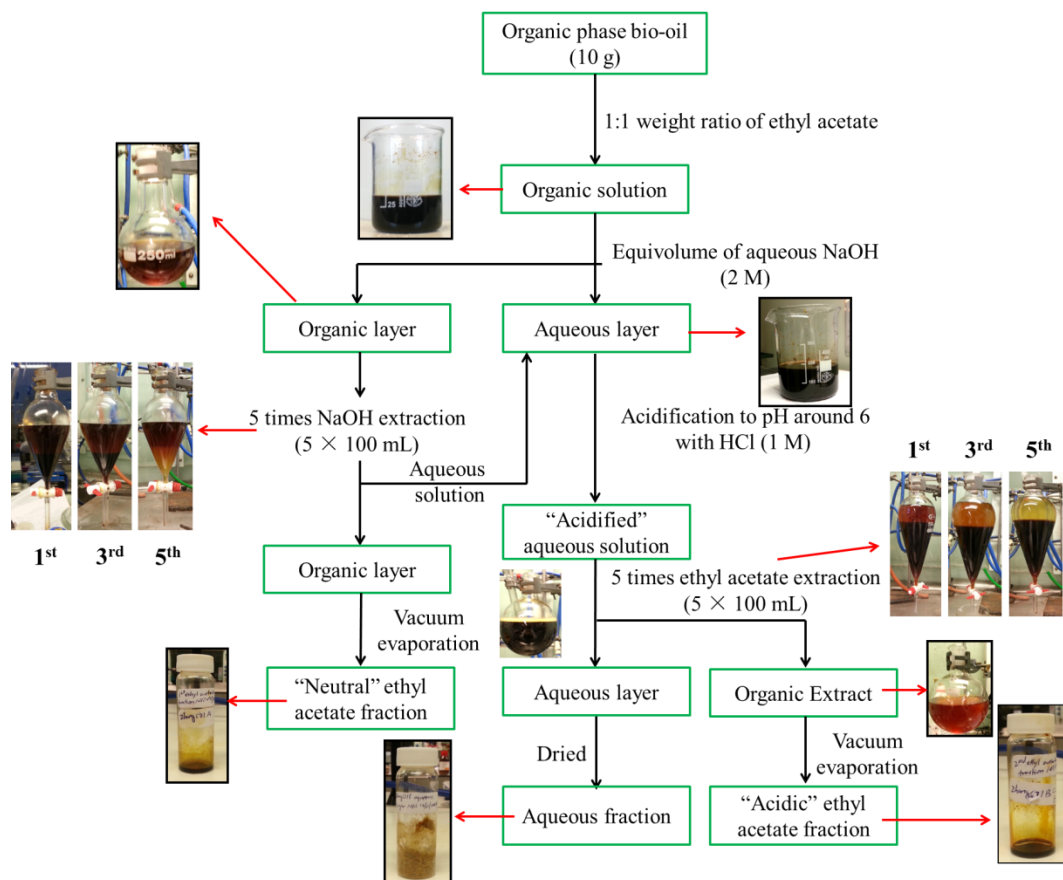


**Figure 110:** Illustration of the procedure for liquid-liquid separation of waste office paper derived organic phase bio-oil and the appearances of samples at crucial separation stages.  
 (Originally in colour)

#### **4.2.15 Solid-state CP/MAS $^{13}\text{C}$ NMR characterization of DIR and its microwave residue**

Solid-state cross-polarization/magic-angle spinning (CP/MAS)  $^{13}\text{C}$  spectra of DIR and its microwave residue were acquired using a 400 MHz Bruker Avance III HD spectrometer equipped with a Bruker 4 mm H(F)/X/Y triple resonance probe and 9.4T Ascend superconducting magnet. The CP experiments employed a 1 ms linearly ramped contact pulse, spinning rates of  $10000 \pm 2$  Hz, optimized recycle delays of 5–7 s, and spinal-64 heteronuclear decoupling (with a nutation frequency,  $\nu_{\text{rf}} = 85$  kHz) and are a sum of 1024 co-added transients. Chemical shifts are reported with respect to tetramethylsilane (TMS), and were referenced using adamantine (29.5 ppm) as an external secondary reference.

#### **4.2.16 Scanning electron microscopy**

Scanning electron micrographs (SEM) of DIR and its thermally treated samples (microwave residue, TG ashes of DIR obtained in nitrogen and air atmosphere) were taken on a JEOL JSM-6490LV (JEOL, Tokyo, Japan). Prior to analysis, samples were mounted on alumina sample holders and coated in a thin film of gold using a high-resolution sputter SC-7640 coating device at a sputtering rate of  $1500 \text{ V min}^{-1}$ .

#### **4.2.17 Powder X-ray diffraction**

X-Ray diffraction pattern of DIR raw material and its thermally treated samples (microwave residue, TG ashes of DIR in both  $\text{N}_2$  and air atmosphere), together with commercial  $\text{CaCO}_3$  (Calcite, Sigma-Aldrich, UK) were acquired using a Bruker-AXS D8 advance diffractometer, which was equipped with a  $\text{Cu K}\alpha$  radiation source. The diffractometer was operated at 40 mA and 40 kV and scans were taken across the angular range of  $10\text{--}90^\circ 2\theta$ .

#### **4.2.18 Solid-state Bloch-decay $^{13}\text{C}$ NMR spectroscopy**

Bloch-decay solid-state  $^{13}\text{C}$  NMR spectra were acquired with a  $30^\circ$  tip-angle pulse at spinning rates of  $10000 \pm 2$  Hz, recycle delays of 480 – 600 s, and spinal-64 heteronuclear decoupling (at  $\nu_{\text{rf}} = 85$  kHz) and are a sum of 32 – 100 co-added transients. Chemical shifts are reported with

respect to TMS and were referenced using adamantane (29.5 ppm) as an external secondary reference.

### 4.3 Experimental details and instrumentation for chapter 3

#### 4.3.1 Expansion of high amylose corn starch

The expansion of high amylose corn starch (HACS) under the trade name Hylon® VII with amylose content up to 75% was achieved through an expansion process mainly including three steps: gelatinisation, retrogradation and solvent exchange. The method used within this project is developed from the method reported by Shuttleworth *et al.* with slight modifications.<sup>283</sup>

HACS (150 g) was added to distilled water (3 dm<sup>3</sup>) in an adapted All American pressure cooker 915. The mixture was stirred vigorously (mechanical stirrer) until all the starch had dispersed before further agitating at 140 °C for 90 minutes to gelatinise the starch. After that, the formed clear starch gel was cooled down to room temperature naturally.

The homogeneous gelatinised starch was kept in a lab fridge at 5 °C for three days (72 h) for retrogradation. Then the water trapped in the aquagel was solvent exchanged (3x) with equivolume of low surface tension solvents (ethanol and toluene). The drying of the starch was carried out in a vacuum oven at 50 °C for 24 h to afford white powdered, expanded starch (143 g, 95.3%) with a surface area (BET) of 176 m<sup>2</sup> g<sup>-1</sup>.

#### 4.3.2 BET surface area measurement

BET surface area measurement (nitrogen adsorption / desorption measurements) of expanded HACS were carried out on a Micromeritics ASAP 2010 volumetric adsorption analyser at 77 K. Prior to analysis, an exact known amount of expanded HACS (around 100 mg) was degassed at 65 °C for at least 3 h and mass differences were corrected after the experiment. The resulted data were subjected to proprietary software for BET specific surface area determination. The reported value is mean value of three measurements.

### 4.3.3 Esterification of expanded starch

A series of HACS propionates with various degrees of substitution (DS) were prepared by changing the amounts of esterifying reagent (propionic anhydride) and reaction time. Expanded HACS (10 g, 0.062 mol) was added to toluene (140 mL) in a 250 mL round bottom flask, and to this, varying amounts of propionic anhydride was added. The mixture was heated to 90 °C and stirred for 5 minutes with a magnetic stirrer. Then the catalyst 4-dimethylaminopyridine (DMAP, 0.4 g, 3.3 mmol) was added. The reaction was kept at 90 °C for 6 h while stirring to allow esterification. In one case with propionic anhydride (40 g, 0.307 mol), the reaction was kept at 90 °C for 12 hours to further increase degree of substitution. Detailed esterification reaction conditions (amounts of propionic anhydride, reaction time *etc.* are summarized in Table 25. After that, the mixture was cooled to room temperature (around 25 °C) naturally and ethanol (100 mL) added. The formed precipitate was stirred for 5 minutes, filtered, and washed. This was repeated a further 4 times with ethanol (100 mL), yielding a white powdered product. Then the resulting material was dried in a vacuum oven for 24 h at room temperature under reduced pressure.

**Table 25:** Summary of esterification reaction conditions

Propionic anhydride (g)	Propionic anhydride (mol)	Expanded HACS <sup>b</sup> (mol)	Reaction time (h)
5.0	0.038	0.062	6
7.5	0.058	0.062	6
10.0	0.077	0.062	6
12.5	0.096	0.062	6
15.0	0.115	0.062	6
17.5	0.134	0.062	6
20.0	0.154	0.062	6
30.0	0.231	0.062	6
40.0	0.307	0.062	6
40.0	0.307	0.062	12

#### 4.3.4 Determination of degree of substitution

Determination of degree of substitution (DS) of starch esters by titration involved complete basic hydrolysis of ester linkages and back titration of excess alkaline. The titration method employed is based on literature.<sup>283, 304, 305</sup>

Accurately weighed starch esters (0.5 g) were finely ground and added to 75% ethanol in distilled water (25 mL). The slurry was agitated at 50 °C for 30 minutes. It was then cooled down to room temperature followed by addition of an exact amount of aqueous solution of potassium hydroxide (0.5 N, 20 mL). After that, the solution was stirred for 72 h at room temperature. Then 2 - 3 drops of indicator (phenolphthalein) was added, and the excess of alkali was back-titrated with hydrochloric acid (0.5 N). Reference samples (original unmodified expanded HACS) and triplicate starch ester samples were tested similarly. For starch propionates, the propionic content (% propionyl) was calculated according to the following equation:

$$\% \text{ propionyl} = \frac{[(V_0 - V_n) \times N \times 0.057 \times 100]}{M}$$

Where, 57 is the molar mass of the propionyl group.  $V_0$  is the volume of HCl (0.5 N) used to titrate reference blank samples (unmodified expanded starch);  $V_n$  is the volume of HCl (0.5 N) used to titrate starch ester samples, N is the molarity of HCl used, and M is the sample weight.

Then the DS could be calculated according to following equation:

$$DS = \frac{162 \times \% \text{ propionyl}}{[5700 - (56 \times \% \text{ propionyl})]}$$

Where, 162 is the molar mass of the repeating unit of starch. 5700 is the molar mass of propionic group multiplied by 100. The value 56 is the actual molar mass increase if one propionic group is added to one starch unit. The reported DS values were the mean value of three measurements with error bars.

#### **4.3.5 ATR-IR characterization**

FT-IR spectra of expanded HACS, starch propionates with various DS and formulated HMAs (before and after DSC measurement) were obtained on a PerkinElmer® Spectrum™ 400 FT-IR/NIR spectrometer (PerkinElmer, Inc., Shelton, CT USA). All the spectra were recorded in attenuated total reflectance (ATR) mode, using a resolution of  $2\text{ cm}^{-1}$  and 64 scans.

#### **4.3.6 Thermogravimetric analysis**

Thermogravimetric analysis (TGA) of expanded HACS and its propionates was carried out on a Netzsch 409 Simultaneous Thermal Analyser (STA) to study their thermal properties. An exact known amount of each sample (around 100 mg) was accurately weighed in a dry and clean porcelain sample cup and heated in the furnace in a nitrogen flow ( $100\text{ mL min}^{-1}$ ) from  $30\text{ }^{\circ}\text{C}$  to  $625\text{ }^{\circ}\text{C}$  at a heating rate of  $10\text{ }^{\circ}\text{C min}^{-1}$ .

#### **4.3.7 Solid-state CP/MAS $^{13}\text{C}$ NMR characterization**

Solid-state  $^{13}\text{C}$  CP/MAS NMR spectra of expanded HACS and its propionate with DS 1.00 were obtained using a Varian VNMRS 400 spectrometer at 100.56 MHz. Chemical shifts are reported with respect to tetramethylsilane (TMS).

#### **4.3.8 Liquid-state $^1\text{H}$ NMR characterization**

$^1\text{H}$  NMR spectra of expanded HACS and its propionates with various DS were recorded on a JEOL ECX-400 NMR spectrometer at 100 MHz for 64 scans at  $25\text{ }^{\circ}\text{C}$ . Prior to analysis, each sample (20 mg) was dissolved in DMSO-d<sub>6</sub> (1 mL, 99.5% atom D) by agitating at  $80\text{ }^{\circ}\text{C}$  for 1 h to obtain homogeneous clear solution, followed by transferring into NMR tubes.

#### **4.3.9 Preparation of hot melt adhesive formulations**

Non-expanded HACS, expanded HACS and its propionates with various DS, together with glycerol and polyvinyl alcohol (PVOH), were incorporated into potentially bio-degradable hot melt adhesive (HMA) formulations by mixing in glass vials.

Each sample (non-expanded HACS, expanded HACS and its propionates) was accurately weighed (2 g) in a glass vial which contains glycerol (2 g). The mixture was mixed using a spatula followed by adding PVOH (2 g) into the glass vial. After that, it was further agitated with a spatula for approximately 10 min until a homogeneous mixture (*i.e.*, formulated hot melt adhesive) was formed.

#### **4.3.10 DSC characterization of hot melt adhesives**

Differential scanning calorimetry (DSC) characterization of the formulated hot melt adhesives (HMAs) was conducted using a TA Q2000 differential scanning calorimeter. Each HMA (10 mg) was accurately weighed into a Tzero hermetic aluminium pan and the lid was attached and crimped. After that, the sample was subjected to a heat – cool – heat – cool cycle according to the following procedure:

- (1) Equilibrate at -50 °C for 10 minutes.
- (2) Heat from -50 °C to 210 °C at a heating rate of 10 °C min<sup>-1</sup>.
- (3) Cool down from 210 °C to -50 °C at 10 °C min<sup>-1</sup>.
- (4) Heat from -50 °C to 210 °C at a heating rate of 10 °C min<sup>-1</sup>.
- (5) Cool down from 210 °C to -50 °C at 10 °C min<sup>-1</sup>.

In addition, the starch propionate (DS: 1.00) based HMA was subjected to 3 more heat – cool cycles according to the above mentioned temperature program as an attempt to investigate the stability/reusability of the formulated HMAs.

#### **4.3.11 Adhesion tests of hot melt adhesives**

The mechanical strengths of the non-expanded HACS, expanded HACS and its propionates based HMA formulations were tested with respect to Al–Al bonding. Each HMA formulation (50 mg) was applied to the middle of an aluminium plate (surface size: 50 mm × 50 mm) and covered using another Al plate with the same surface size. For each HMA formulation, four testing specimens were prepared and bonded at 190 °C for 30 seconds under pressure using a hot press machine.

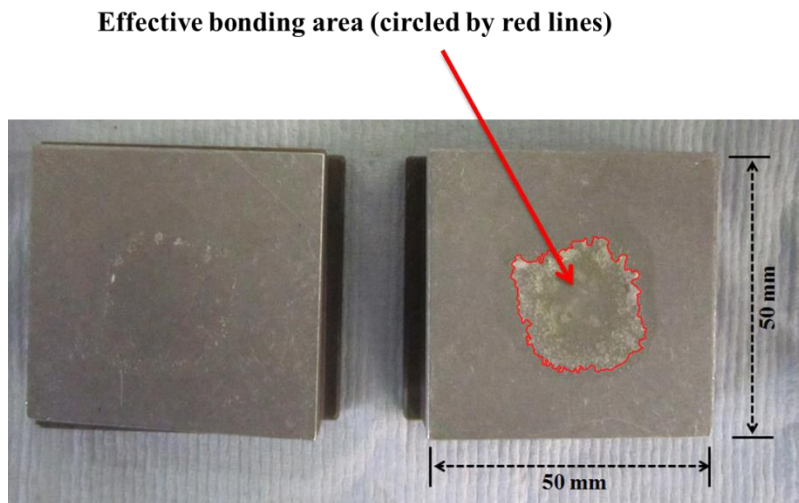


**Figure 111:** Illustration of effective bonding area (the area covered by HMA polymer).  
(Originally in colour)

Tensile strengths of the Al–HMA–Al bonds were measured using an Instron 3367 Dual Column System universal testing machine fitted with a 3000 N capacity load cell at a crosshead speed of 5 mm min<sup>-1</sup>. Obtained tensile strengths were normalized to effective tensile stress by measuring the effective bonding area using Adobe Photoshop CS6. More specifically, as highlighted in Figure 111, the pixels of the effective bonding area (covered by HMA polymer) and those of the Al substrate were measured using Adobe Photoshop CS6, and the effective bonding area was calculated using the following equation:

$$\frac{\text{Effective bonding area}}{\text{Total surface area of Al substrate}} = \frac{\text{Pixels of the area covered by HMA polymer}}{\text{Pixels of the area covered by Al substrate}}$$

Where, the total surface area of Al substrate is 2500 mm<sup>2</sup>.

The measured tensile strengths were normalized to tensile stress according to the following equation:

$$\text{Normalized tensile stress} = \frac{\text{Measured tensile strength}}{\text{Effective bonding area}}$$

The mean value of four measurements for each HMA formulation was reported in the main text of chapter 3 with error bars. In addition, the tensile stress of commercial ethylene vinyl acetate (EVA) based LOCTITE hot melt glue was tested following the same procedure described above for comparison.



# Chapter 5

*Concluding remarks and  
Future work*



Making efficient use of naturally abundant and renewable biomaterials, especially those currently low-value and underutilised biorenewable waste streams, contributes to a significant step towards sustainability and the achievement of a “zero waste” society. In the development of future biorefineries, it is crucially important to use low-environmental-impact technologies and to explore innovative high-value applications for derived products. In the scope of this project, potential routes and applications for the valorisation of three biorenewable waste streams (*i.e.*, waste wood chips, waste office paper and paper deinking residue) as well as waste starch have been demonstrated to very good effect.

The microwave-assisted low-temperature (<200 °C) pyrolysis process allows for the efficient conversion of spruce wood chips, waste office paper and paper deinking residue (DIR) into organic and aqueous phase bio-oil, bio-char (microwave residue) and gas within about 15 min without any additives. The speed of conversion is industrially attractive but this has to be tempered with infra-structure and operational costs. The yield distributions and compositions of pyrolysis products are directly related to their parent materials, as evidenced by ATR-IR, <sup>1</sup>H and <sup>13</sup>C NMR and GC-MS characterization. It was also found that with the aid of the fitted vacuum system during pyrolysis experiments, most organic compounds including carbohydrate sugars and their derivatives, (hetero)-aromatic compounds, ketones, aldehydes and small amounts of carboxylic acids *etc.* were condensed into the organic phase bio-oils. The aqueous phase bio-oils mainly comprise water, carboxylic acids and trace amounts of organic matter. Hence not surprisingly, the organic phase bio-oils were energy-densified in both cases.

The spruce wood chips and waste office paper derived organic phase bio-oils hold great potential to be used as bio-based adhesives towards Al bonding. This represents a potential new market/application opportunity. A small amount of the spruce wood chips and waste office paper derived organic phase bio-oil (70 mg) could effectively adhere two Al substrates (surface sizes: 50 mm × 50 mm) together. The influences of curing temperatures and time periods on the tensile strengths of bio-oil cured Al plates were investigated. Maximum tensile strengths around 2300 – 2600 N could be achieved when specimens were cured around 140 °C to 160 °C for 8 h curing (sufficiently strong to lift an adult without failure). Tensile strengths also increase with

curing time and this effect is more obvious especially when cured at relatively low temperatures (120 °C). High curing temperatures (above 160 °C) results in deterioration of adhesive bonds, the tensile strengths of bio-oil cured Al plates dropped for specimens cured at 180 °C. The reason for this effect is unsure at the moment and needs to be further investigated. The organic phase bio-oil derived from DIR could not bond Al substrates with satisfactory strengths, which were only around 400 N regardless of curing temperature and time. This effect probably resulted from the presence of polycyclic aromatic hydrocarbons (PAHs) in this phase of bio-oil.

To investigate the influences of different categories of compounds within bio-oil on adhesive properties of bio-oil, a liquid-liquid fractionation study of the waste office paper derived organic phase bio-oil using aqueous sodium hydroxide and ethyl acetate, as well as a compound study using HMF, catechol and levoglucosan were carried out. It has been found that there is possibly a *synergistic* and/or *co-operative* effect between various components within bio-oil, and the “acidic” compounds such as furans and (hetero-) aromatic compounds may undergo possible homo- and cross-coupling polymerisation reactions during curing at elevated temperatures. In addition, the bonding behaviour of bio-oil may be similar to phenol-formaldehyde cross-linking reactions.

In furthering the work on bio-oil adhesives it will be necessary to investigate the compositions of released chemicals during curing in oven in terms of safety and large-scale application. Also, it will be interesting to study the adhesive properties of bio-oil towards bonding of other substrates such as glass and stainless steel. Despite the great potential for its use as Al adhesive has been demonstrated and attempts have been made to understand its bonding behaviour, the mechanism still remains uncertain and worth further investigation. For the model compound study, the influences of carboxylic acids (*e.g.*, acetic acid, propionic acid) should be investigated, since these acids are much better catalysts for the polymerization reactions between furans and aromatic compounds.

The microwave-assisted low-temperature (<200 °C) pyrolysis of DIR demonstrates an excellent case study in terms of biorefinery. The microwave-residue was found to be free from organic

matter (as evidenced by the TGA). Solid-state CP/MAS  $^{13}\text{C}$  NMR, XRD and solid-state Bloch-decay  $^{13}\text{C}$  NMR characterization of the microwave residue further confirms this product primarily contains calcite and kaolinite. Hence, the microwave residue could be reused in the paper recycling processes for the production of new paper and cardboard products.

In chapter 3, a series of starch propionates with various DS were prepared from expanded HACS. The expansion of HACS could significantly improve the surface area of non-expanded starch (less than  $5\text{ m}^2\text{ g}^{-1}$ ) to around  $160 - 180\text{ m}^2\text{ g}^{-1}$ . The expansion process opens up the dense packing of starch granules and significantly improves the accessibilities of the hydroxyl groups within starch molecules, allowing esterification to be carried out at relatively mild conditions. A series of potentially biodegradable HMA formulations were prepared by mixing expanded starch, or its propionate derivatives, with the same amounts of polyvinyl alcohol (PVOH) and glycerol. The DSC and ATR-IR characterization of the formulated HMAs confirm the stability/reusability of these HMAs. Maximum tensile stress around 2.3 MPa were achieved with the expanded HACS based HMA, which is much higher than that achieved with non-expanded HACS based HMA. Despite the fact that the tensile stresses of the Al plates cured by starch propionate based HMAs are lower than those obtained with expanded starch based HMA (around 2.3 MPa), this work has for the first time demonstrated the promise of using expanded starch and its esters in HMA formulations.

Since the properties of modified starches significantly depend upon the modification methods used, future work should focus on preparation of other starch esters with various chain lengths and their properties should be investigated. Furthermore, the current potentially biodegradable HMA formulations should be improved to compete with commercial fossil-derived HMAs and/or other natural product derived HMAs.



# **Appendix A**



## **Appendix A: Qualitative and quantitative GC-MS characterization of the organic phase bio-oil generated from microwave-assisted low-temperature (<200 °C) pyrolysis of DIR**

The organic phase bio-oil (60 mg) produced from the microwave-assisted low-temperature (<200 °C) pyrolysis of DIR was dissolved in acetone. After addition of IS-solution (Fluoranthene in Acetone), some white precipitations were observed (probably small amounts of inorganic, *e.g.*, calcite). The analysis was conducted after filtering. Detailed instrumentation and experimental procedures for GC-MS analysis are described in section 4.2.11 in chapter 4. In total 45.66 wt.% of the bio-oil was identified by GC-MS.

(This GC-MS analysis was conducted by the Thunen Institute, University of Hamburg, Germany)

**Table 26:** Summary table of GC-MS characterization of the DIR derived organic phase bio-oil

Substance group	wt.%
<b>NONAROMATIC COMPOUNDS</b>	<b>14.98</b>
Acids	2.11
Nonaromatic Esters	0.62
Nonaromatic Alcohols	1.22
Nonaromatic Aldehydes	8.13
Nonaromatic Ketones	2.91
Hydrocarbons	0.00
<b>HETEROCYCLIC COMPOUNDS</b>	<b>7.44</b>
Furans	6.41
Pyrans	1.02
<b>AROMATIC COMPOUNDS</b>	<b>2.36</b>
Benzenes	1.23
Catechols	n.q.
Aromatic Alcohols	0.00
Aromatic Aldehydes	0.00
Aromatic Ketones	0.00
Aromatic Esters	0.00
Lignin derived Phenols	0.13
Guaiacols (Methoxy phenols)	0.75
Syringols (Dimethoxy phenols)	0.25
<b>CARBOHYDRATES</b>	<b>19.75</b>
Sugars	19.75
<b>OTHER ORGANIC COMPOUNDS</b>	<b>1.13</b>
N-compounds	0.00
Acetates	0.00
Terpenes	0.00
unknown compounds	1.07
Miscellaneous	0.06
<b>Total</b>	<b>45.66</b>

**Table 27:** Detailed GC-MS analysis of the DIR derived organic phase bio-oil

<b>Compound</b>	<b>wt.%</b>	
<b>NONAROMATIC COMPOUNDS</b>		
<b>Acids</b>	<b>2.107</b>	
Acetic acid	1.118	c
Propionic acid	0.989	c
<b>Nonaromatic Esters</b>	<b>0.619</b>	
poss: Oxopropanoic acid methylester, 2- (NIST MQ 77)	0.086	#
poss. Propanoic acid, ethenyl ester (NIST MQ 75)	0.061	#
3-Furancarboxylic acid, methyl ester (NIST MQ 88)	0.117	#
similar Butanoic acid, propyl ester (NIST MQ 67)	0.354	#
<b>Nonaromatic Alcohols</b>	<b>1.217</b>	
Ethylene glycol	1.035	c
Ethene, 1,2-dihydroxy-	0.064	#
unknown aliphatic alcohol	0.042	#
1,2-Ethanediol, monoformate (NIST MQ 89)	0.075	#
<b>Nonaromatic Aldehydes</b>	<b>8.131</b>	
Acetaldehyde, hydroxy-	7.431	c
Propionaldehyde, 3-hydroxy	0.540	#
Butanedral or Propanal (NIST MQ 88)	0.160	#
<b>Nonaromatic Ketones</b>	<b>2.907</b>	
Acetol (Hydroxypropanone)	0.838	c
Butanone, 1-hydroxy-2-	0.159	c
Propan-2-one, 1-acetyloxy-	0.063	c
Cyclopenten-1-one, 2-	0.028	c
Cyclopenten-1-one, 3-methyl-2-	0.044	c
Cyclopenten-1-one, 2-hydroxy-2-	0.261	#
Cyclopenten-3-one, 2-hydroxy-1-methyl-1-	0.717	c
Cyclopenten-1-one, 3-ethyl-2-hydroxy-2-	0.164	c
3-Pantanone	0.027	#
poss: Butan-2-one, 1-(acetyloxy)- (NIST MQ 77)	0.053	#
Isomere of Cyclopenten-1-one, 2-hydroxy-3-methyl-2-	0.361	#
Isomer of Cyclopenten-1-one, 3-ethyl-2-hydroxy-	0.104	#
similar to 1,3-Cyclohexanedione, 2-methyl- (NIST MQ 77)	0.086	#
<b>Hydrocarbons</b>	<b>0.000</b>	
<b>HETEROCYCLIC COMPOUNDS</b>		
<b>Furans</b>	<b>6.414</b>	

Furfuryl alcohol, 2-	0.604	c
Furanone, 2(3H)-	0.111	#
Furanone, 2(5H)-	1.154	c
Furaldehyde, 2-	0.099	c
Furaldehyde, 5-methyl-2-	0.070	c
Furaldehyde, 5-(hydroxymethyl)-, 2-	1.366	c
2(3H)-Furanone, dihydro-4-hydroxy-	0.140	#
Furan-x-on, x,x-dihydro-x-methyl-	0.378	#
Butyrolactone, $\gamma$ -	0.155	c
Butyrolactone, 2-hydroxy-, $\gamma$ -	1.442	c
similar to 2-Furanmethanol, tetrahydro- (NIST MQ 78)	0.030	#
Isomere of 2(3H)-Furanone, dihydro-4-hydroxy-	0.055	#
poss: 2(5H)-Furanone, 5-methyl- (NIST MQ 84)	0.050	#
2,5-Furandione, 3-methyl- (NIST MQ 67)	0.124	#
Furan-2-one, 4-methyl-(5H)- (NIST MQ 88)	0.125	#
Lactone derivative (poss: (S)-(+)-2',3'-Dideoxyribonolactone NIST MQ 84)	0.290	#
Lactone derivative (unspecific spectrum)	0.116	#
Lactone derivative (unspecific spectrum)	0.103	#
<b>Pyrans</b>	<b>1.022</b>	
Maltol (Pyran-4-one, 3-Hydroxy-2-methyl-4H-)	0.322	c
Pyran-4-one, 3-hydroxy-5,6-dihydro-, (4H)-	0.700	#
<b>AROMATIC COMPOUNDS</b>		
<b>Benzenes</b>	<b>1.228</b>	
poss: Biphenyl	0.029	#
Biphenyl, methyl-	0.019	#
1,3-di-iso-propynaphthalene (NIST MQ 87)	0.035	#
Propane, 1,3-diphenyl- CAS#: 1081-75-0 (NIST MQ 92)	0.255	#
1,7-di-iso-propynaphthalene (NIST MQ 87)	0.046	#
1,4-di-iso-propynaphthalene (NIST MQ 87)	0.051	#
x,y-di-iso-propynaphthalene (NIST MQ 87)	0.081	#
2,6-di-iso-propynaphthalene (NIST MQ 87)	0.061	#
unknown not identifiable aromatic compound MW=? (no NIST spectrum found)	0.078	#
poss: 1,1-Diphenylcyclopropane (NIST MQ 82)	0.041	#
Benzene, 1,1'-(1,4-butanediyl)bis- CAS#: 1083-56-3 (NIST MQ 69)	0.030	#
unknown not identifiable aromatic compound MW=? (no NIST spectrum found)	0.016	#
unknown not identifiable aromatic compound MW=220	0.038	#

(no NIST spectrum found)		
unknown not identifiable aromatic compound MW=? (no NIST spectrum found)	0.040	#
unknown not identifiable aromatic compound MW=262 (no NIST spectrum found)	0.028	#
unknown biphenyl compound MW=234 (no NIST spectrum found)	0.040	#
unknown not identifiable aromatic compound MW=262 (no NIST spectrum found)	0.057	#
unknown not identifiable aromatic compound MW=262 (no NIST spectrum found)	0.035	#
unknown not identifiable Benzene compound MW=230 (no NIST spectrum found)	0.045	#
similar to Naphthalene, 1-(phenylmethoxy)- CAS#: 607-58-9 (NIST MQ 67)	0.015	#
unknown not identifiable aromatic compound MW=? (no NIST spectrum found)	0.191	#
<b>Catechols</b>	<b>n.q.</b>	
Hydroquinone (Benzene, 1,4-dihydroxy-)	3.295	n.q.
<b>Aromatic Alcohols</b>	<b>0.000</b>	
<b>Aromatic Aldehydes</b>	<b>0.000</b>	
<b>Aromatic Ketones</b>	<b>0.000</b>	
<b>Aromatic Esters</b>	<b>0.000</b>	
<b>Lignin derived Phenols</b>	<b>0.133</b>	
Phenol	0.093	c
Cresol, o-	0.041	c
<b>Guaiacols (Methoxy phenols)</b>	<b>0.752</b>	
Guaiacol	0.054	c
Guaiacol, 4-methyl-	0.069	c
Guaiacol, 4-vinyl-	0.127	#
Guaiacol, 4-allyl- (Eugenol)	0.041	c
Guaiacol, 4-propenyl- cis (Isoeugenol)	0.077	c
Guaiacol, 4-propenyl-(trans) (Isoeugenol)	0.273	c
Vanillin	0.111	c
<b>Syringols (Dimethoxy phenols)</b>	<b>0.248</b>	
Syringol	0.062	c
Syringol, 4-methyl-	0.054	c

Syringol, 4-(1-propenyl)-, trans	0.131	#
<b>CARBOHYDRATES</b>		
<b>Sugars</b>	<b>19.751</b>	
Anhydro- $\beta$ -D-xylofuranose, 1,5-	0.412	#
Anhydro- $\beta$ -D-glucopyranose, 1,6- (Levoglucosan)	10.092	c
Anhydro- $\alpha$ -D-galactofuranose, 1,6-	0.180	#
Dianhydro- $\alpha$ -D-glucopyranose, 1,4:3,6-	1.309	#
Levoglucosenone	0.880	#
Anhydrosugar unknown (unspecific spectrum)	3.801	#
poss: 2,3-Anhydro-d-galactosan (NIST MQ 78)	0.777	#
poss: 2,3-Anhydro-d-mannosan (NIST MQ 84)	1.196	#
Isomer of 2,3-Anhydro-d-mannosan	0.256	#
Anhydrosugar unknown (unspecific spectrum)	0.325	#
Anhydrosugar unknown (no NIST spectrum found)	0.521	#
<b>OTHER ORGANIC COMPOUNDS</b>		
<b>N-compounds</b>	<b>0.000</b>	
<b>Acetates</b>	<b>0.000</b>	
<b>Terpenes</b>	<b>0.000</b>	
<b>unknown compounds</b>	<b>1.067</b>	
Acetone derived compound = impurity in Acetone	0.097	#
unknown unspecific spectrum (looks like 2-Butanone RT 5.2)	0.017	#
unknown not identifiable compound (no NIST spectrum found)	0.034	#
overlapping not identifiable compounds	0.025	#
overlapping not identifiable compound MW=128 (no NIST spectrum found)	0.104	#
unknown compound (unspecific spectrum) (no NIST spectrum found)	0.125	#
unknown not identifiable compound (no NIST spectrum found)	0.084	#
unknown carbohydrate (unspecific spectrum) (no NIST spectrum found)	0.247	#
unknown not identifiable compound MW=? (no NIST spectrum found)	0.117	#
unknown not identifiable compound MW=? (no NIST spectrum found)	0.059	#
unknown not identifiable compound MW=? (no NIST spectrum found)	0.125	#

unknown not identifiable compound MW=? (no NIST spectrum found)	0.032	#
<b>Miscellaneous</b>	<b>0.064</b>	
4-Phenylcyclohexene CAS#: 4994-16-5 (NIST MQ 77)	0.020	#
Benzenebutanenitrile CAS#: 2046-18-6 (NIST MQ 74)	0.031	#
softener = Isobutyl phthalate	0.013	#
c = calibrated compound		
n.q. = not quantified		
# = estimated response factor		

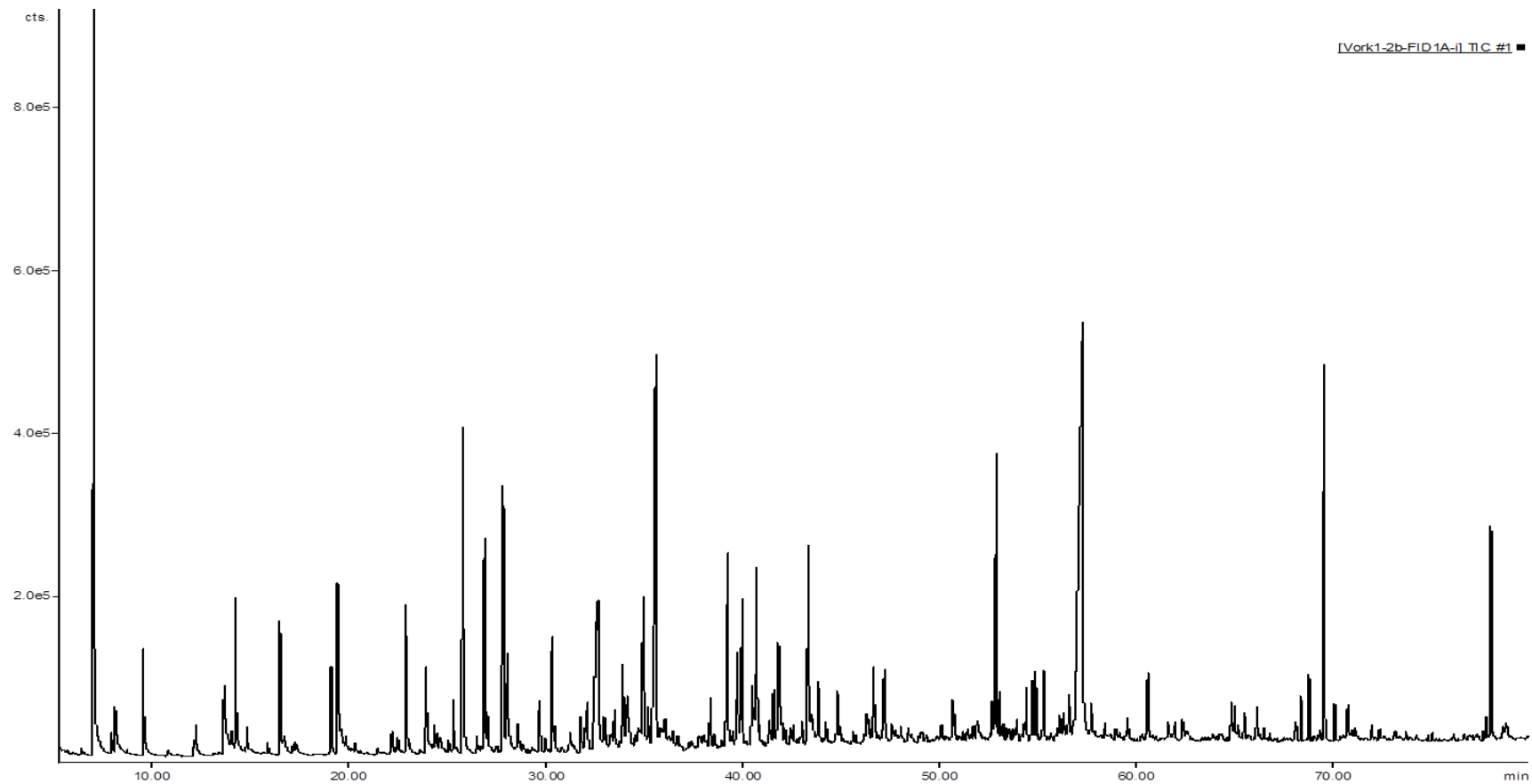


**Figure 112:** Overall gas chromatogram of the DIR derived organic phase bio-oil.

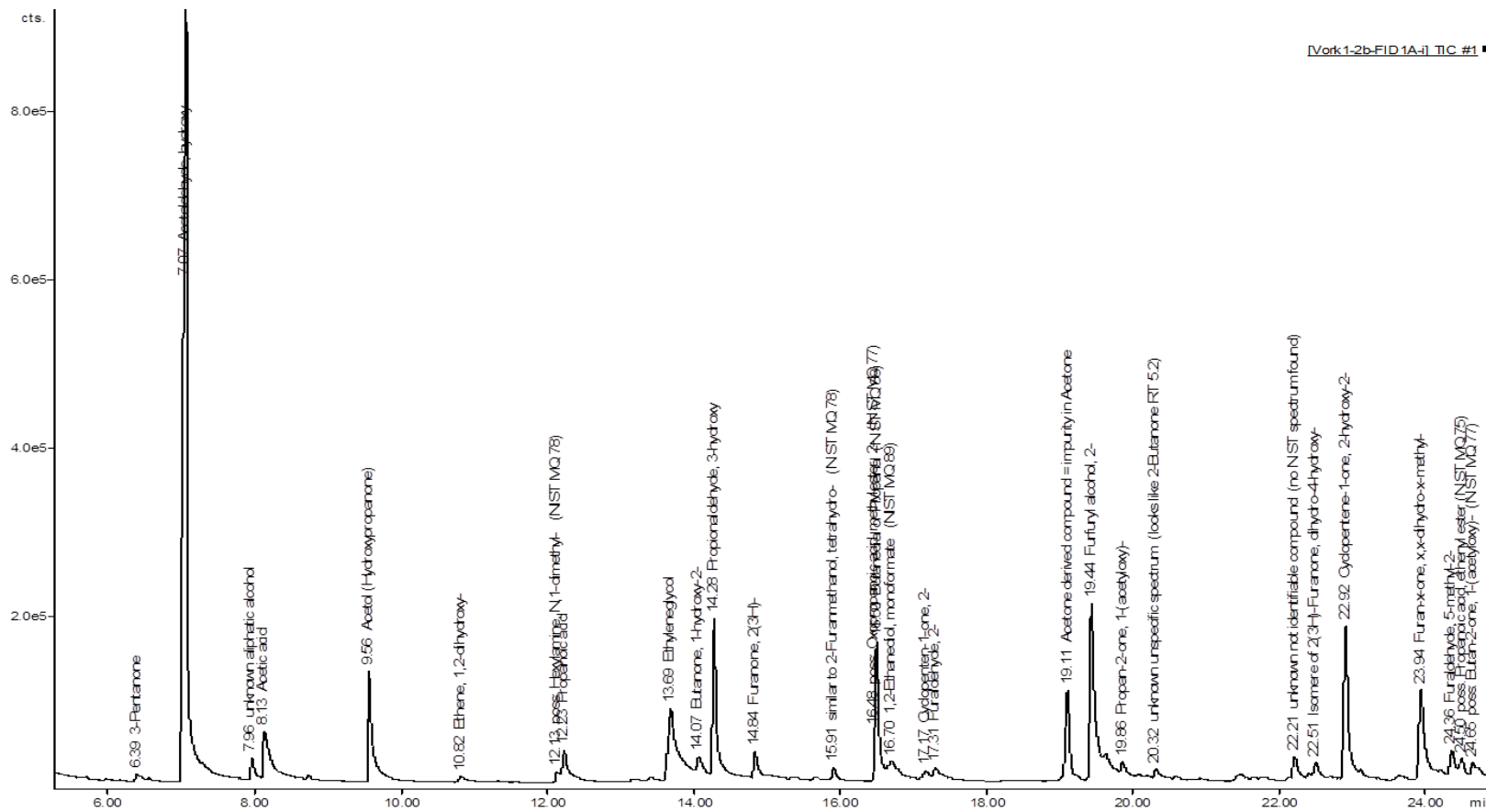


**Figure 113:** Specified gas chromatogram identification of the DIR derived organic phase bio-oil (0-25 min).

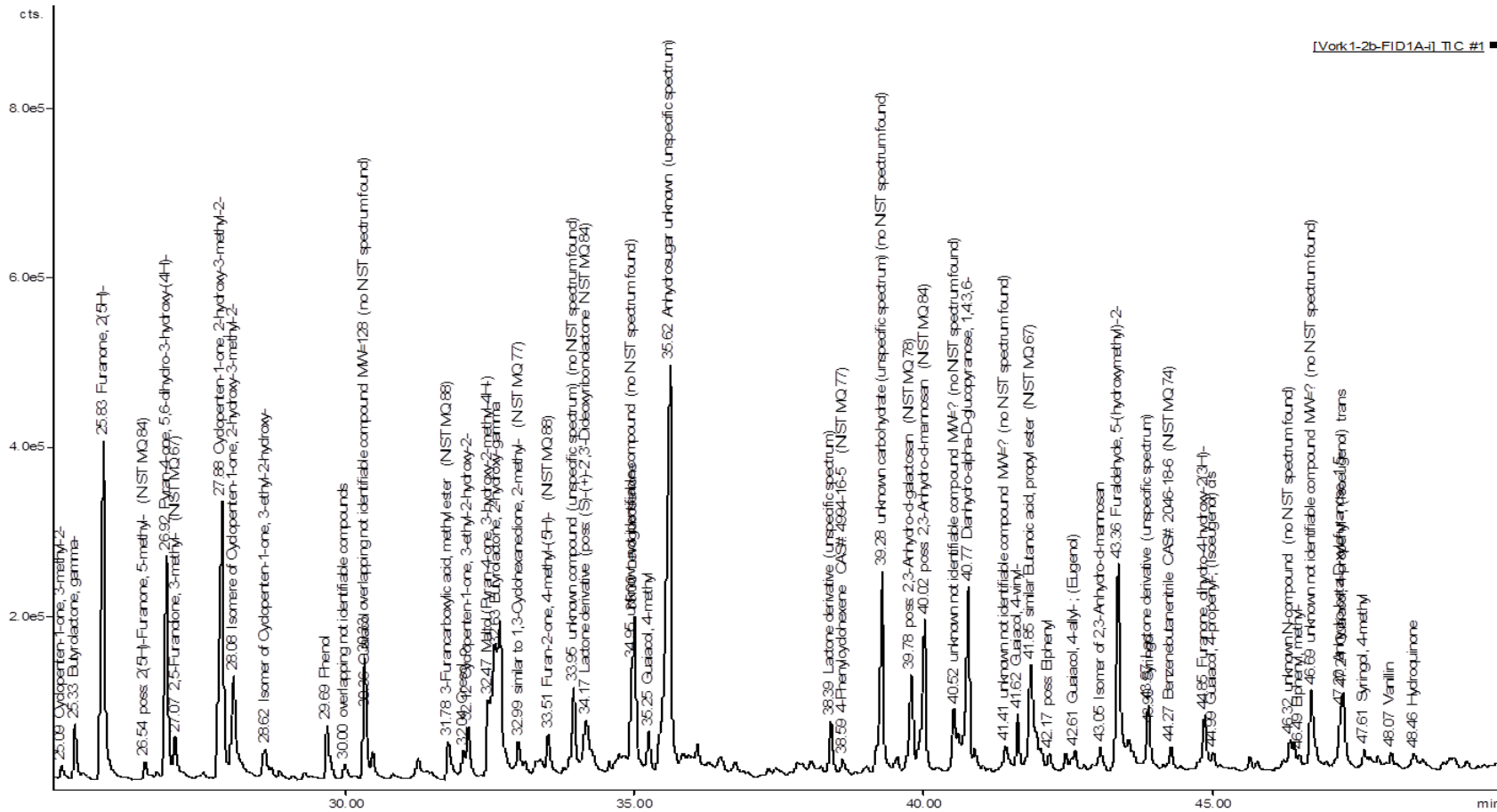


**Figure 114:** Specified gas chromatogram identification of the DIR derived organic phase bio-oil (25-50 min)

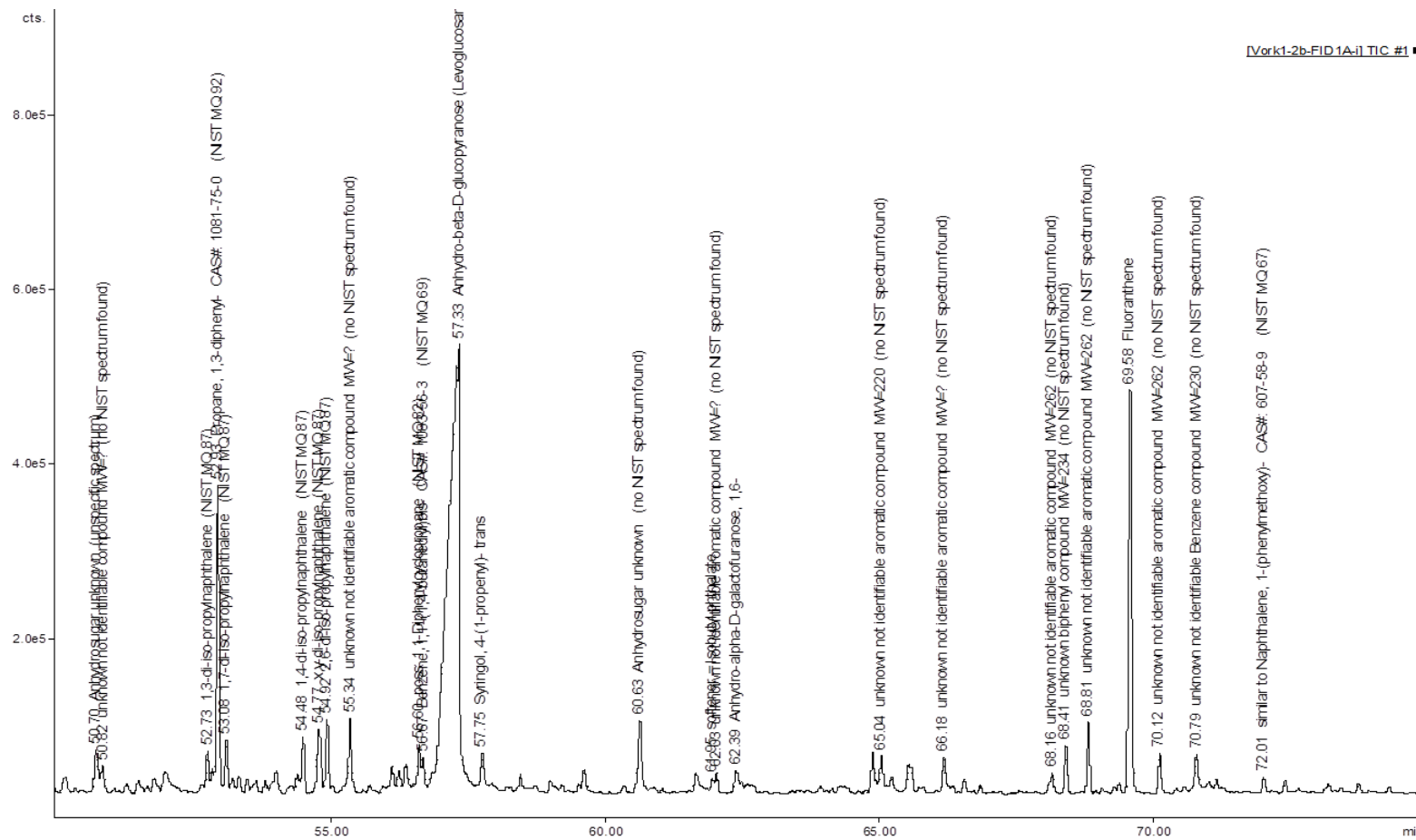


**Figure 115:** Specified gas chromatogram identification of the DIR derived organic phase bio-oil (50-75 min).

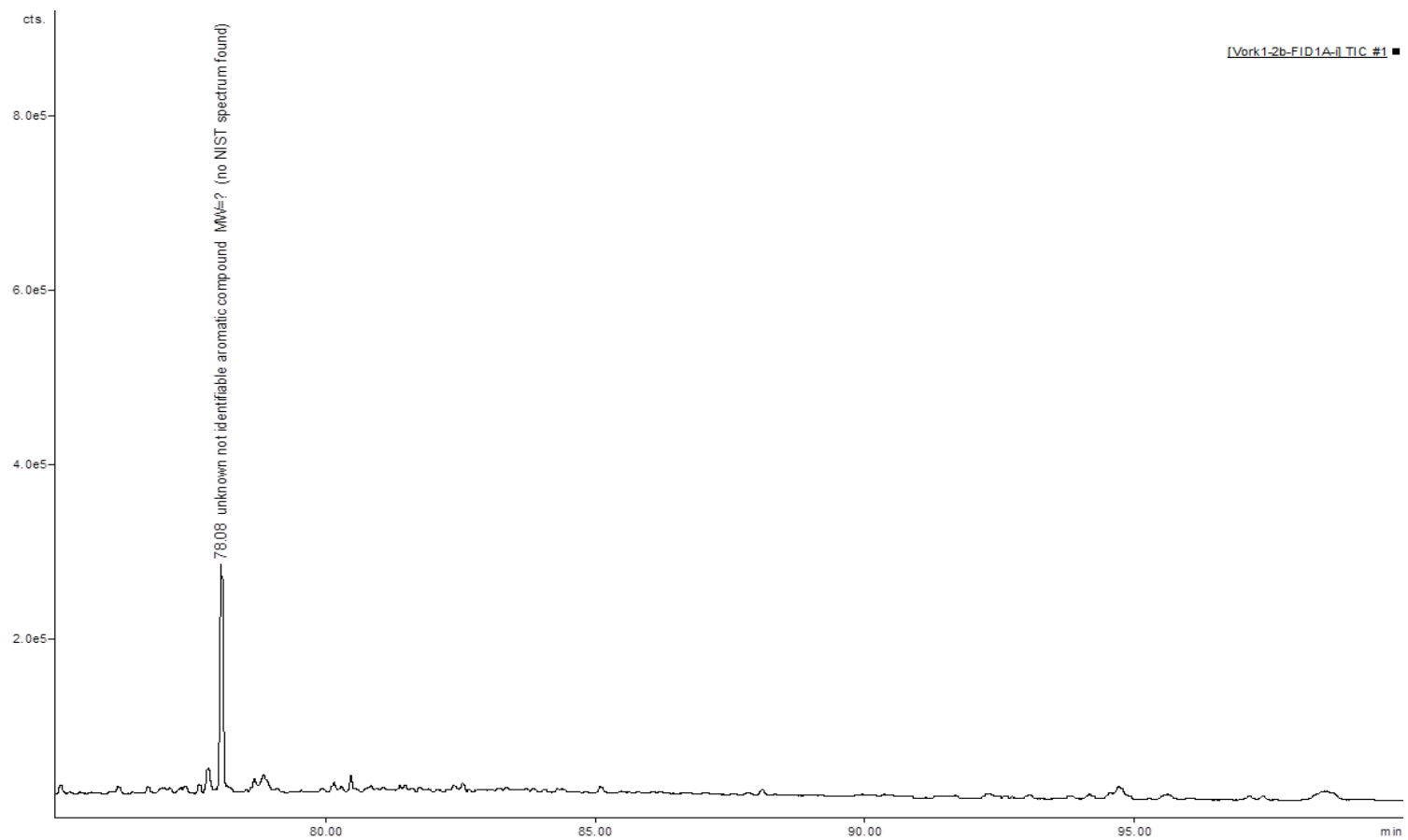


**Figure 116:** Specified gas chromatogram identification of the DIR derived organic phase bio-oil (75-100 min)

# **Abbreviations**



ATR	-	Attenuated total reflectance
BET	-	Brunauer, Emmett and Teller
CAGR	-	Compound annual growth rate
CP/MAS	-	Cross-polarization/magic angle spinning
CV	-	Calorific value
DIR	-	Deinking residue
DMAP	-	4-Dimethylaminopyridine
DMSO	-	Dimethyl sulfoxide
DP	-	Degree of polymerisation
DPS	-	Deinking paper sludge
DRIFT	-	Diffuse reflectance infrared Fourier-Transform spectroscopy
DS	-	Degree of substitution
dTG	-	Derivative thermogravimetric
EPA	-	Environmental Protection Agency
EU	-	European Union
FAO	-	Food and Agriculture Organization of the United Nations
FT-IR	-	Fourier transform-infrared spectroscopy
FWHH	-	Full width at half height
GC	-	Gas chromatography
GC-MS	-	Gas chromatography – mass spectroscopy
GHG	-	Greenhouse gas
GPC	-	Gas permeation chromatography
HACS	-	High amylose corn starch
HMA	-	Hot melt adhesive
HMF	-	5-(Hydroxymethyl)-2-furaldehyde
HPLC	-	High-performance liquid chromatography
ICP-MS	-	Inductively coupled plasma–mass spectrometry
IEA	-	International Energy Agency
LCF	-	Lignocellulosic feedstock biorefinery

MW (1)	-	Microwave
MW (2)	-	Molecular weight
NMR	-	Nuclear magnetic resonance
NREL	-	National Renewable Energy Laboratory
OSB	-	Oriented strand board
PAHs	-	Polycyclic aromatic hydrocarbons
PVOH	-	Polyvinyl alcohol
RT	-	Room temperature
SBS	-	Styrene-butadiene-styrene
SEM	-	Scanning electron microscopy
SIS	-	Styrene-isoprene-styrene
SME's	-	Small and medium enterprises
STA	-	Simultaneous thermal analysis
T <sub>g</sub>	-	Glass transition temperature
TGA	-	Thermogravimetric analysis
TOC	-	Total organic carbon
T <sub>peak</sub>	-	Peak temperature
UK	-	United Kingdom
USA	-	United States of American
USDA	-	United States Department of Agriculture
VOCs	-	Volatile organic compounds
WCED	-	United Nations World Commission on Environment and Development
WFD	-	Waste framework directive
XRD	-	X-ray diffraction

# References



1. United Nations World Commission on Environment and Development, *Our Common Future (Brundtland Report)*, Oxford, 1987.
2. B. Hopwood, M. Mellor and G. O'Brien, *Sustainable Development*, 2005, **13**, 38-52.
3. S. I. Rodriguez, M. S. Roman, S. C. Sturhahn and E. H. Terry, *Sustainability Assessment and Reporting for the University of Michigan's Ann Arbor Campus*, University of Michigan, Ann Arbor, 2002. [http://css.snre.umich.edu/css\\_doc/CSS02-04.pdf](http://css.snre.umich.edu/css_doc/CSS02-04.pdf) (Accessed 06/04/2015)
4. N. Winterton, in *Chemistry for Sustainable Technologies A Foundation*, Royal Society of Chemistry, 2011, ch. 3, pp. 35-51.
5. F. Krausmann, S. Gingrich, N. Eisenmenger, K. Erb, H. Haberl and M. Fischer-Kowalski, *Ecological Economics*, 2009, **68**, 2696-2705.
6. The Organization for Economic Co-operation and Development (OECD), *Material Resources, Productivity and the Environment*, 2015. <http://www.oecd.org/env/waste/material-resources-productivity-and-the-environment-9789264190504-en.htm> (Accessed 06/04/2015)
7. International Energy Agency (IEA), *World Energy Outlook 2014 executive summary*, 2014. <http://www.worldenergyoutlook.org/publications/weo-2014/> (Accessed 06/04/2015)
8. C. McGlade and P. Ekins, *Nature*, 2015, **517**, 187-190.
9. European Commission, *Innovating for Sustainable Growth: A Bioeconomy for Europe*, 2012. [http://ec.europa.eu/research/bioeconomy/pdf/official-strategy\\_en.pdf](http://ec.europa.eu/research/bioeconomy/pdf/official-strategy_en.pdf) (Accessed 06/04/2015)
10. European Commission, *Commission proposes strategy for sustainable bioeconomy in Europe*, 2012. [http://europa.eu/rapid/press-release\\_IP-12-124\\_en.htm](http://europa.eu/rapid/press-release_IP-12-124_en.htm) (Accessed 06/04/2015)
11. L. Landeweerd, M. Surette and C. van Driel, *Interface Focus*, 2011, **1**, 189-195.

12. Germany Federal Ministry of Food and Agriculture, *National Policy Strategy on Bioeconomy*, 2014. [http://www.bmel.de/SharedDocs/Downloads/EN/Publications/NatPolicyStrategyBioeconomy.pdf?\\_\\_blob=publicationFile](http://www.bmel.de/SharedDocs/Downloads/EN/Publications/NatPolicyStrategyBioeconomy.pdf?__blob=publicationFile) (Accessed 06/04/2015)
13. Germany Federal Ministry of Education and Research, *Destination Bioeconomy – Research for a Biobased and Sustainable Economic Growth*, 2014. [http://www.bmbf.de/pub/Destination\\_Bioeconomy\\_bf.pdf](http://www.bmbf.de/pub/Destination_Bioeconomy_bf.pdf) (Accessed 06/04/2015)
14. The White House of United States, *National Bioeconomy Blueprint*, 2012. [https://www.whitehouse.gov/sites/default/files/microsites/ostp/national\\_bioeconomy\\_blueprint\\_april\\_2012.pdf](https://www.whitehouse.gov/sites/default/files/microsites/ostp/national_bioeconomy_blueprint_april_2012.pdf) (Accessed 06/04/2015)
15. L. Staffas, M. Gustavsson and K. McCormick, *Sustainability*, 2013, **5**, 2751-2769.
16. Q. Li, Q. Zhao, Y. Hu and H. Wang, *Biotechnology Journal*, 2006, **1**, 1205-1214.
17. D. Hoornweg, P. Bhada-Tata and C. Kennedy, *Nature*, 2013, **502**, 615-617.
18. J. H. Clark and A. S. Matharu, in *Waste as a Resource*, eds. R. E. Hester and R. M. Harrison, Royal Society of Chemistry, 2013, pp. 66-82.
19. A. B. L. de Sousa Jabbour, C. J. C. Jabbour, J. Sarkis and K. Govindan, *Clean Technologies and Environmental Policy*, 2014, **16**, 7-9.
20. L. A. Guerrero, G. Maas and W. Hogland, *Waste Management*, 2013, **33**, 220-232.
21. D. Hoornweg and P. Bhada-Tata, *What a Waste: A Global Review of Solid Waste Management*, the World Bank, 2012. <https://openknowledge.worldbank.org/handle/10986/17388> (Accessed 06/04/2015)
22. C. S. K. Lin, L. A. Pfaltzgraff, L. Herrero-Davila, E. B. Mubofu, S. Abderrahim, J. H. Clark, A. A. Koutinas, N. Kopsahelis, K. Stamatelatou, F. Dickson, S. Thankappan, Z. Mohamed, R. Brocklesby and R. Luque, *Energy & Environmental Science*, 2013, **6**, 426-464.
23. L.A. Pfaltzgraff, J.H. Clark, in *Advances in Biorefineries*, eds K. W. Waldron, Woodhead Publishing, 2014, ch. 2, pp. 3-33.

24. C. O. Tuck, E. Pérez, I. T. Horváth, R. A. Sheldon and M. Poliakoff, *Science*, 2012, **337**, 695-699.
25. A. J. Ragauskas, C. K. Williams, B. H. Davison, G. Britovsek, J. Cairney, C. A. Eckert, W. J. Frederick, J. P. Hallett, D. J. Leak, C. L. Liotta, J. R. Mielenz, R. Murphy, R. Templer and T. Tschaplinski, *Science*, 2006, **311**, 484-489.
26. R. A. D. Arancon, C. S. K. Lin, K. M. Chan, T. H. Kwan and R. Luque, *Energy Science & Engineering*, 2013, **1**, 53-71.
27. M. Stöcker, *Angewandte Chemie International Edition*, 2008, **47**, 9200-9211.
28. World Economic Forum, *The Future of Industrial Biorefineries*, 2010. [http://www3.weforum.org/docs/WEF\\_FutureIndustrialBiorefineries\\_Report\\_2010.pdf](http://www3.weforum.org/docs/WEF_FutureIndustrialBiorefineries_Report_2010.pdf) (Accessed 06/04/2015)
29. HM Government, *Building a high value bioeconomy - OPPORTUNITIES FROM WASTE*, 2015. [https://www.gov.uk/government/uploads/system/uploads/attachment\\_data/file/408940/BIS-15-146\\_Bioeconomy\\_report\\_-\\_opportunities\\_from\\_waste.pdf](https://www.gov.uk/government/uploads/system/uploads/attachment_data/file/408940/BIS-15-146_Bioeconomy_report_-_opportunities_from_waste.pdf) (Accessed 06/04/2015)
30. House of Lords Science and Technology Committee, *Waste or resource? Stimulating a bioeconomy*, 2014. <http://www.publications.parliament.uk/pa/ld201314/ldselect/ldsctech/141/141.pdf> (Accessed 06/04/2015)
31. United States Department of Agriculture, *Why biobased? Opportunities in the Emerging Bioeconomy*, 2014. <http://www.biopreferred.gov/files/WhyBiobased.pdf> (Accessed 06/04/2015)
32. Council Directive 1999/31/EC of 26 April 1999 on the landfill of waste. <http://eur-lex.europa.eu/legal-content/EN/TXT/PDF/?uri=CELEX:31999L0031&from=EN> (Accessed 06/04/2015)
33. Directive 2008/98/EC of the Europe Parliament and of the council of 19 November 2008 on waste and repealing certain Directives. <http://eur-lex.europa.eu/legal-content/EN/TXT/PDF/?uri=CELEX:32008L0098&from=EN> (Accessed 06/04/2015)

34. Department for Environment Food and Rural Affairs (DEFRA), *Government Review of Waste Policy in England 2011*, 2011. [https://www.gov.uk/government/uploads/system/uploads/attachment\\_data/file/69401/pb13540-waste-policy-review110614.pdf](https://www.gov.uk/government/uploads/system/uploads/attachment_data/file/69401/pb13540-waste-policy-review110614.pdf) (Accessed 06/04/2015)
35. WRAP, *Gate Fees Report 2013*, 2013. [http://www.wrap.org.uk/sites/files/wrap/Gate\\_Fees\\_Report\\_2013\\_h%20%282%29.pdf](http://www.wrap.org.uk/sites/files/wrap/Gate_Fees_Report_2013_h%20%282%29.pdf) (Accessed 06/04/2015)
36. G. Laufenberg, B. Kunz and M. Nystroem, *Bioresource Technology*, 2003, **87**, 167-198.
37. K. R. Hakeem, M. Jawaid and U. Rashid, *Biomass and Bioenergy: Processing and Properties*, Springer, 2014.
38. J. L. Scott and G. Unali, in *Materials for a Sustainable Future*, eds. T. M. Letcher and J. L. Scott, Royal Society of Chemistry, 2012, ch. 10, pp. 279-315.
39. P. Gallezot, *Chemical Society Reviews*, 2012, **41**, 1538-1558.
40. C. Zhou, X. Xia, C. Lin, D. Tong and J. Beltramini, *Chemical Society Reviews*, 2011, **40**, 5588-5617.
41. J. Zakzeski, P. C. A. Bruijnincx, A. L. Jongerius and B. M. Weckhuysen, *Chemical Reviews*, 2010, **110**, 3552-3599.
42. L. P. Christopher, in *Integrated Forest Biorefineries: Challenges and Opportunities*, ed. L. P. Christopher, Royal Society of Chemistry, 2013, ch. 1, pp. 1-66.
43. A. A. Peterson, F. Vogel, R. P. Lachance, M. Froling, J. M. J. Antal and J. W. Tester, *Energy & Environmental Science*, 2008, **1**, 32-65.
44. J. Saini, R. Saini and L. Tewari, *3 Biotech*, 2014, 1-17.
45. D. Mohan, C. U. Pittman and P. H. Steele, *Energy & Fuels*, 2006, **20**, 848-889.
46. A. C. Wiedenhoeft, in *Handbook of wood chemistry and wood composites*, ed. R. M. Rowell, CRC press, 2012, ch. 2, pp. 9-32.
47. G. Garrote, H. Domínguez and J. C. Parajó, *Holz als Roh- und Werkstoff*, 1999, **57**, 191-202.

48. T. Abbasi and S. A. Abbasi, *Renewable and Sustainable Energy Reviews*, 2010, **14**, 919-937.
49. R. Fahmi, A. V. Bridgwater, I. Donnison, N. Yates and J. M. Jones, *Fuel*, 2008, **87**, 1230-1240.
50. A. Demirbaş, *Fuel*, 1997, **76**, 431-434.
51. F. Huang and A. Ragauskas, *Industrial & Engineering Chemistry Research*, 2013, **52**, 1743-1749.
52. T. Fisher, M. Hajaligol, B. Waymack and D. Kellogg, *Journal of Analytical and Applied Pyrolysis*, 2002, **62**, 331-349.
53. A. Gani and I. Naruse, *Renewable Energy*, 2007, **32**, 649-661.
54. P. McKendry, *Bioresource Technology*, 2002, **83**, 37-46.
55. A. O'Sullivan, *Cellulose*, 1997, **4**, 173-207.
56. T. Shibata, in *Renewable Resources for Functional Polymers and Biomaterials: Polysaccharides, Proteins and Polyesters*, eds. B. Tang, P. A. Williams, Royal Society of Chemistry, 2011, ch. 3, pp. 48-87.
57. P. Zugenmaier, *Progress in Polymer Science*, 2001, **26**, 1341-1417.
58. P. L. Dhepe and A. Fukuoka, *ChemSusChem*, 2008, **1**, 969-975.
59. L. D. Gomez, C. G. Steele-King and S. J. McQueen-Mason, *New Phytologist*, 2008, **178**, 473-485.
60. J. Puls, *Macromolecular Symposia*, 1997, **120**, 183-196.
61. L. Laureano-Perez, F. Teymouri, H. Alizadeh and B. Dale, *Applied Biochemistry and Biotechnology*, 2005, **124**, 1081-1099.
62. N. M. L. Hansen and D. Plackett, *Biomacromolecules*, 2008, **9**, 1493-1505.
63. A. J. Ragauskas, G. T. Beckham, M. J. Biddy, R. Chandra, F. Chen, M. F. Davis, B. H. Davison, R. A. Dixon, P. Gilna, M. Keller, P. Langan, A. K. Naskar, J. N. Saddler, T. J. Tschaplinski, G. A. Tuskan and C. E. Wyman, *Science*, 2014, **344**.

64. C. Xu, R. A. D. Arancon, J. Labidi and R. Luque, *Chemical Society Reviews*, 2014, **43**, 7485-7500.
65. F. S. Chakar and A. J. Ragauskas, *Industrial Crops and Products*, 2004, **20**, 131-141.
66. R. Hatfield and R. S. Fukushima, *Crop Sci.*, 2005, **45**, 832-839.
67. K. E. Achyuthan, A. M. Achyuthan, P. D. Adams, S. M. Dirk, J. C. Harper, B. A. Simmons and A. K. Singh, *Molecules*, 2010, **15**, 8641-8688.
68. M. P. Pandey and C. S. Kim, *Chemical Engineering & Technology*, 2011, **34**, 29-41.
69. S. Kang, X. Li, J. Fan and J. Chang, *Renewable and Sustainable Energy Reviews*, 2013, **27**, 546-558.
70. N. Winterton, *Chemistry for sustainable technologies: a foundation*, Royal Society of Chemistry, 2011, ch. 11, pp. 353-406.
71. A. Blennow, M. Hansen, A. Schulz, K. Jørgensen, A. M. Donald and J. Sanderson, *Journal of Structural Biology*, 2003, **143**, 229-241.
72. P. C. Morris, P. Welters and B. Garthoff, in *Renewable Raw Materials*, eds. R. Ulber, D. Sell and T. Hirth, Wiley-VCH Verlag GmbH & Co. KGaA, 2011, ch. 2, pp. 7-32.
73. E. Waltz, *Nature Biotechnology*, 2010, **28**, 8-8.
74. P. S. Shuttleworth and N. Supanchaiyamat, in *The Economic Utilisation of Food Co-Products*, Royal Society of Chemistry, 2013, ch. 5, pp. 110-129.
75. R. F. Tester, J. Karkalas and X. Qi, *Journal of Cereal Science*, 2004, **39**, 151-165.
76. W. Amass, A. Amass and B. Tighe, *Polymer International*, 1998, **47**, 89-144.
77. L. Copeland, J. Blazek, H. Salman and M. C. Tang, *Food Hydrocolloids*, 2009, **23**, 1527-1534.
78. P.T. Anastas and J. C. Warner, *Green Chemistry Theory and Practice*, Oxford University Press, Oxford, 1998.
79. J. H. Clark, *Nature Chemistry*, 2009, **1**, 12-13.

80. P. T. Anastas and J. B. Zimmerman, *Environmental Science & Technology*, 2003, **37**, 94A-101A
81. M. J. Mulvihill, E. S. Beach, J. B. Zimmerman and P. T. Anastas, *Annual Review of Environment and Resources*, 2011, **36**, 271-293.
82. A. Atkinson and C. Wheelock, *Green Chemistry: Bio-based Chemicals, Renewable Feedstocks, Green Polymers, Less-toxic Alternative Chemical Formulations, and the Foundations of a Sustainable Chemical industry*, Pike Research, 2011.  
<http://www.navigantresearch.com/wp-content/uploads/2011/06/GCHEM-11-Executive-Summary.pdf> (Accessed 06/04/2015)
83. J. H. Clark and F. Deswarte, in *Introduction to chemicals from biomass*, John Wiley & Sons, 2014, ch. 1, pp. 1-20.
84. International Energy Agency (IEA), *IEA Bioenergy Task 42 Biorefinery*, 2012. [http://www.biorefinery.nl/fileadmin/biorefinery/docs/Brochure\\_Totaal\\_definitief\\_HR\\_opt.pdf](http://www.biorefinery.nl/fileadmin/biorefinery/docs/Brochure_Totaal_definitief_HR_opt.pdf) (Accessed 06/04/2015)
85. National Renewable Energy Laboratory (NREL), *What is a biorefinery?* <http://www.nrel.gov/biomass/biorefinery.html> (Accessed 06/04/2015)
86. S. Fernando, S. Adhikari, C. Chandrapal and N. Murali, *Energy & Fuels*, 2006, **20**, 1727-1737.
87. B. Kamm and M. Kamm, *Applied Microbiology and Biotechnology*, 2004, **64**, 137-145.
88. D. L. Van Dyne, M. G. Blase and L. D. Clements, *Perspectives on new crops and new uses*. ASHS Press, Alexandria, Va, 1999, 114-123.
89. M. Carus, D. Carrez, H. Kaeb, J. Ravenstiji and J. Venus, Nova paper #1 on bio-based economy 2011–07: Level Playing Field for Bio-based Chemistry and Materials, 2011, <http://bio-based.eu/nova-papers/> (Accessed 06/04/2015)
90. L. Christopher, *Integrated forest biorefineries: challenges and opportunities*, Royal Society of Chemistry, 2012.

91. P. R. Stuart and M. M. El-Halwagi, *Integrated biorefineries: design, analysis, and optimization*, CRC Press, 2012.
92. M. Aresta, A. Dibenedetto and F. Dumeignil, *Biorefinery: from biomass to chemicals and fuels*, Walter de Gruyter, 2012.
93. P. Shuttleworth, V. Budarin and M. Gronnow, in *The Economic Utilisation of Food Co-Products*, eds. A. Kazmi and P. Shuttleworth, Royal Society of Chemistry, 2013, pp. 38-63.
94. Y. Sun and J. Cheng, *Bioresource Technology*, 2002, **83**, 1-11.
95. C. Wu and P. T. Williams, in *Waste as a Resource*, eds. R. E. Hester and R. M. Harrison, Royal Society of Chemistry, 2013, ch. 1, pp. 1-43.
96. V. Kirubakaran, V. Sivaramakrishnan, R. Nalini, T. Sekar, M. Premalatha and P. Subramanian, *Renewable and Sustainable Energy Reviews*, 2009, **13**, 179-186.
97. T. Damartzis and A. Zabaniotou, *Renewable and Sustainable Energy Reviews*, 2011, **15**, 366-378.
98. S. Czernik and A. V. Bridgwater, *Energy & Fuels*, 2004, **18**, 590-598.
99. A. V. Bridgwater, *Biomass and Bioenergy*, 2012, **38**, 68-94.
100. A. V. Bridgwater and G. V. C. Peacocke, *Renewable and Sustainable Energy Reviews*, 2000, **4**, 1-73.
101. A. V. Bridgwater, *Chemical Engineering Journal*, 2003, **91**, 87-102.
102. M. I. Jahirul, M. G. Rasul, A. A. Chowdhury and N. Ashwath, *Energies*, 2012, **5**, 4952-5001.
103. M. F. Demirbas and M. Balat, *Energy Conversion and Management*, 2006, **47**, 2371-2381.
104. F. C. Borges, Z. Du, Q. Xie, J. O. Trierweiler, Y. Cheng, Y. Wan, Y. Liu, R. Zhu, X. Lin, P. Chen and R. Ruan, *Bioresource Technology*, 2014, **156**, 267-274.

105. Y. Wharton, in *Chemical Processes for a Sustainable Future*, eds. T. M. Letcher, J. L. Scott and D. A. Patterson, Royal Society of Chemistry, 2014, ch. 6, pp. 143-156.
106. D. E. Clark and W. H. Sutton, *Annual Review of Materials Science*, 1996, **26**, 299-331.
107. R. Luque, J. A. Menendez, A. Arenillas and J. Cot, *Energy & Environmental Science*, 2012, **5**, 5481-5488.
108. S. S. Lam and H. A. Chase, *Energies*, 2012, **5**, 4209-4232.
109. C. Yin, *Bioresource Technology*, 2012, **120**, 273-284.
110. A. Domínguez, J. A. Menéndez, M. Inguanzo and J. J. Pis, *Fuel Processing Technology*, 2005, **86**, 1007-1020.
111. F. C. Borges, Q. Xie, M. Min, L. A. R. Muniz, M. Farenzena, J. O. Trierweiler, P. Chen and R. Ruan, *Bioresource Technology*, 2014, **166**, 518-526.
112. Y. F. Huang, W. H. Kuan, S. L. Lo and C. F. Lin, *Bioresource Technology*, 2008, **99**, 8252-8258.
113. C. Wu, M. A. Nahil, N. Miskolczi, J. Huang and P. T. Williams, *Environmental Science & Technology*, 2014, **48**, 819-826.
114. V. L. Budarin, J. H. Clark, B. A. Lanigan, P. Shuttleworth and D. J. Macquarrie, *Bioresource Technology*, 2010, **101**, 3776-3779.
115. A. A. Salema and F. N. Ani, *Bioresource Technology*, 2011, **102**, 3388-3395.
116. A. Undri, L. Rosi, M. Frediani and P. Frediani, *Fuel*, 2014, **133**, 7-16.
117. D. Benoso, J. M. Bermúdez, A. Arenillas and J. A. Menéndez, *Journal of Analytical and Applied Pyrolysis*, 2014, **105**, 234-240.
118. A. Undri, M. Frediani, L. Rosi and P. Frediani, *Journal of Analytical and Applied Pyrolysis*, 2014, **105**, 35-42.
119. S. M. Abdul Aziz, R. Wahi, Z. Ngaini and S. Hamdan, *Fuel Processing Technology*, 2013, **106**, 744-750.

120. F. Mushtaq, R. Mat and F. N. Ani, *Renewable and Sustainable Energy Reviews*, 2014, **39**, 555-574.
121. P. Lidström, J. Tierney, B. Wathey and J. Westman, *Tetrahedron*, 2001, **57**, 9225-9283.
122. R. J. Meredith, *Engineers' handbook of industrial microwave heating*, IET, 1998.
123. C. O. Kappe, *Angewandte Chemie International Edition*, 2004, **43**, 6250-6284.
124. D. M. P. Mingos and D. R. Baghurst, *Chemical Society Reviews*, 1991, **20**, 1-47.
125. C. Gabriel, S. Gabriel, E. H. Grant, E. H. Grant, B. S. J. Halstead and D. Michael P. Mingos, *Chemical Society Reviews*, 1998, **27**, 213-224.
126. B. L. Hayes, *Microwave synthesis: chemistry at the speed of light*, CEM Pub. Matthews, NC, USA, 2002.
127. J.-S. Schanche, *Molecular Diversity*, 2003, **7**, 291-298.
128. M. Fröhling, J. Schweinle, J. Meyer and F. Schultmann, in *Renewable Raw Materials*, eds. R. Ulber, D. Sell and T. Hirth, Wiley-VCH Verlag GmbH & Co. KGaA, 2011, ch. 4, pp. 49-94.
129. M. K. Ghose, in *The Biofuels Handbook*, ed. J. G. Speight, Royal Society of Chemistry, 2011, ch. 3, pp. 255-303.
130. J. Buongiorno, R. Raunikar and S. Zhu, *Journal of Forest Economics*, 2011, **17**, 214-229.
131. Food and Agricultural Organization of the United Nations, *Forest products statistics – 2013 Global Forest Products Facts and Figures*, 2014. <http://www.fao.org/forestry/35445-0e287e9c252335f2936d3cdc5b6bbd5ff.pdf> (Accessed 06/04/2015)
132. Food and Agricultural Organization of the United Nations, *Forest products statistics - Forest product consumption and production*, 2014. <http://www.fao.org/forestry/statistics/80938@180723/en/> (Accessed 06/04/2015)
133. European Parliament, *Recycling agricultural, forestry & food wastes and residues for sustainable bioenergy and biomaterials*, 2013. <http://www.europarl.europa.eu/R>

egData/etudes/etudes/join/2013/513513/IPOL-JOIN\_ET%282013%29513513\_EN.pdf

(Accessed 06/04/2015)

134. United States Department of Energy, *Forest Biomass and Wood Wastes*, 2011. [http://www1.eere.energy.gov/bioenergy/pdfs/btu\\_forest\\_biomass.pdf](http://www1.eere.energy.gov/bioenergy/pdfs/btu_forest_biomass.pdf) (Accessed 06/04/2015)
135. Food and Agricultural Organization of the United Nations, *FAO Yearbook of Forest products 2011*, 2013. <http://www.fao.org/forestry/statistics/80570/en/> (Accessed 06/04/2015)
136. A. A. Koutinas, A. Vlysidis, D. Pleissner, N. Kopsahelis, I. Lopez Garcia, I. Kookos, S. Papanikolaou, T. H. Kwan and C. S. K. Lin, *Chemical Society Reviews*, 2014, **43**, 2587-2627.
137. S. N. Dodić, T. Z. Vasiljević, R. M. Marić, A. J. R. Kosanović, J. M. Dodić and S. D. Popov, *Renewable and Sustainable Energy Reviews*, 2012, **16**, 2355-2360.
138. A. Demirbaş, *Energy Conversion and Management*, 2001, **42**, 1357-1378.
139. Department for Environment Food and Rural Affairs (DEFRA), *Wood waste: A short review of recent research*, 2012. [https://www.gov.uk/government/uploads/system/uploads/attachment\\_data/file/82571/consult-wood-waste-researchreview-20120731.pdf](https://www.gov.uk/government/uploads/system/uploads/attachment_data/file/82571/consult-wood-waste-researchreview-20120731.pdf) (Accessed 06/04/2015)
140. J. G. Speight, in *The Biofuels Handbook*, ed. J. G. Speight, Royal Society of Chemistry, 2011, ch. 4, pp. 304-330.
141. C. V. Stevens in *Renewable bioresources: Scope and Modification for Non-food Applications*, eds., C. V. Stevens and R. G. Verhé, John Wiley & Sons Ltd, 2004, ch. 7, pp. 160-188.
142. European Recovered Paper Council, *Paper Recycling Monitoring Report 2012*, 2013. [http://www.paperforrecycling.eu/uploads/Modules/Publications/WEB\\_lowres\\_Monitoring%20report%202012.pdf](http://www.paperforrecycling.eu/uploads/Modules/Publications/WEB_lowres_Monitoring%20report%202012.pdf) (Accessed 06/04/2015)

143. H. Merrild, A. Damgaard and T. H. Christensen, *Resources, Conservation and Recycling*, 2008, **52**, 1391-1398.
144. A. Z. Shi, L. P. Koh and H. T. W. Tan, *GCB Bioenergy*, 2009, **1**, 317-320.
145. Y. Ikeda, E. Y. Park and N. Okuda, *Bioresource Technology*, 2006, **97**, 1030-1035.
146. E. Y. Park, P. N. Anh and N. Okuda, *Bioresource Technology*, 2004, **93**, 77-83.
147. G. Mtui and Y. Nakamura, *Biodegradation*, 2005, **16**, 493-499.
148. M. Alcalde, M. Ferrer, F. J. Plou and A. Ballesteros, *Trends in Biotechnology*, 2006, **24**, 281-287.
149. C. Pothiraj, P. Kanmani and P. Balaji, *Mycobiology*, 2006, **34**, 159-165.
150. P. Bajpai, *Biorefinery in the pulp and paper industry*, Academic Press, 2013.
151. M. C. Monte, E. Fuente, A. Blanco and C. Negro, *Waste Management*, 2009, **29**, 293-308.
152. *Bubbling bed FBC process for the conversion of paper (de-inking) residue. LIFE project to convert a waste material into a valuable product*, LIFE97 ENV/NL/00017, [http://ec.europa.eu/environment/life/project/Projects/files/laymanReport/LIFE97\\_ENV\\_NL\\_000117\\_LAYMAN.pdf](http://ec.europa.eu/environment/life/project/Projects/files/laymanReport/LIFE97_ENV_NL_000117_LAYMAN.pdf) (Accessed 06/04/2015)
153. Confederation of European Paper Industries (CEPI), *Discovering the High Potential of Pulp and Paper Production Residues*, 2004, <http://www.cepi.org/system/files/public/documents/publications/environment/2003/2003Discovering%20the%20High%20Potential%20of%20Pulp%20and%20Paper%20Production%20Residues.pdf> (Accessed 06/04/2015)
154. J. A. Sohara and T. D. Young, Recycling of mineral fillers from the residue of a paper deinking plant, *US Pat.*, 5759258, 2 June 1998.
155. J. J. Camberato, B. Gagnon, D. A. Angers, M. H. Chantigny and W. L. Pan, *Canadian Journal of Soil Science*, 2006, **86**, 641-653.
156. S. Yan, K. Sagoe-Crentsil and G. Shapiro, *Journal of Environmental Management*, 2011, **92**, 2085-2090.

157. S. Kim, H.-J. Kim and J. C. Park, *Resources, Conservation and Recycling*, 2009, **53**, 674-679.
158. A. Taramian, K. Doosthoseini, S. A. Mirshokraii and M. Faezipour, *Waste Management*, 2007, **27**, 1739-1746.
159. J. Soucy, A. Koubaa, S. Migneault and B. Riedl, *Industrial Crops and Products*, 2014, **54**, 248-256.
160. M. Ouadi, J. G. Brammer, Y. Yang, A. Hornung and M. Kay, *Journal of Analytical and Applied Pyrolysis*, 2013, **102**, 24-32.
161. Y. Yang, J. G. Brammer, M. Ouadi, J. Samanya, A. Hornung, H. M. Xu and Y. Li, *Fuel*, 2013, **103**, 247-257.
162. R. Lou, S. Wu, G. Lv and Q. Yang, *Applied Energy*, 2012, **90**, 46-50.
163. J. Jiang and X. Ma, *Applied Thermal Engineering*, 2011, **31**, 3897-3903.
164. C. Xu and J. Lancaster, *Water Research*, 2008, **42**, 1571-1582.
165. L. Zhang, C. Xu and P. Champagne, *Bioresource Technology*, 2010, **101**, 2713-2721.
166. A. Méndez, S. Barriga, J. M. Fidalgo and G. Gascó, *Journal of Hazardous Materials*, 2009, **165**, 736-743.
167. A. Méndez, J. Paz-Ferreiro, F. Araujo and G. Gascó, *Journal of Analytical and Applied Pyrolysis*, 2014, **107**, 46-52.
168. C. Almquist and N. Qin, *Environmental Progress & Sustainable Energy*, 2013, **32**, 524-534.
169. V. L. Budarin, J. H. Clark, B. A. Lanigan, P. Shuttleworth, S. W. Breeden, A. J. Wilson, D. J. Macquarrie, K. Milkowski, J. Jones, T. Bridgeman and A. Ross, *Bioresource Technology*, 2009, **100**, 6064-6068.
170. V. L. Budarin, P. S. Shuttleworth, J. R. Dodson, A. J. Hunt, B. Lanigan, R. Marriott, K. J. Milkowski, A. J. Wilson, S. W. Breeden, J. Fan, E. H. K. Sin and J. H. Clark, *Energy & Environmental Science*, 2011, **4**, 471-479.

171. J. H. Levy, *Energy & Fuels*, 1990, **4**, 146-151.
172. M. Pietro and C. Paola, *Thermochimica Acta*, 2004, **413**, 209-214.
173. A. Mández, J. M. Fidalgo, F. Guerrero and G. Gascó, *Journal of Analytical and Applied Pyrolysis*, 2009, **86**, 66-73.
174. L. Wang, R. Templer and R. J. Murphy, *Applied Energy*, 2012, **99**, 23-31.
175. T. Materne, F. de Buyl and G. L. Witucki, *Dow Corning Review*, 2006.
176. C. I. Basilio and S. W. Sheppard, Deinking of waste paper, *US Pat.*, 8052837 B2, 8 November 2011.
177. M. Schwanninger, J. C. Rodrigues, H. Pereira and B. Hinterstoisser, *Vibrational Spectroscopy*, 2004, **36**, 23-40.
178. A. Naumann, S. Peddireddi, U. Kües and A. Polle in *Wood Production, Wood Technology, and Biotechnological Impacts*, ed. U. Kües, Universitätsverlag Göttingen, 2007, ch. 10, pp. 179-196.
179. A. M. Prima, R. G. Zhbakov and R. Marupov, *Journal of Structural Chemistry*, 1965, **5**, 783-788.
180. P. Rouxhet, N. Samudacheata, H. Jacobs and O. Anton, *Clay Minerals*, 1977, **12**, 171-179.
181. F. W. Langkilde and A. Svantesson, *Journal of Pharmaceutical and Biomedical Analysis*, 1995, **13**, 409-414.
182. C. A. Mullen, G. D. Strahan and A. A. Boateng, *Energy & Fuels*, 2009, **23**, 2707-2718.
183. G. Duman, C. Okutucu, S. Ucar, R. Stahl and J. Yanik, *Bioresource Technology*, 2011, **102**, 1869-1878.
184. A. Oasmaa and D. Meier, in *Fast Pyrolysis of Biomass: A Handbook*, ed. A. V. Bridgwater, Newbury, 2005, Vol. 3, pp. 19-43.
185. M. Garcia-Perez, A. Chaala, H. Pakdel, D. Kretschmer and C. Roy, *Biomass and Bioenergy*, 2007, **31**, 222-242.

186. S. D. Stefanidis, K. G. Kalogiannis, E. F. Iliopoulou, C. M. Michailof, P. A. Pilavachi and A. A. Lappas, *Journal of Analytical and Applied Pyrolysis*, 2014, **105**, 143-150.
187. R. J. Evans and T. A. Milne, *Energy & Fuels*, 1987, **1**, 123-137.
188. G. C. A. Luijkx, F. van Rantwijk and H. van Bekkum, *Carbohydrate Research*, 1993, **242**, 131-139.
189. Z. Liu and F. Zhang, *Energy Conversion and Management*, 2008, **49**, 3498-3504.
190. C. Liao and K. Kannan, *Environmental Science & Technology*, 2011, **45**, 9372-9379.
191. C. J. Beauchamp, M. Charest and A. Gosselin, *Chemosphere*, 2002, **46**, 887-895.
192. H. B. Goyal, D. Seal and R. C. Saxena, *Renewable and Sustainable Energy Reviews*, 2008, **12**, 504-517.
193. S. Xiu and A. Shahbazi, *Renewable and Sustainable Energy Reviews*, 2012, **16**, 4406-4414.
194. S. Tsiantzi and E. Athanassiadou, *PyNe Newsletter*, 2000, **10**, 10-11.
195. S. Cheng, Z. Yuan, M. Anderson, M. Leitch and C. Xu, *Journal of Applied Polymer Science*, 2012, **126**, E431-E441.
196. J. A. von Fraunhofer, *International journal of dentistry*, 2012, **2012**.
197. S. Wang, Y. Wang, Q. Cai, X. Wang, H. Jin and Z. Luo, *Separation and Purification Technology*, 2014, **122**, 248-255.
198. D. Fu, S. Farag, J. Chaouki and P. G. Jessop, *Bioresource Technology*, 2014, **154**, 101-108.
199. Q. Song, J. Nie, M. Ren and Q. Guo, *Energy & Fuels*, 2009, **23**, 3307-3312.
200. J. Li, C. Wang and Z. Yang, *Journal of Analytical and Applied Pyrolysis*, 2010, **89**, 218-224.
201. C. Amen-Chen, H. Pakdel and C. Roy, *Biomass and Bioenergy*, 1997, **13**, 25-37.
202. Z. Zhang, S. Sui, S. Tan, Q. Wang and C. U. Pittman Jr, *Bioresource Technology*, 2013, **130**, 789-792.

203. M. Asadieraghi, W. M. A. Wan Daud and H. F. Abbas, *Renewable and Sustainable Energy Reviews*, 2014, **36**, 286-303.
204. W. Mu, H. Ben, X. Du, X. Zhang, F. Hu, W. Liu, A. J. Ragauskas and Y. Deng, *Bioresource Technology*, 2014, **173**, 6-10.
205. J. R. Gald ámez, L. Garc á and R. Bilbao, *Energy & Fuels*, 2005, **19**, 1133-1142.
206. X. Hu, Y. Wang, D. Mourant, R. Gunawan, C. Lievens, W. Chaiwat, M. Gholizadeh, L. Wu, X. Li and C.-Z. Li, *AIChE Journal*, 2013, **59**, 888-900.
207. M. B. McBride and L. G. Wesselink, *Environmental Science & Technology*, 1988, **22**, 703-708.
208. H. Kono, S. Yunoki, T. Shikano, M. Fujiwara, T. Erata and M. Takai, *Journal of the American Chemical Society*, 2002, **124**, 7506-7511.
209. C. F. Liu, F. Xu, J. X. Sun, J. L. Ren, S. Curling, R. C. Sun, P. Fowler and M. S. Baird, *Carbohydrate Research*, 2006, **341**, 2677-2687.
210. F. Horii, A. Hirai and R. Kitamaru, *Polymer Bulletin*, 1983, **10**, 357-361.
211. R. H. Atalla and D. L. VanderHart, *Solid State Nuclear Magnetic Resonance*, 1999, **15**, 1-19.
212. C. H. Park, Y. K. Kang and S. S. Im, *Journal of Applied Polymer Science*, 2004, **94**, 248-253.
213. H. Zhao, J. H. Kwak, Z. Conrad Zhang, H. M. Brown, B. W. Arey and J. E. Holladay, *Carbohydrate Polymers*, 2007, **68**, 235-241.
214. Y. Su, H. Yang, W. Shi, H. Guo, Y. Zhao and D. Wang, *Colloids and Surfaces A: Physicochemical and Engineering Aspects*, 2010, **355**, 158-162.
215. H. W. Papenguth, R. J. Kirkpatrick, B. Montez and P. A. Sandberg, *American Mineralogist*, 1989, **74**, 1152-1158.
216. M. V. Dungen, *The adhesives and sealants market 2013-2014*, BASAhandbook, pp. 10, <http://www.basaonline.co.uk/publications/basahandbook.aspx> (accessed 06/04/2015)

217. I. K. Khairullin, *Polymer Science Series D*, 2013, **6**, 77-81.
218. *Global Analysis of the Hot Melt Adhesives Market*, Frost & Sullivan, 2013.  
<http://www.frost.com/sublib/display-report.do?id=M967-01-00-00-00>  
(accessed 06/04/2015)
219. *Hot Melt Adhesives Market by Products (EVA, Styrenic Block, Polyolefin, Polyurethane, & Others), By Applications (Packaging, Non-Woven, Pressure Sensitive, Construction, Bookbinding, & Others), by Geography - Global Trends & Forecasts to 2018*, MarketsandMarkets, 2013. <http://www.marketsandmarkets.com/Market-Reports/hot-melt-adhesives-market-1088.html> (accessed 06/04/2013)
220. R. D. Dexheimer and L. R. Vertnik in *Adhesives in Manufacturing*, ed. G. L. Schneberger, Marcel Dekker, 1983, ch. 13, pp. 325-351.
221. S. Ebnesajjad, in *Adhesives Technology Handbook*, William Andrew, 2<sup>nd</sup> edn., 2008, ch. 5, pp. 80-90.
222. A. V. Pocius, in *Physical Properties of Polymers Handbook*, ed. J. E. Mark, Springer, 2<sup>nd</sup> edn., 2007, ch. 27, pp. 483-486.
223. S. Ebnesajjad, in *Handbooks of Adhesives and Surface Preparation: Technology, Applications and Manufacturing*, ed. S. Ebnesajjad, Elsevier, 2011, ch. 8, pp. 154-156.
224. A. V. Pocius, in *Adhesion and Adhesives Technology: An Introduction*, Hanser, 2<sup>nd</sup> edn., 2002, ch. 10, pp. 270-285.
225. H. Dahmane, *International Journal of Adhesion and Adhesives*, 1996, **16**, 43-45.
226. W. Li, L. Bouzidi and S. S. Narine, *Industrial & Engineering Chemistry Research*, 2008, **47**, 7524-7532.
227. G. V. Malysheva and N. V. Bodrykh, *Polymer Science Series D*, 2011, **4**, 301-303.
228. J. P. Kalish, S. Ramalingam, O. Wamuo, O. Vyawahare, Y. Wu, S. L. Hsu, C. W. Paul and A. Eodice, *International Journal of Adhesion and Adhesives*, 2014, **55**, 82-88.
229. P. Kadam, P. Vaidya and S. Mhaske, *International Journal of Adhesion and Adhesives*, 2014, **50**, 151-156.

230. L. L. Ryan, A. Rouyer, E. Pariente and P. Yeboa-Kodie, Biodegradable adhesive packaging, *US Pat.*, 5387623, 7 February 1995.
231. D. V. Varanese and M. D. Hilston, Cohesive reclosure systems and containers using same, *US Pat.*, 2005/0031233 A1, 10 February 2005.
232. D. N. Lewis, G. Schutte, H. Westerhof, J. Janssen and W. E. Kelly, Environmentally degradable polymeric compounds their preparation and use as hot melt adhesive, *US Pat.*, 7465770 B2, 16 December, 2008.
233. K. Cathie, *International Journal of Adhesion and Adhesives*, 1994, **14**, 63-67.
234. S. H. Imam, C. Bilbao-Sainz, B.-S. Chiou, G. M. Glenn and W. J. Orts, *Journal of Adhesion Science and Technology*, 2012, **27**, 1972-1997.
235. A. Dotan, in *Handbook of Thermoset Plastics*, eds. H. Dodiuk and S. H. Goodman, William Andrew Publishing, Boston, 3<sup>rd</sup> edn., 2014, pp. 577-622.
236. L. Jiang and J. Zhang, in *Applied Plastics Engineering Handbook*, ed. M. Kutz, William Andrew Publishing, Oxford, 2011, pp. 145-158.
237. E. Cohen, O. Binshtok, A. Dotan and H. Dodiuk, *Journal of Adhesion Science and Technology*, 2012, **27**, 1998-2013.
238. A. Pizzi, *Journal of Adhesion Science and Technology*, 2006, **20**, 829-846.
239. J. O. Wegner, in *Sustainable Solutions for Modern Economies*, ed. R. Höfer, The Royal Society of Chemistry, 2009, ch. 11, pp. 425-435.
240. E. M. Petrie, Biobased components in hot melt adhesive formulation, SpecialChem, 2012.  
[http://iterg.com/IMG/pdf/biobased\\_components\\_in\\_hot\\_melt\\_adhesive\\_formulation.pdf](http://iterg.com/IMG/pdf/biobased_components_in_hot_melt_adhesive_formulation.pdf)  
(accessed 06/04/2015)
241. R. Kumar, V. Choudhary, S. Mishra and I. Varma, *Journal of Thermal Analysis and Calorimetry*, 2004, **75**, 727-738.
242. R. Kumar, V. Choudhary, S. Mishra and I. K. Varma, *Journal of Adhesion Science and Technology*, 2004, **18**, 261-273.

243. W. Y. Choi, C. M. Lee and H. J. Park, *LWT - Food Science and Technology*, 2006, **39**, 591-597.
244. M. Viljanmaa, A. Södergård and P. Törmälä, *International Journal of Adhesion and Adhesives*, 2002, **22**, 219-226.
245. M. Viljanmaa, A. Södergård and P. Törmälä, *International Journal of Adhesion and Adhesives*, 2003, **23**, 151-154.
246. M. Viljanmaa, A. Södergård and P. Törmälä, *International Journal of Adhesion and Adhesives*, 2002, **22**, 447-457.
247. T. Ke and X. Sun, *Journal of Polymers and the Environment*, 2003, **11**, 7-14.
248. S. Inkinen, M. Stolt and A. Södergård, *Journal of Applied Polymer Science*, 2008, **110**, 2467-2474.
249. M. Labet, K. M. Zakir Hossain, I. Ahmed and W. Thielemans in *Materials for a sustainable future*, eds. T. M. Letcher and J. L. Scott, Royal Society of Chemistry, 2012, ch. 22, pp. 698-727.
250. L. Yu, K. Dean and L. Li, *Progress in Polymer Science*, 2006, **31**, 576-602.
251. T. Mekonnen, P. Mussone, H. Khalil and D. Bressler, *Journal of Materials Chemistry A*, 2013, **1**, 13379-13398.
252. A. K. Mohanty, M. Misra and L. T. Drzal, *Journal of Polymers and the Environment*, 2002, **10**, 19-26.
253. Y. S. Jeon, S. N. Lee, J. Y. Yoon, J. S. Lee and S. O. Kim, Starch-based hot melt adhesive, *US Pat.*, 2015/0045480A1, 12 February 2015.
254. R. J. Billmers, C. W. Paul, S. F. Hatfield and T. F. Kauffman, Starch ester based hot melt adhesive, *US Pat.*, 5360845, 1 November 1994.
255. C. P. Iovine, T. F. Kauffman, J. E. Schoenberg and P. P. Puletti, Polylactide and starch containing hot melt adhesive, *US Pat.*, 5312850, 17 May 1994.

256. D. Neigel, G. A. Sweeey, P. Altieri, C. W. Paul, R. L. Billmers and D. C. Rawlins, Process for production of starch based hot melt adhesives, *US Pat.*, 5434201, 18 July 1995.
257. T. F. Kauffman, J. Wieczorek and S. F. Hatfield, Starch based hot melt adhesives for cigarettes, *US pat.*, 5498224, 12 March 1996.
258. Hot melts can support sustainability, Henkel AI newsletter, 2009. [http://www.quadra.ca/uploadedFiles/Content/Industries/Performance\\_Adhesives\\_Group/GoingGreen\\_Newsletter\\_Summer09.pdf](http://www.quadra.ca/uploadedFiles/Content/Industries/Performance_Adhesives_Group/GoingGreen_Newsletter_Summer09.pdf) (accessed 06/04/2015)
259. C. J. R. Verbeek and J. M. Bier, in *A Handbook of Applied Biopolymer Technology: Synthesis, Degradation and Applications*, eds. S. K. Sharma and A. Mudhoo, Royal Society of Chemistry, 2011, ch. 7, pp. 197-242.
260. A. Rajan, V. S. Prasad and T. Emilia Abraham, *International Journal of Biological Macromolecules*, 2006, **39**, 265-272.
261. O. S. Lawal, *Carbohydrate Research*, 2004, **339**, 2673-2682.
262. L. S. Sciarini, A. Rolland-Sabate, S. Guilois, P. Decaen, E. Leroy and P. Le Bail, *Green Chemistry*, 2015, **17**, 291-299.
263. R. J. White, V. Budarin, R. Luque, J. H. Clark and D. J. Macquarrie, *Chemical Society Reviews*, 2009, **38**, 3401-3418.
264. V. Budarin, J. H. Clark, J. J. E. Hardy, R. Luque, K. Milkowski, S. J. Tavener and A. J. Wilson, *Angewandte Chemie*, 2006, **118**, 3866-3870.
265. G. M. Glenn and D. W. Irving, *Cereal Chemistry*, 1995, **72**, 155-161.
266. G. M. Glenn and D. J. Stern, Starch-based microcellular foams, *US Pat.*, 5958589, 28 September 1999.
267. R. Hoover, *Food Reviews International*, 1995, **11**, 331-346.
268. A.-M. Hermansson and K. Svegmark, *Trends in Food Science & Technology*, 1996, **7**, 345-353.
269. R. Mukerjea, R. Mukerjea and J. F. Robyt, *Carbohydrate Research*, 2006, **341**, 757-765.

270. Z. Huang, X. Xie, Y. Chen, J. Lu and Z. Tong, *Comptes Rendus Chimie*, 2008, **11**, 73-79.
271. S. Doi, J. H. Clark, D. J. Macquarrie and K. Milkowski, *Chemical Communications*, 2002, **22**, 2632-2633.
272. N. J. Atkin, R. M. Abeysekera, S. L. Cheng and A. W. Robards, *Carbohydrate Polymers*, 1998, **36**, 173-192.
273. K. S. Sandhu, N. Singh and M. Kaur, *Journal of Food Engineering*, 2004, **64**, 119-127.
274. Starch, <http://www.food-info.net/uk/carbs/starch.htm> (accessed 06/04/2015)
275. A. A. Karim, M. H. Norziah and C. C. Seow, *Food Chemistry*, 2000, **71**, 9-36.
276. J. H. Clark, V. Budarin, F. E. I. Deswarte, J. J. E. Hardy, F. M. Kerton, A. J. Hunt, R. Luque, D. J. Macquarrie, K. Milkowski, A. Rodriguez, O. Samuel, S. J. Tavener, R. J. White and A. J. Wilson, *Green Chemistry*, 2006, **8**, 853-860.
277. A. I. Bolivar, R. A. Venditti, J. J. Pawlak and K. El-Tahlawy, *Carbohydrate Polymers*, 2007, **69**, 262-271.
278. R. J. White, V. L. Budarin and J. H. Clark, *ChemSusChem*, 2008, **1**, 408-411.
279. M. J. Gronnow, R. Luque, D. J. Macquarrie and J. H. Clark, *Green Chemistry*, 2005, **7**, 552-557.
280. V. Budarin, J. H. Clark, F. E. I. Deswarte, J. J. E. Hardy, A. J. Hunt and F. M. Kerton, *Chemical Communications*, 2005, 2903-2905.
281. X. Ma, X. Liu, D. P. Anderson and P. R. Chang, *Food Chemistry*, 2015, **181**, 133-139.
282. N. Supanchaiyamat, A. J. Hunt, P. S. Shuttleworth, C. Ding, J. H. Clark and A. S. Matharu, *RSC Advances*, 2014, **4**, 23304-23313.
283. P. S. Shuttleworth, J. H. Clark, R. Mantle and N. Stansfield, *Green Chemistry*, 2010, **12**, 798-803.
284. T. Liebert, M. C. V. Nagel, T. Jordan, A. Heft, B. Grünler and T. Heinze, *Macromolecular Rapid Communications*, 2011, **32**, 1312-1318.

285. A. Alissandratos, N. Baudendistel, S. Flitsch, B. Hauer and P. Halling, *BMC Biotechnology*, 2010, **10**, 82.
286. R. L. Shogren, *Carbohydrate Polymers*, 2000, **43**, 309-315.
287. Y. Xu, V. Miladinov and M. A. Hanna, *Cereal Chemistry Journal*, 2004, **81**, 735-740.
288. W. Xie, L. Shao and Y. Liu, *Journal of Applied Polymer Science*, 2010, **116**, 218-224.
289. M. Lukasiewicz and S. Kowalski, *Starch - Stärke*, 2012, **64**, 188-197.
290. U. Neumann, B. Wiege and S. Warwel, *Starch - Stärke*, 2002, **54**, 449-453.
291. A. Lehmann and B. Volkert, *Carbohydrate Polymers*, 2011, **83**, 1529-1533.
292. H. Chi, K. Xu, X. Wu, Q. Chen, D. Xue, C. Song, W. Zhang and P. Wang, *Food Chemistry*, 2008, **106**, 923-928.
293. J. Singh, L. Kaur and N. Singh, *Starch - Stärke*, 2004, **56**, 586-601.
294. B. Laignel, C. Bliard, G. Massiot and J. M. Nuzillard, *Carbohydrate Research*, 1997, **298**, 251-260.
295. M. Tessler and R. Billmers, *Journal of environmental polymer degradation*, 1996, **4**, 85-89.
296. R. Murugan and E. F. V. Scriven, *Aldrichimica Acta*, 2003, **36**, 21-26.
297. S. M. Goheen and R. P. Wool, *Journal of Applied Polymer Science*, 1991, **42**, 2691-2701.
298. S. Thiebaud, J. Aburto, I. Alric, E. Borredon, D. Bikiaris, J. Prinos and C. Panayiotou, *Journal of Applied Polymer Science*, 1997, **65**, 705-721.
299. E. J. Choi, C. H. Kim and J. K. Park, *Macromolecules*, 1999, **32**, 7402-7408.
300. P. Dais and A. S. Perlin, *Carbohydrate Research*, 1982, **100**, 103-116.
301. T. Jordan, S. Schmidt, T. Liebert and T. Heinze, *Green Chemistry*, 2014, **16**, 1967-1973.
302. M. J. Tizzotti, M. C. Sweedman, D. Tang, C. Schaefer and R. G. Gilbert, *Journal of Agricultural and Food Chemistry*, 2011, **59**, 6913-6919.

303. C. J. Donahue and E. A. Rais, *Journal of Chemical Education*, 2009, **86**, 222.
304. R. Santayanon and J. Woothikanokkhan, *Carbohydrate Polymers*, 2003, **51**, 17-24.
305. O. B. Wurzburg, *Methods in Carbohydrate Chemistry*, Academic Press, New York, 1964, vol. IV, pp. 286-288.